Deciphering the transcriptional response of *Saccharomyces cerevisiae* to perturbations of lipid metabolism and graded endoplasmic reticulum stress

Felix Jonas

Submitted for the Degree of Doctor of Philosophy

Supervised by Dr Guy-Bart Stan and Dr Karen Polizzi
Department for Bioengineering
Imperial College London
Centre for Synthetic Biology and Innovation

February 11, 2017

Abstract

Systems Biology combines experimental biology with mathematics and computational simulations to better describe biological phenomena that emerge from the interaction of different players. Extensive prior knowledge and experimental feasibility make the eukaryotic single-cell organism *S. cerevisiae* the preferred model organism for systems biology, while the strongly conserved features might enable conclusions for more complex organisms.

In this thesis, a 'Systems Biology'-approach was taken to better understand how *S. cerevisiae* coordinates different transcriptional and metabolic responses to adapt to two exemplary environmental changes, i.e. inositol depletion and low-level ER stress.

Firstly, a quantitative model guided the construction of fast-folding, actively degraded reporter proteins, which were able to rapidly indicate specific transcriptional changes in single cells.

Secondly, the developed reporter proteins, a fluorescent sphingolipid (SL) intermediate and classical molecular biology techniques were used to investigate the interaction of the signaling pathways, which enable *S. cerevisiae* to survive after inositol depletion, and to understand the role of SL metabolism during this process. The results highlighted the temporal order of transcription factors that follows the removal of inositol, i.e. first INO2/4, then HAC1 and lastly RLM1, and suggested that decreased SL biosynthesis is probably not responsible for the delayed disruption of ER homoeostasis but perturbs cell wall integrity after HAC1 activation.

Thirdly, the adaptation to low ER stress was studied with a reporter protein for HAC1 and established fluorescent labels. The experimental insights then motivated a quantitative model for the adaptation to new environments, which lower the growth rate and change the inheritance of essential resources during cytokinesis. From the results, it emerged that ER stress mainly affects G1 duration in daughter cells and reduces the amount of ER content that is inherited by them. This lower inheritance probably contributed to the daughter-specific HAC1 activation. The analysis of the model implied that such a lower resource inheritance increases the daughter: mother ratio and probably lowers the resource demand of the population.

Overall, the results supported the idea that transcriptional adaptation is primarily performed by daughter cells and is often a multi-step process. This work moreover lays the foundation to investigate transcriptional dynamics during other environmental changes and to further study the role of lipid metabolism for ER homeostasis. It also provided a mathematical model for the long-term impact of changes in the distribution of limiting resources.

.

Declaration

I herewith certify that all the material in this thesis is my own work, except for quotations from published and unpublished sources which are clearly indicated and acknowledged as such. The source of any picture, diagram or other figure that is not my own work is also indicated.

Table of contents

Abstract **2**

Declaration **3**

Table of contents **4**

List of figures **9**

List of tables **13**

List of abbreviations **15**

Acknowledgment **16**

1 Introduction **17**

1.1 Motivation 17

1.2 Scope of this study 19

1.3. Background 20

1.3.1 Structure and function of the endoplasmic reticulum in *S. cerevisiae* 20

1.3.2 Glycerolipid biosynthesis and the impact of inositol starvation 22

1.3.2 Biosynthesis of sphingolipids and ergosterol 23

1.3.3 Protein import, folding and quality control in the ER and the molecular basis of ER homeostasis disruption 26

1.3.4 Regulation of lipid metabolism 31

1.3.5 Control of protein secretion and cell wall integrity by protein kinase C 33

1.3.6 ER homeostasis regulation 34

1.4 Aims of this work 37

2 Materials and Methods **39**

2.1 Chemicals 39

2.2 Growth Media 39

2.3 Polymerase chain reaction (PCR) 41

2.4 Molecular cloning 42

2.5 Plasmids 43

2.6 Yeast Strains 44
2.7 *Escherichia coli* transformation 44
2.8 Plasmid Miniprep 45
2.9 Yeast transformation 45
2.10 Yeast cell preparation for treatments 47
2.11 Growth rate determination 47
2.12 RNA extraction and cDNA Library Preparation 48
2.13 Quantitative Real Time PCR 48
2.14 Yeast synchronisation with Nocodazole 49
2.15 TRITC-ConA staining 49
2.16 Yeast NBD-C6-Ceramide *in vivo* staining 50
2.17 Flow Cytometry - data acquisition 50
2.18 Flow Cytometry - data analysis 51
2.19 Statistical tests 52
2.20 Live cell fluorescent imaging 52
Chapter 3: Improved methods for the detection of metabolic and transcriptional changes in single yeast cells 59
3.1 Introduction 59
3.2 The effect of protein translation, maturation and degradation on reporter dynamics 61
3.3 Implementation guidelines for a dynamic reporter protein in *Saccharomyces cerevisiae* .67
3.4 Robustness of dynamic reporter proteins 70
3.5 Response time of the reporter constructs 72
3.6 Cellular burden of dynamic transcriptional reporter 77
3.7 Fluorescent lipids and the measurement of lipid metabolism 80
3.8 AUR1 activity and the intracellular localisation of NBD fluorescence from NBD-C6-ceramide staining 81
3.9 Total NBD fluorescence after NBD-C6-ceramide staining and AUR1 inhibition 83

3.10 Discussion 84

4 The role of sphingolipid metabolism and the coordination of transcription during the adaptation to inositol starvation 87

4.1 Introduction 87

4.2 Inositol depletion and SUR2-deficiency increased NBD fluorescence after staining with NBD-C6-ceramide 88

4.3 SUR2 knock-out and inositol starvation reduced the growth rate in minimal medium but peptone supplementation recovered the growth rate of SUR2-deficient cells 90

4.4 Peptone supplementation increased SUR2 transcription 92

4.5 The expression of enzymes in SL metabolism correlated with their position in the pathway 93

4.6 SUR2, LAC1 and AUR1 expression are sequentially activated between S and G2 phase 96

4.7 SUR2 deficiency perturbed the trafficking of GAP1 in minimal SC medium 98

4.8 SUR2 deficiency increased PKC activation and transcription of cell wall proteins at an increased growth temperature 100

4.9 HAC1 activity in SUR2-deficient cell remained constant after tunicamycin treatment but increased after ER disruption by DTT 102

4.10 HAC1 activation succeeded INO2/4 activation during inositol starvation 103

4.11 AUR1 inhibition perturbed ER homeostasis but ceramide accumulation was not required for UPR activation during inositol starvation 105

4.12 INO2/4 activation after inositol starvation was independent of UPR activation 107

4.13 UPR activation was necessary for RLM1 induction after inositol removal from minimal SC medium 109

4.14 NBD fluorescence increased after AUR1 inhibition or during inositol starvation independent of UPR activation 111

4.15 Sphingosine hydroxylation or fast growth was required for UPR activation after inositol depletion 112

4.16 INO2/4 activation after inositol depletion required sphingosine hydroxylation or fast growth 114

4.17 Discussion 115

5 Population heterogeneity and adaptation to gradual ER stress 119

5.1 Introduction 119

5.2 ER stress from tunicamycin correlated with its concentration and did not require UPR activation at the IC50 value of the affected biochemical reaction 120

5.3 High tunicamycin concentrations triggered uniform UPR activation and reduced ribosome expression, but low tunicamycin concentrations only triggered heterogeneous UPR activation 122

5.4 Cells born in low tunicamycin concentrations had a higher HAC1 activity than cells born before the treatment 125

5.5 Low tunicamycin concentrations primarily reduced the ER content of younger cells 128

5.6 During low ER stress, daughter cells were born with less ER-resident proteins 130

5.7 At low ER stress, the HAC1 activity of WHI5-deficient mother and daughter cells were more similar in than in wild-type cells 132

5.8 Secreted proteins were enriched in the daughter-specific transcription program 134

5.9 Sphingosine hydroxylation was not required for heterogeneous UPR activation but increased ER stress at low tunicamycin concentrations 136

5.10 Phytoceramide supplementation lowered HAC1 activity at low tunicamycin concentrations 138

5.11 Phytoceramide supplementation increased growth rate of wild-type, UPR-deficient and ERSU-deficient cells at low tunicamycin concentrations 140

5.12 Phytoceramide supplementation increased the inheritance of ER content to the daughter cells at low but not intermediate tunicamycin concentrations 142

5.13 High tunicamycin concentrations or phytoceramide supplementation but not low tunicamycin concentrations induced ER stress in minimal SC medium 144

5.14 Low ER stress delayed the progression of daughter cells from G1- to S-Phase 146

5.15 Tunicamycin increased absolute G1 and G2 duration of both cell types 147

5.16 The fraction of daughter increases with a decreasing relative division rate of daughter cells 151

5.17 Asymmetric inheritance of growth-limiting resources lowers the average resource amount of the total population 157
5.18 Discussion 161
6 Discussion 165
6.1 Summary of results 165
6.2 Evaluation of the approach 167
6.3 Concluding remarks 169
7 Future Directions 173
7.1 Reporter development 173
7.2 Inositol starvation and sphingolipid metabolism 174
7.3 Population asymmetry 176
8 References 178
Appendix A: Coding DNA sequence of the reporter constructs 205
Appendix B: Targets of ACE2 and ASH1 206

List of figures

Figure 1.1: ER structure and organisation 21

Figure 1.2: Synthesis and structure of phospholipids and storage lipid 22

Figure 1.3: Sphingolipid biosynthesis in *Saccharomyces cerevisiae.* 24

Figure 1.4: Structure of ergosterol (A) and sphingolipid (B). 25

Figure 1.5: The co-translational translocation of proteins into ER Lumen via the molecular ratchet 27

Figure 1.6: Protein folding cycle via HSP70 chaperones 28

Figure 1.7: Disulfide bond formation and electron transfer during the folding of secreted proteins. 29

Figure 1.8: CNE1 functions as the pivotal co-chaperone for ER Quality control (ERQC). 30

Figure 1.9: Transcriptional regulation of phospholipid synthesis via PA, INO2/4 and OPI1 32

Figure 1.10: The kinase cascade that maintains cell wall integrity after perturbations 34

Figure 1.11: Important components of and interaction between the different ER homeostasis mechanisms 35

Figure 2.1: General layout for the reporter plasmids 44

Figure 2.2: Visualization of the cell gating procedure 51

Figure 2.3: Visualization of gating procedure to separate TRITC-positive from negative cells 52

Figure 3.1: An extended TX-TL-model for the biochemical processes and entities that precede the detection of a fluorescent reporter protein. 62

Figure 3.2: The simulated dynamics of mRNA, dark protein and fluorescent protein after activation 63

Figure 3.3: 50%-response time (left) and maximal reporter output (right) of a transcriptional reporter system over a range of realistic degradation times. 65

Figure 3.4: Relative impact of maturation time and translation rate on reporter fluorescence. 66

Figure 3.5: The three main modifications from conventional to dynamic transcriptional reporters. 69

Figure 3.6: The median fluorescence of a constitutively expressed reporter protein in different clones and ER stress conditions. 71

Figure 3.7: UPR activation and reporter fluorescence dynamics after DTT exposure. 73

Figure 3.8: RLM1 reporter fluorescence in wild-type cells after temperature elevation. 74

Figure 3.9: INO2/4 activation after inositol depletion from wild-type cells. 75

Figure 3.10: mRNA levels of two INO2/4 targets, CHO1 and INO1, after inositol depletion. 76

Figure 3.11: Growth of wild-type cells with and without reporter constructs in YPD and minimal SC medium. 78

Figure 3.12: The exponential growth rates of the reporter strains at low OD in YPD minimal SC medium. 79

Figure 3.13: NBD-ceramide structure and cellular processing. 81

Figure 3.14: NBD fluorescence localisation before and after AUR1 inhibition. 82

Figure 3.15: Impact of AUR1 inhibition on total NBD fluorescence 83

Figure 4.1: Sphingolipid metabolism in yeast from dihydrosphingosine to inositol phosphorylceramide (IPC) 87

Figure 4.2: NBD fluorescence of wild-type and SUR2-deficient cells after AUR1 inhibition and inositol depletion 89

Figure 4.3: Growth rate of SUR2- and UPR-deficient strains in different media 91

Figure 4.4: SUR2 transcription in wild-type cells from minimal or peptone-supplemented SC medium 92

Figure 4.5: Expression similarities of SL enzymes and related genes in STRING. 94

Figure 4.6: Expression pattern of IPC biosynthetic enzymes during the cell cycle 96

Figure 4.7: GAP1 localisation in wild-type and SUR2-deficient cells in different environments. .99

Figure 4.8: RLM1 activity in wild-type and SUR2-deficient cells at normal and elevated growth temperatures 101

Figure 4.9: HAC1 activity of wild-type and SUR2-deficient cells in normal and ER stress environments 102

Figure 4.10: HAC1 and INO2/4 activity during inositol starvation after minimal SC medium. 104

Figure 4.11: HAC1 activity and the assumed SL ceramide levels in wild-type cells during inositol starvation without ceramide biosynthesis or during total AUR1 inhibition 106

Figure 4.12: INO2/4 activity of UPR-deficient cells during inositol starvation 108

Figure 4.13: RLM1 activity in UPR-deficient cells after inositol starvation or temperature elevation. 110

Figure 4.14: Median NBD-ceramide fluorescence in UPR-deficient strains after inositol depletion. 111

Figure 4.15: HAC1 activity of SUR2-deficient cells from minimal or peptone-supplemented SC medium during inositol starvation or after Aureobasidin A treatment. 113

Figure 4.16: INO2/4 activity of SUR2 deficient strains from different preculture conditions during inositol starvation. 114

Figure 4.17: The temporal order and the causal connection between the metabolic changes and signaling events after inositol depletion. 118

Figure 5.1: Growth rate of wild-type and UPR-deficient yeast strains in YPD medium with different tunicamycin concentrations. 121

Figure 5.2: The reporter fluorescence distribution of HAC1-activity and control reporter cells at different tunicamycin concentrations. 123

Figure 5.3: Quartile ratios of the HAC1-activity and control reporter fluorescence at different tunicamycin concentrations. 124

Figure 5.4: Cell wall staining of growing yeast cells with Concanavalin A (ConA). 126

Figure 5.5: HAC1-activity reporter fluorescence in pre- and post-treatment subpopulations at different tunicamycin concentrations. 127

Figure 5.6: HDEL-GFP fluorescence and forward scatter of pre- and post-treatment wild-type cells. 129

Figure 5.7: Experimental procedure to enrich and distinguish freshly born daughter cells. 130

Figure 5.8: Impact of ER stress on the HDEL-GFP fluorescence and forward scatter of mother and daughter cells after cytokinesis. 131

Figure 5.9: Distribution of HAC1-activity reporter fluorescence in WHI5-deficient cells born before and during the exposure to different tunicamycin concentrations. 133

Figure 5.10: Median and quartile ratio of the HAC1-activity reporter fluorescence of SUR2-deficient cells at different tunicamycin concentrations. 137

Figure 5.11: The effect of phytoceramide supplementation on the fluorescence of the HAC1-activity reporter at different tunicamycin concentrations. 139

Figure 5.12: The effect of phytoceramide supplementation on the growth rate of wild-type, ERSU-deficient and UPR-deficient strains at low tunicamycin concentrations.....141

Figure 5.13: The effect of phytoceramide supplementation on HDEL-GFP inheritance at low tunicamycin concentrations. 143

Figure 5.14: Minimal SC medium reverses the impact of low tunicamycin concentrations and phytoceramide on cell growth of wild-type and UPR-deficient strains. 145

Figure 5.15: Cell cycle progression and UPR activation of mother and daughter cells after weak ER disruption. 147

Figure 5.16: The life cycle of *Saccharomyces cerevisiae.* 148

Figure 5.17: The rate of change of the subpopulation ratio r'(t) depends on the subpopulation r(t) in asymmetric dividing cell populations. 153

Figure 5.18: Stable population of asymmetric dividing cells only depended on the relative subpopulation division rates. 154

Figure 5.19: The ratio of mother and daughter cells converges towards a stable value. 155

Figure 5.20: The evolution of cellular resources in mother and daughter cells over the cell cycle. 158

Figure 5.21: Average cellular resources in asymmetric dividing populations decreases with decreasing inheritance. 160

Figure 6.1: Two alternative ways to activate multiple transcription pathways and adapt to complex perturbation.....170

Figure 6.2: A divided life cycle and population heterogeneity. 171

List of tables

Table 2.1: PCR recipe for 20 or 50 µl PCRs....41

Table 2.2: Cycling program for Phusion™ PCRs:....42

Table 2.3: The recipe of the preincubation solution for the yeast transformation. 45

Table 2.4: The recipe of the PEG-LiAc solution for yeast transformation....46

Table 2.5: Cycling program for quantitative realtime PCR 49

Table 2.6: Name, purpose and sequence of the primers that were used during this study 54

Table 2.7: Name, backbone, insert, source and reference of the plasmids that were used during this study....56

Table 2.8: Name, genotype and source of the yeast strains that were used during this study. ..57

Table 3.1: Definitions, symbols, values and references for all parameters used in the TX-TL model 64

Table 3.2: The names, transcription factors and promoters of the TRP-containing plasmids.....70

Table 4.1: List of genes for enzymes in sphingolipid biosynthesis. 93

Table 4.2: Confirmed transcription factor binding sites (TFBS) in the promoter regions of SUR2, LAC1 and AUR1 97

Table 5.1: GO term enrichment of ACE2 and ASH1 targets. 135

Table 5.2: GO term enrichment in the unified list of ACE2 and ASH1 targets.....136

Table 5.3: Parameters and variables to calculate the absolute phase durations in both cell types 149

Table 5.4: Names, definitions and comments for the variables of the model that was used to analyse the growth of both subpopulations and the total population.....152

Table 5.5: Parameters and variables to calculate the average resource pool size in each subpopulation and the overall population in dependence of the inherited fraction. 159

Table A.1: Sequences of the different features of the coding DNA sequence of the dynamic reporter constructs 205

Table B.1: ORF and Name of all ACE2 targets 206

Table B.2: ORF and name of every ASH1 target....207

Table B.3: ORF and name of every heat-independent ASH1 target 208

List of abbreviations

ConA	Concanavalin A
DNA	Deoxyribonucleic acid
CWI	cell wall integrity
DTT	dithiothreitol
eq.	equation
ER	endoplasmic reticulum
ERAD	endoplasmic reticulum associated degradation
ERSU	endoplasmic reticulum surveillance
FP	fluorescent protein
GFP	green fluorescent protein
ICRE	inositol choline responsive element
ino	inositol
IPC	inositolphosphoryl ceramide
mRNA	messenger RNA
NBD	7-Nitrobenz-2-Oxa-1,3-Diazol-4-yl
ORF	open reading frame
PA	phosphatidic acid
PC	phosphatidylcholine
PE	phosphatidylethanolamine
PI	phosphatidylinositol
PL	phospholipid
RNA	ribonucleotide acid
SC	synthetic complete
S. cerevisiae	*Saccharomyces cerevisiae*
SL	sphingolipid
TF	transcription factor
TM	tunicamycin
TRP	transcriptional reporter protein
UPR	unfolded protein response
YPD	yeast peptone dextrose

Acknowledgment

First of all, I would like to thank my supervisors, Dr Karen Polizzi and Dr Guy-Bart Stan, for giving me a chance to be part of their labs and work on such a fascinating project. Even though I had worked on several research projects before I started my PhD, pursuing my own long-term research project was a completely new experience for me. I needed to learn several skills that I never knew I would need before I started, but thanks to your continued support, valuable advice and constructive criticism I was able to complete this PhD and will benefit from working with you for the rest of my life.

Secondly, I must give mention to both groups, the Stan-group and the Polizzi lab in general, and Rochelle Aw, Pan Wei and Kealan Exley in particular. Interacting with you guys, from early morning chatter with Rochelle to late night discussions with my two fellow PhD mates, made lab and office an enjoyable work environment and also proved to be a nutritious environment for my professional and personal development.

Moreover, I have to thank the whole Ellis lab and Dejana Jovicevic in particular. As you were the only other *S. cerevisiae* group in the centre, my experiments wouldn't have been possible without you willingness to share know-how and equipment with me.

Moreover, I also like to take this opportunity to thank my parents and step-parents, who motivated and enabled me to pursue my dream and work as a scientist.

As this is already the resubmission of my PhD thesis, I also want to express my deep gratitude towards my final examiners, Dr Tom Ellis and Dr Ulrike Eggers, for reading my first submission and allowing me to defend it during the viva. Discussing my research and my thesis with you during my viva helped me to gain a better understanding of the process that makes research into science. I am convinced that the constructive criticism you have had a big impact on this second version of my thesis, and I hope that my resubmission can meet the high standards that you and the other members of the scientific community have.

1 Introduction

1.1 Motivation

Adaptation to new conditions is an important ability of most living organisms that enables them to thrive in a constantly changing environment. It consists of two steps, detection and response, which are connected by a signal transduction cascade that can run through different layers of the cellular organisation.

The lowest layer is the activity of certain proteins, which directly respond to changes in the environment. Several key enzymes are regulated this way to rapidly adjust the metabolism to environmental fluctuations. Phosphofructokinase-1, for example, is activated by high AMP to ATP ratios or fructose 1,6-bisphosphate to accelerate glycolysis and meet the energy need of the organism [1,2]. More complex mechanisms, which divide detection and response among different proteins, expand the number of possible reactions during the adaptational response to a single stimulus. Prominent examples of this mechanism are protein kinases, e.g. protein kinase A (PKA), which phosphorylate and activate several target proteins in response to a single stimulus, e.g. cyclic AMP concentration for PKA [3]. In contrast to these rapid mechanisms that do not change the total amount of participating proteins, mechanisms that can change the absolute amount of affected components take more time and usually respond to slower and less transient environmental changes [4].

Some of these mechanisms change the stability or the translation rate of individual proteins [5,6], while others change the transcription rate for a set of genes to adjust multiple protein levels in response to a stimulus [7]. In particular, transcriptional regulation is very common for the adaptation to various environments as increased transcription can increase the abundance and activity of every possible protein [8], and the set of target genes can easily be adapted during evolution [9,10]. However, this powerful mechanism requires the coordination of three processes, i.e. detection, gene transcription and protein translation, and the components that mediate between them.

Even though some signaling pathways, e.g. regulation of sterol synthesis, use environment-sensitive transcription factors that detect the stimulus and induce the transcriptional change [11,12], many signaling pathways actually benefit from a separation of detection and response. They consist of multiple receptor proteins and several intermediate components to detect different stimuli and amplify the signal, e.g. regulation of cell wall integrity [13].

In addition to these advantages, burst-like transcription makes it difficult to adjust the strength of a transcriptional response to the initial stimulus [14], while the number and duration of the

intermediate biochemical reactions delay the final response, whose strength may then not correlate with the current stress level, and thus increase the probability of wasteful oscillations [15,16]. Due to these problems, even simple adaptation processes in prokaryotes require a complex machinery to enable a perfect response, e.g. chemotaxis [17].

At least two properties of eukaryotic organisms further complicate transcriptional adaptation, and it thus needs to be investigated separately. In contrast to the sigma factors of prokaryotes, eukaryotic transcription factors can only initiate a subset of the transcriptional changes that are required in a new environment [18,19]. Eukaryotes thus need to activate several transcription factors from different signaling pathways to perfectly adapt to a new environment [7].

Secondly, eukaryotic organisms are characterised by the existence of organelles [20]. These membrane-enclosed subcompartments might increase the efficiency of certain biochemical reactions but also separate the transcriptional adaptation process spatially: detection in a certain organelle, the cytoplasm or the extracellular space; gene transcription in the nucleus; protein translation in the cytoplasm; possibly protein secretion and lipid biosynthesis in the endoplasmic reticulum (ER) [21]. This spatial separation further delays the adaptational response and might limit the ability to determine the right strength or to avoid oscillations.

These properties are particularly problematic during changes such as perturbations of lipid metabolism, which not only affect a single process but have long-term consequences for multiple organelles and necessitate extensive transcriptional changes [22,23], or changes that indirectly involve certain organelles and only require the graded activity of a certain adaptation mechanism, e.g. heat stress and ER homeostasis [24].

Comprehensive research in different eukaryotic organisms has uncovered the molecular components and isolated function of various signaling pathways that respond to different environmental stimuli and maintain the homeostasis of different organelles, e.g. the unfolded protein response for the ER, protein kinase C signaling for cell wall integrity, OPI1 for lipid metabolism in *S. cerevisiae* or retrograde signaling for the mitochondria [13,25–27]. However, it is still unclear how the strength and the carriers of a transcriptional response are determined to provide the optimal adaptation to complex perturbations that either require the coordination of different signaling pathways or do not require the full response of a single signaling pathway [28–31].

In order to better understand how eukaryotic cells respond to such complex stimuli during an environmental change, this project therefore investigated how individual cells determine an adequate transcriptional response to deal with graded ER stress and how yeast cells activate

different essential signaling pathways in response to a perturbation that initially only disturbs lipid biosynthesis but ultimately affects the membrane of several organelles.

1.2 Scope of this study

The adaptation of eukaryotic cells to perturbations of ER homeostasis and lipid metabolism can be investigated in different organisms and different experimental set-ups. The unicellular organism *S. cerevisiae* offers several advantages over more complex organisms and was therefore used throughout this study. Most importantly, previous research has already identified different environmental changes such as chemical treatments or nutrient supply that can influence certain cellular processes, e.g. protein folding in the ER, cell wall integrity or lipid biosynthesis [32–34], and also revealed the signaling pathways that connect the initial stimulus to the transcriptional response, e.g. the unfolded protein response (UPR), the protein kinase C (PKC) pathway or the activation of INO2/4 [7,13,26,35,36] (see subchapter 1.3.4 - 1.3.6 for details).

However, the relatively short life cycle of *S. cerevisiae*, its rapid mRNA dynamics and its relatively large cell-to-cell differences make it necessary to investigate transcriptional adaptation on a single-cell level and with high temporal resolution [37–40]. Therefore, fluorescent techniques, which enable live observation and single-cell resolution, were primarily used in this work.

Several conditions such as protein overexpression, chemical treatment or genetic perturbation of ER-resident proteins can be used to perturb ER homeostasis and trigger adaptation [41–43] (see subchapter 1.3.3 for details), but only the addition of chemicals exposes all cells of the population to the same stress, is easily reproducible and does not remove a potential component of the adaptive response. In this project, it was thus investigated how individual yeast cells combine different adaptational mechanisms for ER homeostasis, e.g. the unfolded protein response (UPR) and ER inheritance [44,45], to respond adequately to graded levels of chemically induced ER stress, and a mathematical model was then applied to predict the population-wide consequences from single-cell behaviour.

In contrast to the well-studied direct perturbations of ER homeostasis, perturbations of lipid metabolism affect different organelles (e.g. ER and plasma membrane) and cellular processes (e.g. lipid biosynthesis and protein folding) in ways that are not completely understood [23,46] (see subchapter 1.3). Therefore, the investigation of adaptation to lipid metabolism perturbations first requires a sufficient knowledge of how they affect different cellular processes.

The removal of inositol from the growth medium, which was chosen as an exemplary perturbation for this work, depletes an important precursor of lipid metabolism and over time affects several

biosynthetic processes, e.g. phospholipid biosynthesis, sphingolipid biosynthesis and the synthesis of certain extracellular proteins [47–49] (see subchapter 1.3.1 and 1.3.2 for details). Ultimately, inositol depletion also perturbs the homeostasis of at least two subcellular compartments, i.e. the ER and the cell wall [50,51]. This connection between organelle perturbation and lipid metabolism is not perfectly understood, but sphingolipids, which are associated with various roles in cell physiology [52–55], might be crucial in this respect.

Previous research already identified the main components of the signaling pathways, i.e. UPR, INO2/4 or protein kinase C [45,56,57], that adjust lipid metabolism and maintain organelle homeostasis during inositol starvation and also studied the role of sphingolipid metabolism for processes such as apoptosis that are not directly connected to inositol starvation [58]. In this project the interconnection between sphingolipid metabolism and ER homeostasis, cell wall integrity or cell division [32] was hence explored, before the coordination of the participating signaling pathways during inositol starvation was investigated.

1.3. Background

1.3.1 Structure and function of the endoplasmic reticulum in *S. cerevisiae*

In *S. cerevisiae* and other eukaryotes, the endoplasmic reticulum (ER) consists of a single lipid bilayer and the enclosed lumen. It forms a large network that extends from the nucleus, where it blends with the nuclear membrane (i.e. perinuclear ER), to other cellular organelles and the plasma membrane (i.e. cortical ER). The contact sites with these other organelles, e.g. mitochondria or peroxisomes [59,60], are stabilised by dedicated protein complexes and may serve to exchange lipids or other molecules (see figure 1.1) [61]. A close interaction with the cytoskeleton supports its extended structure and also enables the active transport of vesicles to and from the ER [62].

The endoplasmic reticulum houses the synthesis of most proteins that reside in the membrane or lumen of cellular organelles and the extracellular space, is the main location of lipid metabolism and also serves as intracellular calcium storage [63–65]. Due to the first two functions, the ER is essential for the *de novo* synthesis of other cellular organelles, like peroxisomes or the Golgi apparatus [66,67], and itself cannot be generated *de novo.* Therefore, dedicated molecular mechanisms ensure its homeostasis in changing environments and its inheritance to both descendent cells after cytokinesis [25,44] (see subchapter 1.3.6).

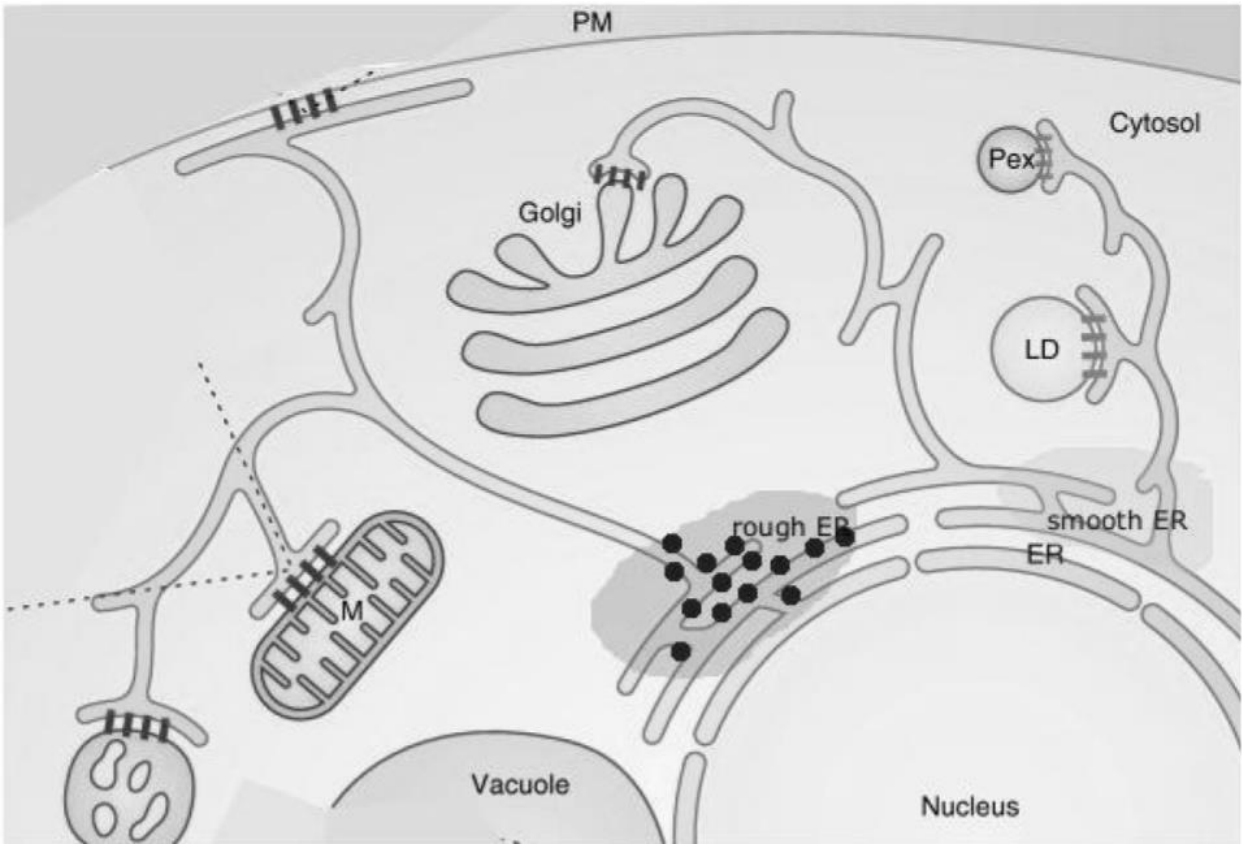

Figure 1.1: ER structure and organisation

Diagram of an eukaryotic cell with the ER, mitochondria (M), Golgi apparatus (Golgi), lipid droplets (LD), peroxisomes (Pex), ribosomes (black dots) and the plasma membrane (PM). Shaded areas indicate the different functional domains of the ER (rough ER, smooth ER) and bars indicate verified (dark grey) and proposed (light grey) membrane contact sites between the ER and other organelles (adapted from [61] copyright Elsevier).

Lipid metabolism on the ER membrane comprises the main synthesis steps of the four lipid classes in eukaryotic organisms, i.e. triacylglycerol (TAG), phospholipids (PL), sphingolipids (SL) and sterols (ergosterol in yeast), and their biophysical characteristics then determine their polymerisation and cellular function [68]: Hydrophobic TAGs are mainly used for energy storage. Amphiphilic PLs form sheets in aqueous environments and are the main component of cellular membranes [69]. Rigid Ergosterol and SL closely associate and form transiently stable subcompartments in lipid bilayers, which serve as an anchor point for protein complexes and confer mechanical stability to certain membrane structures [70].

The ER does not contain its own DNA or ribosomes, and secreted proteins are thus still translated in the cytoplasm and translocated into the ER only during or after their translation. The translocated proteins then refold in the ER lumen and are afterwards transported via the Golgi apparatus to their final destination [20].

1.3.2 Glycerolipid biosynthesis and the impact of inositol starvation

The synthesis of glycerolipids, i.e. phospholipids and storage lipids, starts at the ER membrane with the synthesis of phosphatidic acid (PA) from two acyl-CoA and glycerol-3-phosphate but diverges afterwards (see figure 1.2A).

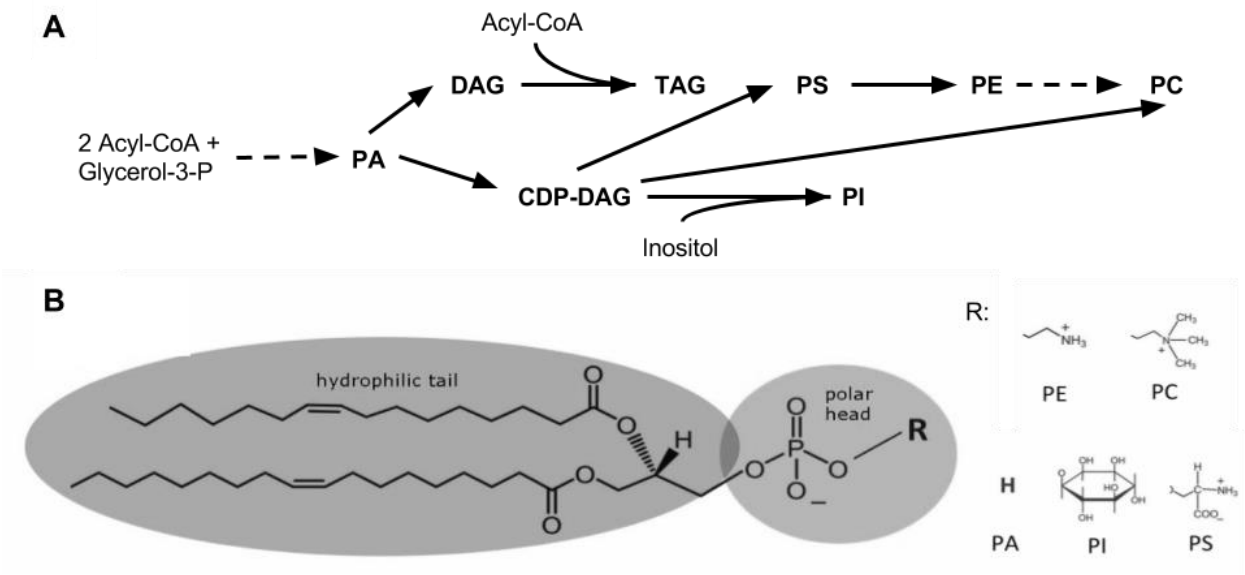

Figure 1.2: Synthesis and structure of phospholipids and storage lipid

A, the synthesis of phosphatidic acid (PA), CDP-diacylglycerol (CDP-DAG), phosphatidylinositol (PI), diacylglycerol (DAG), triacylglycerol (TAG) and phosphatidylserine (PS) from acyl-CoA and glycerol-3-phosphate happens entirely in the ER. However, the synthesis of PE and PC necessitate an intermediate step (PS to PE) that happens in the mitochondria. (solid lines, single step chemical reaction, dashed lines: multiple reactions, bold names: lipids). **B**, the amphipathic structure of phospholipids: hydrophobic tail (dark grey) and polar/ hydrophilic head group (grey), (R indicates the residues that define the phospholipid class) (images are taken from [26]).

On one hand, the exothermic phosphate group removal from the glycerol backbone generates diacylglycerol (DAG), which can accept an additional acyl-CoA to produce triacylglycerols (TAG) that are also known as storage lipids [71].

On the other hand, the activation of PA with cytidine triphosphate (CTP) produces cytidine diphosphate-DAG (CDP-DAG) and initiates phospholipid biosynthesis. CDP-DAG, a high-energy intermediate, can directly react with serine, choline or inositol to yield three of the four essential phospholipids, phosphatidylserine (PS), phosphatidylcholine (PC) or phosphatidylinositol (PI) [72]. PS can further be transferred to the mitochondria, where it is converted into the last major PL, i.e. phosphatidylethanolamine (PE) [73].

To generate PC in the absence of choline, PE can be transferred back to the ER and be converted into PC through the addition of three methyl groups [74]. The two other head group precursors, i.e. serine and inositol, are either taken up from the environment or *de novo* synthesised by the cell, i.e. inositol from glucose by INO1 [75] and serine from phospho-glycerate by SER1 and SER2 [76]. During inositol/choline starvation, lower inositol/choline levels decrease PI/PC production and trigger PA accumulation [48]. Higher substrate concentrations subsequently increase PS and DAG formation, but the metabolic changes also trigger a transcriptional response over the INO2-INO4-complex (see subchapter 1.3.4 for details) to increase inositol synthesis and PE-to-PC conversion for permanent adaptation [26].

1.3.2 Biosynthesis of sphingolipids and ergosterol

Sphingolipid biosynthesis (see figure 1.3) starts on the ER membrane with the condensation of palmitoyl-CoA and serine to the long chain base 3-ketosphinganine. Two enzymes, TSC10 and SUR2, then catalyse two oxidations that convert 3-ketosphingosine to dihydrosphingosine (DHS) and phytosphingosine (PHS). The attachment of a very long chain fatty acid (VLCFA) to the sphingosine backbone by ceramide synthases, i.e. LAC1 and LAG1, is the last essential step in the ER and yields phytoceramide (PHC) from PHS or dihydroceramide (DHC) from DHS [63,77]. However, an optional VLCFA hydroxylation by ER-resident SCS7 increases sphingolipid diversity [78,79]. In the Golgi apparatus, the attachment of phosphatidylinositol (PI) to the different ceramides by AUR1 yields inositol phosphorylceramide (IPC), the first mature sphingolipid [80]. The attachment of a mannose sugar and an additional PI then yields the two other mature sphingolipids, mannosyl-inositol phosphorylceramide (MIPC) and mannosyl-di-inositol phosphorylceramide ($M(IP)_2C$) [52].

Inositol starvation, which lowers PI levels, decelerates the synthesis of IPC and $M(IP)_2C$ and leads to the accumulation of ceramide and other upstream metabolites [48]. Genetic perturbations of SL metabolism, e.g. gene knock-outs, are lethal for most enzymes upstream of IPC synthesis. Notable exceptions are ceramide synthesis, which is catalysed by two redundant proteins, and the two oxidations by SUR2 and SCS7, which are not essential for IPC synthesis and only change SL hydroxylation pattern [78]. Alternatively, specific inhibitors can disturb different enzymatic steps in SL metabolism, e.g. myriocin for LCB1 [81], Fumonisin B1 for LAC1 and LAG1 [82], or Aureobasidin for AUR1 [83], and are highly toxic for yeast.

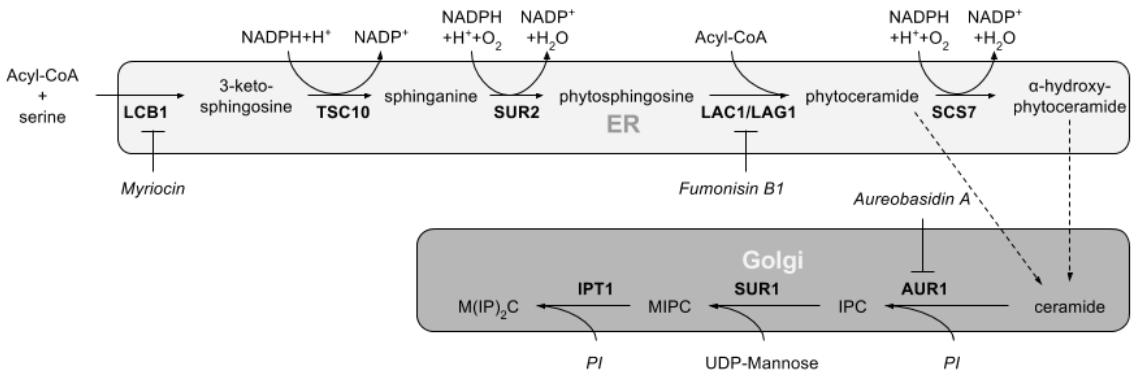

Figure 1.3: Sphingolipid biosynthesis in *Saccharomyces cerevisiae.*

The reactions (solid arrows), enzymes (in bold), substrates (normal font) and inhibitors (italic font) of sphingolipid biosynthesis are mainly localised in the membrane of the endoplasmic reticulum (ER) or the Golgi apparatus (Golgi). While the ER-resident reactions only consume NADPH and acyl-CoA, the synthesis of all three mature sphingolipids, i.e. $M(IP)_2C$, MIPC and IPC, requires phosphatidylinositol (PI) or UDP-Mannose and happens in the Golgi apparatus.

The regulation of SL biosynthesis, which is less understood than the regulation of phospholipid synthesis, happens mainly via the inhibition of the initial step, i.e. 3-ketosphingosine synthesis, by the ORM1 and ORM2 proteins [84] (see subchapter 1.3.4 for details). A molecular mechanism for the regulation of downstream steps has not been reported so far but might require ergosterol [85]. Due to their very long hydrophobic tail (see figure 1.4B), sphingolipids can support the mechanical stability of membranes, while the interaction with bulky cholesterol generates transiently stable subcompartments inside the lipid bilayer, i.e. lipid rafts, that are characterised by a greater depth than that of the surrounding phospholipid bilayer [70].

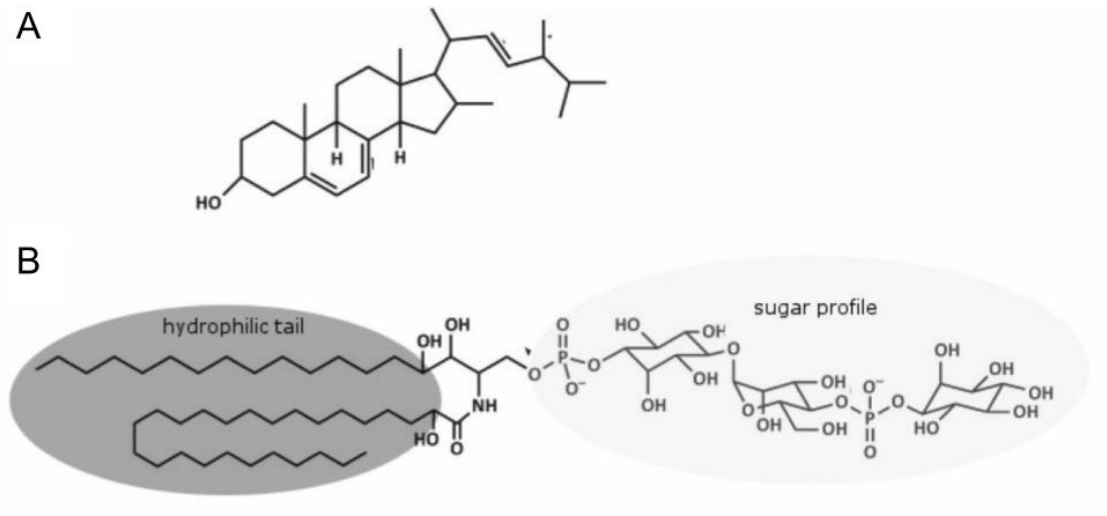

Figure 1.4: Structure of ergosterol (A) and sphingolipid (B).

A, The four interlinked carbon rings make ergosterol, the fungal cholesterol equivalent, a very rigid and hydrophobic lipid. **B**, The very long fatty acid makes up the long hydrophobic tail of sphingolipids (dark grey shading) and depending on the sugar profile (light grey shading) the head group can either serve as protective coat in fungi or a molecular recognition pattern in humans (adapted from [86]))

Ergosterol biosynthesis does not start from acyl-CoA but from squalene - a linear chain of 30 carbons that is synthesized from acetyl-CoA via the mevalonate pathway [87]. In the endoplasmic reticulum, multiple oxidation and cyclisation reactions, which are catalysed by the enzymes of the ERG cluster, convert this 30-carbon backbone into a complex 28-carbon structure, which is characterised by four ring structures [88,89] (see figure 1.4A). Two negative feedback loops, one in the mevalonate pathway via the stability of a rate-limiting enzymes [90] and one in the ergosterol pathway via the transcription of the ERG cluster genes [91], maintain a stable sterol production in a changing environment (see subchapter 1.3.4 for details). Ergosterol biosynthesis does not require inositol and inositol starvation has probably no direct impact on ergosterol metabolism.

1.3.3 Protein import, folding and quality control in the ER and the molecular basis of ER homeostasis disruption

While lipid biosynthesis resides in the ER membrane, the main function of its lumen is to provide an intermediate environment for the controlled and facilitated folding of peptide chains into functional three-dimensional structures, before they are transported to their less controllable final destinations [92]. Moreover, the oxidising environment and the presence of specialised chaperones in the ER can enable protein conformations that are not possible in the reducing environment of the cytoplasm or the nucleus [93]. Secreted or transmembrane proteins, which are still translated by cytoplasmic ribosomes, fist need to translocate into the ER lumen or the ER membrane via co- or post-translational mechanisms.

For co-translational translocation (see figure 1.5), most secretory proteins contain a short, hydrophobic signal sequence on their N-terminus. This sequence is recognised by the signal recognition particle (SRP) during translation and then triggers the relocalisation of the entire translation unit, i.e. ribosome, mRNA and the nascent peptide chain, to the translocon at the ER membrane [94]. The translocon is a protein complex that forms a tunnel in the hydrophobic lipid bilayer and enables the passage of unfolded peptide chains from the cytoplasm into the ER lumen [95]. The subsequent binding of chaperones, i.e. KAR2, to the nascent peptide chain inside the ER lumen provides a pulling force from ATP hydrolysis and regulates the directionality of the transport process, i.e. molecular ratchet [96]. With enough distance from the ATPase-activating function of the translocon, KAR2 ceases to hydrolyse freshly bound ATP, dissociates from the peptide chains and initiates their folding [97].

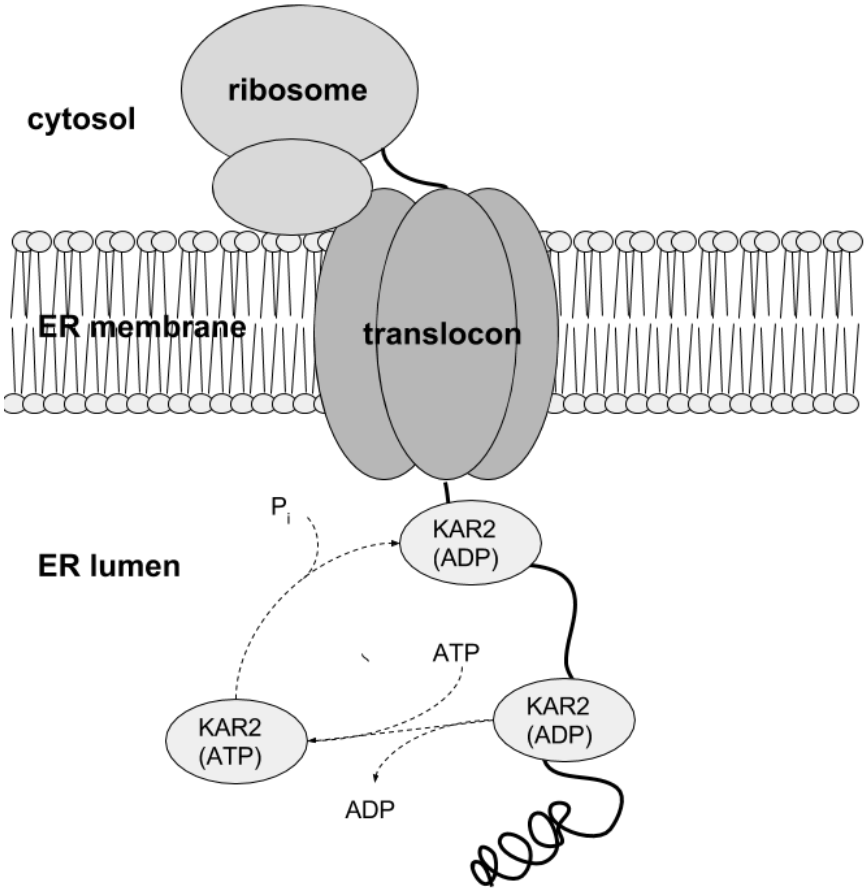

Figure 1.5: The co-translational translocation of proteins into ER Lumen via the molecular ratchet
Sequential binding of ADP-bound KAR2 to newly appearing parts of the peptide chains (solid black line) prevents back-diffusion and represents a molecular ratchet. With enough distance from the translocon, ADP exchange triggers KAR2 release and initiates the folding of peptide chain.

In addition to its role during translocation and like other HSP70 chaperones, KAR2 also promotes protein folding inside the ER lumen via the well-studied ATPase cycle (shown in figure 1.6) [98,99]: Exposed hydrophobic peptides of unfolded or misfolded proteins are recognised by J proteins that recruit ATP-bound KAR2 to their client proteins [100]. Subsequent ATP hydrolysis promotes the unfolding of the client protein and releases the J protein from the complex. The ADP-bound KAR2 is subsequently recognised by a nucleotide exchange factor (NEF), which catalyses the exchange of ADP for ATP on substrate-bound KAR2. After this exchange, ATP-bound KAR2 loses the affinity for unfolded peptides and releases its client protein. While free ATP-bound KAR2 can now participate in another folding cycle, the unfolded client protein either folds into its native state and is secreted from the endoplasmic reticulum or misfolds and performs another folding cycle. The over-expression of secreted proteins or misfolded substrate proteins

such as CPY* overloads this folding mechanism and leads to an accumulation of unfolded or misfolded proteins, which eventually perturbs the ER homeostasis [41].

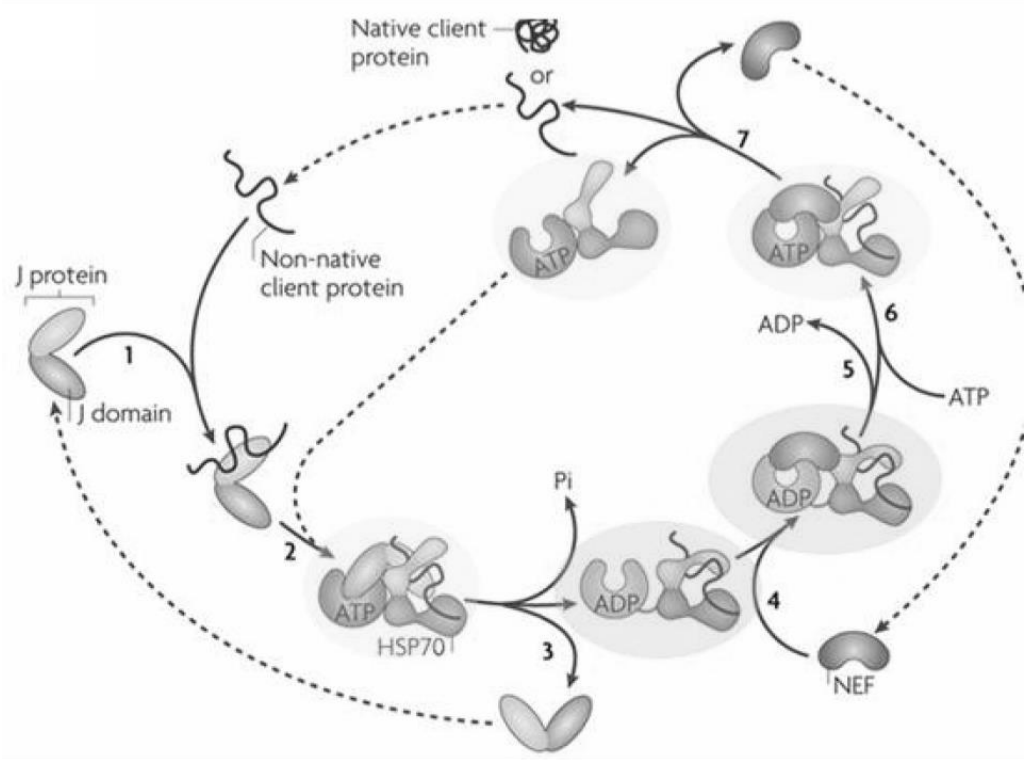

Figure 1.6: Protein folding cycle via HSP70 chaperones

1, J protein binds to the hydrophobic peptide of the non-native client protein. **2,** J protein recruits ATP-bound HSP70 chaperone. **3,** After the J protein triggers ATP hydrolysis, the ADP-bound chaperone unfolds the peptide and releases the J protein. **4, 5, 6,** the binding of a nucleotide exchange factor (NEF) promotes the exchange of ADP for ATP, and the ATP-bound chaperone releases the unfolded client protein, which now reinitiates its folding process. (Pi: inorganic phosphate) (Adapted from [101] copyright: Nature Publishing Group)

Due to the oxidative redox potential in the lumen of organelles or outside the cell, disulfide bonds, which are neither formed in the reducing environment of the cytoplasm nor the nucleus, are a common feature of proteins along the secretory pathway and in the extracellular space. Multiple cysteine residues on the surface of most secreted proteins increase the proportion of dysfunctional disulfide bond combinations and complicate the folding process [102]. Because the redox potential of functional disulfide bonds is usually lower than that of non-functional ones, *S. cerevisiae* and other eukaryotic organisms maintain an intermediate redox environment in the ER and use dedicated redox enzymes, i.e. PDI1 and ERO1 [103,104], to decrease the likelihood of the formation of non-functional low-energy disulfide bonds and to promote the formation of functional high-energy ones [93] (see figure 1.7).

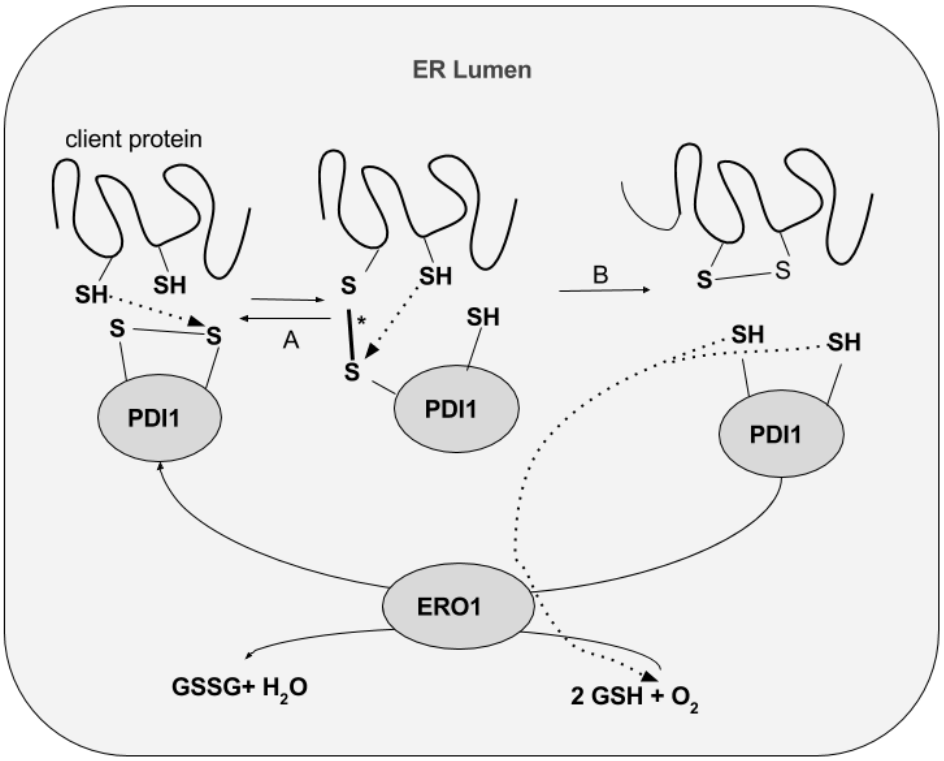

Figure 1.7: Disulfide bond formation and electron transfer during the folding of secreted proteins.
Unfolded proteins with reduced cysteine residues attract PDI1 and thereby trigger a series of inter- and intramolecular redox reaction that transfer electrons (dotted arrows) from the unfolded protein over PDI1 and ERO1 to molecular oxygen. The initial formation of the labile inter-molecular disulfide bond (bold and asterisk) is reversible (A) and only the irreversible formation of a functional disulfide bond (B) in the client protein enables the final dissociation of substrate and PDI1.

After PDI1 recruitment to misfolded or unfolded client proteins, PDI1's unstable disulfide bond reversibly oxidizes cysteine residues on the client protein through the formation of an intermolecular disulfide bond [105]. This fragile inter-molecular disulfide bond can be displaced by either (A) the initial disulfide bond of PDI1 or (B) a high-energy disulfide bond between two cysteines of the client protein. While the first route releases the original, reduced substrate protein, the second route leads to the formation of a functional disulfide bond in the client protein and reduces PDI1. The subsequent regeneration of PDI1 by ERO1 consumes reduced glutathione and oxygen to generate oxidised glutathione, water and oxidised PDI1 [106,107]. The regeneration of reduced glutathione consumes NADPH, which is generated in the cytoplasm.
Reducing agents such as dithiothreitol (DTT) and beta-mercaptoethanol reduce the chemical environment of the ER, prevent the formation of new disulfide bonds and dissolve existing bonds.

This immediately unfolds most proteins in the secretory pathway and rapidly perturbs ER homeostasis [50].

Many secreted proteins are glycoproteins and CNE1, the only calmodulin homologue in *Saccharomyces cerevisiae,* can via its lectin domain exclusively bind to their newly attached N-glycan chains. CNE1 thus performs a crucial function during ER quality control and protein degradation [108,109] (see figure 1.8).

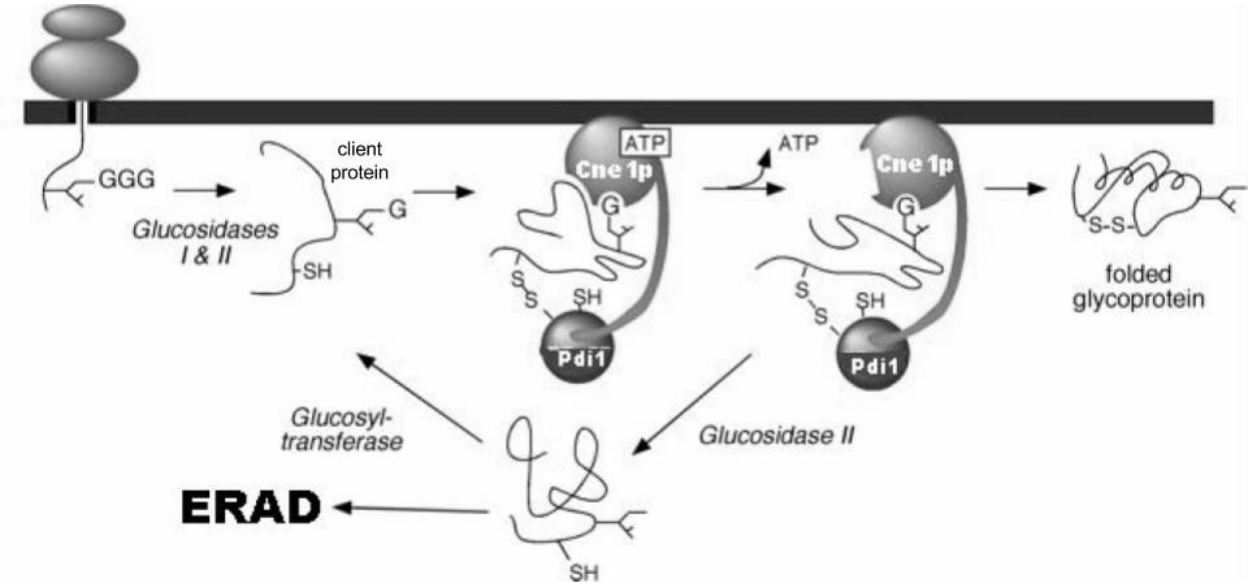

Figure 1.8: CNE1 functions as the pivotal co-chaperone for ER Quality control (ERQC).

The membrane-bound CNE1 (Cne1p) binds to unfolded glycosylated (G) client proteins. It subsequently functions as a co-chaperone and recruits PDI1 (Pdi1) or other chaperones to promote disulfide bridge formation and refolding. During client protein release, it recruits glucosidases to shorten the glycan chain. While folded proteins can now be transported to the Golgi, the shortened glycan chain either triggers re-glycosylation and CNE1 re-binding or ER-associated degradation of unfolded proteins. (http://biochemistry.utoronto.ca/person/david-b-williams/)

After CNE1 recognises unfolded, glycosylated client proteins via its lectin domain [110], it promotes their interaction with PDI1 or possibly other chaperones. Release from CNE1 triggers the removal of another glucose subunit from the glycan chain, and properly folded proteins are then transferred to the Golgi apparatus. However, misfolded proteins are either recognised by a glucosyltransferase that elongates the glycan chain and initiates another folding cycle or recognised by the lectin protein YOS9, which initiates ER-associated degradation (ERAD) [111]. As multiple unsuccessful folding cycles increase the likelihood of YOS9 binding, non-folding N-glycosylated proteins are usually degraded via ERAD [112] (see subchapter 1.3.6 for details).

Tunicamycin and 2'-deoxy-glucose inhibit the formation of N-glycan chains and prevent the interaction between secretory proteins and CNE1, which facilitates their folding. Depending on the rate of protein secretion, the accumulation of non-glycosylated and misfolded proteins can then perturb ER homeostasis [113,114].

While the presented mechanisms are usually sufficient to enable the correct processing of most secreted proteins, certain soluble proteins are further attached to a lipid anchor, which links them permanently to the membrane [115]. For extracellular proteins, this lipid anchor consists of glycosylphosphatidylinositol (GPI) and is necessary for their proper secretion from the ER [116]. The depletion of inositol also reduces GPI synthesis and thus perturbs the proper processing of this class of proteins, i.e. GPI-anchored proteins.

After their successful folding, secreted or transmembrane proteins are recognised by cargo receptors in the ER membrane and recruited into coat protein II (COPII) vesicles, which pinch off the ER and deliver cargo proteins to the Golgi apparatus [117]. In the Golgi, falsely secreted proteins can be transferred back via COPI vesicles, whereas the rest of the proteins are sorted and trafficked to their final destination [118,119].

If applied on mammalian cells, Brefeldin A inhibits the formation of COPI vesicles, prevents the physiological recycling of ER proteins, e.g. chaperones, and increases the likelihood of an accidental fusion between the Golgi apparatus and the endoplasmic reticulum. Once fused with the Golgi apparatus, the homeostasis of the ER is inevitably lost [120].

1.3.4 Regulation of lipid metabolism

As mentioned earlier, *Saccharomyces cerevisiae* possesses several mechanisms that control lipid metabolism and adjust it to the current environmental conditions.

For phospholipid metabolism, a transcriptional feedforward mechanism via phosphatidic acid (PA), the OPI1 protein and the heterodimeric transcription factor complex between INO2 and INO4 (INO2/4), ensures an efficient utilisation of PA as the substrate for TAG and PL synthesis [26,121] (see figure 1.9).

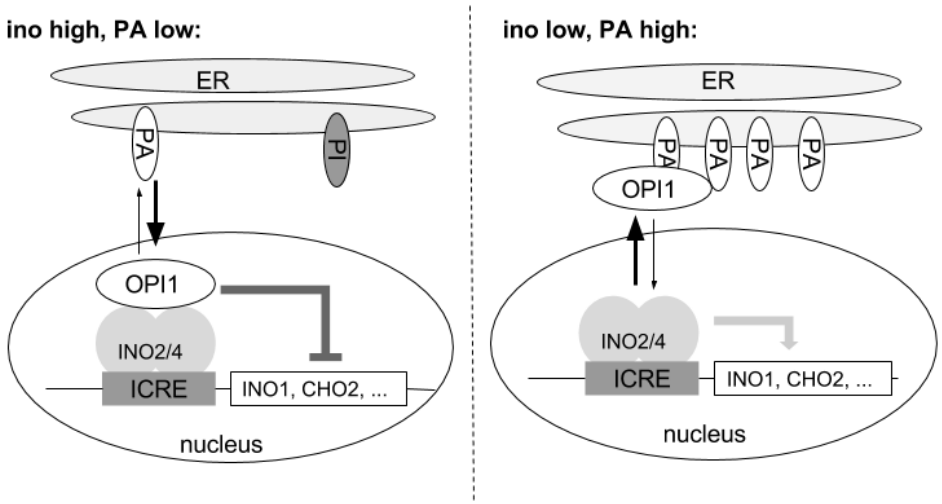

Figure 1.9: Transcriptional regulation of phospholipid synthesis via PA, INO2/4 and OPI1

Phosphatidic acid (PA) is continuously produced on the ER membrane during exponential growth. In the presence of head group precursors, e.g. inositol, it is immediately converted to phospholipids, e.g. phosphatidylinositol (PI), but accumulates in the ER in the absence of precursors. Depending on PA concentration, OPI1 either resides inside the nucleus, binds to INO2/4 and represses the transcription of ICRE-regulated genes, e.g. enzymes for phospholipid biosynthesis (left side, PA low), or it binds to PA on the ER membranes, releases INO2/4 inhibition and enables the transcription of ICRE-regulated genes (right side, PA high).

The promoters of many genes in PL metabolism such as the inositol synthase INO1 and the methyltransferases that convert PE to PC, i.e. OPI3 and CHO2, contain the inositol choline responsive element (ICRE) [122–124]. This ICRE-sequence is recognised by the INO2/4 complex, which can activate gene transcription but is repressed by OPI1 binding at low PA concentrations [125]. If inositol depletion, decreased DAG synthesis or faster PA synthesis increase the PA concentration in the ER [126,127], the accumulated PA and ER-resident SCS2 recruit OPI1 from the nucleoplasm to the ER membrane [128]. After this releases INO2/4 inhibition, the expression of ICRE-containing genes increases PA consumption and re-establishes lipid homeostasis via increased inositol production and faster PE to PC conversion. In addition to PA concentration, the cytoplasmic pH and glucose can also influence OPI1 localisation [129].

Ergosterol biosynthesis is in part controlled by flux-dependent ubiquitination and degradation of HMG2, i.e. the enzyme that catalysis the rate-limiting step of mevalonate biosynthesis: Fast mevalonate synthesis triggers ubiquitination and degradation of HMG2 through the ERAD pathway [90,130]. Furthermore, two transcription factors UPC2 and ECM22 regulate the transcription of genes for the conversion of squalene to ergosterol, i.e. the ERG cluster. In the presence of sterols, UPC2 and ECM22 reside in the cytoplasm, and the transcription of ERG

genes is repressed. Upon sterol depletion, they relocalise to the nucleus, where they depend on heme to induce the expression ERG genes [131–133].

Sphingolipid biosynthesis is mainly regulated by the conserved proteins ORM1 and ORM2 that can directly bind to LCB1 and inhibit its initial step, i.e. the formation of 3-ketosphingosine by LCB1/2 [134]. The activity of these inhibitors is controlled on the transcriptional level by the unfolded protein response during ER stress [135] and via phosphorylation of ORM2 by kinases of various signaling pathways, e.g. SLT2 [136,137].

1.3.5 Control of protein secretion and cell wall integrity by protein kinase C

Cell wall integrity is critical for cell growth, division and survival [138–140]. A crucial function of the endoplasmic reticulum is the secretion of enzymes and structural proteins that maintain it.

Under normal conditions, the production of these proteins is regulated by the life cycle of *S. cerevisiae*. Fresh-born daughter cells, for example, induce the expression of enzymes that separate them from the mother cells after cytokinesis [141]. After cell wall perturbation due to higher growth temperatures, environmental stress or changes in the lipid composition of the membrane, a dedicated response mechanism, i.e. the cell wall integrity (CWI) pathway, triggers transcriptional changes that promote cell wall synthesis [51,57] (see figure 1.10). This pathway is a prototypical kinase cascade with five transmembrane receptors (WSC1-3, MID1 and MTL1), which are interlinked with the cell wall and can recruit the GTP exchange factors, i.e. ROM1 and ROM2, upon cell wall perturbation. At the plasma membrane, ROM1 and ROM2 subsequently interact with RHO1 and exchange RHO1-bound GDP for GTP [142]. RHO1-GTP then activates protein kinase C 1 (PKC1) [143], and this activation triggers a phosphorylation cascade that culminates in SLT2 activation and the phosphorylation of the transcription factor RLM1 [13]. Activated RLM1 induces the transcription of cell wall proteins (CWP) and enzymes for chitin synthesis [144]. The elevated CWP expression and chitin production can restore cell wall integrity and counteract the initial stimulus but perturbs ER homeostasis [24].

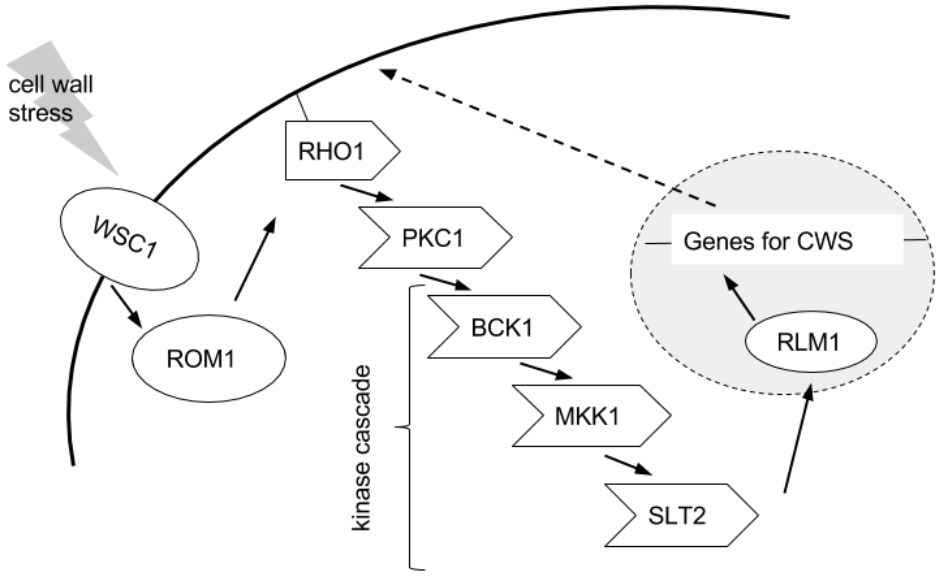

Figure 1.10: The kinase cascade that maintains cell wall integrity after perturbations

Environmental stress perturbs cell wall integrity and activates WSC1 or another sensor in the plasma membrane. This sensor then recruits the GTP exchange factor (GEF) ROM1 or ROM2, which catalyses the exchange of RHO1-bound GDP for GTP. The activated GTPase then activates PKC1 and triggers a kinase cascade that consists of BCK1, MKK1 and SLT2. SLT2 phosphorylates RLM1, and RLM1 induces the expression of genes for cell wall synthesis (CWS) such as cell wall proteins and chitin synthases that reestablish cell wall integrity.

Other secreted proteins, e.g. pheromones, receptors and intracompartmental enzymes, also necessitate ER homeostasis, but their expression is regulated by less understood mechanisms that have not yet been be investigated.

1.3.6 ER homeostasis regulation

S. cerevisiae coordinates different control mechanisms to maintain ER homeostasis and ensure the proper folding of secreted proteins, the activity of ER-resident enzymes and the continuous production of lipid intermediates (see figure 1.11). The unfolded protein response (UPR) and ER-associated degradation (ERAD) are relatively specific to the ER, while ER inheritance, ER surveillance (ERSU) and ER-phagy share many components with similar pathways for other cellular organelles [25,44,145–147].

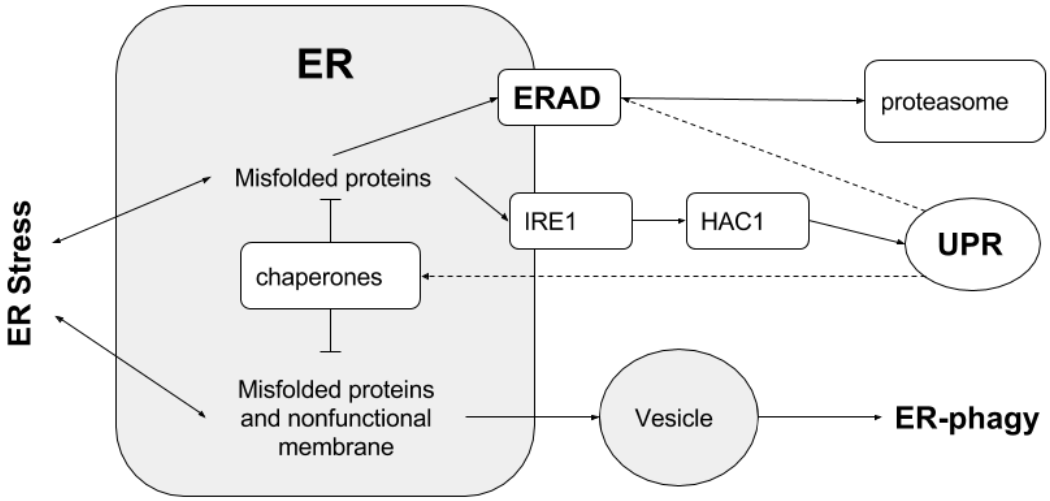

Figure 1.11: Important components of and interaction between the different ER homeostasis mechanisms
ER stress leads to the accumulation of misfolded proteins or nonfunctional membrane fragments. Misfolded proteins can either be transported out of the ER by the ERAD (ER associated degradation) machinery and degraded by the proteasome or activate IRE1 and induce the UPR response. UPR activation increases the expression of ERAD components and chaperones that help to clear misfolded proteins. Non-functional ER membrane fragment and proteins in the ER lumen can also split from the ER, and the vesicles can then be degraded via ER-phagy.

In *S. cerevisiae*, the UPR is the main mechanism that triggers a transcriptional response to ER stress and consists of at least three different components:
(I) IRE1, a transmembrane protein with four different domains, i.e. a lumenal domain that binds to unfolded proteins in the ER, a transmembrane domain plus a kinase and an RNAse domain in the cytoplasm.
(II) HAC1, a transcription factor that induces the expression of genes with an unfolded protein response element (UPRE) in their promoter sequence.
(III) ER-resident chaperones such as KAR2 and PDI1 that support ER homeostasis and are upregulated after UPR activation [45,50].

Under normal conditions and with low protein secretion, the ER chaperone KAR2 binds IRE1 and keeps it in an inactive state. Increased protein secretion or perturbed protein folding depletes KAR2 from IRE1 [148], and unfolded proteins subsequently bind to the lumenal IRE1 domain. This facilitates IRE1 dimerisation and increases the proximity of two inactive kinase domains [149]. Binding of additional unfolded proteins and transphosphorylation between the kinase domains of adjacent IRE1 proteins trigger IRE1 oligomerization and activate its RNAse domain [150]. The activated RNAse domain initiates the splicing and enables the translation of HAC1

mRNA [151]. This transcription factor subsequently passes to the nucleus and induces the expression of chaperones and other UPRE-containing genes that promote protein folding and re-establish ER homeostasis [152,153]. The IRE1 kinase and RNAse domain have also been associated with less understood, HAC1-independent mechanisms that might be more relevant for higher organisms (e.g. regulated IRE1-dependent decay of mRNAs (RIDD)) [154,155].

Independent of UPR activation, ERAD continuously removes terminally misfolded proteins from the ER, but some ERAD components, e.g. HRD1 and HRD3, are further upregulated after UPR induction to complement the increased chaperone activity [156]. Through its interaction with YOS9 and the binding of terminally trimmed glycan chains and unstructured peptides, HRD3 recruits proteins that failed ER quality control by CNE1 (see subchapter 1.3.3) [157,158] and facilitates their back-translocation to the cytoplasm via a transmembrane tunnel, which is formed by HRD1, HRD3 and DER1 [112,159]. On the cytoplasmic face of the ER membrane, the ubiquitin ligase HRD1 attaches ubiquitin to the emerging peptide chains and labels them for proteasomal degradation.

ER-phagy is an additional control mechanism that degrades entire ER fragments [160]. The name describes two different processes that either use macroautophagy to continuously recycle newly generated excess ER membrane during nitrogen starvation, or use microautophagy to degrade existing cortical ER fragments after ER stress exposure [161,162]. While the former requires the core autophagic machinery, stress-triggered microautophagy bypasses the autophagosome, delivers ER fragments directly to the vacuole and resembles other organelle-specific microautophagy processes, e.g. for the mitochondria or the peroxisome [147].

To ensure ER inheritance to mother and daughter cell after cell division, the perinuclear ER is transmitted to the bud alongside the nucleus during mitosis [44], while the motor protein MYO4 actively transports cortical ER along actin filaments into the emerging bud during the entire budded phase [163]. A ceramide-dependent diffusion barrier in the bud neck additionally prevents the passive diffusion of cortical ER components and contains possibly toxic protein aggregates in the mother cell [164,165]. Upon strong ER stress, CWI-dependent ER surveillance (ERSU) decelerates cortical ER transport, prevents the inheritance of protein aggregates and ensure the survival of both cells after cell division [146,166]

1.4 Aims of this work

Most of the presented knowledge on the molecular basis for ER function and homeostasis was gained as part of research that primarily focused on the long-term adaptation or the population-wide response to environmental stimuli [7,154,167,168]. As a consequence, very few genetic tools are available to measure the short-term transcriptional response and the metabolism in individual cells, which are possibly important during the adaptation to environments that require the coordination of different transcription factors or the graded response of a certain signaling pathway. To overcome this shortage and investigate the metabolic and transcriptional changes during transient responses after experimental perturbations of ER homeostasis or lipid metabolism in single cells and at the desired temporal resolution, this PhD project was divided into three parts with different complementary aims, outlined here as follows:

(1) Develop reporters for transcriptional changes during the adaptation of lipid metabolism and ER homeostasis under new conditions and find an appropriate tool to evaluate the direct impact of a new condition on the sphingolipid metabolism of single cells.
(2) Investigate the role of SL metabolism in cell physiology and determine the temporal and causal connection between transcriptional and metabolic changes after inositol depletion.
(3) Investigate the adaptation to qualitatively different levels of ER stress on a single-cell level and theoretically assess the consequences of this behaviour for the overall population and over evolutionary time scales.

These objectives were key steps to extract the underlying principles that govern the adaptation of *S. cerevisiae* in new environments that not only necessitate the full activation of a single signaling pathway but require a weighted combination of different signaling pathways. Each of the objectives is addressed in a separate chapter of this thesis after chapter 2, which describes the materials and the methods that were applied throughout the whole study.

Chapter 3 describes an innovative approach to design and build three different single-cell reporters that can dynamically track the essential transcriptional changes that are triggered by three different signaling pathways after changes of lipid metabolism or ER homeostasis. The feasibility of a fluorescent sphingolipid, i.e. NBD-C6-ceramide, as a reporter for lipid metabolism changes was also evaluated in this chapter.

In chapter 4, the transcriptional changes after inositol depletion or SUR2 knock-out were monitored with the developed reporter proteins and were then used to estimate the temporal and causal sequence that leads to the transcriptional adaptation after inositol depletion. The

fluorescent sphingolipid intermediate was further used to estimate the impact of both perturbations on sphingolipid biosynthesis.

In the first part of chapter 5, the reporter for UPR activity and established fluorescent markers were used to determine the contribution of asymmetric cell division to the adaptation of single cells in different levels of ER stress. The different experimental observations influenced the development of an abstract model to analyse the effect of asymmetric inheritance on population growth and resource demand in the second part of this chapter.

2 Materials and Methods

2.1 Chemicals

Unless otherwise specified, chemicals for growth media or buffer preparation were purchased from Sigma Aldrich. Antibiotics and chemicals were prepared as >/=500 x stock solutions in water (i.e. 100 mM Inositol and 1 M DTT), DMSO (i.e. 1 mg/ml tunicamycin, 1 mM Aureobasidin, 1 mg/ml myriocin, 5 mg/ml nocodazole, and 1 mg/ml rapamycin) or 50% ethanol (50 mg/ml Ampicillin) as required. Inositol, yeast nitrogen base without amino acids and yeast nitrogen base without amino acids or inositol were purchased from Formedium. NBD-C6-ceramide stain and the Tetramethylrhodamine Conjugate of Concanavalin A (TRITC-ConA) were purchased from Invitrogen (now ThermoFisher Scientific™).

2.2 Growth Media

Escherichia coli were cultured on Luria-Bertani (LB) agar or in liquid LB medium supplemented with antibiotics. For 1 L of liquid LB medium, 25 g of an LB premix (NaCl (2) : yeast extract (1) : tryptone (2)) premix were diluted in 1 L of double distilled water and autoclaved at 128 °C for 15 minutes. For 1 L of LB - Agar, 40 g of an LB Agar premix (NaCl (2) : yeast extract (1) : tryptone (2) : agar agar (3)) were diluted in 1 L of double distilled water and autoclaved at 128 °C for 15 minutes.

For *Saccharomyces cerevisiae* three different liquid growth media, i.e. minimal synthetic complete (SC), synthetic dropout (SD) and yeast peptone dextrose (YPD) medium, were prepared according to Gietz *et al.* [169] with the recipes stated below and autoclaved at 128 °C for 15 minutes. For culture plates, SD or YPD agar was prepared as the liquid medium but an additional 16 g of agar agar added before autoclaving.

YPD Media:

10 g/l Yeast extract
20 g/l Peptone
20 g/l Glucose
(16 g/l Agar agar for YPD agar)

SD Media:

6.7 g/l Yeast Nitrogen Base without amino acids (Sigma)
1.9 g/l Yeast Synthetic Drop-out Medium Supplements*
20 g/l Glucose
(16 g/l agar agar for SD agar)

* exact composition depends on the specific prototrophy of the cultured yeast strain, i.e. without histidine for histidine prototroph strains (reporter strains) or without uracil for uracil prototroph strains.

Minimal SC media with (or without) inositol:

6.7 g/l Yeast Nitrogen Base without amino acids (or inositol) (Formedium)
0.5 g/l amino acid mix (see below)
(20 g/l autoclaved glucose were added after autoclaving)

Amino Acid mix (36.2 g):

2.0 g Adenine hemisulfate
2.0 g Arginine HCl
2.0 g Histidine HCl
2.0 g Isoleucine
2.0 g Leucine*
2.0 g Lysine HCl
2.0 g Methionine
3.0 g Phenylalanine
2.0 g Serine
2.0 g Threonine
3.0 g Tryptophan
2.0 g Tyrosine
1.2 g Uracil
9.0 g Valine

2.3 Polymerase chain reaction (PCR)

All PCRs were performed in 20 µl or 50 µl, with the NEB Phusion™ polymerase enzyme, the respective primer sets (see table 2.6 at the end of this chapter for sequences) and according to the manufacturer's protocol:

20 or 50 µl of the reaction mix (see table 2.1) were prepared at room temperature and subsequently incubated in a thermocycler with primer and template specific modifications of the annealing temperature and the elongation time in the general PCR protocol (see table 2.2).

Table 2.1: PCR recipe for 20 or 50 µl PCRs

Stock	**Volume**	**Final concentration**
10 µM forward primer	1 (2.5) µl	0.5 µM
10 µM reverse primer	1 (2.5) µl	0.5 µM
Template DNA	2 (5-10) µl	Variable
5x Phusion™ HiFiBuffer	4 (10) µl	1x
10 mM dNTPs	0.4 (1) µl	200 µM
Phusion™ enzyme (2 units/µl)	0.2 (0.5) µl	0.02 units/µl
ddH_2O	Ad 20 (50) µl	-

Table 2.2: Cycling program for Phusion™ PCRs:

Step	Duration	Temperature
Initial denaturation	20 sec	98 °C
25-35 Cycles:		
- *Denaturation*	15 sec	98 °C
- *Annealing*	15 sec	55 - 65 °C
- *Elongation*	15-30 sec per kb template	72 °C
Final Elongation	5 min	72 °C

2.4 Molecular cloning

Restriction digests, dephosphorylations and ligations were carried out with NEB enzymes and according to the manufacturer's protocol. 20 or 50 µl of double digest reaction (see below) were prepared at room temperature and subsequently incubated at 37 °C for 1 hour.

20 (50) µl DNA digest reactions:

DNA (plasmid or PCR product)	1 µg
CutSmart Buffer™ 10x	2 (5) µl
First restriction enzyme	0.5 µl
Second restriction enzyme	0.5 µl
ddH_2O	ad 20 (50) µl

Calf Intestinal Phosphatase enzyme (1 µl) was subsequently added to the reaction to dephosphorylate the digested DNA fragments. Digested plasmid fragments were separated with gel electrophoresis and purified with the Wizard DNA purification kit™ (Promega). Digested PCR products do not need to be separated and were immediately used for DNA purification with the same kit.

For plasmid assembly, 10 µl of ligation reaction were prepared with the purified DNA fragments and the T4 DNA ligase:

Dephosphorylated Vector (20 - 50 ng/µl)	3 µl
DNA insert(s) (~15-25 ng/µl)	5 µl
T4 DNA ligase buffer 10x	1 µl
T4 DNA ligase	1 µl

After the reactions were incubated for 1 hour at room temperature, they were used for the transformation of chemically competent NEB® Turbo Competent Cells.

2.5 Plasmids

The different reporter plasmids (see table 2.7 at the end of this chapter for details) all shared the same general layout (depicted in figure 2.1) and were assembled with established molecular biological techniques (see subchapter 2.3 and 2.4), i.e. polymerase chain reaction (PCR), overlap extension PCR, restriction digest and DNA ligation. The individual parts of the transcriptional unit of each reporter construct, i.e. promoter, ubiquitin gene, superfolder GFP and CYC1 terminator sequence, were amplified by PCR from the matching template and with specific primers pairs (see table 2.6 at the end of this chapter). After gel purifying the amplicons with the Wizard DNA purification kit™ (Promega), the full transcriptional unit was created from the individual parts via overlap extension PCR. The full transcriptional unit was subsequently cloned into the pRS403 backbone vector or another reporter plasmid with the restriction enzymes SacI and ClaI or SacI and SpeI, respectively. The complete plasmid was transformed into *E.coli* cells, and its organisation and sequence were confirmed after Miniprep and with restriction digest or commercial Sanger DNA sequencing, respectively (the full sequence of the common, coding DNA sequence of all reporter plasmids, i.e. UBI4, linker and yeast codon-optimised superfolder GFP, can be found in appendix A).

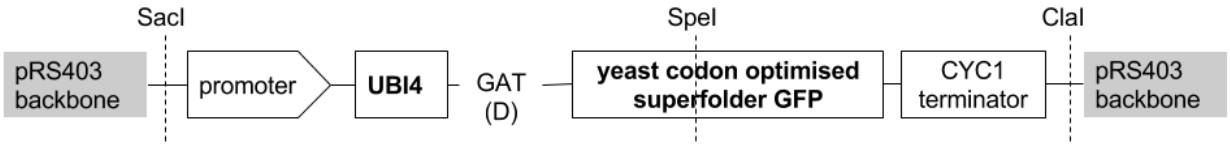

Figure 2.1: General layout for the reporter plasmids

The transcription factor specific promoter, the endogenous ubiquitin gene (UBI4), the linking aspartate codon (GAT (D)), the yeast codon optimised sequence for GFP and the endogenous CYC1 terminator were integrated into the pRS403 backbone that contains the HIS3 gene for yeast selection, and an OriC and AMP resistance cassette for the amplification in *Escherichia coli.* (dashed lines indicate the cutting sites of the different restriction enzymes, bold indicates the translated coding DNA sequence).

2.6 Yeast Strains

All yeast strains used in this study (listed in table 2.8 at the end of this chapter) were either part of the yeast knock-out collection [170] and purchased from GE Dharmacon™ (e.g. BY4741 and knock out mutants) or created via yeast LiAc/SS/PEG - transformation [171] (see subchapter 2.9). Linear DNA fragments for the transformation were either created by PCR amplification with integration specific primers (see table 2.6) and on the pMaM175 plasmid [172] or single restriction digests with NheI for reporter plasmids, i.e. pFJ1, 4, 8 and 25, and NdeI for pFJ17. Plasmid transformation was verified with selection medium and fluorescence measurements, and the insertion of PCR fragments was PCR-verified with the primers specified in table 2.6.

The genomic DNA template for PCR verification was isolated using the sodium hydroxide method [173]: Single yeast colonies were picked from an agar growth plate and resuspended in 20 µl 0.02M NaOH by vortexing. The suspension was incubated at 99 °C for 10 minutes and briefly centrifuged. 1.5 µl of the supernatant were subsequently used as a template for PCR (see subchapter 2.3).

2.7 *Escherichia coli* transformation

To prepare chemically competent *E. coli* cells, NEB® Turbo Competent Cells were exponentially grown in 300 ml of liquid LB medium until an OD of ~0.5. The culture was then cooled on ice for at least 10 minutes. Afterwards, the cooled cells were collected during a 10-minute centrifugation at 2880x g, and supernatant discarded. After the cell pellet was washed twice with ice-cold 0.1 M $CaCl_2$, it was resuspended in 15% glycerol and 0.1M $CaCl_2$. Resuspended cells were immediately dispensed into 50-100 µl aliquots and stored at -80 °C for further use.

For transformation, chemically competent *E. coli* cells from -80 °C, were thawed on ice, and 10 µl of ligation reaction were added to thawed cells. After a 30-minute incubation on ice, the cells were

transferred for 1 minute to 42 °C. After this heat shock, cells were kept on ice for additional 5 minutes. The cells were then spread on prewarmed LB + ampicillin (50 mg/ml) agar plates and incubated at 37 °C overnight.

2.8 Plasmid Miniprep

5 ml of liquid LB media with 50 mg/ml ampicillin were inoculated with a single transformed *E. coli* colony and incubated overnight at 37 °C. After the saturated overnight culture was collected at 6000x g for 1 minute, the plasmid was extracted with the Plasmid Miniprep Kit I peqGOLD (Peqlab) and DNA concentration was determined with NanoDrop1000™.

2.9 Yeast transformation

The LiAc/SS/PEG transformation method of Gietz *et al.* [169] was slightly modified to generate all non-commercial yeast strains that were used in this study:
Before transformation, saturated overnight cultures of the original strain in the respective media (e.g. YPD for BY4741 and knock-out mutants and SD-His for the reporter strains) were diluted 1:10 into fresh prewarmed YPD (500 µl per transformation). Cultures were grown for 6 hours to reach exponential phase and collected via centrifugation for 1 minute at 1500x g. Pellets were then washed once with 0.1 M LiAc. Cells were subsequently resuspended in 50 µl of transformation mix (see table 2.3) and incubated for 30 minutes at 30 °C.

Table 2.3: The recipe of the preincubation solution for the yeast transformation.

Stock	**Volume**	**Final concentration in 50 µl**
Yeast cells	var.	-
1 M LiAc	5 µl	0.1 M LiAc
10 mg/ml ssDNA	10 µl	2 mg/ml
1 µg DNA (digested plasmid or purified PCR)	var.	20 ng/µl
ddH_20	Add. 50 µl	-

After this incubation period, 450 µl of PEG-LiAc solution (see table 2.4) were added to the cells, and the cells then mixed carefully by pipetting.

Table 2.4: The recipe of the PEG-LiAc solution for yeast transformation

Stock	**Volume**	**Final concentration in 500 µl**
50 % PEG 3800	300 µl	30 %
1 M LiAc	50 µl	0.1M LiAc
DMSO	50 µl	10% DMSO
ddH_20	Add. 450 µl	-

The Yeast/LiAc-PEG mix was incubated for another 30 minutes at 30 °C, mixed, i.e. flicking the tube, and exposed to a 30 minute heat shock at 42 °C. After heat shock, cells were collected via centrifugation, i.e. for 2 minutes at 1000 x g, resuspended in 70 µl 5 mM $CaCl_2$ and plated on selective media plates, e.g. SD without histidine for the reporter strains.

2.10 Yeast cell preparation for treatments

If not noted differently for a specific experiment, cells for all treatments were prepared according to same general scheme:

On the day before the experiment, three different colonies of a strain were picked from an agar plate and incubated in appropriate medium for strains with a selective marker, e.g. SD medium without histidine for the reporter strains, or YPD medium for strains without a selective marker. On the next day the three cultures, i.e. biological replicates, were 100- to 200-fold diluted (~OD600 = 0.05 - 0.1) into minimal SC medium or YPD medium and incubated in a shaking incubator at 30 °C.

After 4.5 (YPD medium) to 6 (YPD medium and minimal SC medium) hours, the exponential cultures were treated according to the experimental procedure: synchronised with Nocodazole (optional); stained with TRITC-ConA (optional) and put into the prewarmed treatment medium. For inositol starvation, the growing cells were always collected with centrifugation (i.e. 600x g for 1 minute) and washed with inositol-free medium before they were resuspended in inositol-free or inositol-supplemented medium.

2.11 Growth rate determination

Growth rate determination was adopted from Toussaint *et al.* [174] and performed as follows:

Exponentially growing yeast cultures were 100-fold diluted into the treatment medium, and 2*200 µl of each culture were dispensed into two neighbouring wells of a clear 96-well, flat-bottom microtiter plate (Corning® CLS3370), i.e. 2 technical repeats. After the plate was covered with a Breathe-Easy® sealing membrane (DiversifiedBiotech), it was incubated at 30 °C with shaking and for at least 20 hours in a Synergy™ HT plate reader (BioTek®). Every 5 or 10 minutes, the optical density at 600 nm (OD600) of each well was measured.

Because the OD600 of each well with strongly diluted cells did not differ by more than 5% from the OD600 of a well with the same medium but without cells, the lowest OD600 during the first 10 measurements of each well was subtracted from all OD600 values of the same well to yield blanked OD600 values. Blanked OD600 values of each well were subsequently converted into log space. As this curve was almost linear during the exponential growth at low ODs (see subchapter 3.6), i.e. between 0.05 and 0.2 for minimal SC medium or between 0.1 and 0.3 for YPD medium, the slope of a fit to this linear part was used as the exponential growth rate.

The exponential growth rate of the two technical replicates was subsequently compared and their average used. For all discussed experiments, the mean and standard deviation of the average

growth rates of three different colonies, i.e. biological replicates, from one strain were used to determine the growth rate and standard variation of this strain in a certain media.

2.12 RNA extraction and cDNA Library Preparation

The RiboPure™ RNA Purification Kit for yeast (ThermoScientific™) was used according to the manufacturer's instructions to extract RNA from ~10^7 yeast cells, i.e. 2 ml of a culture with OD 0.5. The RNA concentration was determined via spectroscopy on the Nanodrop 1000™ (ThermoScientific™). 1 µg of the RNA was immediately used for a reverse transcriptase reaction. The reverse transcription was carried out with the Tetro™ cDNA Synthesis Kit (BioLine) and random hexamers according to the manufacturer's protocol.
The generated cDNA libraries were stored at -20 °C and the remaining RNA was stored at -80 °C for later use.

2.13 Quantitative Real Time PCR

Mastercycler Realplex (Eppendorf) was calibrated according to the manufacturer's manual: 10 µl of ddH_20 were dispensed into each well of a 96-well qPCR plate (Eppendorf CatNr: 0030132734) covered with sealing films (Eppendorf, CatNr: 0030132904), and this plate was then used to determine the background fluorescence for correction.
For each measurement and according to the manufacturer's instructions, a fresh target-specific non-template qPCR mix (see below) was prepared and kept on ice.

qPCR mix per technical replicate:

5 µl	2x SYBR green master mix (S9194 SIGMA)
0.5 µl	target-specific forward primer (see table 2.6)
0.5 µl	target-specific reverse primer (see table 2.6)
ad. 8 µl	ddH_2O

For each of the technical triplicates and each target gene, 8 µl of a qPCR mix were pipetted into a precooled 96-well plate and 2 µl of cDNA sample (or ddH_2O for no template control) were added to each of the gene-specific triplicates. The cDNA was subsequently amplified and detected in the Mastercycler Realplex and with a 2-step 40-cycle protocol (see table 2.5).

Table 2.5: Cycling program for quantitative realtime PCR

Step	Temperature	Duration
Initial melting and enzyme activation	95 °C	5 minutes
40 Cycles:		
- *Melting*	95 °C	15 seconds
- *Annealing + amplification*	63.4 °C	40 seconds
- *Fluorescence measurement*	-	-
Melting curve program	98 - 25 °C	15 minutes

The melting point, which was determined in the subsequent melting curve program (a linear 15 minute cooldown from 98 °C to 25 °C), was used to verify the purity of the gene-specific amplicons.

The built-in software was then used to determine the C_t, i.e. cycle of fluorescence threshold crossing, for each technical replicate and the average C_t value of the three replicates of each primer - template combination determined. Relative mRNA amounts in the different samples were determined with the delta delta C_t method as described by Livak *et al.* [175]:

mRNA (Gene A, sample 1) / mRNA (Gene A, sample 2) = 2^X

x = (C_t (Gene A, sample 1) - C_t (Ref. Gene, sample 1)) -
(C_t (Gene A, sample 2) - C_t (Ref. Gene, sample 2))

2.14 Yeast synchronisation with Nocodazole

Nocodazole was added at a concentration of 3 nM to exponentially growing yeast cells in YPD medium. After 2 hours, the cells were collected for 2 minutes at 3000 rpm in a MiniSpin® centrifuge (Eppendorf®), i.e. 600x g, and used for TRITC-ConA staining (see below).

2.15 TRITC-ConA staining

Exponentially growing cells were collected for 2 minutes at 3000 rpm in a MiniSpin® centrifuge (Eppendorf®), i.e. 600x g, washed in PBS and resuspended in 0.1 mg/ml TRITC-ConA in PBS. After 15 minutes incubation at room temperature, cells were collected, washed once in PBS and

resuspended in prewarmed treatment medium, i.e. YPD with DMSO or different tunicamycin concentrations.

2.16 Yeast NBD-C6-Ceramide *in vivo* staining

According to the supplier's manual, a highly concentrated 25-fold staining solution (125 µM NBD-ceramide + 125 µM BSA) in PBS was prepared from a 1 mM NBD-C6-ceramide in DMSO stock and a sterile 10 mg/ml BSA in PBS solution. After a 15-minute preincubation at room temperature, this concentrated staining solution was added to yeast cultures at a final concentration of 5 µM and incubated for at least 30 minutes or the rest of the experiment. Samples were then taken for flow cytometry or epifluorescence microscopy.

2.17 Flow Cytometry - data acquisition

Samples from NBD-C6-ceramide-stained cells or cells with the transcriptional reporter protein were diluted 1:100 (overnight cultures) or 1:10 (exponentially growing cultures) in 200 µl flow cytometry buffer, i.e. 6.9 g/l yeast nitrogen base in ddH_20, in 96-well flat-bottom plates. The samples from cells with the HDEL-GFP construct, i.e. pFJ17, were diluted 1:10 in 200 µl flow cytometry buffer with 10 mM DTT, due to their redox-sensitive GFP fluorophores [168].

The automatic multi sampler (AMS) from Cytek was then used to sequentially inject the samples in the BD Bioscience FACScan for flow cytometry measurements. GFP or NBD fluorescence was excited using a 488 nm Argon laser and photomultiplier tubes at a fluorophore-specific voltage, i.e. 540 mV for most reporter plasmids (pFJ1, 4 and 8) or 640 mV for the other plasmids and NBD-C6-Ceramide, used to record the fluorescence emission at 510 nm. TRITC-ConA fluorescence was excited at 510 nm and measured at 590 nm using a photomultiplier at 750 mv. Each sample was measured for only 17 seconds to minimise the time delay between different samples. A threshold for the forward scatter of each measurement event was subsequently applied to avoid saving and analysing fluorescence measurement of non-cell particles, e.g. salt crystals. The fluorescent measurements were subsequently analysed in FlowJo (see subchapter 2.18).

Two experiments with NBD stain (see chapter 3.9 and chapter 4.3) were performed on a different FACS machine e.g. Fortessa X30, and the median fluorescence values thus differ from the other experiments, but the data was still analysed with FlowJo (see subchapter 2.18).

2.18 Flow Cytometry - data analysis

After data acquisition, flow cytometry data was analysed using FlowJo™ (Version 10) (Tree Star Inc.). First and to exclude non-yeast contaminations, i.e. cell fragments, and cell clumps, yeast populations were gated according to their forward and sideward scatter (see figure 2.2):

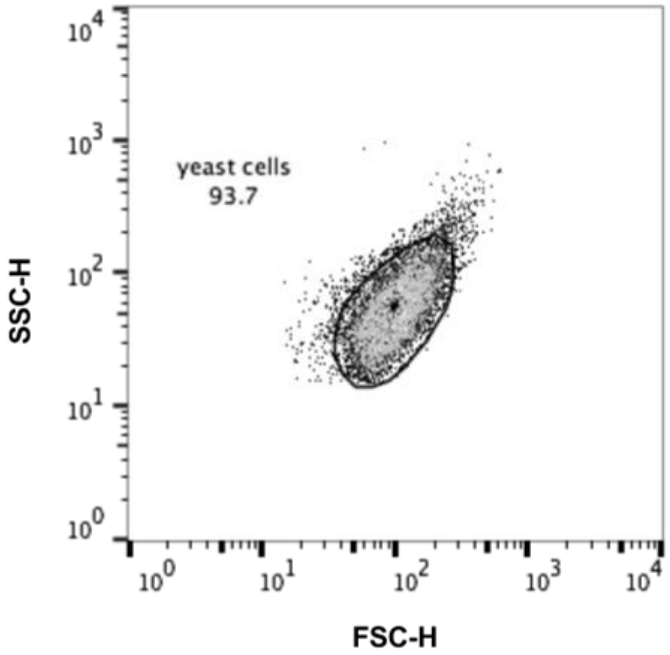

Figure 2.2: Visualization of the cell gating procedure

Forward (FSC-H) and sideward scatter (SSC-H) of each event that crosses the size threshold is visualised by a dot. The black line corresponds to the gating boundary for further analysed yeast cells and excluded cell clumps or cell fragments.

If necessary and possible, the intensity of the red TRITC fluorescence was used to separate TRITC-positive mother and TRITC-negative daughter cells in the samples (see figure 2.3). Their ratio was used to estimate the number of cell cycles since the staining, e.g. one daughter per mother cell corresponds to one doubling after staining and 3 daughters per mother corresponds to 2 doublings after staining.

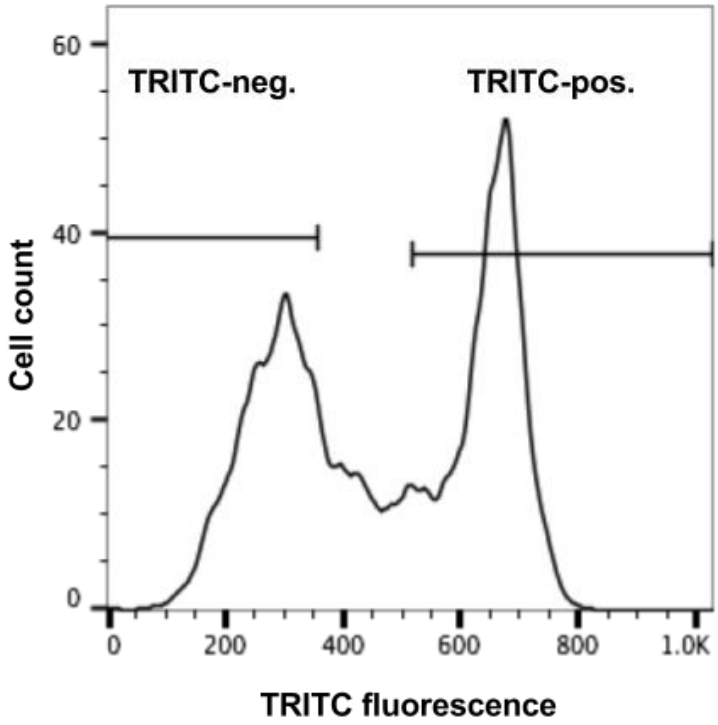

Figure 2.3: Visualization of gating procedure to separate TRITC-positive from negative cells

After gating the TRITC fluorescence of each fluorescence event is used to separate older, ConA stained and TRITC fluorescent cells (mothers) from younger, TRITC negative cells (daughters).

If not stated otherwise, all reporter measurements were done in biological triplicates. Because the distribution of green fluorescence resembled a log normal distribution with outliers (see subchapter 5.3 for example), the median fluorescence was chosen to represent the fluorescence level of the population or a subpopulation in the sample. Moreover, the data in the results section is sometimes presented on a logarithmic scale to account for the large differences in the fluorescence level between the different conditions.

2.19 Statistical tests

If not indicated otherwise, the star represents p-values smaller than 0.05 in a non-paired or paired student's t-test for different biological samples (different genotypes) or of the same biological replicate (different treatments), respectively. Tests were performed with Excel™ from Microsoft™.

2.20 Live cell fluorescent imaging

Live samples for fluorescent imaging were collected at 600x g for 2 minutes, washed in PBS and resuspended in 1/20 of the initial volume in PBS or SC minimal media for a single image or live

imaging, respectively. Cells were then placed on agar pads that were prepared as described by Rines *et al.* [176]:

In brief, 1.3 % molecular grade agarose was dissolved at 95 °C and in PBS or SC minimal medium. 80 µl of liquid agarose was then pipetted onto a preheated microscope slide and covered with a 1 mm-gap-casting slide. For polymerisation, “slide-agar-slide-sandwich” was incubated for at least 15 minutes at 4 °C. Agar pads were then prewarmed to 30 °C before the cells were added at the start of the actual imaging.

After the cells were added, 40*15 mm cover glass was placed on top of the agarose and the remaining gaps between the cover glass and slide closed with petroleum jelly. Phase contrast and epifluorescence imaging were then carried out and analysed on an inverted Nikon Ti-E microscope at 63x magnification and with the probe specific filters, i.e. with excitation and emission filters at 480 nm and 535 nm for the sfGFP and NBD ceramide or 532 nm and 590 nm for TRITC.

Table 2.6: Name, purpose and sequence of the primers that were used during this study

The primers were ordered from Sigma-Aldrich and either used during qPCR (qPCR) to construct the different reporter plasmid (pFJ1 - pFJ27) or to generate and verify the C-terminal GFP insertion (GAP1-GFP).

Name	Purpose	Sequence	Template
ACT1-1000 for	qPCR	CATGAAGTGTGATGTCGATGTCCGT	ACT1 cDNA
ACT1-1000 rev	qPCR	CGGCAATACCTGGGAACATGGTGG	ACT1 cDNA
HAC1 spliced for	qPCR	TGCGACGATATAGCGGGAAACAGT	HAC1s cDNA
HAC1 spliced rev	qPCR	TTCAAACCTGACTGCGCTTCTGGA	HAC1s cDNA
INO1 for	qPCR	CGGGGACTCAAAAGTGGCAATGGA	INO1 cDNA
INO1 rev	qPCR	CGATGATCAAGGGCGTAGCCAGT	INO1 cDNA
CHO1 for	qPCR	GGTGTGGCTCCGGCTGCAAT	PAH1 cDNA
CHO1 rev	qPCR	TCTCGCTAAGCCGCAAAGGACA	PAH1 cDNA
ERO1 for	qPCR	TCCGGTTTCCATGCCTCTATCGGT	ERO1 cDNA
ERO1 rev	qPCR	TCCAGATTGGGCTCCCATTTACCA	ERO1 cDNA
UPRE for	pFJ1	GGTTTTCCCAGTCACGACG	pPM47
UPRE-Ubi rev	pFJ1	AGTCTTGACGAAAATCTGCATTATTAATTTAGTGTGTGTATTTG	pPM47/p1434
UPRE-Ubi for	pFJ1	CAAATACACACACTAAATTAATAATGCAGATTTTCGTCAAGACT	pTW45
Ubi-sfGFP-rev:	pFJ1	AGCTCTTCACCCTTGGAAACCATGGTGGCGACAGG	pTW45
Ubi-sfGFP-fwd:	pFJ1	GTCGCCACCATGGTTTCCAAGGGTGAAGAGCTATT	pMaM175
sfGFP-Xbai-rev	all pFJ	AATAGTCTAGATTAGGATCCCTTATAAAGCTCGT	pMaM175
SacI-pIno1	pFJ4	CTAAGAGCTCGTCGGGGACTCAAAAGT	yeast gDNA
pIno1-Ubi rev:	pFJ4	AAAATCTGCATTGTTACTTCTTTTTCACTG	yeast gDNA
pIno1-Ubi fwd:	pFJ4	GAAGTAACAATGCAGATTTTCGTCAAGACT	pFJ1
SacI-RLM1 for *	pFJ8	ATAAGAGCTCGGGAGCAAGATCAAGATGT	p1434
SacI-Rpl19A for	pFJ25	ATTAGAGCTCCACTTCAGGTAAACCGTCTTCA	yeast gDNA
Rpl19A-Ubi rev	pFJ25	GACGAAAATCTGCATTTTTGCTTTGGAGTTCTTAATCAAC	yeast gDNA
Rpl19A-Ubi for	pFJ25	ATTAAGAACTCCAAAGCAAAAATGCAGATTTTCGTCAAGACT	pFJ1
SacI-Sur2	pFJ27	TTATGAGCTCTGCGGGAGTCCTTGTTGAAG	yeast gDNA
Sur2-Ubi rev	pFJ27	AGTCTTGACGAAAATCTGCATCGTATATTTTCTTTTCGTATACACCCT	yeast gDNA

Sur2-ubi for	pFJ27	AGGGTGTATACGAAAAGAAAATATACGATGCAGATTTTCGTCAAG ACT	pFJ1
GAP1-S3 for	GAP1-GFP	ATGGCCACAAAGCCAAGATGGTATAGAATCTGGAATTTCTGGTGT CGTACGCTGCAGGTCGAC	pMaM175
S2-GAP1 rev	GAP1-GFP	TGATTATCTAAAAAATAAAGTCTTTTTTTGTCGTTGTTCGATTCA ATC GATGAATTCGAGCTCG	pMaM175
GAP1-GFP check	GAP1-GFP	GCTGTCACATCTGCATTCGG	Yeast gDNA

Table 2.7: Name, backbone, insert, source and reference of the plasmids that were used during this study

All pFJ plasmids, except pFJ17, follow the general scheme that is depicted in figure 2.1, and were used to generate the strains that are described in table 2.8 via single-site genome integration (tcyc1: terminator of the CYC1 gene, pXYZ1: promoter of the gene XYZ1, HSRE: heat shock response element, UPRE: unfolded protein response element)

Name	Backbone	Insert	Source	Reference
pRS403	pRS403	-	Addgene	[177]
pPM48	pRS416	UPRE-mCherry-tyc1;pGDH3-eroGFP-tcyc1	Addgene	[168]
pMaM175	-	sfGFP URA3 sfGFP(C)	Knob lab	[172]
p1434	-	HSRE-LacZ-tcyc1	Levine lab	[178]
pTW45	-	UBI4-D-GFP	Ellis Lab	Master thesis of T. Weenike
pFJ1	pRS403	UPRE-UBI4-D-sfGFP-tcyc1	this study	-
pFJ4	pRS403	pINO1-UBI4-D-sfGFP-tcyc1	this study	-
pFJ8	pRS403	HSRE-UBI4-D-sfGFP-tcyc1	this study	-
pFJ17	pRS403	pTDH3-eroGFO-tcyc1	this study	-
pFJ25	pRS403	pRPL19A-UBI4-D-sfGFP-tcyc1	this study	-
pFJ27	pRS403	pSUR2-UBI4-D-sfGFP-tcyc1	this study	-

Table 2.8: Name, genotype and source of the yeast strains that were used during this study.

Strain	Genotype	Source
BY4741	*MAT a his3Δ1 leu2Δ0 met15Δ0 ura3Δ0*	GE Dharmacon
BY4741HAC1Δ	*MAT a hac1Δ::kanMX4 his3Δ1 leu2Δ0 met15Δ0 ura3Δ0*	GE Dharmacon
BY4741IRE1Δ	*MAT a ire1Δ::kanMX4 his3Δ1 leu2Δ0 met15Δ0 ura3Δ0*	GE Dharmacon
BY4741SUR2Δ	*MAT a sur2Δ::kanMX4 his3Δ1 leu2Δ0 met15Δ0 ura3Δ0*	GE Dharmacon
BY4741SLT2Δ	*MAT a slt2Δ::kanMX4 his3Δ1 leu2Δ0 met15Δ0 ura3Δ0*	GE Dharmacon
FJ4741.1	*BY4741 his3Δ1::pFJ1*	this study
FJ4741.4	*BY4741 his3Δ1::pFJ4*	this study
FJ4741.8	*BY4741 his3Δ1::pFJ8*	this study
FJ4741.17	*BY4741 his3Δ1::pFJ17*	this study
FJ4741.25	*BY4741 his3Δ1::pFJ25*	this study
FJ4741.27	*BY4741 his3Δ1::pFJ27*	this study
FJ4741.GAP1GFP	*BY4741 gap1:: gap1-sfGFP URA3*	this study
FJ4741HAC1Δ.4	*BY4741HAC1Δ his3Δ1::pFJ4*	this study
FJ4741HAC1Δ.8	*BY4741HAC1Δ his3Δ1::pFJ8*	this study
FJ4741IRE1Δ.4	*BY4741IRE1Δ his3Δ1::pFJ4*	this study
FJ4741IRE1Δ.8	*BY4741IRE1Δ his3Δ1::pFJ8*	this study
FJ4741SUR2Δ.1	*BY4741SUR2Δ his3Δ1::pFJ1*	this study
FJ4741SUR2Δ.4	*BY4741SUR2Δ his3Δ1::pFJ4*	this study
FJ4741SUR2Δ.8	*BY4741SUR2Δ his3Δ1::pFJ8*	this study
FJ4741SUR2Δ.GAP1GFP	*BY4741SUR2Δ gap1:: gap1-sfGFP URA3*	this study

BY4741WHI5Δ	*MAT a whi5Δ::kanMX4 his3Δ1 leu2Δ0 met15Δ0 ura3Δ0*	GE Dharmacon
FJ4741WHI5Δ.1	*BY4741WHI5Δ his3Δ1::pFJ1*	this study

Chapter 3: Improved methods for the detection of metabolic and transcriptional changes in single yeast cells

3.1 Introduction

Despite extensive research on the adaptation of *Saccharomyces cerevisiae* to ER stress and perturbations of lipid metabolism [46,179,180], some questions still remain open:

(1) How does inositol starvation or other perturbations of lipid metabolism disturb ER homeostasis and trigger UPR activation [46]?

(2) What interconnects metabolism and transcription in the multi-layered response of *Saccharomyces cerevisiae* to complex perturbations, e.g. inositol depletion [181]?

(3) Is ER adaptation in yeast as uniform and switch-like as the conventional UPR pathway suggests or it more gradual and can possibly differ between individual cells in the same population [150,168,179]?

There are at least two different explanations for this gap of knowledge: (A) there is no reason to expect any difference in the UPR response between different stresses and between different cells, or (B) the currently available tools are not suited to experimentally address these questions.

Firstly, a thorough review of the literature already highlights differences between the UPR activation after perturbations of protein folding via chemicals and perturbations of lipid homeostasis such as inositol starvation [182]:

- Genetic mutations that perturb ER folding, e.g. CRZ1 or HRD1 knock-out, increase the sensitivity to dithiothreitol (DTT) and tunicamycin (TM) treatment but not to inositol starvation [23,183,184].
- Tunicamycin co-treatment leads to inositol auxotrophy in certain genetic mutants [185].
- Mutations that perturb phospholipid biosynthesis can rescue the inositol auxotrophy of UPR-deficient cells [181].
- The IRE1 activation mechanism and UPR dynamics after inositol depletion differ from those after chemically induced ER stress [156,168,179].

Secondly, even though there are fewer direct indications for possible cell-to-cell differences in the transcriptional response during the adaptation to ER stress, a careful review of published results and a comparison to other challenging conditions suggest that cell-to-cell differences might exist during ER stress adaptation:

- Mother and daughter yeast cells differ in the transcription level of secreted enzymes, the protein composition of intracellular membranes and the homeostasis of other organelles [186–189]
- Cell-to-cell differences increase during cellular adaptation to other challenging conditions such as non-glucose carbohydrates [190–193].
- UPR activation varies during the cell cycle [194,195].
- UPR-deficient mother and daughter cells stop growing with a different ER redox potential after inositol depletion [168].

However, the experimental methods that were applied to study adaptation can roughly be classified into three categories with complementary characteristics:

- Growth experiments indicated ER-sensitive phenotypes in genome-wide screens and revealed the role of specific genes for the steady-state after adaptation [23,46,183,196];
- The investigation of batch cultures provided an insight into population-wide transcriptional dynamics after ER stress and revealed the signaling pathways that triggered the adaptation mechanism [156,197,198];
- *In vivo* studies of signaling pathways with long-lived reporter proteins delivered a single-cell resolution of ER homeostasis and UPR activation but responded much slower than the population-wide mRNA concentration measurements [36,168,199];

and none of these methods has been chosen to assess the response dynamics of single cells on a temporal resolution that would be sufficient to reveal transient cell-to-cell differences during adaptation or distinct transcriptional phases in the adaptation mechanism.

For lipid metabolism, the high material demand of conventional lipidomic techniques such as mass spectrometry or chromatography limits the investigation of metabolic processes to large sample sizes. They were thus primarily used to measure steady-state profiles of several genotypes or the adaptive changes in selected genotypes in big populations but not on a single-cell level [46,181,200]. There was also no attempt to measure the transcriptional and metabolic changes in the same experimental set-up and at a high temporal resolution, as it would be necessary to reveal the dynamic interaction between them.

Conventional tools were probably not able to measure at the required resolution and do not seem appropriate to answer the remaining questions on the adaptation to ER stress and perturbations of lipid metabolism. I thus explored novel single-cell methods to measure the changes of lipid

metabolism after inositol depletion and to rapidly determine the transcriptional changes during the adaptation to inositol starvation or ER stress in this chapter.

3.2 The effect of protein translation, maturation and degradation on reporter dynamics

The transcriptional changes after inositol depletion and ER stress are mainly triggered by the transcription factors of three process-specific signaling pathways, i.e. INO2/4 for phospholipid metabolism, HAC1 for ER homeostasis and RLM1 for cell wall integrity [23,51,201,202]. In contrast to biochemical methods to analyse mRNA abundance and pathway activation that can mainly determine the pathway activation after cell lysis [203–205], fluorescent proteins can be observed in living cells. Therefore, GFP-tagged regulatory proteins and the expression of transgenic fluorescent reporters are theoretically able to indicate the dynamics of these signaling pathways in individual living cells but have their own disadvantages.

Fluorescently labeled regulatory proteins, for example, have been used to observe kinetic processes previously [128], but the GFP tag might interfere with protein function. Moreover, their read-out usually depends on a subcellular relocalisation during the response and can only be assessed with imaging techniques but not flow cytometry [129,206].

Transcriptional reporter proteins (TRP), i.e. fluorescent proteins whose expression is controlled by a pathway-specific promoter sequence, on the other hand, do not interfere with the transcription factor function and can be measured with flow cytometry. However, their activity depends on mRNA transcription and protein expression, and the duration of these processes might hide transient transcriptional changes that are sometimes observed during the adaptation to environmental changes [207].

Recent publications suggested that active proteasomal degradation can reduce the response time of TRP and represents a possible way to overcome this problem [208,209], but reporter degradation might occupy the proteasome and burden cell metabolism [210]. The tuning of other participating processes, e.g. faster mRNA degradation, might equally optimise the TRP dynamics but possibly places less burden on cell metabolism.

To theoretically determine the main factors for TRP dynamics, differential equations, which summarise the underlying biochemical reactions, i.e. transcription (TX), translation (TL), folding, maturation and degradation, were used to quantify the impact of different changes, e.g. faster protein degradation or increased protein expression, on the response time and amplitude of the fluorescent signal (see figure 3.1).

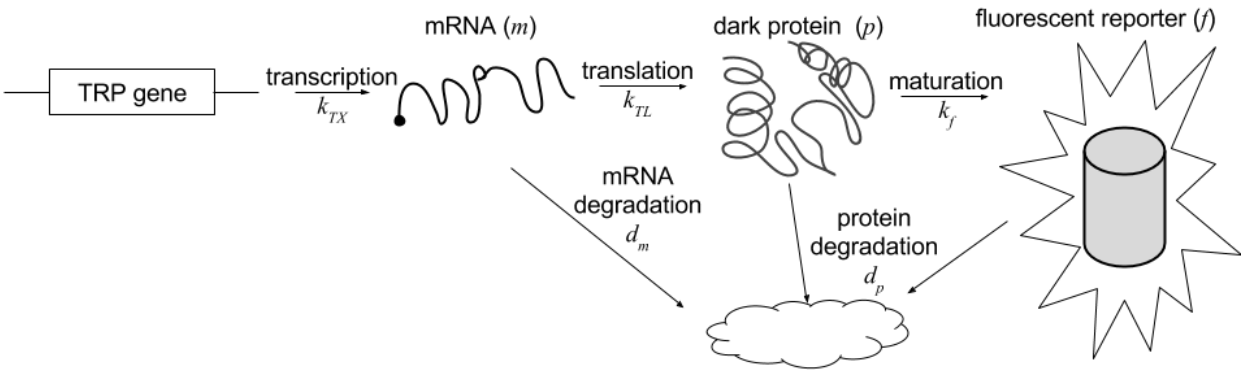

Figure 3.1: An extended TX-TL-model for the biochemical processes and entities that precede the detection of a fluorescent reporter protein.

The transcription and translation of the reporter gene results in a dark unfolded protein, which only fluoresces after maturation. Proteins and mRNAs are subject to degradation, while the gene is stably integrated into the host genome. (Italic symbols in brackets indicate the respective variable in the mathematical model and the italic symbols below the arrows represent the rate constants of the individual processes that were used in the mathematical description of the model (see equations 3.1 to 3.3).

In this model, transcriptional activation, whose molecular multi-step mechanism might differ between the signaling pathways, was simplified into a single signal-dependent switch from an OFF-state without transcription to an ON-state with full transcription to focus on post-transcriptional processes. Reporter expression after transcription activation was then simulated as the evolution from an unstable initial state with activated transcription but no protein or mRNA towards a new state with activated transcription, increasing protein and mRNA levels for a limited amount of time. Further, the production and degradation of mRNA (m), dark protein (p) and fluorescent protein (f) were assumed to follow the law of mass action with first order kinetics and their dynamics (m', p', f') summarised in the equations 3.1, 3.2 and 3.3:

$$m'(t) = \frac{d}{dt}m(t) = k_{TX} - d_m m(t) \quad \textbf{(3.1)}$$

$$p'(t) = \frac{d}{dt}p(t) = k_{TL}m(t) - (d_p + k_f)p(t) \quad \textbf{(3.2)}$$

$$f'(t) = \frac{d}{dt}f(t) = k_f p(t) - d_p p(t) \quad \textbf{(3.3)}$$

The necessary parameter values for mRNA degradation rate (d_m), translation rate (k_{TL}), fluorescence maturation (k_f), protein degradation (d_P), and activated mRNA transcription after gene activation (k_{TX}) were subsequently derived from the existing literature (summarised in table 3.1).

Due to the prior assumptions of the model and independent of the chosen parameter set, the simulations of all variables (m, p and f) always resulted in a monotonically increasing curve that approaches a stable steady-state, x_{ss}, with $m'(x_{ss})=p'(x_{ss})=f'(x_{ss})=0$ (see equations 3.4-3.9 and figure 3.2):

$$m'(x_{ss}) = 0 = k_{TX} - d_m m(x_{ss}) \Leftrightarrow m(x_{ss}) = \frac{k_{TX}}{d_m} \textbf{ (3.4)}$$

$$p'(x_{ss}) = 0 = k_{TL} m(t) - (d_p + k_f) p(t) \Leftrightarrow p(x_{ss}) = \frac{k_{Tl} m(x_{ss})}{d_m + k_f} \textbf{ (3.5)}$$

$$f'(x_{ss}) = 0 = k_f p(x_{ss}) - d_p p(x_{ss}) \Leftrightarrow f(x_{ss}) = \frac{k_f p(x_{SS})}{d_p} \textbf{ (3.6)}$$

$$\forall\, m(t) < m(x_{ss}) \Rightarrow m'(t) > 0 \textbf{ (3.7)}$$

$$\forall\, p(t=0) = 0 \; and \; m'(t) > 0 \Rightarrow p(t>0) < \frac{k_{Tl} m(t)}{d_p + k_f} \Rightarrow p'(t) > 0 \textbf{ (3.8)}$$

$$\forall\, f(t=0) = 0 \; and \; p'(t) > 0 \Rightarrow f(t>0) < \frac{k_f p(t)}{d_p} \Rightarrow f'(t) > 0 \textbf{ (3.9)}$$

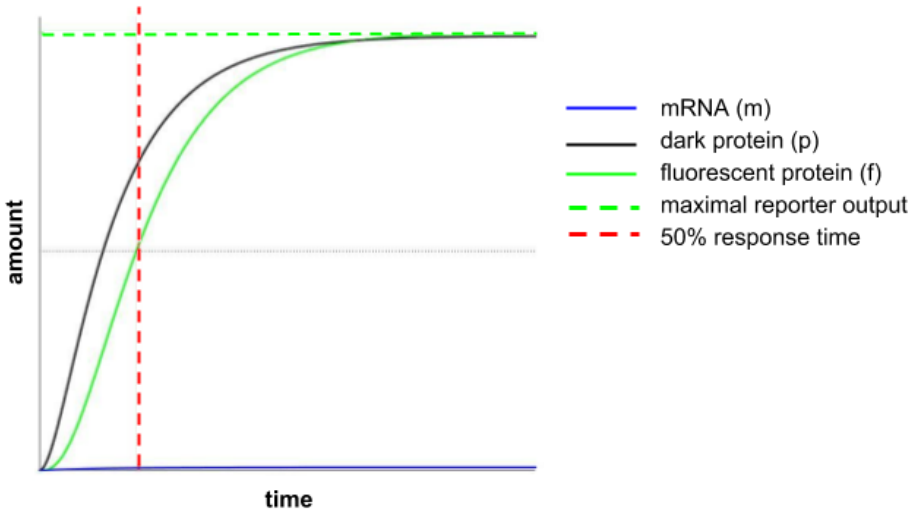

Figure 3.2: The simulated dynamics of mRNA, dark protein and fluorescent protein after activation

The curves represent the dynamics of mRNA (m), dark protein (p) and fluorescent protein (f) for every reporter whose kinetics are defined by formulas 3.1, 3.2 and 3.3. The absolute values of the final amounts (green dotted line) and the 50%-response time (vertical dotted line) depend on the actual choice of parameters.

Moreover, the simulations with any arbitrary parameters bigger than zero further indicated that the synthesis of the first half of the final fluorescent protein amount is much faster than the synthesis of the second half (see figure 3.2). This suggested that input signals shorter than the time needed to reach 50% of the steady-state fluorescence might miss the main fluorescence increase and that the gain from longer signals is relatively small.

This 50%-response time, which probably correlated with the optimal signal duration that is required for detection by the reporter, was subsequently used to evaluate the impact of protein and mRNA degradation on TRP dynamics.

The cellular amount of mRNA and proteins either declines via dilution during cell division or active degradation. MATLAB was thus used to calculate the 50%-response times for three reasonable mRNA decay rates and over a realistic range of reporter protein half-lives, i.e. from five minutes for actively degraded proteins to 120 minutes for the division time of *Saccharomyces cerevisiae* in synthetic complete medium [40,211](see figure 3.3, left).

The TX-TL model was also used to calculate the maximal reporter output, i.e. amount of fluorescent proteins at steady-state, $f(x_{ss})$, for the same range of mRNA degradation rates and protein half-lives (see figure 3.3, right).

Table 3.1: Definitions, symbols, values and references for all parameters used in the TX-TL model

The parameter values are chosen based on the published literature.

Definition	Symbol	Value	Reference
Transcription rate	k_{TX}	0.069 min^{-1}	1 - 10 degradable mRNAs per gene per cell [212]
mRNA decay	d_m	0.207, 0.069, 0.023 min^{-1}	Degradation rate of unstable, normal and stable mRNAs, with half-lives ($t_{1/2}$) 3.3, 10 or 30 minutes, respectively [211]
Translation rate	k_{TL}	40 min^{-1}	10 ribosomes per mRNA and 4 proteins per ribosome per minute [212]
Maturation rate	k_f	0.14 min^{-1}	Maturation time superfolder GFP (5 min) [213]
Protein decay	d_p	0.0059 - 0.14 min^{-1}	*In vivo* half-life of CLN3 (5 min) and doubling time of *S. cerevisiae* in SC (120 min) [193,214]

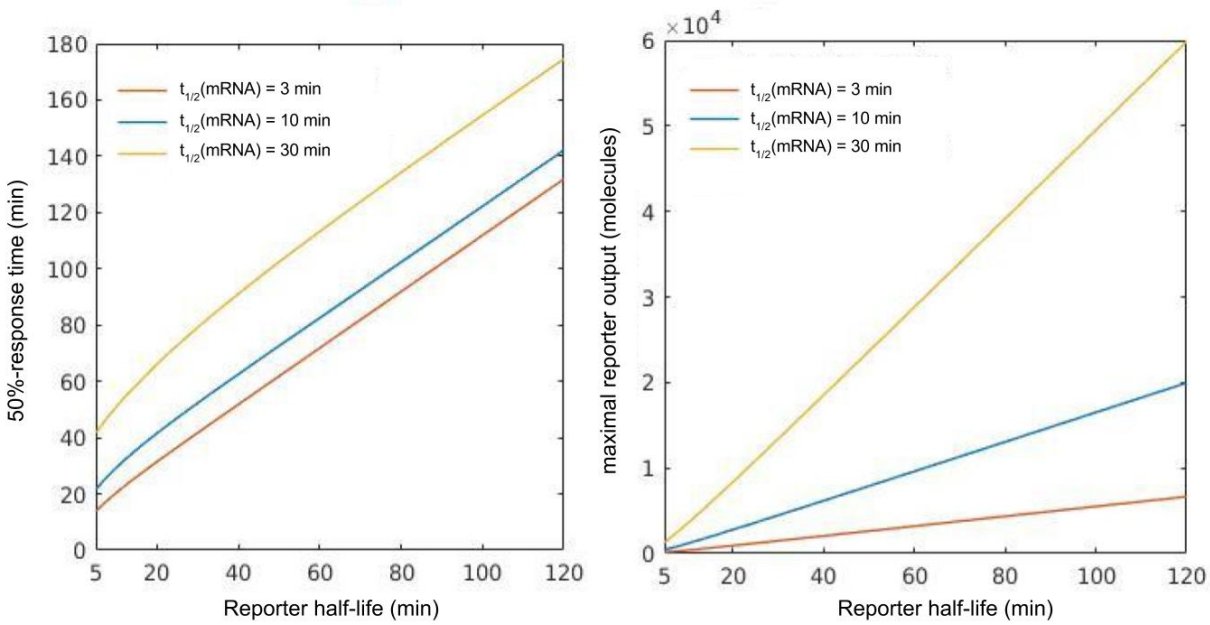

Figure 3.3: 50%-response time (left) and maximal reporter output (right) of a transcriptional reporter system over a range of realistic degradation times.

The 50%-response time and the maximal reporter output were derived by simulating a permanent input change from 0 to 1 with the formulas 3.1 to 3.3 and the parameters in table 3.1.

For all three mRNA half-lives, the calculated response time increased with protein half-life. The response time was lowest at the shortest protein half-life and amounted to 13, 21 or 41 minutes for the unstable, normal and stable mRNA, respectively. The response time at the longest protein half-life was highest and amounted to 132, 142 or 175 minutes depending on the mRNA stability. While the 50%-response time increased by up to 10-fold between the shortest and longest protein half-life (13 min vs. 132 min), it only increased by maximally 3-fold for the three different mRNA half-lives (13 min vs. 41 min).

This difference indicated that protein half-life is probably more important than mRNA degradation for the response time in the biologically relevant parameter space. The relatively big response time difference between the three exemplary mRNA half-lives at the shortest protein half-life (>200%), and the small relative difference at the longest protein half-life (<50%) further indicated that mRNA degradation influenced the response time more if it happens on a similar time scale as protein degradation.

Because protein degradation in yeast is generally slower than mRNA degradation [40,211], most actively degraded proteins are probably suited to indicate TF activation after several minutes, ~ 15 minutes, and detect transient transcriptional changes existing for this timespan.

Over the range of protein half-lives, the reporter output increased from 144, 434 and 1304 proteins for the three different mRNA stabilities to 6651, 20 000 and 60 000 proteins. This strong correlation between reporter output and protein or mRNA half-life over their entire range showed that both are equally important for reporter output. It further indicated that rapidly detected TRPs with fast protein and mRNA degradation have a very small fluorescence output and might not be detected at all.

A further optimisation of other post-transcriptional processes might help to increase reporter fluorescence and improve the output detection of actively degraded TRPs. The TX-TL model was subsequently used to evaluate the impact of fluorescence maturation speed and translation rate on maximal reporter output.

To this end, the reporter output for the previous range of protein half-lives and a reasonable range of maturation times, i.e. from 5 minutes for superfolder GFP to 40 minutes for mCherry, or translation rates, i.e. 20 to 100 ribosomes per mRNA per minute, was first calculated with MATLAB. The output amplification of each protein half-life maturation time (or translation rate) combination was then defined as the ratio between reporter output at this combination and that at the same protein half-life and the longest maturation time (or lowest translation rate) (see figure 3.4).

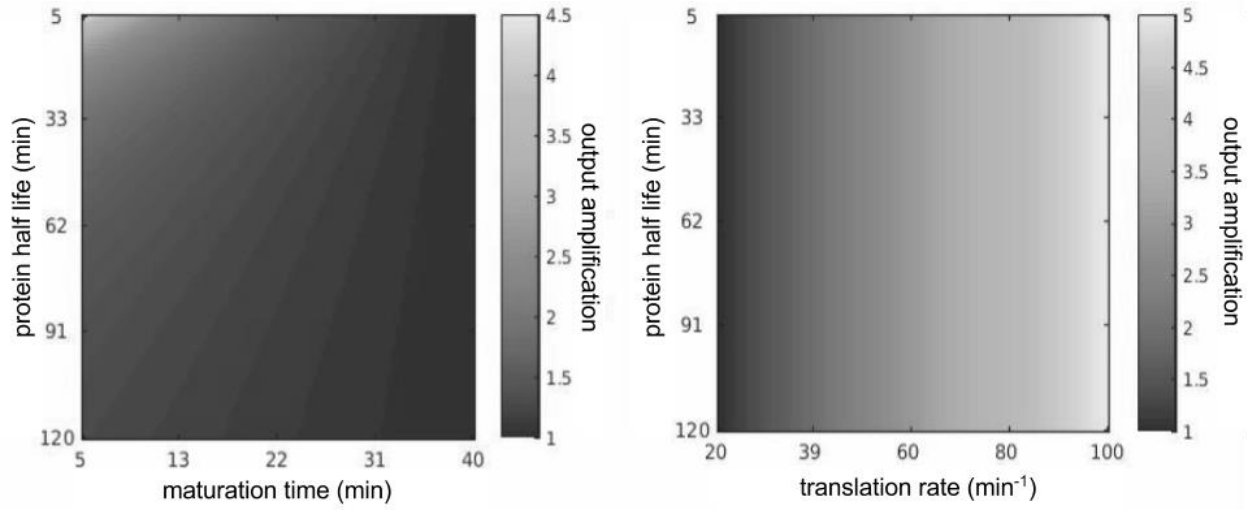

Figure 3.4: Relative impact of maturation time and translation rate on reporter fluorescence.

The relative amplitude of at a certain maturation time (left) or translation rate (right), was calculated by taking the steady-state amount of the fluorescence protein for a given maturation time (or translation rate) protein half-life combination and dividing it by the steady-state amount of the fluorescence protein for the same protein half-but the maximal maturation time (or the minimal translation rate).

Regarding the maturation time, the strongest output amplification, i.e. around 4.5, was calculated at the shortest maturation time and the shortest protein half-life, but the positive impact of the shortest maturation time was much smaller at longer protein half-lives, e.g. 1.5 for the longest protein half-life. For translation rates, the strongest output amplification was calculated at the fastest translation rate and independent of the protein half-life.

The model therefore suggested that fluorescent proteins with short maturation times are especially important to improve the fluorescence detection from fast-degrading TRPs, while increased translation efficiency equally benefits slow and fast degrading proteins.

The predicted response time improvement via active protein degradation was repeatedly observed in experiments [208,215], and I subsequently wanted to select specific modifications of the transcriptional unit, i.e. promoter, coding DNA sequence and terminator, that can increase translation rate, shorten maturation time and accelerate protein degradation to improve the dynamics of TRPs.

3.3 Implementation guidelines for a dynamic reporter protein in *Saccharomyces cerevisiae*

The minimal transcriptional unit consist of a promoter, a coding DNA sequence (CDS) and a terminator. As the promoter sequence primarily determines the transcription factor specificity and the effect of the terminator is less understood, I only considered CDS modifications as a way to accelerate protein decay, translation and maturation to optimise the response time and output of a reporter protein.

For accelerated protein decay, the protein decay rate can be determined by the speed of two different biological processes, (A) passive diffusion during cell division and (B) active degradation by the proteasome. While diffusion applies to all proteins in a dividing cell, degradation only applies to misfolded or polyubiquitinated proteins. Polyubiquitination via the ubiquitin pathway requires one of two possible features in the primary sequence: an internal PEST (proline, glutamate, serine and threonine)-rich sequence or an N-terminal amino acid that differs from methionine [216,217].

PEST-rich sequences are mainly responsible for the regulated degradation of signaling proteins such as G1 cyclins [216]. Their effect on protein half-life might thus depend on the cell cycle stage or their accessibility, which is defined by the three-dimensional structure of the protein.

N-terminal amino acids, on the other hand, are easily accessible and usually indicate non-native protein modifications if they differ from methionine. Specific residues can thus lead to half-lives

from 2 or 3 minutes for arginine or aspartate to several hours for proline or glycine of any protein [218,219]. Internal protein cleavage, which can be triggered by an N-terminal ubiquitin fusion, is a reliable way to generate a specific destabilizing residue and was chosen to yield N-terminal aspartate for the rapid TRP degradation in this project [220].

As the translation rate of each codon contributes to the translation rate of the complete protein, the codon choice in the CDS has a big impact on the protein translation rate. The translation rate of a codon correlates with the relative abundance of the respective tRNA and can be estimated from the overall codon usage in an organism [221]. An over-representation of slow and rare codons might additionally deplete the pool of loaded tRNAs and interfere with host cell physiology [222,223]. The substitution of rare codons by those with abundant tRNAs, i.e. codon optimisation, is thus particularly important for the expression of transgenes in host organisms with a different codon usage than that of their original host. For example, the rare arginine codons in the original GFP sequence from *Aequorea victoria* should be exchanged for the more abundant AGA via site-directed mutagenesis or *de-novo* DNA synthesis to optimise protein translation in *Saccharomyces cerevisiae* [224–227].

After protein translation, maturation of fluorescent proteins consists of two steps, protein folding and fluorophore maturation.

The folding rate of proteins mainly depends on their size and secondary structure, but single amino acid substitutions can overcome energetic traps and accelerate this process [228,229]. The structural analysis of protein folding has led to the development of rapidly folding isoform of fluorescent proteins that incorporate such point mutations, e.g. GFP mut3 and mCherry [230–234].

For fluorophore maturation, the type and rate of the chemical reaction that leads to fluorophore formation are specific for the spectral class of the fluorescent protein and range from rapid one-step oxidations for GFP and its derivatives to slow, oxygen-dependent two-step oxidations for red fluorescent proteins [235,236].

Together these criteria suggested that a yeast codon-optimised version of a fast-folding GFP isoform such as superfolder GFP should be the optimal basis for an actively degraded reporter protein [237]. Khmelinskii *et al.* [172] recently synthesized such a GFP sequence but did not use it for an actively degraded reporter protein.

These promoter-independent steps of CDS optimization should enable the construction of dynamic TRPs for every transcription factor (TF) that can activate a specific promoter sequence (see figure 3.5).

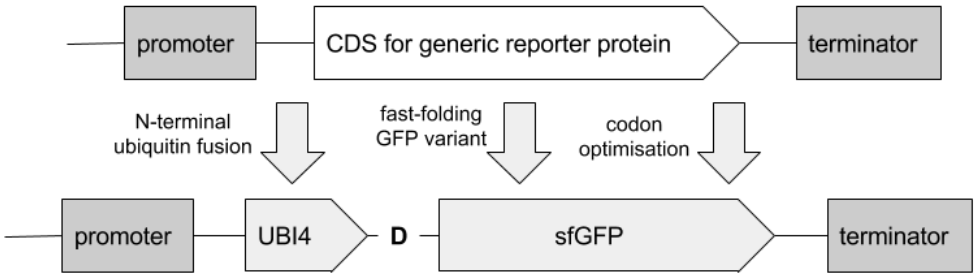

Figure 3.5: The three main modifications from conventional to dynamic transcriptional reporters.
Three synergistic CDS modifications, i.e. codon optimisation for efficient translation, AA changes to accelerate folding (i.e. sfGFP) and N-terminal aspartate (D) after constitutive cleavage of an ubiquitin fusion protein (UBI4), can be combined with every promoter sequence to yield dynamic transcriptional reporter proteins.

Pathway-specific TRPs for HAC1, RLM1 and INO2/4 activation were subsequently constructed with the optimised CDS and transcription factor-specific promoter sequences: four UPRE upstream of a minimal CYC1 promoter for HAC1 activity [50], the endogenous INO1 promoter for INO2/4 activity [122], and two RLM1-binding sites upstream of a minimal CYC1 promoter for RLM1 activity [238] (see table 3.2). To also evaluate the effect of changes in general cell physiology on reporter expression, the optimised CDS was also fused to the promoter of a ribosomal protein (RPL19A) that is not regulated by HAC1, INO2/4 or RLM1 [239]. For stable and reproducible transformation, these four transcriptional units were integrated into the pRS403 vector, which enables a targeted single-site integration and confers histidine prototrophy to histidine-auxotroph yeast strains such as BY4741 [177,240] (see materials and methods 2.9 and Table 3.2 for details). These plasmids were subsequently transformed into BY4741 and used to investigate the robustness, response time and metabolic burden of dynamic reporter proteins.

Table 3.2: The names, transcription factors and promoters of the TRP-containing plasmids.

The TF-specific promoter regions were based upon published reporter plasmids for HAC1, INO2/4 and RLM1 activity. The ribosomal promoter for pFJ25 was chosen as constitutive expressed gene that is not regulated by any of three different transcription factors. TRPs were inserted into the pRS403 backbone and verified by DNA sequencing [177].

Plasmid	**pFJ1**	**pFJ4**	**pFJ8**	**pFJ25**
Transcription factor	HAC1	INO2/4	RLM1	not HAC1, INO2/4 or RLM1
Promoter	4x UPRE [50]	pINO1 [122]	2x RLM1 binding site [238]	pRPL19A [239]

3.4 Robustness of dynamic reporter proteins

The fluorescence level of an ideal transcriptional reporter should only depend on promoter activity and be robust against possible changes in post-transcriptional processes that are triggered during an environmental change. Protein translation and proteasomal degradation represent two links between host cell physiology and reporter fluorescence that could increase the sensitivity of transcriptional reporter proteins (TRP) against post-transcriptional changes and lead to false positives during an experiment [210].

The control reporter, which combines a constitutively and strongly expressed ribosomal promoter (RPL19A) with the optimised CDS, relies on the same post-transcriptional processes but is not affected by the investigated transcription factors [239,241]. This reporter was thus used as a negative control to evaluate reporter sensitivity against possible changes of post-transcriptional processes that follow perturbations of ER homeostasis or lipid metabolism, which are studied during this project: inhibition of protein glycosylation by tunicamycin, inhibition of AUR1 and SL biosynthesis with Aureobasidin A, inositol starvation and redox changes in the ER from DTT.

To this end three different wild-type clones with the control reporter were cultured for 6 hours in minimal SC medium. To induce ER stress or lipid perturbations, each of these cultures was then split and transferred to minimal synthetic complete medium (SC), minimal SC medium without inositol or minimal SC medium with 2 mM DTT, 1 mg/ml tunicamycin or 2 µM Aureobasidin A. After 2 hours, the fluorescence of each culture was determined with flow cytometry and analysed with FlowJo (see figure 3.6 and materials and methods subchapter 2.17 and 2.18 for data acquisition and analysis).

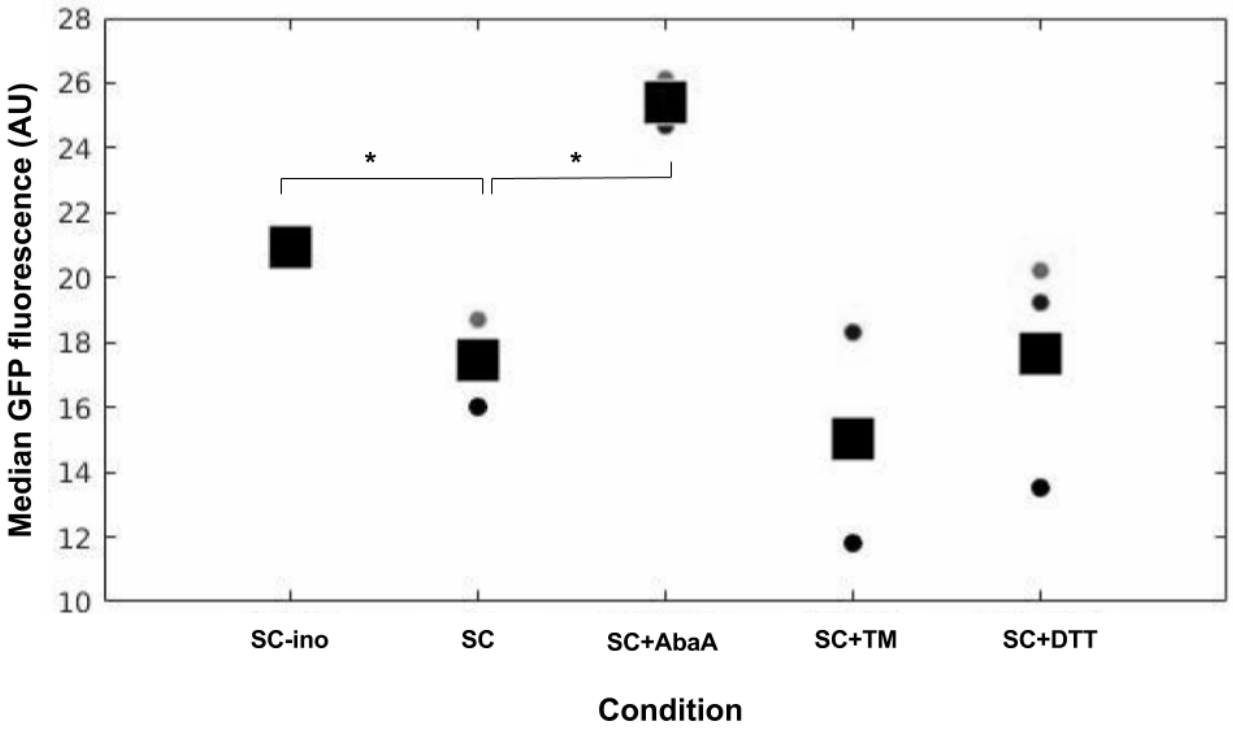

Figure 3.6: The median fluorescence of a constitutively expressed reporter protein in different clones and ER stress conditions.

Median GFP fluorescence levels of wild-type cells with a constitutively expressed, actively degraded reporter after 2 hours in minimal SC medium (SC), inositol-free minimal SC medium (SC-ino), minimal SC medium with 2 µM Aureobasidin A (SC+AbaA), minimal SC medium with 1 mg/ml tunicamycin (SC+TM) or minimal SC medium with 2 mM DTT (SC+DTT) was measured with flow cytometry and analysed in FlowJo (n=3, dots represent the individual biological replicates and squares the mean, asterisk indicates significant differences with $p<0.05$).

The median fluorescence of the control reporter varied by up to 50% in isogenic clones at the same environmental condition (i.e. SC + tunicamycin) and by up to 40% in the same clone under two different environmental conditions (i.e. SC vs Aureobasidin A treatment). Average GFP fluorescence of all clones varied less than 20% between the stressed and the unstressed conditions, and only inositol starvation and Aureobasidin A treatment significantly increased fluorescence in all biological replicates ($p<0.05$ student's t-test).

The different fluorescence level in different clones suggested that internal factors differed between isogenic populations and influenced the reporter expression even under unperturbed conditions. Moreover, the fluorescence increase during inositol starvation and AUR1 inhibition might indicate a common cellular response that influenced cellular reporter fluorescence, e.g. unbalanced growth [242].

Internal factors and the cellular response possibly act via post-translational mechanisms and also affect the fluorescence of pathway-specific reporter proteins. To minimise clone-specific effects during experiments, it is possible to compare reporter fluorescence after a stimulation to that of the same clone before the stimulation, i.e. paired t-test. To further exclude fluorescence changes that might be independent of transcription factor activity, I only considered relative fluorescence changes above 100%, i.e. two times the strongest non-transcriptional fluorescence change, as indicators for transcription factor activity changes in the following experiments.

3.5 Response time of the reporter constructs

The main objective of the design was to decrease the response time of the reporter constructs, i.e. the delay between gene activation and detectable fluorescence change. To evaluate response time, the TF activity of wild-type cells with a reporter construct was stimulated with an environmental change that is known to activate the respective TF, and the *in vivo* reporter fluorescence in single cells was measured at different timepoints after the stimulus. The fluorescence dynamics were then compared to direct measures of gene transcription and pathway activation in batch cultures.

For the HAC1 reporter construct with four UPREs in the promoter region, i.e. pFJ1, the reporter fluorescence was compared to an endogenous measure of IRE1 activation (i.e. HAC1 splicing) and target gene activation (i.e. ERO1 transcription) at different timepoints after ER stress exposure [50,156]. For ER stress induction and UPR activation, exponentially growing wild-type yeast cells (BY4741) for HAC1 splicing and ERO1 transcription and exponentially growing wild-type cells with the HAC1 reporter (FJ4741.1) for reporter fluorescence from synthetic complete medium were exposed to 2 mM DTT.

The abundance of spliced HAC1 and ERO1 mRNA in wild-type cells before and at three timepoints, i.e. 3, 15 and 90 minutes, after DTT exposure was determined with quantitative real-time PCR (qPCR) and normalised by the housekeeping gene ACT1 (see figure 3.7, left). The reporter fluorescence of wild-type cells with the HAC1-activity reporter (FJ4741.1) was measured at technically feasible times, i.e. 15, 45 and 90 minutes, after stress exposure and compared to the fluorescence of untreated control cells (see figure 3.7, right).

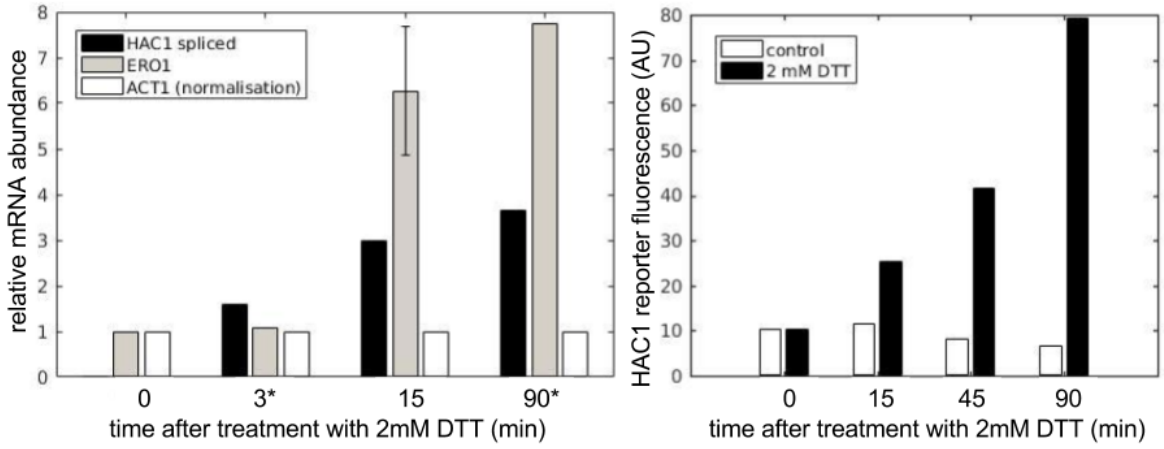

Figure 3.7: UPR activation and reporter fluorescence dynamics after DTT exposure.

(left) Exponentially growing wild-type cells were exposed to 2 mM DTT and spliced HAC1 and ERO1 mRNA levels were measured with qPCR before (0) and 3, 15 or 90 minutes after the treatment (n=2, *: n=1). The resulting C_t-values were normalised with ACT1 to calculate the relative mRNA abundance after DTT exposure according to the double delta C_t method (see materials and methods 2.13). (right) At time=0 exponentially growing wild-type cells with the HAC1-activity reporter (FJ4741.1) were diluted into DTT-treated (2 mM DTT) or untreated (control) minimal SC medium. At indicated timepoints, i.e. before (0), 15, 45 and 90 minutes after treatment, samples of both cultures were taken. The single-cell fluorescence was then measured with flow cytometry and analysed with FlowJo (n=1).

Compared to ACT1 and ERO1 mRNA levels, the spliced HAC1 mRNA was not detected before DTT addition. However, it could be detected 3 minutes after DTT addition and increased by almost 2-fold over the next 12 minutes. Relative ERO1 abundance stayed constant during the first 3 minutes but increased by 8-fold 15 minutes after DTT addition. After 90 minutes, the relative abundance of spliced HAC1 mRNA and ERO1 mRNA increased slightly from their 15-minute level.

The rapid accumulation of spliced HAC1 mRNA indicated IRE1 activation and suggested that DTT addition immediately disrupted ER homeostasis, caused protein unfolding and activated IRE1 [150]. The delayed increase in ERO1 mRNA indicated a time-shifted target gene transcription and suggested that several minutes were necessary for HAC1 translation and the activation of target genes by this transcription factor.

A previous genome-wide analysis, which showed the broad induction of UPR target genes after 15 minutes [156], further supported this notion and suggested that reporter expression from the HAC1-specific promoter should also be detectable from 15 minutes onwards.

In the analogous experiment, the HAC1 reporter fluorescence increased by 1.5, 2.5 and 6.5-fold in 15, 45 and 90 minutes after DTT exposure and decreased by 50% at later timepoints in untreated cells (see figure 3.7 right).

After 15 minutes, the relative change of reporter fluorescence in the DTT-treated culture already exceeded the previously set significance threshold and this strong increase suggested that HAC1 activation triggered TRP expression and that TRP fluorescence reacted in less than 15 minutes after gene activation. This response time was shorter than that of other UPR reporter constructs and should enable the observation of transcriptional differences between different cells or different genes that last more than 15 minutes [168]. At later timepoints, the increased reporter fluorescence and the stronger transcription of UPR target genes suggested that the chosen timeframe is too short to observe full adaptation [156].

To evaluate if the optimised CDS also enabled rapid TF activity measurements in other signaling pathways, the fluorescence dynamics of the RLM1-activity reporter were measured after heat shock, a stimulus that rapidly lowers cell wall integrity and activates RLM1 via PKC [243,244]. Therefore, wild-type cells with the RLM1-activity reporter (FJ4741.8) were grown in synthetic complete medium at 30 °C and then shifted to 39 °C. The median reporter fluorescence before and at 3 timepoints after the temperature change was determined with flow cytometry and analysed with FlowJo (see figure 3.8).

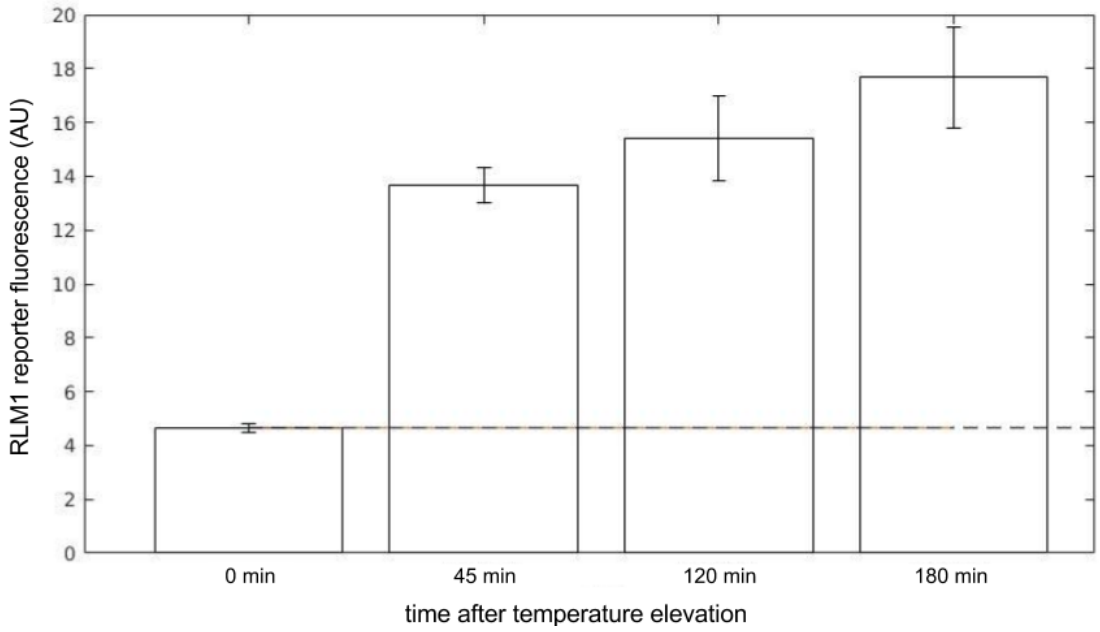

Figure 3.8: RLM1 reporter fluorescence in wild-type cells after temperature elevation.

Wild-type cells with the RLM1-activity reporter (FJ4741.8) were first cultured in SC medium at 30 °C and then changed to 39 °C. Before (0 min) and at the indicated timepoints after temperature elevation (45, 120 and 180 minutes), samples were taken. Cellular fluorescence was determined with flow cytometry and analysed with FlowJo (n=3, bars represent the mean and error bars indicate the standard deviation of the median fluorescence level).

After 45 minutes at 39 °C, the median fluorescence of the RLM1-activity reporter increased by more than 200% and remained at an elevated expression level for the rest of the experiment.
The main increase in reporter fluorescence already occurred in the first 45 minutes of the treatment and between the peak of RNA transcription (15 minutes) and the commonly used detection time of competing reporter proteins, i.e. beta-galactosidase, which were both determined in previous experiments [243,245].
The fluorescence of both new reporter constructs and other actively degraded reporter proteins increased faster than the fluorescence of stable reporter constructs with similar promoter sequences [168,208,245], and this suggested that the conducted CDS modifications were sufficient to reduce the response time independent of the promoter sequence.
Inositol starvation, a well-studied perturbation that triggered INO2/4 activation in wild-type cells [202], was used to evaluate the response time of the INO2/4-activity reporter. The median reporter fluorescence level of exponentially growing wild-type cells with the INO2/4-activity reporter (FJ4741.4) at different timepoints after the transfer from inositol-supplemented to inositol-free or inositol-supplemented medium was determined with flow cytometry and analysed with FlowJo (see figure 3.9 and materials and methods 2.10 for treatment).

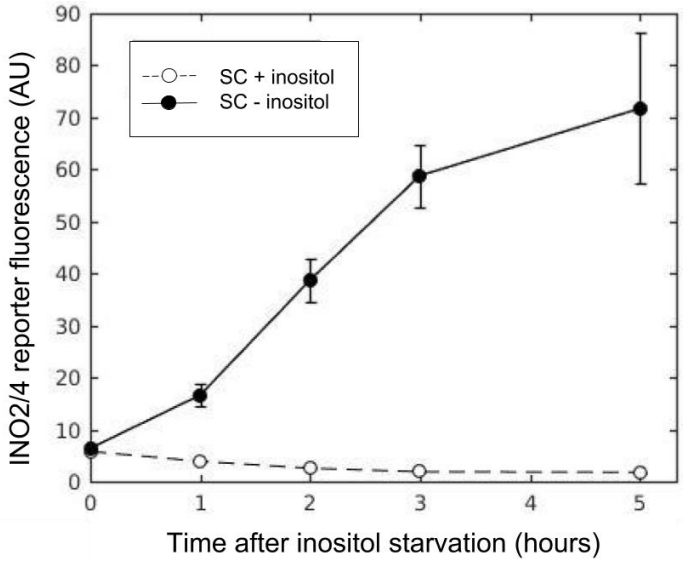

Figure 3.9: INO2/4 activation after inositol depletion from wild-type cells.
Exponentially growing wild-type cells with the INO2/4 reporter (FJ4741.4) were collected from inositol-supplemented SC medium, resuspended in prewarmed inositol-free (filled dots) or inositol-supplemented SC medium (hollow dots) and incubated for 5 hours at 30 °C. At indicated timepoints, the fluorescence of cells from both cultures was measured with flow cytometry and analysed with FlowJo. (The dots represent the mean reporter fluorescence in 3 different biological replicates and the bars represent the standard derivation).

During the first 5 hours after the medium change, the median reporter expression continuously increased up to 20-fold in the inositol-depleted cells and decreased by 50% in the inositol-supplemented cells when compared to the initial reporter fluorescence.

However, the main fluorescence increase occurred more than one hour after the media change and this delay suggested either a slower induction of transcription or a time delay in the post-transcriptional processes. As the INO2/4 reporter shared the CDS and the post-transcriptional regulation with the fast-responding reporters for HAC1 and RLM1 activity but contained a different, non-synthetic promoter sequence, i.e. INO1, this delay probably resulted from delayed transcription.

To investigate if a generally delayed INO2/4 activity or a promoter-specific delay is responsible for the slow fluorescence increase after inositol depletion, the transcriptional activation of the endogenous promoter template, i.e. INO1, was compared to the induction of another endogenous INO2/4 target, i.e. CHO1, after inositol depletion [56]. To this end, the mRNA abundance of both genes, i.e. INO1 and CHO1, in wild-type cells before and at three timepoints after inositol depletion was determined with qPCR and normalised by ACT1 mRNA abundance (see figure 3.10).

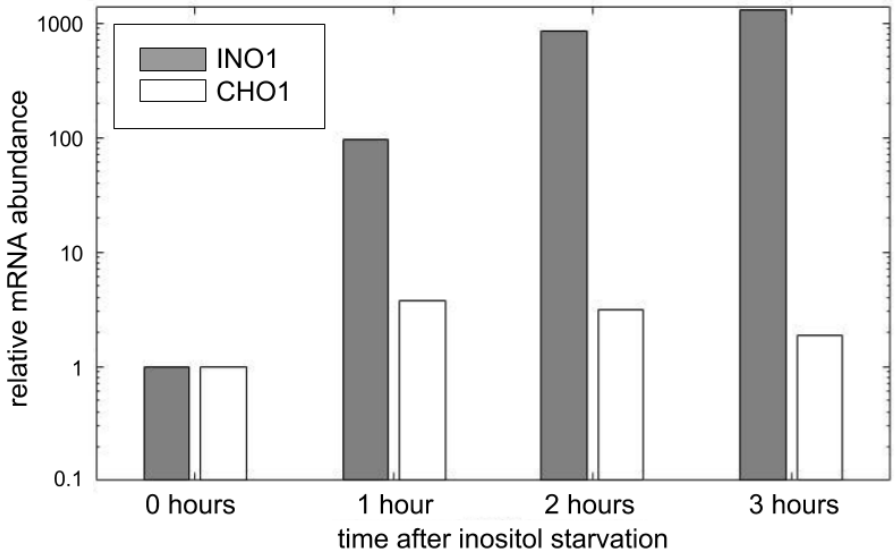

Figure 3.10: mRNA levels of two INO2/4 targets, CHO1 and INO1, after inositol depletion.

Exponentially growing wild-type cells (BY4741) were collected and resuspended in prewarmed inositol-free media. Samples were taken before resuspension and one, two and three hours afterwards, the mRNA levels were measured with qPCR, and relative mRNA abundance calculated via the double delta C_t method with ACT1 and normalised by the initial expression level (n=1, y-axis in log scale with basis 10)

CHO1 mRNA abundance tripled during the first hour after the treatment but remained relatively constant afterwards. INO1 mRNA levels increased by 80-times during the first hour but reached up to 1000-times the basal expression level 3 hours after inositol depletion.

CHO1 mRNA dynamics indicated a rapid and sustained increase in gene expression and suggested that one hour is enough to activate INO2/4. In contrast to CHO1, slow INO1 expression dynamics argued for a gradual gene activation, which is INO1-specific and probably conserved to the reporter for INO2/4 activity that shares the same promoter sequence. Despite this gradual response which might indicate an additional regulatory mechanism, INO1 activation primarily depends on INO2/4 activity [246], and increased reporter fluorescence should thus always require their activation.

3.6 Cellular burden of dynamic transcriptional reporter

The expression of transgenes can have a negative impact on cell physiology and cell growth [247]. Stress from basal TRP expression might hence decelerate growth and dominate the effect of the environment, and their permanent integration might prevent the investigation of an adaptive response after an environmental change.

To determine the growth effect of basal TRP expression, the growth of wild-type culture with or without the promoter constructs and in nutrient-enriched (YPD) or amino-acid-low (minimal synthetic complete) medium at 30 °C was measured via optical density at 600 nm (OD600) in 96-well microtiter plates and every 5 minutes during an incubation from non-detectable starting amounts to full confluency, i.e. 15 to 20 hours (see figure 3.11 and materials and methods 2.11).

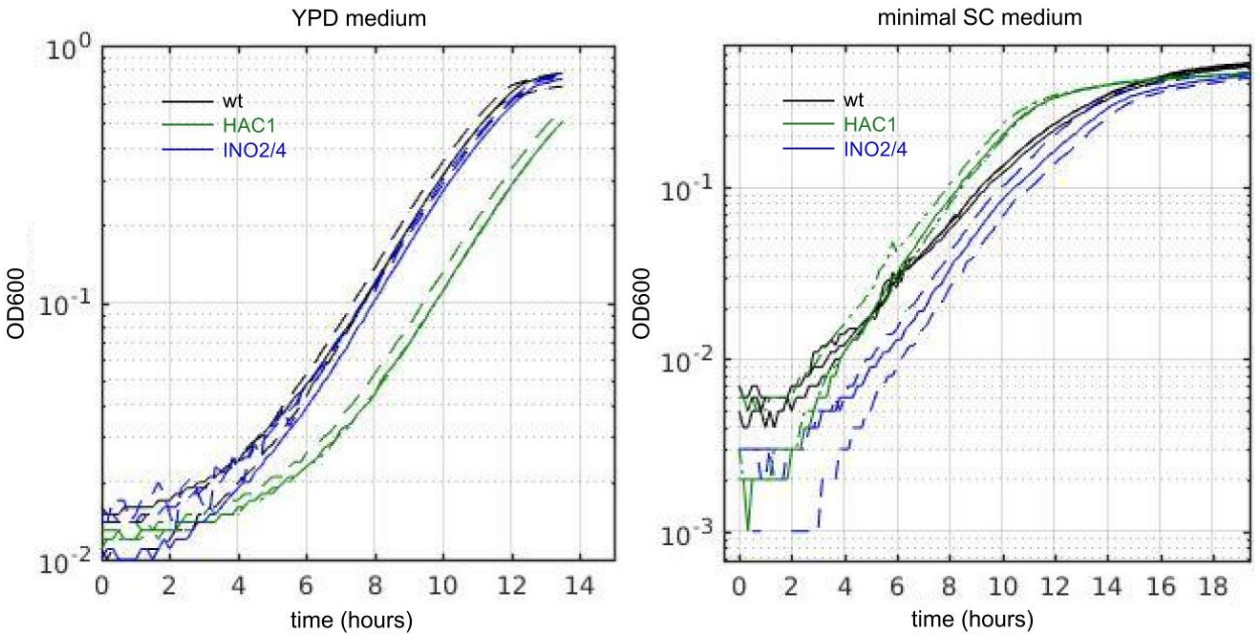

Figure 3.11: Growth of wild-type cells with and without reporter constructs in YPD and minimal SC medium. The optical density at 600 nm (OD600) of three different cell types, wild-type cells without reporter construct (BY4741, wt: black line), with HAC1-activity reporter (FJ4741.1, HAC1: green line) or INO2/4 reporter (FJ4741.4, INO2/4: blue line), was measured during the growth in YPD or minimal SC medium (the solid and dashed line represent the biological replicate of the different cell-types, n=3, y-axis in log scale with basis 10).

In all cultures, the shape of the growth curve in a semi-log plot was linear at low ODs (0.04 - 0.3 for YPD and 0.02 - 0.2 for SC) and indicated exponential growth with a constant growth rate. This suggested that the depletion of extracellular resources did not inhibit population growth at low ODs. The maximal growth rate, a robust indicator of cell physiology, is equal to the slope of the curve at lower ODs and was determined for each genotype and in each medium (see materials and methods 2.11).

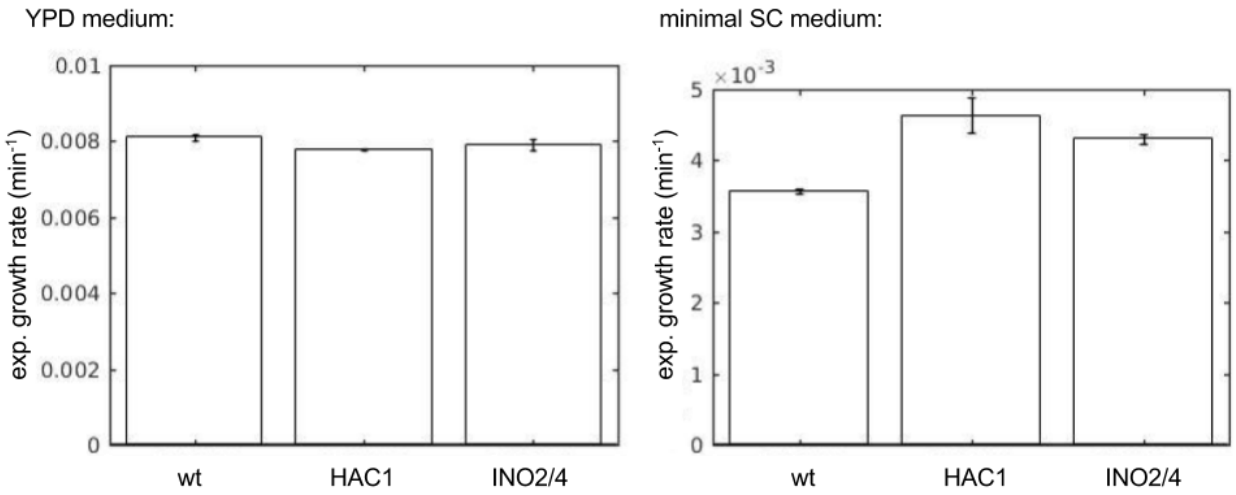

Figure 3.12: The exponential growth rates of the reporter strains at low OD in YPD minimal SC medium.
The exponential growth rates of the strains without reporter construct (wt, BY4741), with HAC1 reporter (HAC1, FJ4741.1) and with INO2/4 reporter (INO2/4, FJ4741.4) in two different media, i.e. YPD medium (left) or SC medium (right), were calculated from the growth curves in figure 3.11 at very low ODs. (n=3, bars represent the mean average slope of the different biological replicates, and the error bars indicate the standard deviation).

Firstly, the higher exponential growth rate of all strains in YPD (~0.008 min^{-1} doubling time: 86 minutes) than minimal SC medium (~0.004 min^{-1}; doubling time: 170 minutes) probably resulted from the additional nutrients in YPD medium, i.e. peptone and yeast extract, which alleviated most limitations of the minimal medium.

In minimal medium, the growth rates of the transformed strains were 10 to 20% higher than that of the original strain, while the difference between the different strains was less than 10% in rich medium. The similar growth rates of the different strains in rich medium suggested that the reporter constructs did not decrease the optimal metabolic rate of the cells. The faster growth of reporter strains at low ODs in minimal SC medium further suggested that they were less affected by the growth limitations in amino acid-poor media, and this possibly resulted from the histidine prototrophy that was used for colony selection.

In addition to the growth rate, the decreasing slope at higher ODs indicated the existence of an environmental limit that might result from nutrient depletion. The earlier decrease in SC minimal (OD600 >0.2) than in YPD (OD600 >0.5) medium (see figure 3.11) implied that the higher nutrient concentration of YPD medium also supports bigger yeast populations.

In both media, the final OD of the reporter strains was not significantly different from that of the untransformed strain. This indicated that histidine prototrophy or TRP expression did not change the environment capacity and suggested that histidine is not limiting the final population size in minimal SC medium.

3.7 Fluorescent lipids and the measurement of lipid metabolism

In contrast to gene transcription, methods to investigate the general metabolism or lipid metabolism of individual cells are still in their infancy [248]. The current approaches, which compromise mass spectrometry, optical spectroscopy and fluorescent biosensors, can only be performed by specialists and cannot easily be modified to answer a new scientific question [192,249,250].

Analogous to fluorescent NBD-glucose, which is already commercialised as a quantitative indicator of glucose metabolism in single cells [251], the localisation and amount of lipid intermediates such as ceramide can be visualised via the conjugation of fluorescent NBD and might then be used as a proxy for sphingolipid lipid metabolism in single cells [252,253].

The NBD fluorophore can be attached to different carbon atoms of ceramide, and its chemical environment then influences the optical properties of NBD: Quenching by water molecules reduces its fluorescence. Non-polar environments such as cellular membranes enable a GFP-like fluorescence [254,255]. When attached to the lipid side chain like in NBD-C6-ceramide, NBD only fluoresces in cellular membranes, and this can be used to distinguish between membrane-integrated and free NBD-C6-ceramide (see figure 3.13).

Low levels of extracellular NBD-C6-ceramide are not toxic to wild-type yeast cells, which can take them up and metabolise them into NBD-IPC but not further [256]. Similarly to endogenous ceramide, the conversion of NBD-C6-ceramide to NBD-IPC by AUR1 also triggers its cellular relocalisation from the ER to the Golgi, where it accumulates until cell division [256]. After NBD-C6-ceramide staining, the subcellular localisation and total NBD fluorescence might hence be good ways to study sphingolipid metabolism, but the feasibility of NBD-C6-ceramide as a quantitative *in vivo* probe for yeast has not been explored before (see figure 3.13).

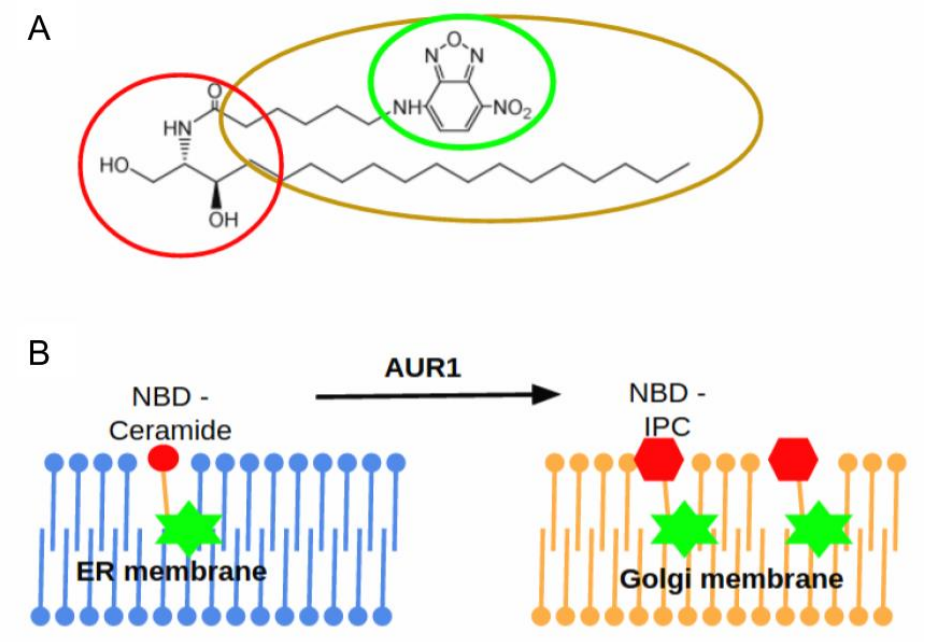

Figure 3.13: NBD-ceramide structure and cellular processing.

A, Chemical structure of NBD-C6-ceramide with fluorophore (green), polar head group (red) and hydrophilic tail (brown). **B,** Cellular relocalisation after processing of NBD-C6-ceramide into its *physiological* end product, i.e. NBD-IPC).

3.8 AUR1 activity and the intracellular localisation of NBD fluorescence from NBD-C6-ceramide staining

To evaluate how the subcellular localisation of NBD fluorescence after NBD-C6-ceramide staining reacts to a reduced AUR1 activity as it possibly occurs during inositol starvation [55], the localisation of NBD fluorescence after total chemical AUR1 inhibition with Aureobasidin A was investigated [257].

To this end, exponentially growing wild-type cells from minimal SC medium were incubated for 3 hours at 30 °C in minimal SC medium with 5 µM NBD-C6-ceramide/BSA complex and with or without 2 µM Aureobasidin A [258]. After three hours, samples were taken and the localisation of NBD fluorescence in living cells investigated with epifluorescence microscopy (see materials and methods 2.16 and 2.20 for the details of the procedure and figure 3.14 for exemplary pictures).

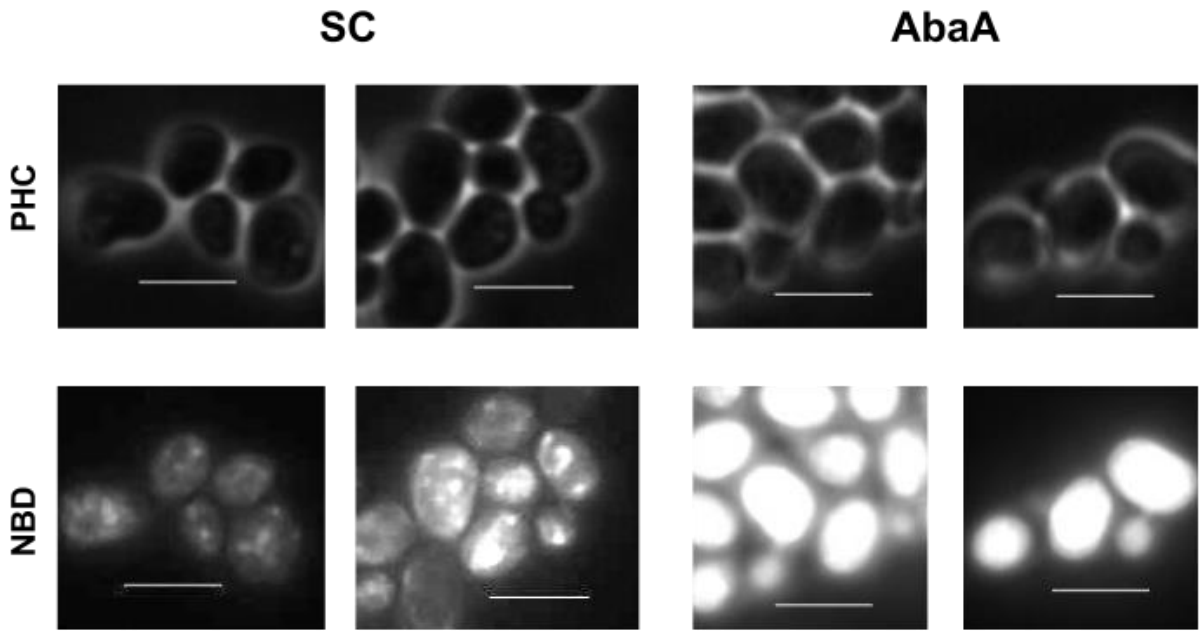

Figure 3.14: NBD fluorescence localisation before and after AUR1 inhibition.

Phase contrast (PHC, upper row) and NBD fluorescence (NBD, lower row) pictures of yeast cells two hours after NBD-C6-ceramide staining in SC medium with (AbaA) or without (SC) 2 µM Aureobasidin A (n=3, pictures show the two channels of representative cells from one of the three replicates. White scale bars correspond to 5 µm).

In wild-type cells and without AUR1 inhibition, NBD fluorescence localized to intracellular punctae. After long-term AUR1 inhibition, NBD fluorescence was uniform throughout the entire cell.

The intracellular punctae indicated that NBD-C6-ceramide was taken up, and NBD was incorporated into intracellular membranes. The punctae probably corresponded to Golgi vesicles where NBD-IPC resides in non-perturbed yeast cells [256]. The absence of fluorescence from the plasma membrane further suggested that NBD-C6-ceramide and NBD-IPC are somehow excluded from the plasma membrane.

As Aureobasidin A treatment prevents the synthesis NBD-IPC and all endogenous sphingolipids, the uniform NBD fluorescence probably corresponded to NBD-C6-ceramide in the plasma membrane and suggested that long-term AUR1 inhibition and the loss of mature sphingolipids eventually permitted NBD-C6-ceramide to localise to the plasma membrane, which was probably occupied by mature sphingolipids, i.e. IPC, MIPC and $M(IP)_2C$, before.

As the uniform staining hid organelle-localised NBD fluorescence, it was impossible to determine if the complete inhibition of IPC synthesis also prevented ceramide uptake or changed the subcellular localisation.

3.9 Total NBD fluorescence after NBD-C6-ceramide staining and AUR1 inhibition

The cellular NBD-C6-ceramide amount does not change significantly and NBD-IPC production ceases after AUR1 treatment [256]. AUR1 inhibition thus probably lowers the total NBD content of the cell, while the new localisation in the plasma membrane might further influence NBD fluorescence and lead to the strong NBD fluorescence that was observed in epifluorescence microscopy (see figure 3.14).

To quantify the impact of AUR1 inhibition on total NBD fluorescence, wild-type cells were incubated in SC medium with NBD-C6-ceramide or with NBD-C6-ceramide and 2 µM Aureobasidin A. The total NBD fluorescence of single cells at two different timepoints during the incubation was subsequently measured with flow cytometry (see figure 3.15).

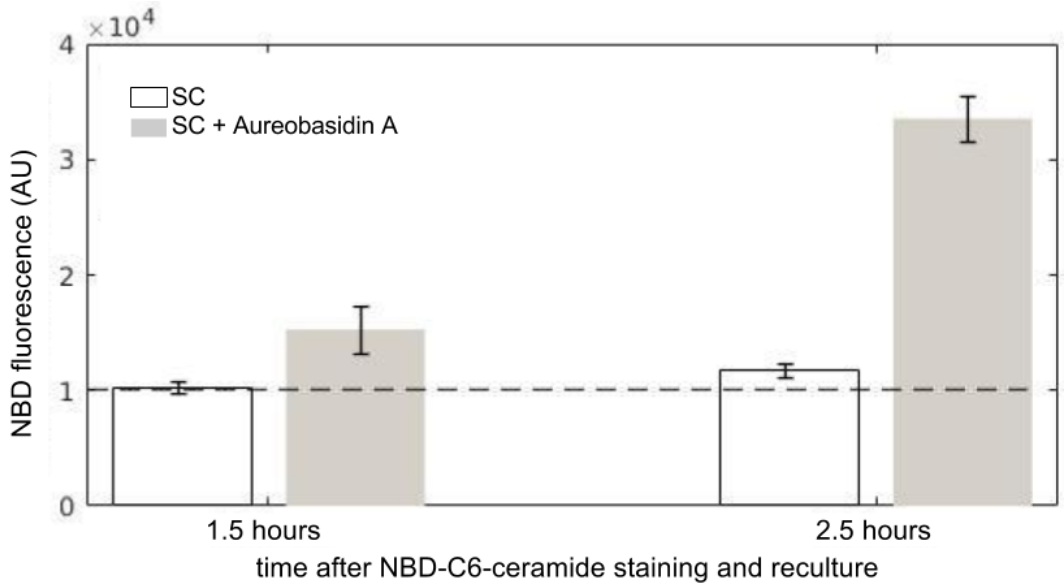

Figure 3.15: Impact of AUR1 inhibition on total NBD fluorescence

Exponentially growing wild-type cells (BY4741) in minimal SC medium were incubated with 5 µM NBD-C6-ceramide or with 5 µM NBD-C6-ceramide and 2 µM Aureobasidin to inhibit AUR1 activity. The total NBD fluorescence in single cells at two timepoint during the incubation (1.5 hours and 2.5 hours) was determined with flow cytometry and analysed with FlowJo (n=3, and error bars represent the standard deviation of the three biological replicates).

The NBD fluorescence of unperturbed yeast cells was very similar between the different biological repeats and did not change by more than 20% in minimal SC medium between 1.5 and 2.5 hours after the exposure to NBD-C6-ceramide. With Aureobasidin A exposure, the NBD fluorescence increased by 40% after 90 minutes and by 250% after 150 minutes.

The constant NBD fluorescence of unperturbed cells indicated no big changes in the amount or environment of NBD and suggested that a balance between NBD-C6-ceramide uptake, NBD-IPC production and cell division probably established a stable cellular NBD pool. The strong increase in NBD fluorescence after AUR1 inhibition suggested that the concentration of NBD derivatives, i.e. NBD-C6-ceramide and NBD-IPC, or the fluorescence efficiency of individual NBD molecules increased after AUR1 inhibition.

Previous work has shown that short-term AUR1 inhibition had no significant impact on intracellular NBD-C6-ceramide levels and prevented NBD-IPC synthesis [256], it is thus unlikely that long-term AUR1 inhibition increased the concentration of NBD derivatives. Because the fluorescence of individual NBD molecules is also affected by their chemical environment, a different lipid composition in the plasma membrane (see subchapter 3.8) or unknown changes of lipid metabolism after AUR1 inhibition probably increased the fluorescence of existing NBD molecules. Overall, the localisation and strength of NBD fluorescence in single cells after NBD-C6-ceramide staining was highly sensitive to the inhibition of AUR1 activity by Aureobasidin A and might also react to similar changes of sphingolipid metabolism that occur during inositol starvation [55].

3.10 Discussion

One objective of this chapter was to develop fluorescent reporter proteins that can track the transcriptional changes of single cells and have a minimal impact on host cell physiology.

A theoretical model for fluorescent protein expression suggested that slow protein degradation is the main obstacle for fast-responding reporter proteins and that active degradation disproportionately lowers the signal output of slow-maturing fluorescent proteins. For optimal detection, active degradation should thus be combined with sequence modifications that maximise translation and accelerate maturation. A review of the existing literature indicated specific modifications of the coding DNA sequence, i.e. codon optimisation, ubiquitin tagging and fast-folding GFP variants, that can accelerate protein degradation and increase reporter fluorescence.

The fluorescence of a control reporter with these modifications and a ribosomal promoter was relatively robust against perturbations of ER homeostasis or lipid metabolism. This suggested that these perturbations had a small impact on the translation, folding or degradation of reporter proteins and that transcriptional changes primarily lead to the fluorescence changes of the other reporter proteins in the following experiments.

The fluorescence of the constructed HAC1 reporter indicated an increased transcription factor activity 15 minutes after an environmental change. The other reporter proteins also closely

followed gene expression, i.e. INO2/4 reporter, or responded faster than existing reporter proteins, i.e. RLM1 reporter. The growth rate of reporter carrying strains in two different media further indicated no negative impact of basal reporter expression on cellular metabolism.

Promoter specificity and the positive impact of the individual CDS modifications, i.e. improved dynamics from active protein degradation via an N-terminal ubiquitin or a PEST-rich sequence and several fold higher fluorescence yields from codon-optimised GFP constructs [208,259,260], were already investigated earlier [50,238,261]. It thus seemed not necessary to further investigate how their combination contributed to the specificity, fluorescence output and response time of the new reporter constructs. Moreover, their dynamic properties and the low burden from basal reporter expression should already enable them to detect transient transcriptional changes, which might happen during the adaptation to environmental changes that were investigated in the following chapters of the thesis. In addition to transcription factor activity measurements, the newly constructed CDS could also be fused to an endogenous promoter sequence and should subsequently indicate the transcriptional changes of a specific gene.

So far, reporter robustness was only validated in the set of environments that was of interest for this PhD and with a negative control that is regulated by ribosome-specific transcription factors and might be affected by other environments [262]. When applying the reporters in other conditions, the impact of proteasomal degradation or translation rate should thus again be estimated with a degradable reporter protein that is at best not controlled by any transcription factor [263].

The main advantages of the developed reporter proteins over GFP-labeled regulatory proteins were their low impact on cell physiology, their independence of cellular localisation and their possible application to other transcriptional changes. Nevertheless, the spectral overlap of GFP with cyan fluorescent protein (CFP) and yellow fluorescent protein (YFP), which are the two alternative fluorescent proteins with sufficient short maturation times to enable fluorescence detection from rapidly degraded reporter proteins [264–266], prevents the parallel observation of two different signaling pathway in the same cell and is probably the main disadvantage of the reporter proteins. An improved reporter toolset should therefore use fast-folding and codon-optimised CFP and YFP variants. However, other factors of the experimental setup, e.g. laser configuration for flow cytometry or filter combinations in microscopy, might then still limit their application to one pathway per cell. Moreover, the physiologic impact of reporter proteins was only evaluated in non-induced conditions, but the physiologic burden of multiple reporters or a fully expressed reporter might also limit the application of the developed reporter proteins.

Towards the development of a fluorescent indicator for sphingolipid metabolism, the evaluation of NBD-C6-ceramide *in vivo* staining has shown that the localisation and intensity of NBD fluorescence are stable in unperturbed cells but very sensitive to chemical AUR1 inhibition.

While the stable NBD fluorescence most likely resulted from tightly regulated IPC levels [267], it remains unclear which consequence of AUR1 inhibition actually led to the relocalisation of NBD-C6-ceramide to the plasma membrane and increased its fluorescence intensity. A possible explanation for the latter is that a higher ergosterol content in the plasma membrane increased NBD fluorescence similar to cholesterol in mammalian cells [69,268].

Even though phytoceramide concentration could increase after long-term AUR1 inhibition, it is not known if it also localises to new cellular membranes, e.g. the plasma membrane. However, the existence of ceramidases and other ceramide processing enzymes probably limits the accumulation and prevents the relocalisation of endogenous ceramide species [269]. Therefore, NBD-C6-ceramide probably did not reflect natural ceramide metabolism but rather responded to other parallel changes in lipid metabolism during AUR1 inhibition.

A better understanding of these lipid changes and their effect on the localisation, concentration and fluorescence of NBD-C6-ceramide would require lipid content measurements in different cellular membranes after AUR1 inhibition and NBD-C6-ceramide staining with liquid chromatography or mass spectrometry, but these exceeded the scope of this project.

Nevertheless and based on the high sensitivity of NBD fluorescence to AUR1 inhibition, I decided to use NBD-C6-ceramide staining as a rough proxy for perturbations of lipid metabolism that affect AUR1 activity, e.g. lower PI levels after inositol depletion, but not as a probe for ceramide metabolism in single cells. Alternatively, NBD-phytosphingosine, which is based on the metabolic phytoceramide precursor, could be more suited to investigate the route of endogenous phytoceramide at lower AUR1 activities but was not established at the start of my PhD [270].

Overall, the utilization of different state-of-the-art techniques has led to the development of a versatile reporter for transcriptional changes and a rather confined reporter for AUR1 activity, which might still be useful in this project.

4 The role of sphingolipid metabolism and the coordination of transcription during the adaptation to inositol starvation

4.1 Introduction

In *S. cerevisiae,* inositol is the substrate for an important metabolite of lipid biosynthesis and cellular signaling, i.e. phosphatidylinositol (PI) [26,271]. The adaptation to inositol-free environments causes remarkable physiological and transcriptional changes, which cannot be explained by the activation of a single transcription factor and represent a good example to study the coordination different signaling pathways during adaptation [33,48,202,272].

The effects of inositol starvation and lower PI synthesis on the fluxes and transcriptional regulation of glycerolipid biosynthesis via INO2/4 are extensively studied but do not explain the additional transcriptional changes, e.g. UPR and PKC activation [50,51], which are required for the final adaptation [23,26]. PI is also an essential substrate for inositolphosphoryl ceramide (see figure 4.1) - the simplest of the mature sphingolipids that seem to regulate various cellular processes such as ER homeostasis or cell wall integrity [53]. Reduced SL biosynthesis at lower PI levels might thus trigger or demand the INO2/4-independent transcriptional changes after inositol starvation.

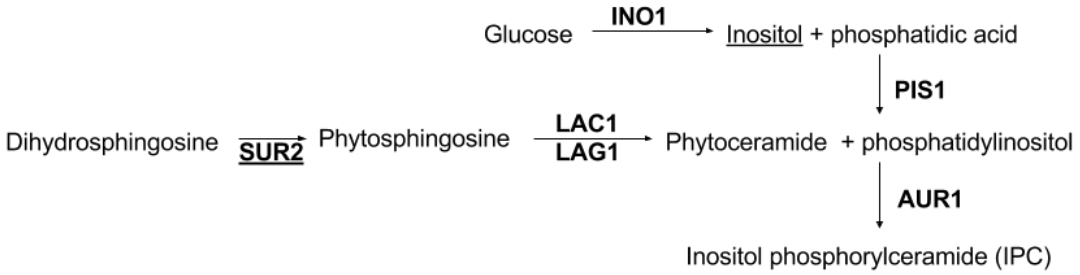

Figure 4.1: Sphingolipid metabolism in yeast from dihydrosphingosine to inositol phosphorylceramide (IPC). Schematic overview of the partial sphingolipid metabolism that is investigated during this chapter: Metabolic intermediates (normal font), participating enzymes (bold font) and the perturbations (underlined).

The role of SL biosynthesis in cell physiology was extensively studied with chemical inhibitors and genetic mutants that target specific steps of sphingolipid synthesis but only once during inositol starvation [81,82,258,273–276]. However, as the adaptational response enables cells to survive inositol starvation, its effect on SL metabolism probably differs from the exposure to toxic inhibitors or genetic perturbations, which permanently affect optional steps downstream of PI consumption

or reduce the activity of distant steps upstream of PI consumption [277–279]. It could be more similar to non-lethal perturbations of steps upstream of PI consumption that reduce IPC synthesis. Ceramide and PI are the only substrates for IPC synthesis, and sphingosine hydroxylation by SUR2, which accelerates ceramide biosynthesis [280], could possibly determine the rate of IPC synthesis similar to inositol availability (see figure 4.1). The SL metabolism changes after SUR2 knock-out might thus resemble those during inositol starvation but are unlikely to have the same effect on the phospholipid biosynthesis and INO2/4 activity. The physiologic consequences after this knock-out possibly help to determine SL-dependent transcriptional changes after inositol starvation but have not been studied yet.

To understand the adaptation to inositol starvation, the impact of both perturbations on lipid metabolism and cell growth was first compared, before genetic tools and published data were used to evaluate the role of SL metabolism in cell division, cell wall integrity, protein secretion and ER homeostasis. Afterwards, the developed reporters (see chapter 3) were used monitor the transcriptional and metabolic changes after inositol starvation and to assess the temporal and causal connections between the participating signaling pathways. Finally, the importance of the growth rate during inositol starvation was evaluated with the slow-growing SUR2 knock-out mutant.

4.2 Inositol depletion and SUR2-deficiency increased NBD fluorescence after staining with NBD-C6-ceramide

Inositol starvation and SUR2-deficiency, which target different enzymatic steps upstream of IPC synthesis, probably both affect AUR1 activity and IPC synthesis. Lower PI levels during inositol starvation probably decrease AUR1 activity during inositol starvation [55], but the impact of sphingosine hydroxylation has not been investigated so far.

As NBD-C6-ceramide staining responded to changes of AUR1 activity in earlier experiments (see chapter 3), the same method was used to investigate the lipid metabolism during inositol starvation and after SUR2 knock-out. To this end, exponentially growing wild-type (BY4741) or SUR2-deficient cells (BY4741SUR2Δ) were collected from minimal SC medium, stained with NBD-C6-ceramide and then transferred to minimal SC medium, inositol-free medium or SC medium with 2 µM Aureobasidin A (AbaA) that all also contained NBD-C6-ceramide. After 1.5 and 2.5 hours, the total NBD fluorescence of individual cells in each sample was determined with flow cytometry and analysed with FlowJo (see figure 4.2).

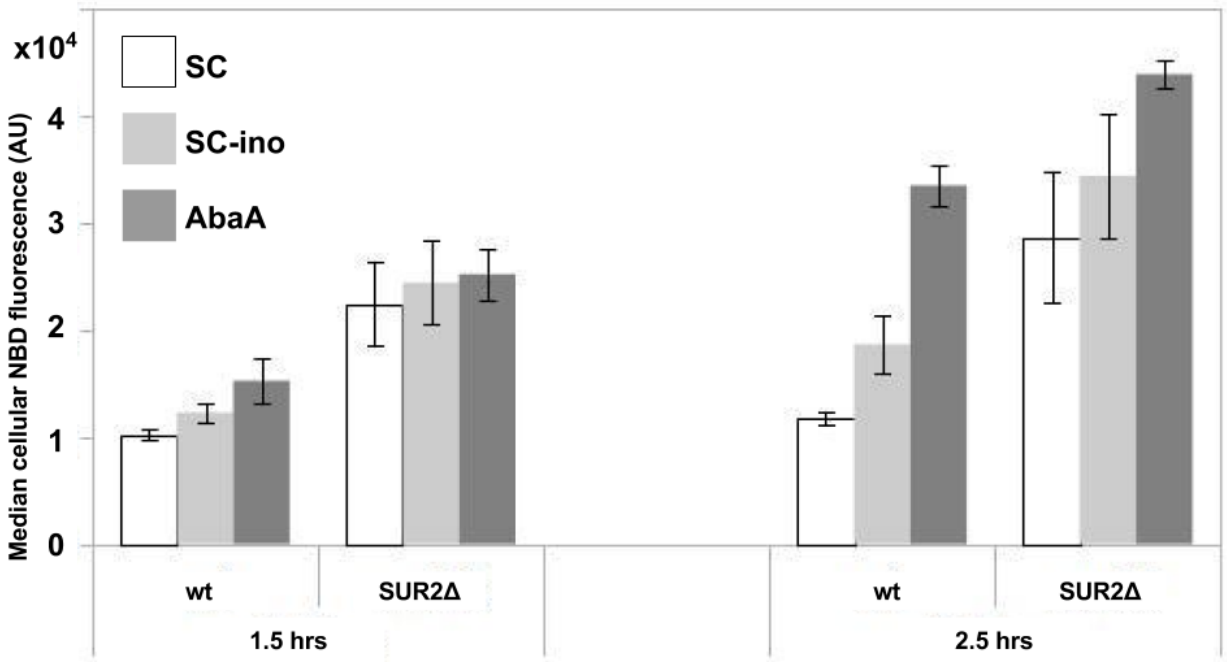

Figure 4.2: NBD fluorescence of wild-type and SUR2-deficient cells after AUR1 inhibition and inositol depletion
The NBD fluorescence in wild-type (BY4741, wt) and SUR-deficient (BY4741SUR2Δ, SUR2Δ) cells after NBD-C6-ceramide staining and 1.5 hours or 2.5 hours growth in normal minimal (SC), inositol-free minimal (SC-ino) or minimal medium with 2 µM Aureobasidin A (AbaA) was determined with flow cytometry and analysed with FlowJo (n=3, and the error bars represent the standard deviation between the biological replicates).

In minimal SC medium, the NBD fluorescence of SUR2-deficient cells was higher and more variable than the NBD fluorescence of wild-type cells. 1.5 hours after inositol depletion or AbaA addition and compared to minimal SC medium, the NBD fluorescence only increased slightly in wild-type and even less in SUR2-deficient cells. After 2.5 hours and compared to minimal SC medium, Aureobasidin A treatment increased the NBD fluorescence in SUR2-deficient cells (50%) but less than in wild-type cells (200%). After 2.5 hours inositol starvation, NBD fluorescence of all wild-type samples increased by at least 50% compared to 2.5 hours in minimal SC medium but increased less and only in two of the three biological replicates of SUR2-deficient cells when compared to NBD fluorescence of SUR2-deficient cells in minimal SC medium.
The higher NBD fluorescence of SUR2-deficient cells in minimal medium and of wild-type cells after Aureobasidin A treatment (i.e. AUR1 inhibition) or during inositol starvation indicated a changed lipid metabolism. The increase after inositol starvation and Aureobasidin A treatment in wild-type cells accompanied a reported lower AUR1 activity under both conditions [55,257], and this further supported that NBD fluorescence reacts to the changes of lipid metabolism that result from lower IPC synthesis. Even though the higher NBD fluorescence of the SUR2 knock-out strain

might result from IPC-independent lipid metabolism changes, the smaller relative effect of AUR1 inhibition and inositol starvation suggested that a decreased ceramide concentration after sphingosine knock-out already lowered AUR1 activity before those additional perturbations [280].

4.3 SUR2 knock-out and inositol starvation reduced the growth rate in minimal medium but peptone supplementation recovered the growth rate of SUR2-deficient cells

Both perturbations, SUR2 knock-out and inositol starvation, possibly reduce AUR1 activity, but while *S. cerevisiae* undergoes big transcriptional changes to survive inositol starvation [202], SUR2 deficiency is unlikely to trigger a targeted compensatory response. Therefore, the growth rate after both perturbations probably highlights different aspects of cell physiology:

During inositol starvation, the growth rate of wild-type cells might indicate the burden of the adaptational changes on the overall metabolism, and the growth rate of UPR-deficient cells, i.e. after IRE1 or HAC1 knock-out, might additionally highlight the impact of those changes on ER homeostasis. The growth rate of SUR2-deficient cells, on the other hand, might indicate the importance sphingosine hydroxylation and fast IPC synthesis for cell physiology in a certain environment.

To measure the growth rate, exponentially growing wild-type (BY4741), SUR2-deficient (BY4741SUR2Δ) and UPR-deficient (BY4741IRE1Δ, BY4741HAC1Δ) cells from minimal SC medium, minimal SC medium without inositol or minimal SC medium with peptone supplementation were diluted 100-fold and cultured in a 96-well microtiter plate. Every 5 minutes during a 20-hour incubation at 30 °C, the cell density of individual wells was measured via OD600, and the growth curves were then used to calculate the exponential growth rate of each strain in the different media (see figure 4.3).

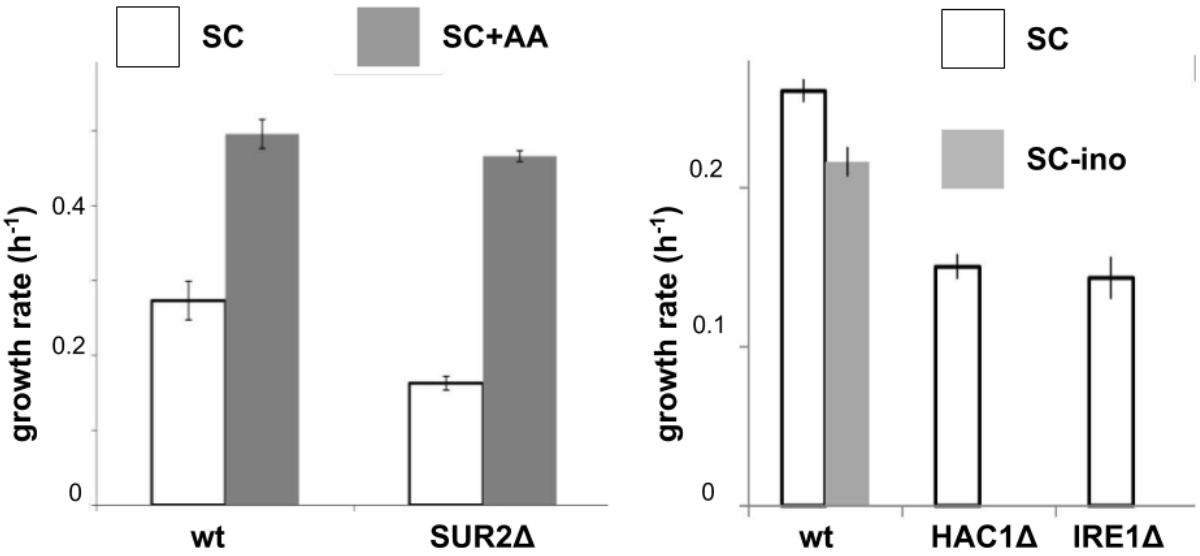

Figure 4.3: Growth rate of SUR2- and UPR-deficient strains in different media

The different strains, wild-type (BY4741, wt), SUR2-deficient (BY4741SUR2Δ, SUR2Δ) and UPR-deficient (i.e. BY4741IRE1Δ, IRE1Δ and BY4741HAC1Δ, HAC1Δ) were cultured in the respective medium, minimal SC (SC), minimal SC + 2% peptone (SC+AA) or inositol-free minimal SC (SC-ino), and in 96-well microtiter plates. The growth rate was subsequently determined from the optical density as described in materials and methods 2.11 (n=3, and the error bars indicate the standard deviation between the different biological replicates).

UPR-deficient and SUR2-deficient cells grew much slower than wild-type cells in minimal synthetic complete medium, but SUR2-deficient cells almost grew as fast as wild-type cells in peptone-supplemented SC medium (see figure 4.3, left). In inositol-free SC medium (see figure 4.3 right), wild-type cells grew a little slower than in minimal SC medium, and the UPR-deficient strains did not grow at all.

Firstly, the faster growth of wild-type and SUR2-deficient cells in peptone-supplemented medium suggested that amino acids limited the growth in minimal SC medium. The stronger growth defect of SUR2-deficient cells in minimal SC medium further indicated that SUR2 activity, sphingosine hydroxylation and accelerated ceramide synthesis were very important for growth in minimal medium, but less for growth in peptone-supplemented medium [280]. The growth defect of wild-type strains in inositol-free medium was smaller than that after SUR2 knock-out and suggested that transcriptional adaptation enabled the cells to better deal with this perturbation of lipid metabolism than with SUR2 deficiency. The growth rates of UPR-deficient strains indicated that UPR functionality was important for yeast growth in minimal SC medium and essential during inositol starvation.

4.4 Peptone supplementation increased SUR2 transcription

In addition to the growth rate, the transcriptional regulation of later steps of SL biosynthesis is relatively unknown but might indicate their physiological role. For a few special genes and certain conditions the fitness defect of knock-out mutants correlates with a higher gene expression in wild-type cells under the respective condition, e.g. galactose utilisation cluster in galactose-supplemented medium [281].

The transcriptional regulation of SUR2 and sphingosine hydroxylation was thus investigated with a new reporter construct, i.e. dynamic GFP under the control of the SUR2 promoter (see figure 4.4A), and in the two previous nutrient conditions, i.e. minimal and peptone-supplemented SC medium, which determined the growth defect of SUR2-deficient cells.

The reporter construct was integrated into the HIS3 locus of wild-type cells, and saturated overnight cultures of the transformed cells (FJ4741.27) were diluted and cultured in minimal (SC) or peptone-supplemented SC (SC+AA) medium. After 6 hours of undisturbed growth, the single-cell fluorescence of all samples was measured with flow cytometry and analysed with FlowJo (see figure 4.4B).

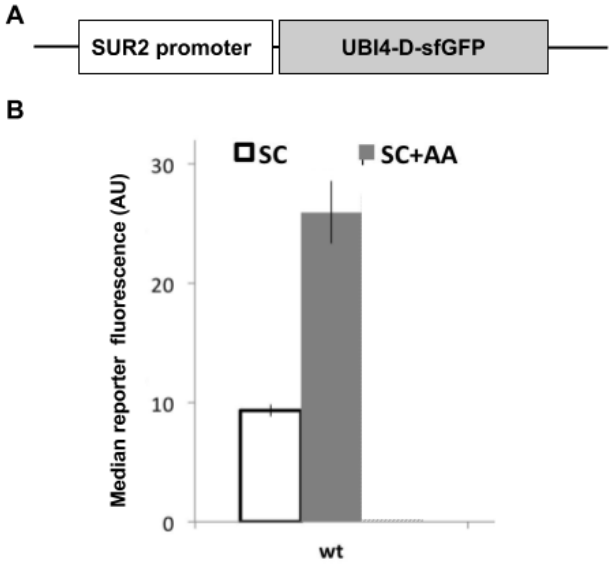

Figure 4.4: SUR2 transcription in wild-type cells from minimal or peptone-supplemented SC medium

A, Scheme of the new reporter construct: SUR2 promoter comprises 800 bases upstream of the SUR2 start codon, and UBI4-D-sfGFP corresponds to the common CDS of the dynamic reporter construct (see chapter 3). The remaining plasmid features, i.e. HIS3 locus, CYC1 terminator, origin of replication and antibiotic resistance, are omitted for simplicity. **B**, The reporter fluorescence of wild-type cells that express dynamic GFP under the control of the SUR2 promoter (FJ4741.27, wt) after 6 hours of exponential growth in minimal synthetic complete medium with (SC+AA, grey bar) or without (SC, white bar) 2% peptone was recorded with flow cytometry, and median fluorescence determined with FlowJo (n=3, the error bars indicate the standard deviation between the different biological replicates)

During exponential growth, the SUR2 reporter fluorescence of wild-type cells was 2.5 times higher in peptone-supplemented than in minimal SC medium (see figure 4.4B).

The higher reporter fluorescence indicated an increased SUR2 transcription in peptone-supplemented medium, which might result from the binding sites of two nitrogen-dependent transcription factors, i.e. GLN3 and DAL80, in the SUR2 promoter [282,283]. As SUR2 protein abundance also increases by around 3-fold in YPD medium [38], the strong growth defect from SUR2 deficiency probably does not correlate with higher protein expression in minimal SC medium. The strong growth defect of the SUR2 knock-out in minimal medium and the increased SUR2 expression in peptone-supplemented medium implied that SUR2 is probably important for growth in amino-acid-rich as well as amino-acid-poor environments.

4.5 The expression of enzymes in SL metabolism correlated with their position in the pathway

Even though sphingosine hydroxylation might promote IPC synthesis, it is not sufficient to investigate the regulation of SUR2, but necessary to study the regulation of all participating enzymes under different environmental conditions to understand the transcriptional regulation and the physiological role of SL biosynthesis.

STRING, an online bioinformatics tool to analyse publicly available experimental data, was subsequently used to compare the regulation of all enzymes in SL metabolism (see table 4.1), reveal correlations between their expression profiles and highlight the potential co-regulation of individual enzymes in SL biosynthesis [284].

Table 4.1: List of genes for enzymes in sphingolipid biosynthesis.

The enzymes are ordered according to their position along the biosynthetic process (see chapter 1) and essential genes are defined according to Gievar *et al*. [281]

Gene	**LCB1**	**LCB2**	**TSC10**	**SUR2**	**LAC1**	**LAG1**	**SCS7**	**AUR1**	**IPT1**
Essential?	yes	yes	yes	no	no	no	no	yes	no

A standard STRING query combines different kinds of biological interaction data, e.g. co-expression, physical interaction and co-occurrence in different organisms, to calculate the confidence score for interactions between the query genes and find additional related genes of the organism. The search parameters were thus modified to only consider expression data and to determine the 5 closest interaction partners, which might highlight the integration of SL

biosynthesis into general physiology (figure 4.5). As no co-expression between the different genes passed the standard confidence threshold for interactions (0.4), the threshold was lowered to the lowest recommended threshold (0.15) and even less probable interactions were considered. While this lenient threshold increased the likelihood of false positive detection, it might also account for the fact that no previous experiment focused on the transcriptional regulation of sphingolipid biosynthesis.

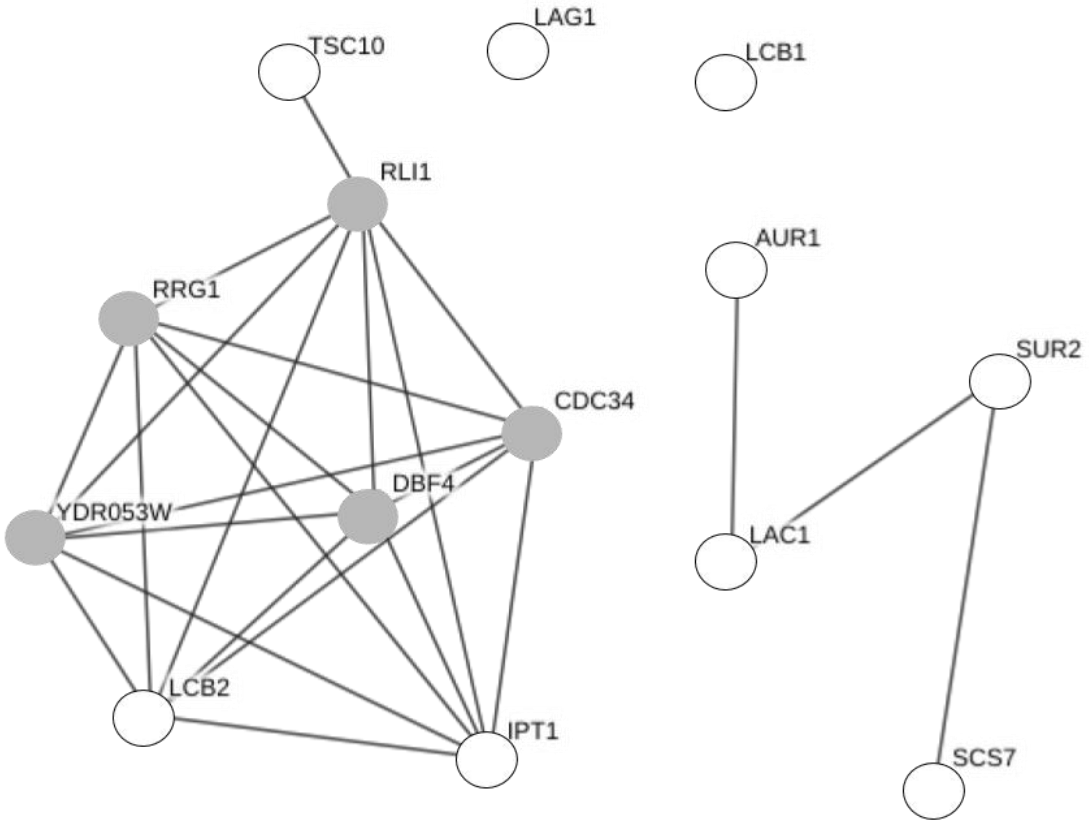

Figure 4.5: Expression similarities of SL enzymes and related genes in STRING.
The white circles represent the different genes in SL biosynthesis, and the grey circles represent the five genes with the most similar expression profiles (RLI1, DBF4, CDC34, YDR053W and RRG1), which were found via the STRING algorithm [284]. The connections indicate correlating expression profiles, as defined by the algorithm.

Based on the similarity of their expression profiles in various experiments, the STRING algorithm separated the enzymes into two distinct expression clusters (see figure 4.5). Interestingly and except for IPT1, these clusters reflected their respective position upstream and downstream of dihydrosphingosine: LCB2, TSC10 on the one side and SUR2, LAC1, SCS7 and AUR1 on the

other side, whilst the expression profiles of the remaining enzymes, LCB1 and LAG1, were not assigned to any cluster.

The five closest interaction partners, RLI1, DBF4, CDC34, YDR053W and RRG1, were not involved in SL biosynthesis and exclusively assigned to the LCB2/TSC10 cluster. The first three are essential proteins in three basic processes for yeast physiology: ribosome biosynthesis (RLI1) [285], DNA replication (DBF4) [286], and cell cycle progression (CDC34) [287]. YDR053W is an unannotated gene [288], and its co-expression probably resulted from the genomic overlap with DBF4 and not any biological connection. RRG1 is not essential for yeast growth but required for mitochondrial genome maintenance and mitochondrial ribosome production [289]. The co-expression of essential LCB2 and TSC10 with these basic genes suggested that their transcriptional activity is more robust and used less to regulate DHS synthesis, which is connected to essential processes in the cell [290].

The expression of SUR2 correlated with that of downstream enzymes. This correlation suggested a common regulation and that the adjustment of IPC biosynthesis to new conditions might be the main purpose for the transcriptional regulation of SUR2, LAC1, SCS7 and AUR1.

To account for the increased risk of false positives, the correlation between the expression profiles of these four genes was verified with an additional online tool, i.e. SPELL [291]. SPELL compares the expression profile of a certain gene against all other genes of the same organism in many published experiments, e.g. more than 400 experiments for *S. cerevisiae*, and ranks them according to their expression similarity. When SUR2 or LAC1 was queried using SPELL, the three other enzymes of the cluster were among the 20 genes with the most similar expression profiles. This also suggested co-expression and thus supported the previous findings from the STRING algorithm, i.e. co-regulation of SL biosynthesis under certain environment conditions. However, when SCS7 or AUR1 was queried in SPELL, only two (SUR2 and LAC1 for SCS7) or none of the other three enzymes were among the 20 highest genes. The difference between SCS7 or AUR1 and the other genes suggested that their regulation might be more specific than that of SUR2 and LAC1.

4.6 SUR2, LAC1 and AUR1 expression are sequentially activated between S and G2 phase

Based on above results, the higher SUR2 expression of fast-growing cells in peptone-supplemented SC medium could correlate with increased LAC1 and AUR1 expression and might indicate a higher sphingolipid demand during cell growth and division. Cyclebase.org was subsequently used to investigate the transcription of SUR2, LAC1 and AUR1 during the cell cycle and highlight a possibly role of SL synthesis during specific cell cycle phases [292] (see figure 4.6).

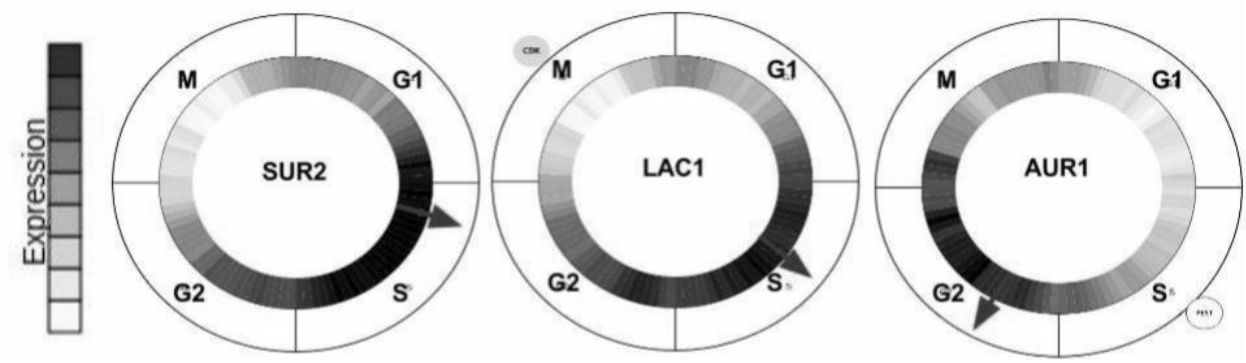

Figure 4.6: Expression pattern of IPC biosynthetic enzymes during the cell cycle

The cell-cycle-dependent expression profile of SUR2, LAC1 and AUR1 from 7 different datasets with 3 different synchronisation methods [293–296] (white to dark grey bars: low to strong average expression), were evaluated with Cyclebase.org to determine the peak expression time during the cell cycle (arrow head) of each gene.

For each gene, Cyclebase.org combines the expression data from seven different cell cycle experiments with three different synchronisation methods to estimate the peak expression time during the cell cycle and to rank the periodicity of gene expression during cell cycle progression against all other genes in the yeast genome (around 5000), i.e. rank 1 is assigned to the most periodic gene [292–296].

The high ranking of SUR2, LAC1 and AUR1, i.e. 146, 127 and 447, indicated a higher periodicity of their gene expression then for 90% of the *S. cerevisiae* genes and all other enzymes in SL biosynthesis. Even though the rank was lower than that of most cell cycle regulators (e.g. CLN1, CLN2) or S-phase-specific histones, it still suggested that the expression of all three genes is probably regulated during the cell cycle. Interestingly, the determined temporal order (figure 4.6, arrows) also reflected their position in SL biosynthesis: first SUR2 in early S, then LAC1 in late S and finally AUR1 in early G2. This sequence further suggested that IPC synthesis might be

synchronised with cell cycle progression but did not reveal a causal relationship between the two processes.

To identify potential transcriptional regulators of SL biosynthesis during the cell cycle, the promoter sequences of the three different enzymes were scanned for transcription factor binding sites (TFBS) with the Yeast Promoter Atlas and YEASTRACT [241,297] (see table 4.2).

Table 4.2: Confirmed transcription factor binding sites (TFBS) in the promoter regions of SUR2, LAC1 and AUR1

The name and binding site (BS) count of the transcription factors (TF), which have verified TFBS in the promoter regions of the three genes, were determined with YEASTRACT and the Yeast Promoter Atlas [241,297]. The potential role of the identified transcription factors in cell cycle progression was assigned from the collected literature.

Gene	TF	Number of BS	TF activity peak during the cell cycle
SUR2	MBP1	2	G1 to S transition [298]
LAC1	SWI4	4	Late G1 [299]
AUR1	GTS1/ABF1	5 and 1	Metabolic oscillations [300]

Both databases contain experimentally verified TFBS in *Saccharomyces cerevisiae*, and the analysis showed that the cell-cycle-regulated transcription factors (TF), MBP1 and SWI4, recognise specific sequences in the promoters of SUR2 or LAC1 and also bind their target *in vivo* [301–303].

None of the publicly available datasets indicated or predicted a binding site of a cell-cycle-dependent TFs in the AUR1 promoter. As the main regulator of AUR1 expression GTS1 is important for metabolic oscillations [300], the correlation between AUR1 expression and cell cycle progression might thus just be an experimental artefact.

In accordance with other expression data [202,304], the tools did not predict an INO2/4, HAC1 or RLM1 binding site in the LAC1 or AUR1 promoter, but YEASTRACT contained one physical interaction between INO4 and the SUR2 promoter.

Together the high rank in Cyclebase.org and the confirmed TFBS in the SUR2 and LAC1 promoters strongly suggested that both are regulated by the cell cycle machinery to increase ceramide production and satisfy the demand of ceramide-dependent processes during the cell cycle, e.g. ER inheritance [165]. For AUR1, the lower rank and missing TFBSs indicated that it might not be a direct target of cell cycle control and that the co-expression of AUR1 with the other

two enzymes (see subchapter 4.5) might correspond to environmental conditions that increase IPC demand but not cell cycle progression.

4.7 SUR2 deficiency perturbed the trafficking of GAP1 in minimal SC medium

As cells divided faster in peptone-supplemented medium, the stipulated role of sphingosine hydroxylation during cell division might explain higher SUR2 expression in peptone-supplemented SC medium but cannot explain the stronger growth defect of SUR2-deficient cells in minimal SC medium (see figure 4.3). This defect possibly resulted from an additional role of sphingosine hydroxylation in nutrient-poor environments. Lower nitrogen consumption and mis-trafficking of membrane proteins have already been reported previously for SUR2-deficient cells [305,306], and mis-trafficking of amino acid transporters could specifically lower amino acid import and growth rate in minimal SC medium.

GAP1 (general amino acid permease 1), for example, is first synthesized and folded at the ER membrane. Without perturbations, it is then transported over the Golgi apparatus and the endosome to the vacuole. If the external conditions require a greater presence of amino acid transporters on the cell membrane, GAP1 is recruited from the vacuole to the plasma membrane to increase amino acid import [307]. Vacuolar localisation therefore indicates a functional folding and trafficking of GAP1 and probably other transmembrane proteins that are processed similarly [117].

As the localisation of similar GFP-tagged proteins has already been used to investigate protein folding and trafficking [306,308], the localisation of GAP1-GFP was subsequently evaluated in wild-type or SUR2-deficient yeast cells from amino-acid-rich (YPD medium) or amino-acid-poor (minimal SC medium) environments.

First, the genomic locus of GAP1 in wild-type and SUR2-deficient cells was C-terminally tagged with a superfolder GFP variant [172], and the functional insertion confirmed with PCR and flow cytometry (see material and methods, subsection 2.6 for DNA extraction, and 2.3 for PCR verification). Colonies from both genotypes, FJ4741.GAP1GFP and FJ4741SUR2Δ.GAP1GFP, were grown in selective medium (SD-Ura) overnight and diluted into minimal SC medium or YPD medium. After 6 hours of exponential growth, the subcellular localisation of GFP in all samples was visualised with epifluorescence microscopy (see figure 4.7).

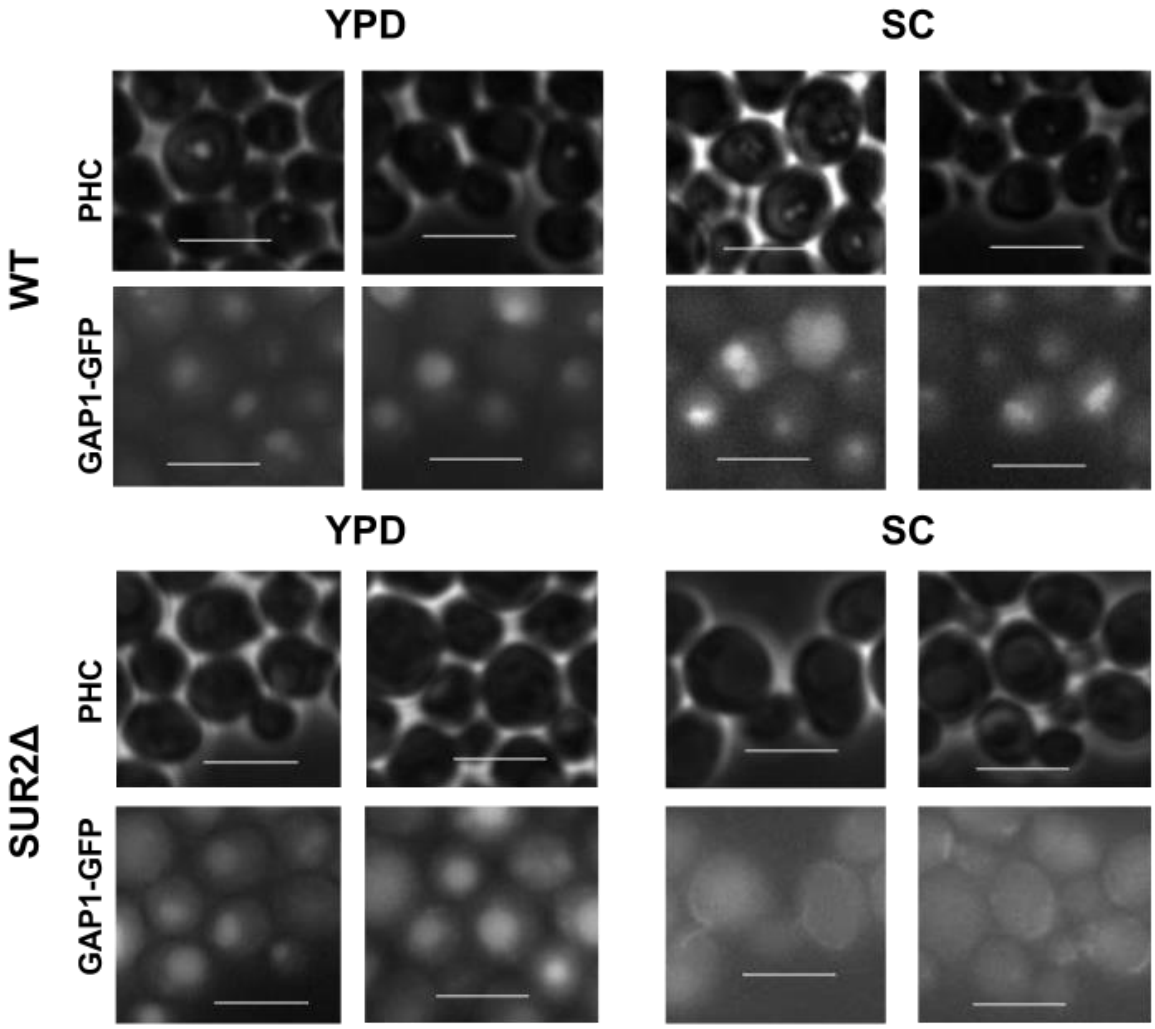

Figure 4.7: GAP1 localisation in wild-type and SUR2-deficient cells in different environments.

The phase contrast (PHC) and GFP fluorescence (GAP1-GFP) of wild-type (FJ4741.GAP1GFP, WT) or SUR2-deficient (FJ4741SUR2Δ.GAP1GFP, SUR2Δ) cells that express an endogenously GFP-tagged GAP1 protein during exponential growth in YPD or SC medium. (Pictures are representative cells for each condition that were observed in three different biological replicates, white bars correspond to 5 µm).

In most wild-type cells from both media, GFP localised exclusively to a circle in the centre of the cell. In SUR2-deficient cells, GFP fluorescence localised to a circle in YPD medium, but was much weaker and accumulated at the cell cortex below the plasma membrane of occasional yeast cells in minimal SC medium.

The GFP localisation in wild-type cells was consistent with trafficking to the vacuole and suggested correct folding and trafficking of GAP1 in peptone-rich and minimal medium. For SUR2-deficient cells, wild-type-like GFP localisation and correct trafficking was only observed in

YPD medium, while the low and cortical GFP fluorescence in minimal medium indicated a perturbed folding or trafficking in this genotype-environment combination.

A genome-wide screen already identified a perturbed trafficking along the secretory pathway in yeast mutants with deficiencies in sphingolipid metabolism, which was attributed to a non-functional Golgi sorting in these mutants [306]. Accordingly, the cortical stripes could match to the trans-Golgi compartment, where GAP1-GFP might be stuck due to a perturbed sphingolipid metabolism.

If this improper trafficking and localisation also extended to other membrane transporters, it would lower the import of growth-limiting amino acids and decrease the growth rate of SUR2-deficient cells in minimal medium (see figure 4.3).

In YPD medium, the wild-type-like localisation of GAP1 suggested that sphingosine hydroxylation is less important for trafficking in amino acid-rich environments. Because the rate of sphingosine synthesis also depends on serine concentration [309], peptone supplementation, which probably increases the serine concentration, might accelerate ceramide production via higher sphingosine levels independent of sphingosine hydroxylation. Restored transporter trafficking and higher external amino acid concentration together might improve amino acid import and reduce the growth deficit of SUR2-deficient cells in peptone-supplemented medium.

4.8 SUR2 deficiency increased PKC activation and transcription of cell wall proteins at an increased growth temperature

Mis-trafficking of membrane proteins and lower IPC synthesis are two ways in which SUR2-deficiency and reduced IPC synthesis could perturb cell wall integrity (CWI) under normal and stress conditions [55,310]. The dynamic reporter for the activity of RLM1, a PKC-dependent transcription factor for cell wall proteins that is activated by cell wall perturbations (see chapter 1 and 3) [311], was subsequently used to assess the impact of sphingosine hydroxylation on cell wall integrity in minimal medium and at elevated growth temperatures, i.e. 39 °C.

Saturated overnight cultures of reporter-carrying wild-type and SUR2-deficient cells, FJ4741.8 and FJ4741SUR2Δ.8, were diluted in minimal SC medium and grown exponentially at 30 °C for 6 hours. The cultures were then diluted and incubated at 39 °C. Before and 45, 120 or 180 minutes after the transfer to the higher growth temperature the reporter fluorescence in both strains was determined with flow cytometry and analysed with FlowJo (see figure 4.8).

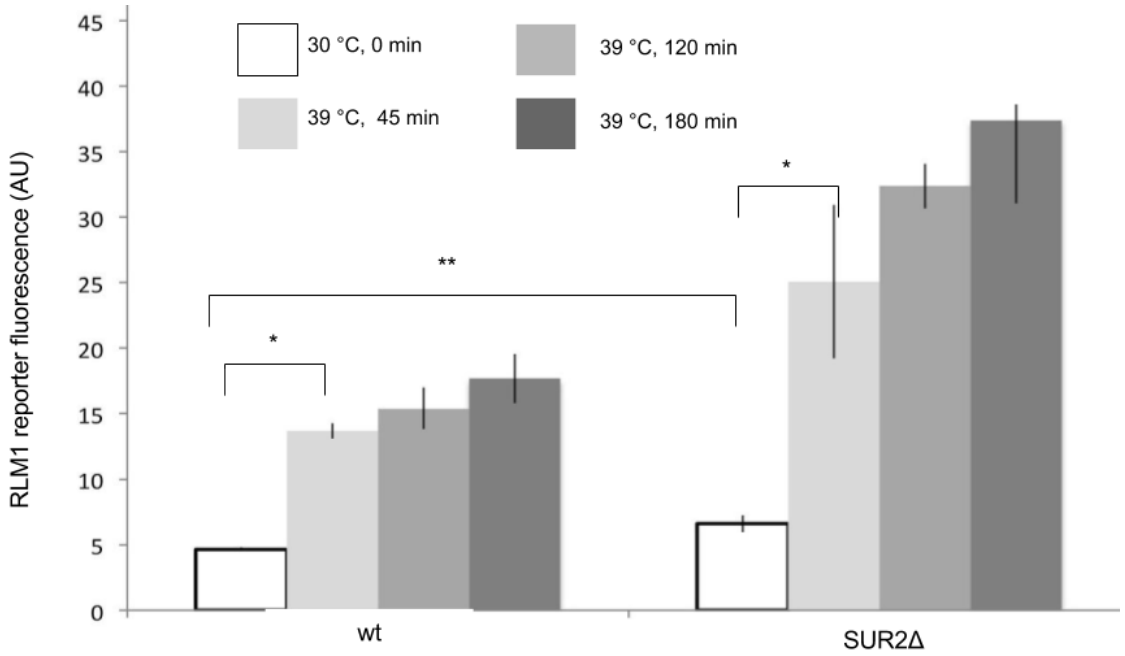

Figure 4.8: RLM1 activity in wild-type and SUR2-deficient cells at normal and elevated growth temperatures
Reporter fluorescence of wild-type and SUR2-deficient cells with the RLM1-reporter construct (BY4741.8, wt and BY4741SUR2Δ.8, SUR2Δ) before (0 min) and 45, 120 and 180 minutes after a temperature change from 30 °C to 39 °C was determined with flow cytometry and analysed with FlowJo (n=3, and the error bars represent the standard deviation between the different biological replicates, double asterisk indicate a significant difference with $p<0.05$ in an unpaired t-test, single asterisk indicate a significant different with $p<0.05$ in a paired t-test.)

When compared to the reporter fluorescence at 30 °C, the higher growth temperature increased the fluorescence of the RLM1-activity reporter in wild-type cells by 150% to 200% in the first three hours after the temperature shift. In SUR2-deficient cells, the reporter fluorescence was slightly higher than that of wild-type cells at normal growth temperatures (~25%) but increased to much higher levels during the incubation at 39 °C (400-500%).

These results indicated that RLM1 activity and cell wall synthesis of SUR2-deficient cells is slightly elevated at 30°C but strongly increased at higher growth temperatures, where it probably compensates existing CWI deficiencies. This result further suggested that SUR2 is less important for cell wall integrity at normal growth temperatures but supported CWI at higher temperatures, when an increased secretion of cell wall proteins, a higher IPC production and heat shock signalling possibly depend on sphingosine hydroxylation for faster ceramide synthesis [312,313].

4.9 HAC1 activity in SUR2-deficient cell remained constant after tunicamycin treatment but increased after ER disruption by DTT

After cell growth and cell wall integrity, the disturbed trafficking and perturbed SL biosynthesis in SUR2-deficient cells might also affect ER homeostasis. The fluorescence of the dynamic HAC1-activity reporter, which indicates UPR activation after ER stress, was subsequently compared between wild-type and SUR2-deficient cells under normal or ER-perturbing conditions to assess the importance of sphingosine hydroxylation for ER homeostasis under normal and challenging conditions.

Overnight cultures from wild-type or SUR2-deficient cells with the HAC1 reporter were diluted in minimal SC medium and exponentially grown for 6 hours. To induce ER stress, the cultures were collected, resuspended and incubated in minimal SC medium with three different chemicals: DMSO as solvent control, 1 µg/ml tunicamycin or 2 mM DTT. After one and three hours, the cellular reporter fluorescence of each sample was determined with flow cytometry and analysed with FlowJo (see figure 4.9).

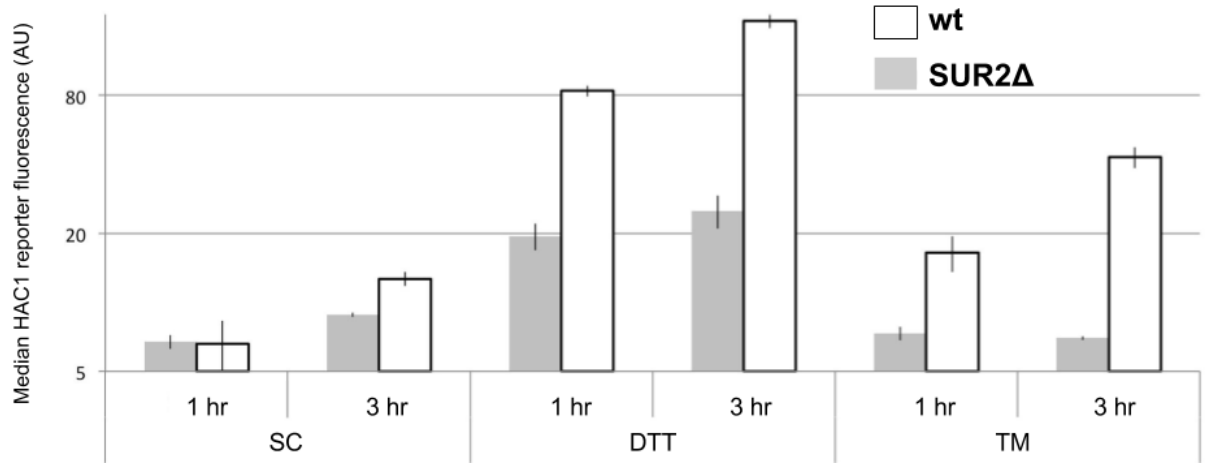

Figure 4.9: HAC1 activity of wild-type and SUR2-deficient cells in normal and ER stress environments

Reporter fluorescence of wild-type and SUR2-deficient cells with the HAC1 reporter construct (FJ4741.1, wt and FJ4741SUR2Δ, SUR2Δ) was determined at different timepoints, i.e. one and three hours, after transfer from minimal SC medium into minimal SC medium (SC) with DMSO, minimal SC medium with 2 mM DTT (DTT) or minimal SC medium with 1 µg/ml tunicamycin (TM) with flow cytometry and analysed with FlowJo (n=3, and error bars indicate the standard deviation between the biological replicates, y-axis in log scale with basis 4, e.g. 1*5, 4*5 and 16*5).

In the DTT-treated samples of both genotypes, the reporter fluorescence after one hour was already higher than in the solvent control, but the effect was stronger in wild-type than in SUR2-deficient cells. Two additional hours further increased reporter fluorescence in cells from both

genotypes. The tunicamycin treatment slightly increased the reporter fluorescence of wild-type cells after one hour and stronger after 3 hours but did not change the reporter fluorescence of the SUR2-deficient cells.

The low reporter fluorescence of both cell types in unperturbed medium indicated a low HAC1 activity and suggested that SUR2 is not required for ER homeostasis in minimal medium. The increased reporter fluorescence in DTT-treated cells indicated a strong UPR activation and suggested (A) that protein unfolding after changes in redox environment disrupted ER homeostasis independent of sphingosine hydroxylation and (B) that sphingosine hydroxylation is not required for UPR activation.

After tunicamycin treatment, the low reporter fluorescence in SUR2-deficient cells and the slower fluorescence increase in wild-type cells indicated no and a delayed UPR activation, respectively. The delayed UPR induction and ER disruption in wild-type cells possibly resulted from a slow accumulation of glycoproteins after tunicamycin treatment [314]. In SUR2-deficient cells, low UPR activity correlated with slow growth in minimal SC medium (see subchapter 4.3) and suggested that the effect of tunicamycin depended on sphingosine hydroxylation or the growth rate. As tunicamycin resistance is generally enriched in slow-growing yeast mutants [315], the ER disruption by tunicamycin might depend on the growth rate rather than on SUR2 specifically.

Overall, from the collected results emerged that SUR2 knock-out reduced IPC synthesis, decelerated growth, caused mis-trafficking and reduced cell wall integrity in minimal SC medium similarly to inositol starvation but had no effect on ER homeostasis [32,51]. For amino-acid-rich medium, the results suggested that sphingosine hydroxylation might be less important for growth but is still upregulated to support the increased ceramide demand during cytokinesis [316].

4.10 HAC1 activation succeeded INO2/4 activation during inositol starvation

In contrast to the positive effect of SUR2 knock-out and slow growth on ER homeostasis after tunicamycin treatment, the inositol auxotrophy of UPR-deficient mutants (see subchapter 4.3) already suggested that ER perturbation and induction of UPR target genes are a critical step in the adaptation to inositol starvation. A lower inositol concentration is not known to directly activate IRE1, and subsequent changes such as a lower AUR1 activity possibly disturb ER homeostasis and induce the UPR after inositol depletion. To better classify the mechanism of UPR activation, the novel reporter proteins were used to compare dynamics of HAC1 activation to that of INO2/4 activation, which directly depends on phosphatidic acid (PA) accumulation [128], after inositol depletion.

To assess transcriptional dynamics, two wild-type strains with different reporter constructs, i.e. one for HAC1 (FJ4741.1) and one for INO2/4 activity (FJ4741.4), were first grown in minimal SC medium. After 6 hours of exponential growth, the cultures were collected, washed and resuspended in fresh minimal SC medium without inositol. Immediately before the medium change and at different timepoints during the adaptation (i.e. 1 hour, 2 hours and 3.5 hours), the reporter fluorescence of cells from each sample was determined with flow cytometry and analysed with FlowJo (see figure 4.10).

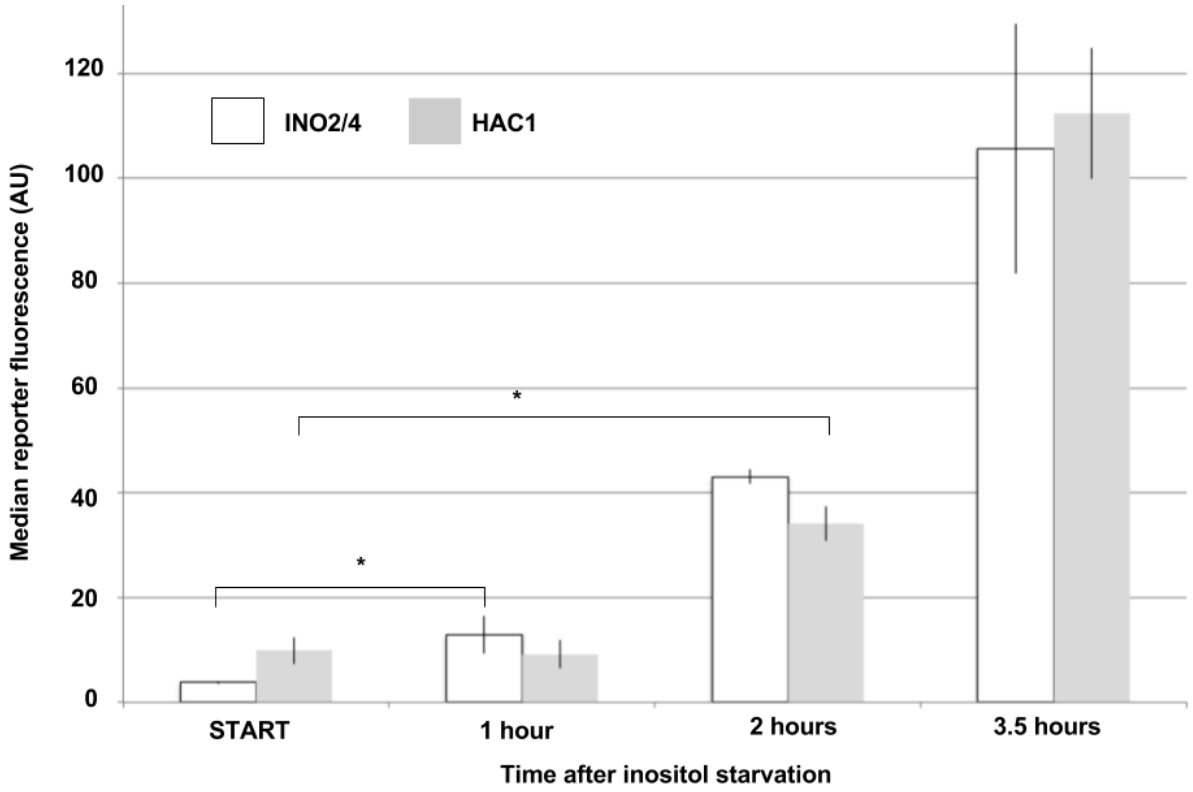

Figure 4.10: HAC1 and INO2/4 activity during inositol starvation after minimal SC medium.
Reporter fluorescence of wild-type cells with the INO2/4 reporter (FJ4741.4, white bars) or HAC1 reporter (FJ4741.1, grey bars) before and at three timepoints during inositol starvation was measured with flow cytometry and analysed with FlowJo (n=3, asterisk indicates significant differences between the fluorescence in a unpaired t-test with $p<0.05$).

The reporter fluorescence of both reporters increased strongly after 3.5 hours of inositol starvation. The INO2/4 reporter fluorescence already increased significantly during the first hour of the treatment, but HAC1 reporter fluorescence did not change during the first hour of the treatment and only increased 2 hours after inositol depletion.
The strong fluorescence of both reporters at later timepoints indicated a high activity of HAC1 and INO2/4 during inositol starvation and suggested that INO2/4 and HAC1 targets are equally

induced after the adaptation to inositol-free environments. The fast increase in INO2/4 reporter fluorescence further proposed that PA accumulation rapidly released INO2/4 from OPI1 inhibition after inositol depletion [129,181]. The time delay between the onsets of both reporters additionally suggested that UPR induction and ER stress either required a higher PA concentration than INO2/4 or did not directly result from PA accumulation.

A negative genetic interaction of the PA synthesizing enzyme DGK1 with HAC1 and IRE1 also suggested that low rather than high PA concentrations disturb ER homeostasis and supported the notion that other changes of phospholipid or sphingolipid metabolism possibly perturbed ER homeostasis during inositol starvation [317].

4.11 AUR1 inhibition perturbed ER homeostasis but ceramide accumulation was not required for UPR activation during inositol starvation

The previous results suggested that even though SUR2 knock-out and inositol depletion lowered IPC synthesis, only inositol starvation perturbed ER homeostasis and triggered UPR activation and that inositol-starvation-specific PA accumulation does not induce ER stress. Therefore, ceramide, i.e. the metabolic intermediate between sphingosine hydroxylation and the inositol-consuming step of SL-biosynthesis, might accumulate and perturb ER homeostasis after inositol starvation or AUR1 inhibition but not in SUR2-deficient cells.

If ER disruption and UPR activation depends on ceramide accumulation, ceramide synthesis inhibition could prevent it. To test this hypothesis, the UPR activity of wild-type cells with a decreased AUR1 activity, i.e. after Aureobasidin A (AbaA) treatment or during inositol starvation, and with or without the inhibition of ceramide synthesis by Fumonisin B1 (FB1) was assessed with the HAC1 reporter construct [82].

Exponential growing wild-type cells with the HAC1 reporter (FJ4741.1) were collected from minimal SC medium and transferred to five different media: minimal SC medium with or without Fumonisin B1 (+ino con and +ino FB1), inositol-free medium with or without 150 nm FB1 (-ino con and -ino FB1) and minimal SC medium with 2 µM AbaA. After three hours, the cellular reporter fluorescence of all samples was determined with flow cytometry and analysed with FlowJo. (Due to the high toxicity and cost of FB1 this experiment could not be conducted in biological replicates) (see figure 4.11).

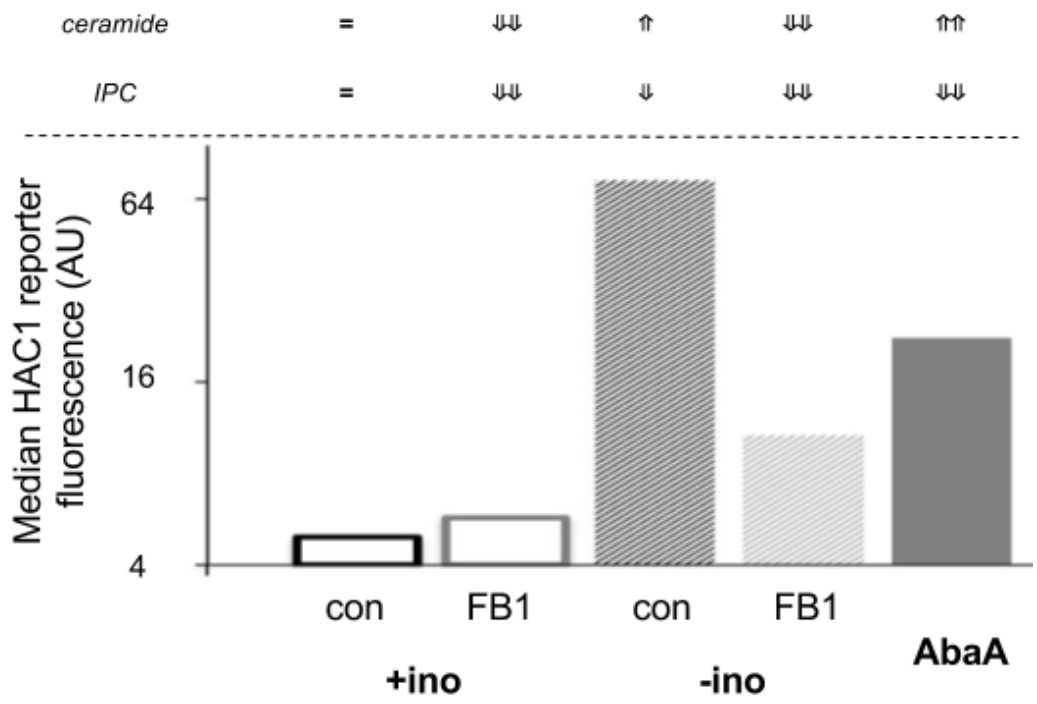

Figure 4.11: HAC1 activity and the assumed SL ceramide levels in wild-type cells during inositol starvation without ceramide biosynthesis or during total AUR1 inhibition

Median reporter fluorescence of wild-type cells with the HAC1 reporter (FJ4741.1) 3 hours after transfer to minimal medium with inositol (+ino, con), minimal medium with inositol and 150 nm Fumonisin B1 (+ino, FB1), minimal medium without inositol (-ino, con), minimal medium without inositol and FB1 (-ino, FB1) or minimal medium with 2 µM Aureobasidin A (AbaA) was measured with flow cytometry and analysed with FlowJo (n=1, log scale with basis 4). The upper two rows indicate the changes of the ceramide and IPC concentration that are stipulated by the action of the different treatments, i.e. decrease (⇓), unchanged (=) and increase (⇑).

The reporter fluorescence increased strongest after inositol starvation without FB1 but also increased during the Aureobasidin A treatment or after inositol depletion with FB1 addition. FB1 alone only slightly increased the reporter fluorescence of wild-type cells.

The increased reporter fluorescence indicated an increased UPR activity in the three conditions with lower AUR1 activity, i.e. AbaA, -ino con and -ino FB1, and suggested that AUR1 inhibition alone is sufficient to disturb ER homeostasis, albeit not to the same extent as inositol starvation. According to the hypothesis, the increased fluorescence in the FB1-treated cells during inositol starvation further suggested that ceramide accumulation is not required for ER disruption. The high toxicity of FB1 might prevent continuous protein synthesis and explain the difference between the reporter fluorescence during inositol starvation with and without ceramide synthesis inhibition.

In previous experiments, ceramide degradation could not rescue the growth defect of IRE1-deficient cells with a reduced IPC synthesis [276], and this also supported that ceramide has only a minor effect on the ER homeostasis during conditions with low IPC production.
Overall, neither ceramide accumulation nor PA accumulation is probably responsible for ER stress and UPR activation after inositol starvation.

4.12 INO2/4 activation after inositol starvation was independent of UPR activation

INO2/4-deficient and UPR-deficient cells are both inositol auxotrophs, but while INO2/4 induces the essential INO1 expression and inositol production [318], the benefit from classical UPR target genes, i.e. chaperones, during inositol starvation is less obvious. UPR-dependent INO2/4 activity could explain the inositol auxotrophy of UPR-deficient strains (see figure 4.3), but the rapid INO2/4 activity and slow UPR induction after inositol depletion rather suggested that INO2/4 activation is independent of UPR activation. To directly test the UPR dependence of INO2/4 activation, the INO2/4 induction of UPR-deficient cells after inositol depletion was determined with the INO2/4 reporter.
HAC1- (BY4741HAC1Δ) and IRE1-deficient (BY4741IRE1Δ) cells were transformed with the INO2/4 reporter construct and successful insertions selected on histidine-free medium. For inositol depletion, overnight cultures with reporter-containing wild-type (FJ4741.4) or UPR-deficient (FJ4741HAC1Δ.4 and FJ4741IRE1Δ.4) cells were diluted in minimal SC medium and collected after 6 hours of exponential growth. The cells were then washed and cultured in inositol-free medium. The cellular reporter fluorescence immediately after the medium change and at different timepoints during the adaptation was measured with flow cytometry and analysed with FlowJo (see figure 4.12)

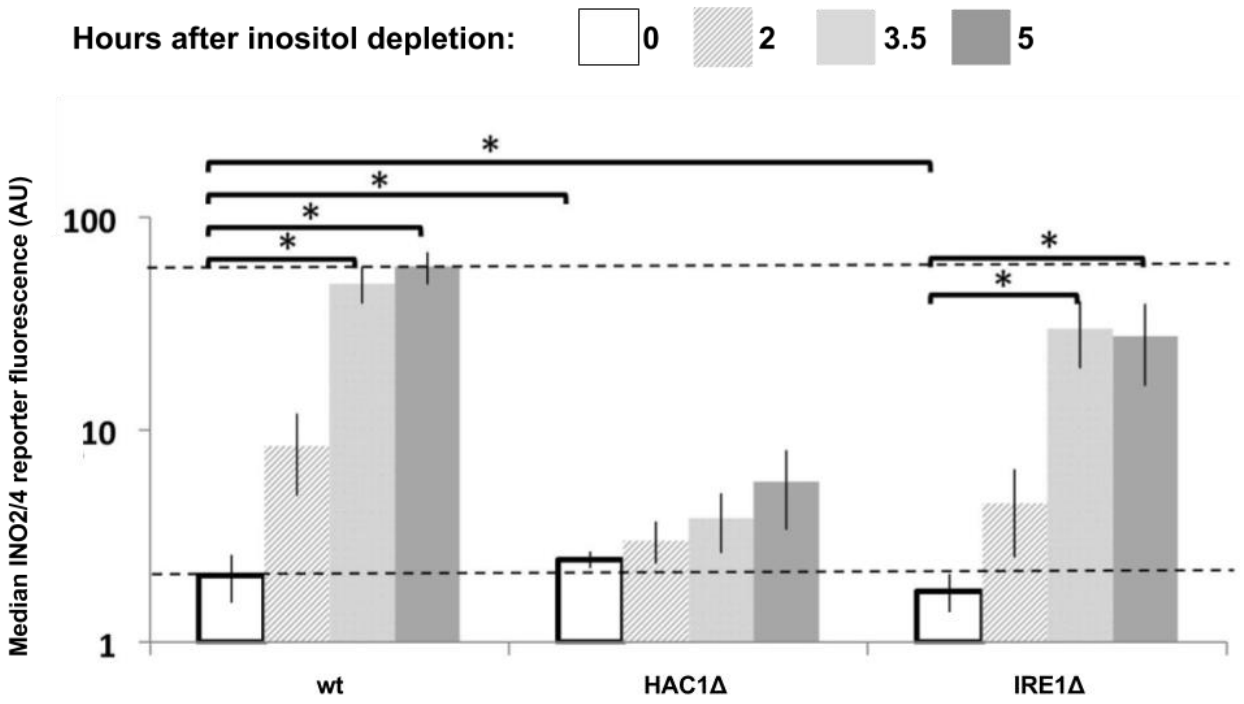

Figure 4.12: INO2/4 activity of UPR-deficient cells during inositol starvation

Median fluorescence of wild-type (wt), HAC1- (HAC1Δ) and IRE1-deficient (IRE1Δ) cells with the INO2/4-activity reporter at different timepoints during inositol starvation was determined with flow cytometry and analysed with FlowJo (n=3, error bars indicate the standard deviation between the biological replicates and asterisks indicate statistically significant differences between different strains or conditions, y-axis in log scale with basis 10).

INO2/4 reporter fluorescence of the HAC1-deficient cells only increased slightly during inositol starvation, but the reporter fluorescence of IRE1-deficient cells increased strongly and with dynamics similar to wild-type cells during the first 3.5 hours of the treatment.

For IRE1-deficient cells, the increased reporter fluorescence indicated an increased INO2/4 activity and suggested that INO2/4 activity and INO1 expression after inositol starvation are independent of UPR activation.

The different fluorescence of IRE1-deficient cells and wild-type cells at later timepoints agreed with reported differences of the INO1 mRNA level [319], and could result from a UPR-dependent, long-term activity of INO2/4 or the increased fraction of dead cells in the inositol-auxotroph mutant. Previous experiments already indicated a lower PA concentration in HAC1-deficient cells [181], and this difference might explain the low INO2/4 activity of HAC1-deficient cells after inositol starvation.

4.13 UPR activation was necessary for RLM1 induction after inositol removal from minimal SC medium

The previous experiments could neither determine the trigger for UPR activation nor explain auxotrophy of UPR-deficient cells in inositol-free medium. Previous work already indicated a perturbed CWI and PKC activation during inositol starvation, which possibly resulted from lower sphingolipid biosynthesis [55]. Accordingly, UPR activation could either be required to maintain ER homeostasis after PKC activation or actually reduce sphingolipid production via ORM1/2 expression and trigger PKC activation [156]. The UPR should then either precede or succeed PKC activation, and UPR-deficient strains should either have a disturbed CWI and strong PKC signaling or a lower PKC activation during inositol starvation.

The PKC dynamics in wild-type and UPR-deficient cells during inositol starvation were subsequently investigated to distinguish between these two possible roles of UPR activation and maybe understand the inositol auxotrophy of UPR-deficient cells. Wild-type and UPR-deficient yeast cells with the RLM1 reporter (FJ4741.8, FJ4741IRE1Δ.8 and FJ4741.HAC1Δ.8) were collected during exponential growth in minimal SC medium and resuspended in inositol-free or inositol-containing SC medium. The reporter fluorescence three and five hours after the medium change was determined with flow cytometry. As a positive control for reporter fluorescence and PKC activation, cells from all genotypes were also incubated for 3 hrs at 39 °C, and their fluorescence measured with flow cytometry (see figure 4.13).

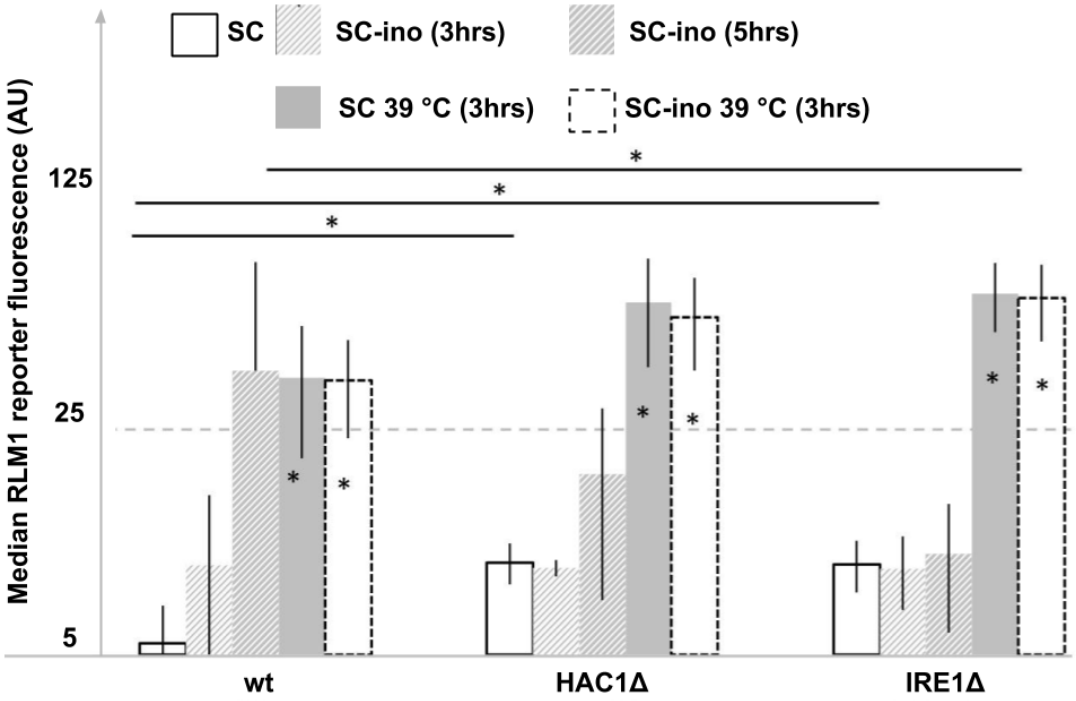

Figure 4.13: RLM1 activity in UPR-deficient cells after inositol starvation or temperature elevation.
Reporter fluorescence of wild-type (wt), HAC1- (HAC1Δ) or IRE1-deficient (IRE1Δ) cells with the RLM1 reporter construct (FJ4741.8, FJ4741HAC1Δ.8 or FJ4741IRE1Δ.8) at different timepoints after inositol starvation at 30 °C, i.e. 3 and 5 hours (SC-ino), or 3 hours after temperature elevation to 39 °C (SC 39 °C) was determined with flow cytometry and analysed with FlowJo (n=3, error bars represent the standard deviation between the biological replicates, asterisk on a line indicate significant differences between two samples $p<0.05$ and asterisk in a bar indicate significant difference between a sample and the SC control, log scale with basis 5).

In wild-type cells, the reporter fluorescence increased three hours after the transfer to higher growth temperatures but only after 5 hours in inositol-free medium at 30 °C. The reporter fluorescence of both UPR-deficient strains similarly increased after 3 hours at 39 °C but did not change significantly after 5 hours in inositol-free medium at 30 °C.

In wild-type cells, the delayed reporter fluorescence during inositol starvation indicated late RLM1 activation and suggested that cell wall perturbation succeeded INO2/4 and UPR induction after inositol depletion (see figure 4.10). For UPR-deficient cells, the increased reporter fluorescence at normal and higher growth temperatures indicated a functional PKC pathway and stronger RLM1 activity than in wild-type cells. In line with previous reports [24], this result suggested that ER homeostasis and UPR activation support CWI during normal and stress conditions.

However, the late PKC activation in wild-type or missing one in UPR-deficient cells implied that the UPR possibly decreases SL biosynthesis and contributes to PKC activation but is not only induced after PKC activation to maintain ER homeostasis.

4.14 NBD fluorescence increased after AUR1 inhibition or during inositol starvation independent of UPR activation

The missing RLM1 activation in UPR-deficient cells (see figure 4.13) is in line with the role of some UPR target genes, e.g. ORM2, in sphingolipid metabolism and cell wall integrity [135,304]. To better evaluate the role of UPR activation in sphingolipid metabolism during inositol starvation, I decided to determine the impact of UPR activation on the rise of NBD fluorescence during inositol starvation, which indicates changes in lipid metabolism and possibly responds to a lower IPC synthesis, with UPR-inducing conditions and inositol-starved UPR-deficient strains.

Exponentially growing, wild-type and UPR-deficient cells, i.e. BY4741, BY4741HAC1Δ and BY4741IRE1Δ, were collected from minimal SC medium and stained with NBD-C6-ceramide. Afterwards, the stained cells were cultured for three additional hours in four different media with NBD-C6-ceramide supplementation: minimal SC medium, minimal SC medium without inositol, minimal SC medium with 2 mM DTT and minimal SC medium with 2 µM Aureobasidin A. The cellular NBD fluorescence was determined with flow cytometry and analysed with FlowJo (see figure 4.14).

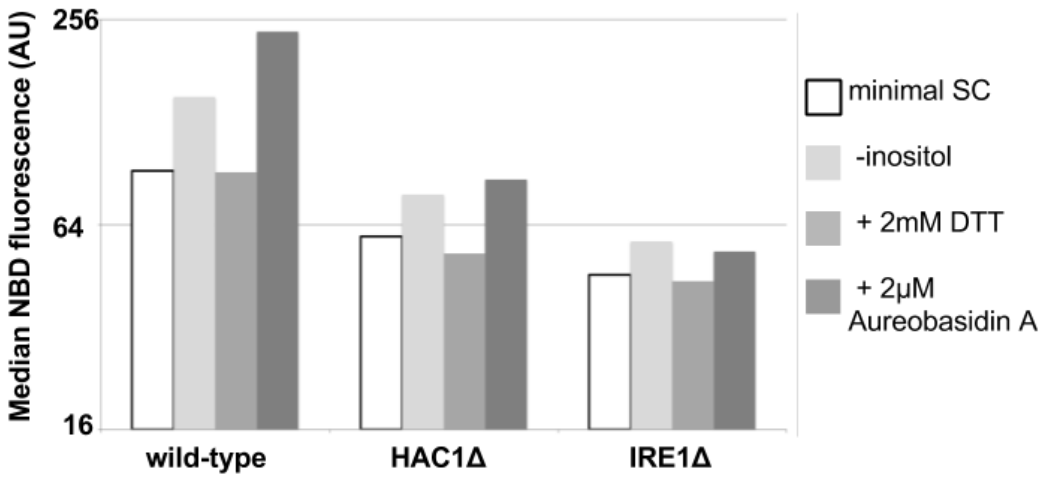

Figure 4.14: Median NBD-ceramide fluorescence in UPR-deficient strains after inositol depletion.

Median NBD fluorescence of wild-type (wt), HAC1- (HAC1Δ) or IRE1-deficient (IRE1Δ) cells after NBD-C6-ceramide staining and 3 hours in minimal SC medium (SC), minimal SC medium without inositol (-inositol), minimal SC medium with 2 mM DTT or 2 µM Aureobasidin A (n=1, y-axis in log scale with basis 4).

Like in the wild-type cells, the median NBD fluorescence of UPR-deficient cells was higher after the growth in inositol-free and Aureobasidin A-supplemented medium than after minimal SC medium or the DTT treatment.

Firstly, the lower NBD fluorescence of UPR-deficient cells probably indicated a generally perturbed lipid metabolism and highlighted the importance of ER homeostasis for lipid metabolism [46]. However, the increased NBD fluorescence of UPR-deficient cells after inositol starvation indicated further lipid metabolism changes and suggested together with the stable fluorescence in DTT-treated wild-type cells that UPR activation is neither required nor sufficient to trigger the changes in lipid metabolism that increased NBD fluorescence.

Overall, from the presented results emerged that UPR activation is neither required for INO2/4 activation or to change NBD fluorescence but still necessary for cell wall perturbation and PKC activation after inositol depletion.

4.15 Sphingosine hydroxylation or fast growth was required for UPR activation after inositol depletion

The smaller relative increase in NBD fluorescence of slow-growing SUR2-deficient mutants after inositol depletion from poor media (see subchapter 4.3) suggested that sphingosine hydroxylation or fast growth might contribute to the effect of inositol starvation on lipid metabolism, and they could also be important for other effects of inositol starvation such as the ER perturbation. The HAC1 reporter and the two different media compositions that enabled slow or fast growth of SUR2-deficient cells (see subchapter 4.3) were used to investigate the effect of SUR2 activity and cell growth on ER homeostasis after inositol depletion or AUR1 inhibition.

Before the treatment, wild-type and SUR2-deficient yeast cells with the HAC1-reporter (FJ4741.1 and FJ4741SUR2Δ.1) were exponentially grown in minimal or peptone-supplemented SC medium. Both cultures were then collected, washed and transferred to minimal SC medium with inositol (SC), without inositol (SC-ino) or with 2 µM Aureobasidin A (AbaA). After three hours, the cellular reporter fluorescence of all samples was determined with flow cytometry and analysed with FlowJo (see figure 4.15).

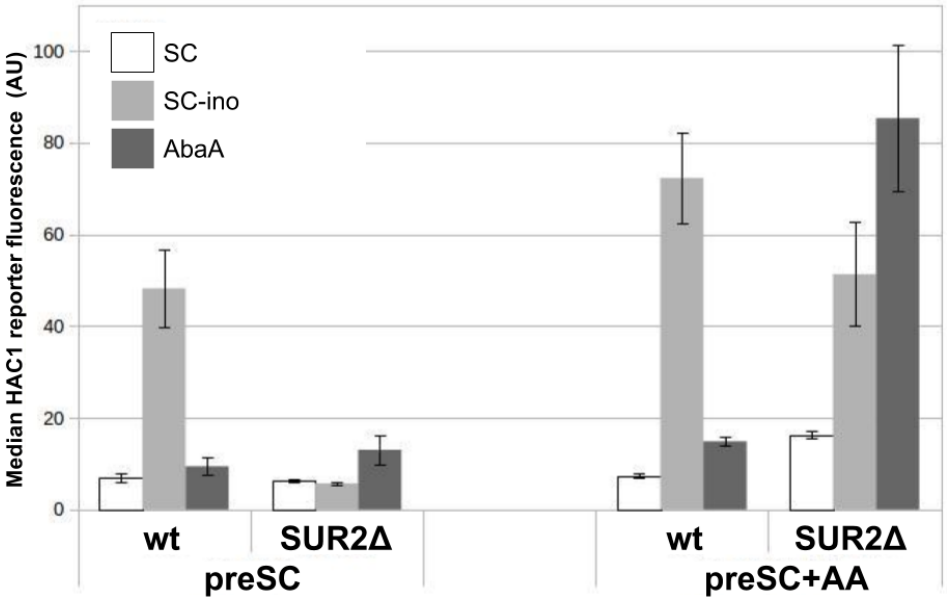

Figure 4.15: HAC1 activity of SUR2-deficient cells from minimal or peptone-supplemented SC medium during inositol starvation or after Aureobasidin A treatment.

Reporter fluorescence of wild-type (wt) or SUR2-deficient (SUR2Δ) cells with the HAC1-reporter construct 3 hours after transfer from minimal (preSC) or peptone-supplemented (preSC+AA) SC medium to minimal SC medium (SC), minimal SC medium without inositol (SC-ino) or minimal SC medium with 2 µM Aureobasidin A (AbaA) was determined with flow cytometry and analysed with FlowJo (n=3, error bars indicate the standard deviation between the different biological replicates).

After preculture in minimal SC medium, the HAC1 reporter fluorescence of wild-type cells was higher in inositol-free than inositol-containing medium, while the reporter fluorescence of slow-growing SUR2-deficient cells remained low in inositol-free and inositol-containing medium (figure 4.15, preSC).

After preculture in peptone-supplemented SC medium (preSC+AA), the reporter fluorescence of both cell types was much higher in inositol-free than in inositol-containing minimal medium. Interestingly, the reporter fluorescence of SUR2-deficient cells from the peptone-supplemented preculture in minimal SC medium with Aureobasidin A was much higher than the reporter fluorescence of equally treated wild-type cells.

The strong increase in reporter fluorescence after AUR1 inhibition and inositol starvation in fast-growing SUR2-deficient cells from peptone-supplemented medium indicated a strong UPR activation and suggested that sphingosine hydroxylation is not required for ER stress in both treatments. The low reporter fluorescence of slow-growing, SUR2-deficient cells from minimal SC medium after inositol starvation indicated no UPR activation and suggested that fast growth probably disrupted ER homeostasis in wild-type cells during inositol starvation.

4.16 INO2/4 activation after inositol depletion required sphingosine hydroxylation or fast growth

The non-disturbed ER homeostasis indicated an interesting phenotype of slow-growing cells in inositol-free medium. At slow-growth, endogenous inositol production by INO1, for example, might prevent inositol starvation, PA accumulation and make transcriptional changes after inositol depletion superfluous. The INO2/4 reporter was subsequently used to evaluate the impact of slow growth and SUR2 deficiency on PA accumulation and INO2/4 induction.

To this end, wild-type and SUR2-deficient INO2/4 reporter cells (FJ4741.4 and FJ4741SUR2Δ.4) were pre-cultured in minimal or peptone-supplemented SC medium. After 6 hours, the exponentially growing cells were collected and cultured in inositol-free medium. The reporter fluorescence immediately and three hours after the medium change was determined with flow cytometry and analysed with FlowJo (see figure 4.16).

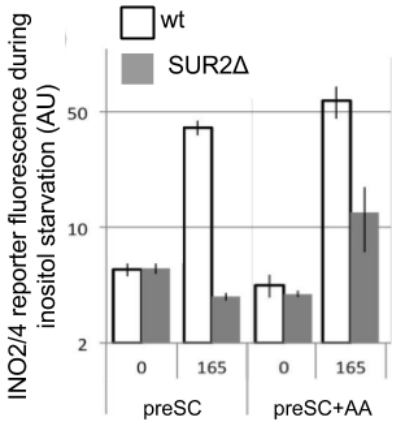

Figure 4.16: INO2/4 activity of SUR2 deficient strains from different preculture conditions during inositol starvation.

Reporter fluorescence of wild-type or SUR2-deficient cells with the INO2/4 reporter construct immediately (0) or 165 minutes (165) after the transfer from minimal (preSC) or peptone-supplemented SC medium (preSC+AA) to inositol-free medium was determined with flow cytometry and analysed with FlowJo (n=3, error bars represent the standard deviation between the different biological replicates, y-axis in log scale with basis 5, e.g. 1*2, 5*2, 25*2)

The reporter fluorescence of wild-type cells from both preculture conditions and SUR2-deficient cells from the peptone-supplemented preculture increased during inositol starvation. Only the fluorescence of SUR2-deficient cells from minimal SC medium remained low after inositol depletion. The low reporter fluorescence of SUR2-deficient cells from minimal SC medium indicated a low INO2/4 activity and suggested that endogenous inositol production is sufficient to avoid PA accumulation in slow-growing, SUR2-deficient cells. The strong INO2/4 induction in

SUR2-deficient cells after peptone-supplemented medium further suggested that fast growth not SUR2 activity is required for inositol depletion, PA accumulation and ER disruption during inositol starvation.

4.17 Discussion

In this chapter, the previously developed reporter constructs and genetic mutants were used to investigate the physiological consequences of two sphingolipid metabolism perturbations, inositol starvation and SUR2 deficiency. SUR2 knock-out is a genetic modification that removes an optional enzymatic step of SL biosynthesis and is unlikely to occur in nature [320]. Inositol starvation is a physiological state of *Saccharomyces cerevisiae*, which is triggered by the lack of inositol in the environment and affects SL metabolism but also other cellular processes [23,202]. By comparing the phenotypes of these two perturbations, I aimed to better understand the role of sphingolipids in different cellular processes and to assign the transcriptional changes during inositol starvation to SL metabolism or independent processes.

Growth rate and NBD fluorescence were initially measured to gauge the impact of both perturbations on overall cell physiology and lipid metabolism, respectively. For inositol starvation, the small growth defect suggested that wild-type cells are well adapted to inositol-less conditions, and the rise of NBD fluorescence most probably resulted from a reduced IPC synthesis that was reported earlier [55]. However, the results from SUR2-deficient cells, i.e. higher NBD fluorescence at steady-state and strong growth defect in medium without peptone supplementation, revealed a peptone sensitivity and a lipid perturbation that could only be understood through further experiments.

The GAP1 localisation in SUR2-deficient cells implied that the growth defect in minimal medium probably resulted from a perturbed trafficking of membrane transporters that is re-established by a faster sphingosine synthesis after peptone supplementation [309]. In addition to the increased NBD fluorescence and the smaller rise after Aureobasidin A inhibition, the increased PKC activation at elevated temperatures supported the hypothesis that sphingosine hydroxylation also accelerates IPC synthesis through higher ceramide levels [280]. Additionally, the previously reported increase in the MIPC to IPC ratio of SUR2-deficient mutants resembles the changes after inositol starvation and could equally result from decreased IPC synthesis [55,320]. However, conclusive results should be obtained with quantitative lipidomics of SUR2-deficient cells to reveal the impact of sphingosine hydroxylation on lipid metabolism kinetics.

Increased RLM1 activity further suggested that SUR2 deficiency increased PKC activity and probably aggravated the CWI perturbation at higher temperatures. The growth defect after SUR2

knock-out in other cell wall perturbing conditions, e.g. high salt concentrations or caffeine supplementation [315,321,322], supported the notion that sphingosine hydroxylation is already required for cell wall integrity at normal temperatures. As other reports already highlighted the role of later steps of IPC synthesis for cell wall integrity [55,276], cell wall perturbation can probably be attributed to a lower IPC synthesis in SUR2 knock-out and inositol-starved cells.

The mis-trafficking of membrane proteins that was observed in SUR2-deficient cells agrees with the mis-trafficking after other perturbations of SL biosynthesis. Together with the Aureobasidin A sensitivity of cells with a perturbed protein secretion [270,276,306], it highlighted the close interaction between protein secretion and SL biosynthesis.

Interestingly, similar trafficking defects were also reported for mutants with a perturbed ergosterol metabolism [306]. Because perturbations of SL metabolism also affect ergosterol metabolism and vice versa [85,323], it is currently impossible to attribute mis-trafficking to one of the two processes. To address this question, it might help to test if external ergosterol and sphingolipid supplementation can rescue the mis-trafficking phenotype after genetic perturbations of SL metabolism, ergosterol metabolism or both.

However, based on the current knowledge, vesicle trafficking is less likely to depend on sphingolipids, which reside in the outer leaflet of membranes, than on ergosterol, which increases membrane rigidity and facilitates membrane fusion complex assembly [324–327]. Moreover, ergosterol directly binds to several protein domains and could thereby recruit regulatory proteins for vesicle transport [328,329].

In addition to the role of SL metabolism in protein secretion and cell wall integrity, the transcriptional regulation of SUR2 and LAC1 suggested increased ceramide synthesis during the budding process, where it is necessary to establish the diffusion barrier between the bud and the mother cell [165]. Mature sphingolipids could further stabilise the plasma membrane of the emerging bud [330]. Such an IPC-dependent process could also cause the elongated G2 phase of inositol-starved cells [331].

The main difference between inositol starvation and SUR2 knock-out was their effect on UPR activation and ER homeostasis. While SUR2 deficiency and slower growth seemed to promote ER homeostasis after tunicamycin treatment, the presented results indicated that inositol starvation disturbed ER homeostasis and activated the UPR probably independent of ceramide accumulation and other SL-independent rearrangements of lipid metabolism. Interestingly, the ratio between two major phospholipids, i.e. phosphatidylcholine (PC) and phosphatidyl-ethanolamine (PE) increases during inositol starvation [181], and their balance is critical for ER homeostasis [46]. Moreover, genetic modifications, such as overexpression of a PC-degrading

enzyme or knock-out of the choline kinase, which lower the PC concentration, rescue the inositol auxotrophy of UPR-deficient strains [181,185]. Accordingly, this change of PL metabolism is more likely than ceramide accumulation to disrupt ER homeostasis and necessitate UPR activation after inositol removal. As the relative amount of PC is even higher in UPR-deficient strains [181], lipid enzymes among the HAC1 targets possibly limit PC accumulation or increase PE synthesis after the transmembrane domain of IRE1 detected the changed ratio [156,179,332,333].

While conventional reporters for INO2/4, HAC1 and RLM1 activity could also show that lower SL biosynthesis primarily perturbs CWI during inositol starvation [55], the dynamic reporters allowed to assess the temporal sequence of events after inositol starvation. The results suggested that a UPR-independent INO2/4 activation was probably triggered by PA accumulation rapidly after inositol removal, while ER disruption, UPR activation and increased NBD fluorescence depended on a slower change in the lipid metabolism. According to the results, the perturbation of cell wall integrity and RLM1 activation were even later steps in the adaptation process [51].

However, this temporal sequence is no indicator for the causal connections, which are necessary to understand the interaction between the three signaling pathways during the adaptation to inositol starvation. Interestingly, OPI1-deficient cells like inositol-starved wild-type cells have a permanently increased INO2/4 activity and activated UPR [196,334]. INO2/4 activation might thus trigger changes in lipid metabolism, e.g. increase the PC to PE ratio via OPI3 and CHO2 expression [202], that then perturb ER homeostasis and causally connect the immediate effects of inositol depletion, i.e. PA accumulation, to the later changes.

As PKC activation during inositol starvation most probably resulted from decreased SL biosynthesis, the missing RLM1 activation of UPR-deficient strains highlighted a connection between mid-term UPR activation and long-term CWI disruption that might rely on ORM1/2 expression. However, the classical PKC targets are not triggered during a normal UPR response [304], and it is thus very unlikely that UPR activation and ORM production can sufficiently lower SL biosynthesis to perturb CWI and trigger PKC activation independent of inositol depletion. Accordingly, increased NBD fluorescence of UPR-deficient strains and constant NBD fluorescence of wild-type cells after ER disruption also argued against a dominant role of UPR activation in sphingolipid metabolism. As PKC activation, which probably indicated CWI perturbation, was only observed several hours after inositol depletion, continuous cell growth and cell division, which are enabled by UPR activation, might actually perturbed cell wall integrity.

After all, the work in this chapter has shown that the transcriptional adaptation after inositol depletion is not switch-like but rather a sequence of events, which is determined by causal connections between the signaling pathways that are only partially understood (see figure 4.17).

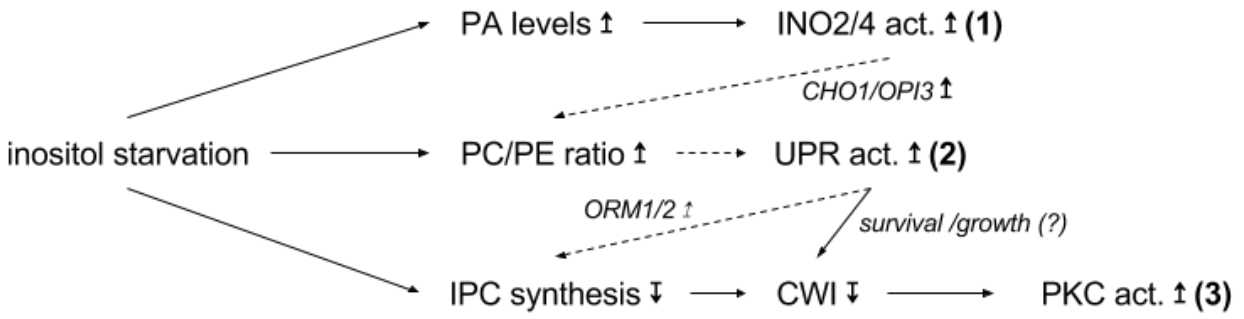

Figure 4.17: The temporal order and the causal connection between the metabolic changes and signaling events after inositol depletion.

Solid arrows indicate experimentally verified causal connections. Dashed arrows indicate new causal connection that were proposed after a comparison of the results of this chapter with the collected literature, and the italic gene names indicate possible actors for these connection. The numbers indicate the temporal sequence that was determined in this project. (PA: phosphatidic acid, PC: phosphorylcholine, PE: phosphorylethanolamine, IPC: inositol phosphorylceramide)

The missing HAC1 activity and INO2/4 activity in slow-growing SUR2-deficient cells further indicated that fast growth actually triggered transcriptional adaptation and agree with the hypothesis that inositol-less death of inositol-auxotrophic strains results from an imbalance between macromolecule synthesis and membrane synthesis [335].

5 Population heterogeneity and adaptation to gradual ER stress

5.1 Introduction

Adaptation is the basic mechanism that enables organisms to thrive in a changing environment. After sensing an environmental change, *S. cerevisiae* mainly uses transcriptional but also post-transcriptional regulation to adjust its metabolism to the demands of the new environment [243,336]. Qualitatively different stresses are detected by specific sensors and trigger different transcriptional responses. However, it is less clear how quantitatively-different stresses are distinguished and how cells respond to them.

The unfolded protein response (UPR) is a highly conserved adaptation mechanism that enables cells to maintain ER homeostasis in the face of increased protein secretion or impeded protein folding through an increased production of ER-resident chaperones and other compensative measures [156,180]. An initially proposed feedback loop involved the linear sensing of unfolded proteins and allowed the cell to respond adequately to quantitatively different perturbations. However, this model is hard to reconcile with the switch-like activation mechanism of the sensory protein, IRE1, that has been reported more recently [50,149,150,337].

To overcome this problem and understand the mechanism that enables cells to deal with different levels of ER stress, researchers have focused on the molecular interaction between IRE1 and other proteins or signaling pathways. This approach has revealed a direct interaction between IRE1 and ER chaperones, which can explain the temporal decline of UPR activity after the initial activation, or cross-talk with other signaling pathways, which enables very strong UPR activation in the presence of multiple environmental stresses [154,338–340]. However, these additional components and interactions complicated the simple and elegant model of adaptation and are probably not conserved alongside the UPR in other organisms.

Nevertheless, an alternative mechanism could enable yeast populations to deal with different levels of ER stress despite a simple switch-like UPR activation: temporal heterogeneity. Instead of keeping the same intermediate UPR level for their entire life, cells could activate the full UPR during a limited time and benefit from the increased ER capacity afterwards [31,341]. It is unlikely that all cells respond with the same UPR activity pattern, and asynchronous expression dynamics in single cells probably lead to a heterogeneous UPR activation in the overall population at a given time [342].

Even though temporal heterogeneity is a tempting theory that could apply to different adaptation mechanisms and other organisms, it also presupposes more complex organisms, which do not maintain a single steady state throughout their life but proceed through different states over time

[343]. Such multiple states are established during cell cycle progression of *S. cerevisiae,* but the experimental evidence for temporal differences in UPR activation are sparse [194,195,293].
Similar to temporal heterogeneity, permanent differences between individual cells in the population, i.e. cellular heterogeneity, could also result in an intermediate average UPR activity but seem less likely in autonomous, unicellular organisms such as budding yeast.
Previous studies focused on strong ER stress or population-wide responses and might have overlooked the differences between individual cells at low ER stress [43]. In this study, the internal and external conditions that set the ER stress level were first explored, before an actively degraded reporter protein was used to investigate the molecular basis of the transient differences in the transcriptional response of single cells during the adaptation. Finally, a quantitative model was developed to simulate the impact of the observed changes on the permanent characteristics of the adapted population.

5.2 ER stress from tunicamycin correlated with its concentration and did not require UPR activation at the IC50 value of the affected biochemical reaction

ER stress and UPR activation can be achieved with different experimental protocols, e.g. protein overexpression, inositol starvation or chemical treatment. In contrast to binary stresses like inositol starvation, the degree of chemically-induced ER stress, i.e. via tunicamycin and DTT, can be adjusted through the concentration [43]. However, most previous investigations still used saturating chemical concentrations to achieve a complete and fast UPR activation, and the scaling between concentration and ER stress for different chemicals remained unknown.
Tunicamycin inhibits a certain step of protein glycosylation, i.e. the transfer of glucose-N-acetyl phosphate to the carrier lipid dolichol phosphate, which is catalysed by ALG7 in *S. cerevisiae* [314]. As the IC50 value of the pig homologue of ALG7 is around 100 ng/ml of tunicamycin [113], concentrations around and above this value might lead to different degrees of ALG7 inhibition and induce quantitatively different levels of ER stress. Quantitatively different ER perturbations should then differ in the growth inhibition of wild-type cells and might also differ in their ability to prevent the growth of UPR-deficient cells.
To quantify the scaling between tunicamycin concentration and ER stress, the growth rates of wild-type and UPR-deficient cells at different tunicamycin concentrations above the biochemical IC50 value (100 ng/ml) were determined.
Exponentially growing wild-type (BY4741) and HAC1-deficient (BY4741HAC1Δ*)* cells from YPD medium were diluted into 96-well microtiter plates with YPD medium and different concentrations of tunicamycin (100, 200, 500 and 1000 ng/ml) or dimethyl sulfoxide (DMSO, solvent control).

Every 5 minutes during a 30-hour incubation, the OD600 of every well was measured and the growth curve used to calculate the exponential growth rate of each culture (see materials and methods, section 2.11 for details). The relative growth rate of each strain at every tunicamycin concentration was then defined as the ratio between the growth rate in YPD medium with tunicamycin supplementation and the growth rate in YPD medium with DMSO (see figure 5.1).

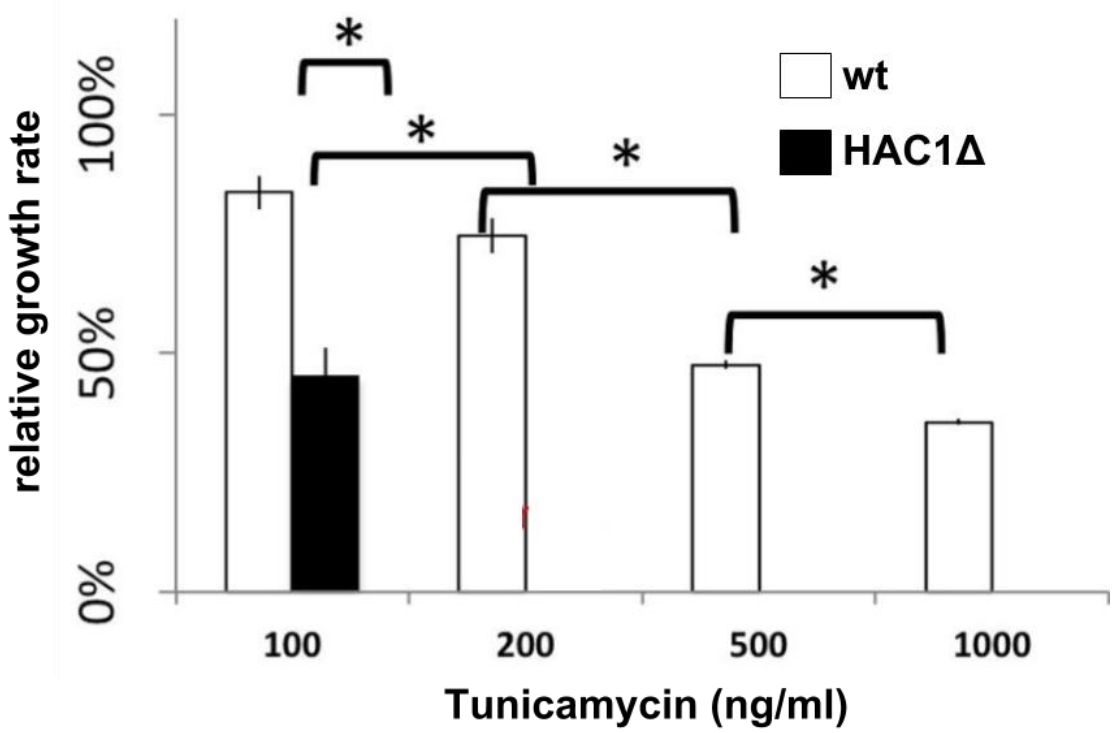

Figure 5.1: Growth rate of wild-type and UPR-deficient yeast strains in YPD medium with different tunicamycin concentrations.

Exponential growth rate of wild-type (BY4741, wt: white bars) and HAC1-deficient (BY4741HAC1Δ, HAC1Δ: black bars) cells in different tunicamycin concentrations was determined from the OD600 curves of a 30-hour incubation in a 96-well microtiter plate. The relative growth rate for each genotype was subsequently calculated as the ratio between its growth rate at a certain tunicamycin concentration and its growth rate in YPD medium with DMSO (solvent control). HAC1-deficient cells failed to grow above 100 ng/ml tunicamycin and their relative growth was therefore not determined. (n=3, and the error bars indicate the standard deviation between the biological replicates; asterisks indicate significant differences $p<0.05$ with student's t-test).

Wild-type and HAC1-deficient cells were able to grow at 100 ng/ml tunicamycin, but with very different relative growth rates: 100 ng/ml tunicamycin reduced the growth rate of wild-type cells by 20% and that of HAC1-deficient cells by 55% when compared to their growth rate in YPD medium. Higher tunicamycin concentrations further reduced the growth rate of wild-type cells and prevented the exponential growth of HAC1-deficient cells (see figure 5.1).

The stronger effect of tunicamycin on the HAC1-deficient cells suggested that all tunicamycin concentrations primarily induced ER stress. The different growth rates of the wild-type cells thus indicated different ER stress levels that scaled with the tunicamycin concentration from 100 to 1000 ng/ml.

5.3 High tunicamycin concentrations triggered uniform UPR activation and reduced ribosome expression, but low tunicamycin concentrations only triggered heterogeneous UPR activation

The slow growth of UPR-deficient cells at 100 ng/ml tunicamycin suggested that UPR activation is not essential but still beneficial at this level of ER stress. The HAC1-activity reporter and the control reporter, i.e. a similarly constructed reporter with a promoter from a ribosomal gene (RPL19A) that is strongly expressed and not directly regulated by UPR, were subsequently used to assess the transcriptional response of wild-type cells at different tunicamycin concentrations (see chapter 3.4).

Exponentially growing wild-type cells with the HAC1-activity reporter (FJ4741.1) or the control reporter (FJ4741.25) in YPD medium were diluted and split into fresh YPD medium with DMSO (organic solvent control) or different tunicamycin concentrations (100, 200 and 400 ng/ml). After 2.5 hours, the cellular reporter fluorescence of both strains was measured at each tunicamycin concentration using flow cytometry, and the distribution of the reporter fluorescence was then analysed using FlowJo (see figure 5.2).

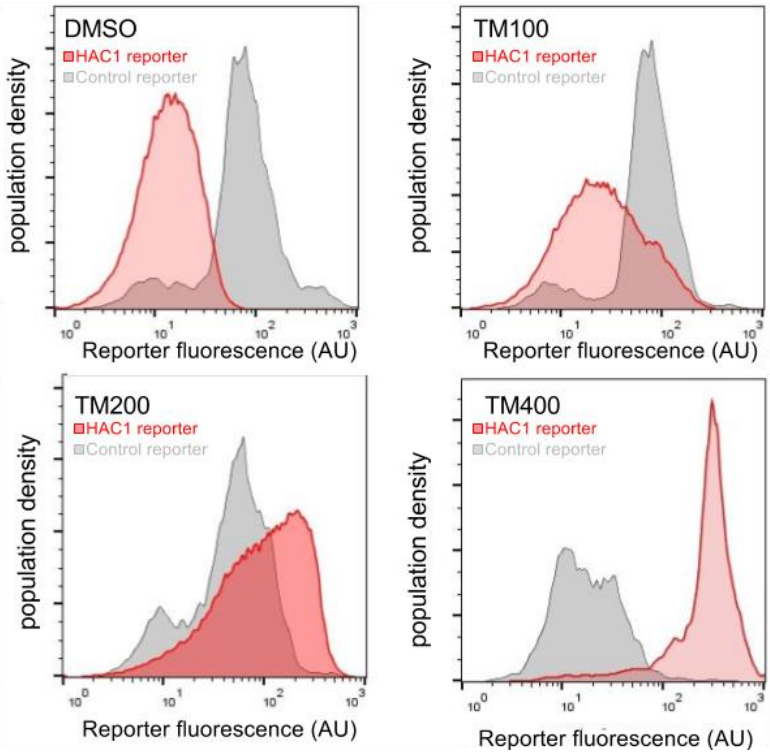

Figure 5.2: The reporter fluorescence distribution of HAC1-activity and control reporter cells at different tunicamycin concentrations.

The reporter fluorescence of wild-type cells with the HAC1-activity reporter (FJ4741.1, red) or the control reporter (FJ4741.25, grey) after a 2.5-hour incubation in YPD with DMSO or different tunicamycin concentrations, i.e. 100 (TM100), 200 (TM200) or 400 (TM400) ng/ml, was measured with flow cytometry and analysed with FlowJo (for the HAC1 reporter a representative replicate was selected n=3, and n=1 for the control reporter, x-axis in log scale with basis 10).

In YPD medium without tunicamycin, the single-cell fluorescence of both reporters covered a wide range (2 - 100 AU for the HAC1-activity reporter and 3 - 1000 AU for the control reporter) and can best be described by a lognormal distribution with different medians or modes and standard deviations [344,345]. The addition of tunicamycin gradually increased overall fluorescence of the HAC1-activity reporter, and the two higher tunicamycin concentrations, 200 and 400 ng/ml, also decreased overall fluorescence of the presumably constitutive control reporter.

Since the control reporter contained the promoter of a ribosomal protein (RPL19A), whose downregulation after ER stress was observed in genome-wide studies alongside other ribosomal proteins [304], the fluorescence of the HAC1-activity reporter and the control reporter at higher tunicamycin concentrations indicated a stronger UPR activation and a lower ribosome production at high ER stress. This anticorrelation suggested that strong ER perturbation in nutrient-rich environments (YPD medium) not only triggered UPR activation but also reduced ribosome

expression and cell growth [346]. At the lowest tunicamycin concentration, the intermediate reporter fluorescence of the HAC1-activity reporter and the high fluorescence of the control reporter indicated a partial UPR activation with constant ribosome expression and suggested that 100 ng/ml tunicamycin perturbed ER homeostasis but had less impact on overall cell physiology. In addition to the changes in overall reporter fluorescence, the range of the distribution, an indicator for cell-to-cell differences, changed with the tunicamycin concentration. The fluorescence spread of the HAC1-activity reporter was widest at 100 or 200 ng/ml and narrower at 400 ng/ml or without stress. The width of the control reporter fluorescence distribution did not change at the lowest tunicamycin concentration but increased at higher tunicamycin concentrations.

To quantify and compare the cell-to-cell differences for different reporter constructs and in different environmental conditions, the quartile ratio (75% quantile divided by 25% quantile) - a modified version of the interquartile distance for log-normal distributed data, which increases with increasing population heterogeneity ($log\ q_{75\%}-log\ q_{25\%}=log(q_{75\%}/q_{25\%})\rightarrow q_{75\%}/q_{25\%}$) - was subsequently calculated for all samples (see figure 5.3).

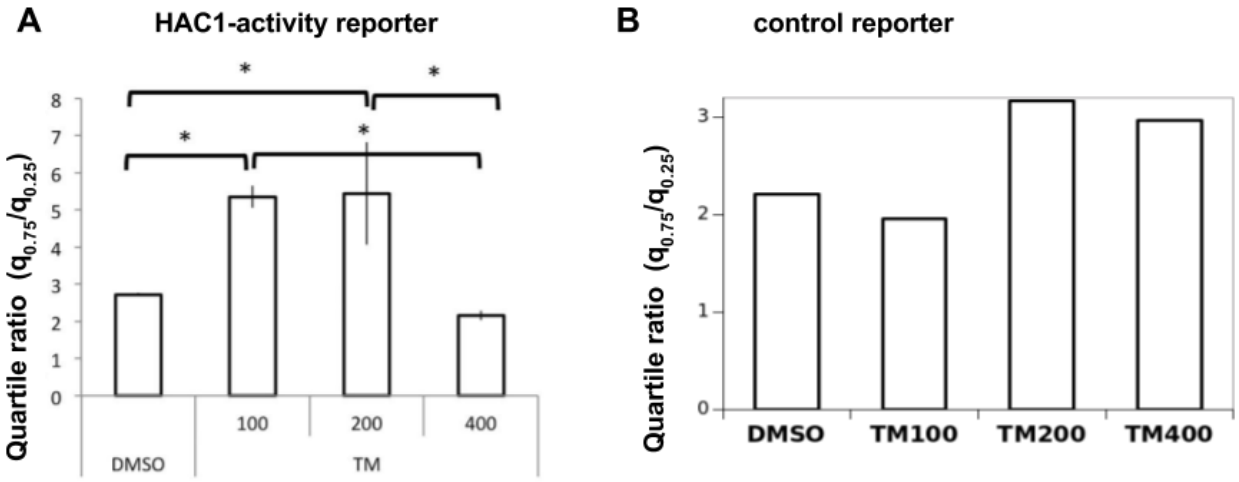

Figure 5.3: Quartile ratios of the HAC1-activity and control reporter fluorescence at different tunicamycin concentrations.

The quartile ratios for the HAC1-activity reporter (A) and the control reporter (B) fluorescence were calculated from the fluorescence distribution after 2.5 hours at the different tunicamycin concentrations (DMSO: solvent control, TM100, 200 and 400: 100, 200 and 400 ng/ml tunicamycin). (A: n=3, the asterisks indicate a significant difference $p<0.05$ with student's t-test, and the error bars represent the standard deviation between the different biological replicates. B: n=1)

The quartile ratio of the HAC1-activity reporter fluorescence was below 3 for unsupplemented YPD medium and the highest tunicamycin concentration, but above 5 for 100 and 200 ng/ml tunicamycin. The quartile ratio of the control reporter remained below 3 for all tested conditions.

The lower quartile ratio indicated smaller cell-to-cell differences and suggested a more homogeneous reporter expression and HAC1 activity in conditions with no or high ER stress than at 100 or 200 ng/ml tunicamycin. The relatively small differences in the quartile ratio of the control reporter indicated small cell-to-cell differences and suggested rather uniform changes in ribosome transcription at higher tunicamycin concentrations. At 100 and 200 ng/ml tunicamycin, the higher quartile ratio of the HAC1-activity reporter and low quartile ratio of the control reporter further suggested that cell-to-cell differences are more pronounced in genes that are regulated by HAC1 and belong to the UPR.

5.4 Cells born in low tunicamycin concentrations had a higher HAC1 activity than cells born before the treatment

The previous experiments indicated cell-to-cell differences in the UPR activity at low ER stress. Better characterisation of UPR-activating cells might help to understand the heterogeneity-generating mechanism. One possible source for heterogeneous UPR activity in growing yeast populations are existing differences between mother and daughter cells after cell division [347]. The cell wall, for example, remains with the mother cell, and Concanavalin A (ConA) which binds to sugar residues in the cell wall [348], can thus be used to distinguish pre-existing cell from those that were born later (see figure 5.4). ConA-based staining was subsequently combined with the HAC1-activity reporter to test the impact of replicative age (zero for daughters and larger than zero for mothers) on the UPR activity of individual cells.

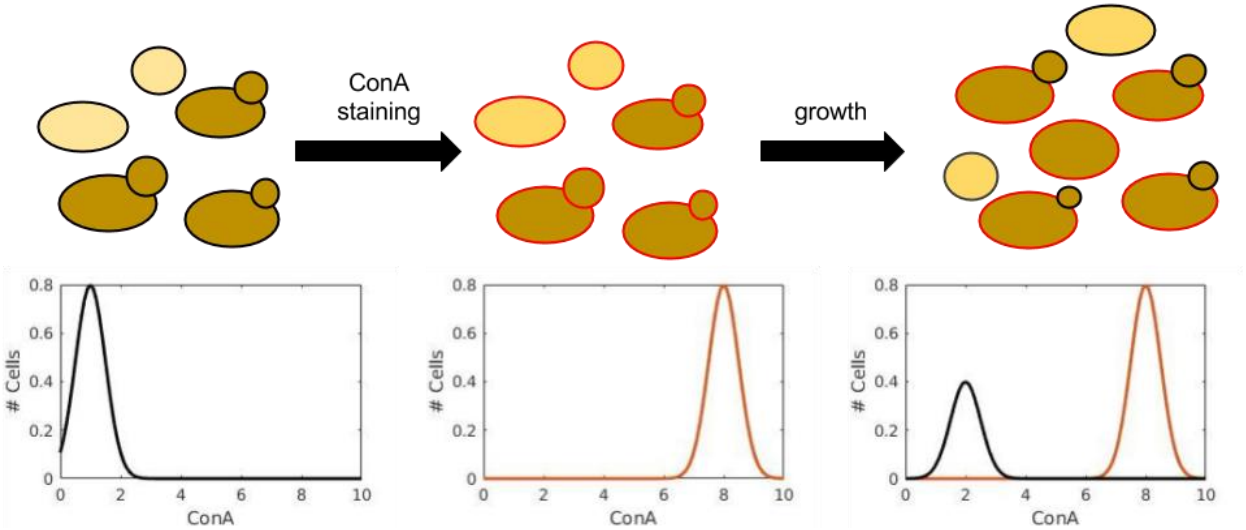

Figure 5.4: Cell wall staining of growing yeast cells with Concanavalin A (ConA).

Schematic of individual yeast cells (upper panels) and theoretical flow cytometry profiles (lower panels) of asynchronous yeast cultures before and after ConA-based staining of the cell wall (mother cells: dark brown; daughter cells: light brown, cell wall: black, ConA stained cell wall: red). The labeled subpopulation that results from the ConA staining of asynchronous yeast cultures consists initially of mother and daughter cells, but consists exclusively of mother cells after the daughter cells have completed their first cell cycle. The unlabeled population, appears with the first cell division of the original cells and initially consists of daughter cells but matures into a mixed population where daughter cells represent the majority.

Exponentially growing HAC1-activity reporter cells (FJ4741.1) were stained with red fluorescent ConA, i.e. TRITC-ConA, and diluted into prewarmed tunicamycin-containing (100 or 200 ng/ml) or DMSO-containing YPD medium. At the indicated timepoints (i.e. 45, 90, 135, 190 and 260 minutes), the cellular HAC1-activity reporter and TRITC fluorescence of all samples was determined with flow cytometry. During the subsequent analysis of the HAC1-activity reporter fluorescence in FlowJo, younger and older cells were distinguished according to their red fluorescence (see figure 5.5 for one representative sample).

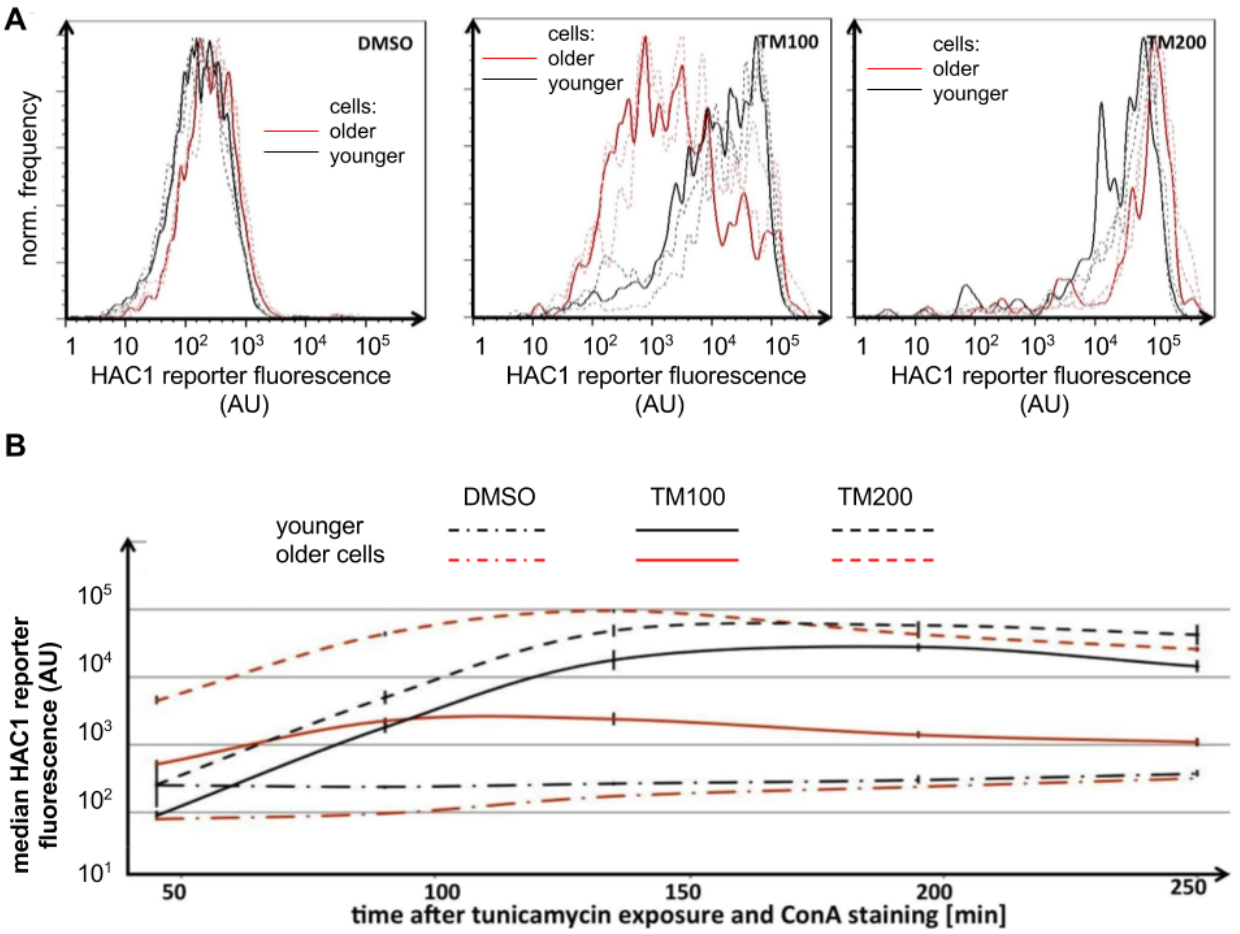

Figure 5.5: HAC1-activity reporter fluorescence in pre- and post-treatment subpopulations at different tunicamycin concentrations.

HAC1-activity reporter cells were pre-grown in YPD medium, stained with TRITC-ConA and incubated in YPD medium with DMSO or tunicamycin (TM100: 100 ng/ml, TM200: 200 ng/ml). The cellular reporter fluorescence at different timepoints (45, 90, 135, 190 or 250 minutes) after the treatment was measured with flow cytometry (n=3). **A**, Histogram of the HAC1-activity reporter fluorescence in all treatments after 190 minutes (red line: TRITC-positive subpopulation, black line: TRITC-negative subpopulation; solid lines: one representative biological replicate, dotted lines: two additional replicates, x-axis in log scale with basis 10). **B**, Time evolution of the median reporter fluorescence after the treatment (as the dynamics slightly differed between the biological replicates, the curve only displays one representative biological replicate, y-axis in log scale with basis 10)

In YPD medium with DMSO, the median HAC1-activity reporter fluorescence of both subpopulations was similarly low and remained low throughout the treatment (see figure 5.5B, interrupted lines and figure 5.5A DMSO). At low tunicamycin concentrations (100 ng/ml), the median HAC1-activity reporter fluorescence of TRITC-negative cells rose faster and higher than the reporter fluorescence of the TRITC-positive cells (see figure 5.5B, solid black and red lines). Accordingly, the reporter fluorescence distribution differed strongly between younger and older

subpopulations after 190 minutes in 100 ng/ml tunicamycin (see figure 5.5A, TM100). At 200 ng/ml tunicamycin (see figure 5.5B, dashed lines, and figure 5.5A TM200) the median reporter activity of both populations rose rapidly and to similarly high levels.

The strong HAC1-activity reporter fluorescence in TRITC-positive and TRITC-negative cells at 200 ng/ml tunicamycin indicated a high UPR activity in both subpopulations and suggested that all cells are equally able to induce the UPR after ER stress. TRITC-negative cells were born after the treatment and were predominantly daughter cells. Their higher reporter fluorescence at 100 ng/ml tunicamycin indicated a higher HAC1 activity and suggested a higher UPR activity and stronger ER stress in daughter cells that were born after the treatment. At least half of the pre-existing cells were also daughter cells, and the difference between TRITC-positive and TRITC-negative cells at 100 ng/ml thus further suggested that the time of birth, i.e. pre- or post-treatment, and the replicative age were both important factors for the HAC1 activity and ER stress at low tunicamycin concentrations.

5.5 Low tunicamycin concentrations primarily reduced the ER content of younger cells

Asymmetric separation of ER content during cytokinesis at low ER stress or different expression profiles in mother and daughter cells after cytokinesis could both contribute to the stronger UPR activation in cells born after the tunicamycin treatment.

To address ER content separation during cytokinesis, the distribution of ER content in younger and older cells of a population was determined with ConA-based staining and HDEL-GFP, a fluorescent protein that localises to the ER due to a secretion and ER retention signal [168,349]. The forward scatter of each cell was additionally determined to estimate cell size and investigate the relation between cell size and ER content in both subpopulations at different ER stress levels [350].

Exponentially growing wild-type cells with a constitutively expressed HDEL-GFP (FJ4741.17) were stained with TRITC-ConA and cultured in YPD medium with DMSO or 100 ng/ml tunicamycin. After 200 minutes (~ two cell doublings), forward scatter and fluorescence of single cells were measured with flow cytometry, and the TRITC fluorescence was used to distinguish between older and younger cells during the analysis with FlowJo (see Figure 5.6).

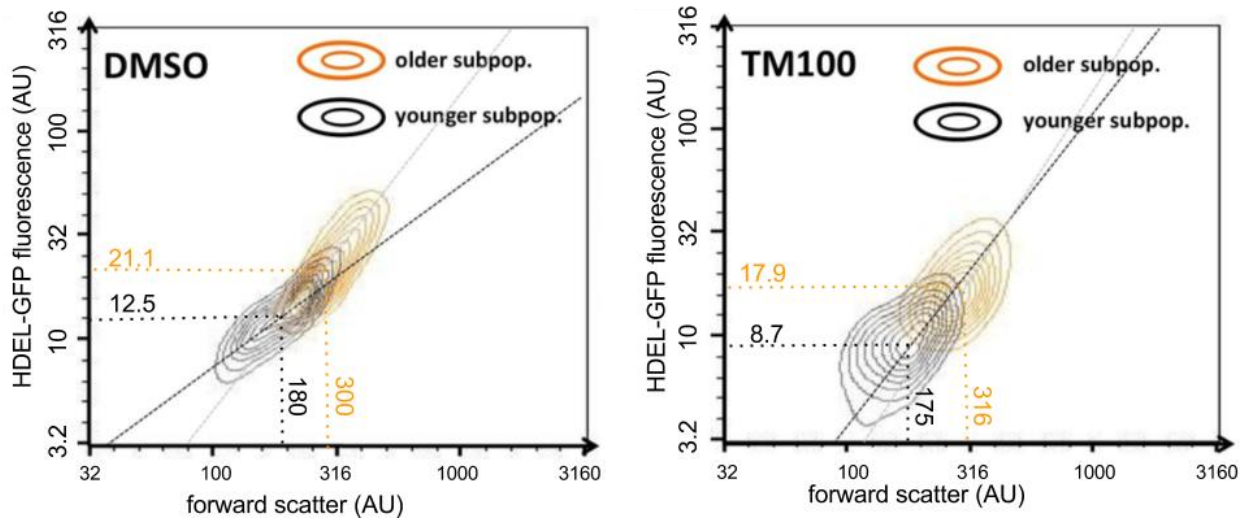

Figure 5.6: HDEL-GFP fluorescence and forward scatter of pre- and post-treatment wild-type cells.

GFP fluorescence and forward scatter in arbitrary units (AU) of TRITC-ConA stained wild-type cells with a constitutively expressed ER-localised GFP (HDEL-GFP FJ4741.17) after 200 minutes in YPD medium with DMSO (DMSO) or 100 ng/ml tunicamycin (TM100) was measured with flow cytometry. The contour plots represent the forward scatter and HDEL-GFP fluorescence distribution in 90% of the TRITC-negative (younger subpopulation, black) and TRITC-positive (older subpopulation, orange) cells, the numbers indicate the median of both parameters in the respective subpopulation and the diagonal orange or diagonal black line is the manual fit of the relation between both parameters in the respective subpopulations, the horizontal and vertical line indicate the medians of both values in both subpopulations (n=1, both axis in log scale with basis 3.16).

After 200 minutes in YPD medium with DMSO, the median HDEL-GFP fluorescence and the median forward scatter of the TRITC-negative cells was 12.5 and 180 arbitrary units (AU), and the medians of the TRITC-positive subpopulation were 21.1 AU and 300 AU. The two parameters also correlated, and the slope of the linear fit was steeper in older than in younger cells. The higher median fluorescence and forward scatter of older cells indicated bigger cell size and larger HDEL-GFP content, while the correlation between both parameters indicated a close connection between cell size and HDEL-GFP content in both subpopulations. After 200 minutes in YPD medium with 100 ng/ml tunicamycin, the median HDEL-GFP fluorescence of the younger subpopulation is 3.8 AU (30%) lower than in YPD medium with DMSO, while the median forward scatter decreased by 5 AU (2.5%). The median HDEL-GFP fluorescence of mother cells only decreased by 3.2 AU (15%) and the median forward scatter increased by 16 AU (5%). The strong correlation between both parameters remained in both subpopulations.

The GFP fluorescence in single cells is determined by their starting HDEL-GFP amount and their HDEL-GFP expression. The constitutive expression of HDEL-GFP implied that cells accumulate HDEL-GFP alongside other proteins during growth and probably caused the strong correlation

between cell size and HDEL-GFP content in both subpopulations. Because the contribution of constitutive HDEL-GFP expression to the fluorescence at low tunicamycin concentrations should not differ between younger and older cells, the stronger decrease in HDEL-GFP fluorescence in TRITC-negative cells primarily suggested a strongly reduced starting amount in younger cells at low tunicamycin concentrations.

5.6 During low ER stress, daughter cells were born with less ER-resident proteins

As the unstained subpopulation also contained older daughter cells that have already expressed HDEL-GFP and partially compensated for reduced ER content inheritance, the impact of low ER stress on ER inheritance can be better investigated in newly born daughter cells.

Nocodazole or other compounds synchronize the cell cycle of yeast populations and increase the fraction of new-born cells, which is relatively small in asynchronous populations [351]. Cell synchronisation can further be combined with ConA-based staining to distinguish new-born daughter from mother cells after cell division.

Nocodazole prevents cell cycle progression in the M-Phase [352], so that ConA binds to the cell wall of cells and their very large buds. The first cell division immediately after the release from Nocodazole thus results in stained mother and daughter cells. The second cell division yields stained mother cells and unstained daughter cells (see figure 5.7).

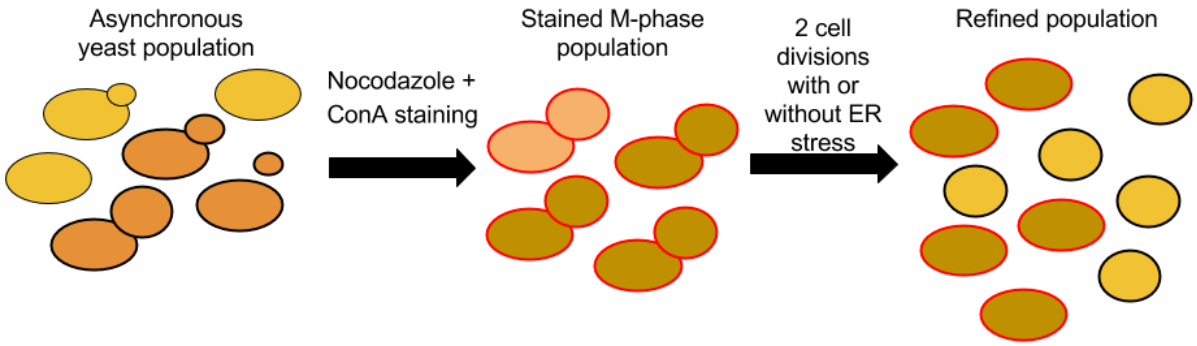

Figure 5.7: Experimental procedure to enrich and distinguish freshly born daughter cells.
Nocodazole arrests the growing mother (dark brown) and daughter (light brown) cells during M-phase and shortly before cell division, i.e. with a very large bud. ConA binds to the cell wall of all existing cells and their buds (red outline). The first cell division separates the large ConA-bound bud from the ConA-bound cells and only the second synchronous cell division gives rise to daughter cells without ConA (black outline).

This method of daughter selection was subsequently applied in HDEL-GFP expressing wild-type cells before growth in YPD medium with DMSO, low tunicamycin concentrations or low 2'-deoxy-glucose (2'DG, which is an alternative ER-stressing agent) concentrations to investigate the inheritance of ER content with and without low ER stress [353].

After a two-hour treatment with Nocodazole in unsupplemented YPD medium, the M-phase-arrested HDEL-GFP-expressing cells (FJ4741.17) were stained with TRITC-ConA and released into prewarmed YPD medium with DMSO, 100 ng/ml tunicamycin or 1 mM 2'DG. Samples were frequently taken to monitor the appearance of unlabeled daughter cells with flow cytometry until this subpopulation formed 50% of the population, i.e. the end of the second cell division. The forward scatter and cellular fluorescence at this timepoint were determined with flow cytometry and analysed with FlowJo. During the analysis in FlowJo, mother and daughter cells were separated according to their TRITC fluorescence (see figure 5.8).

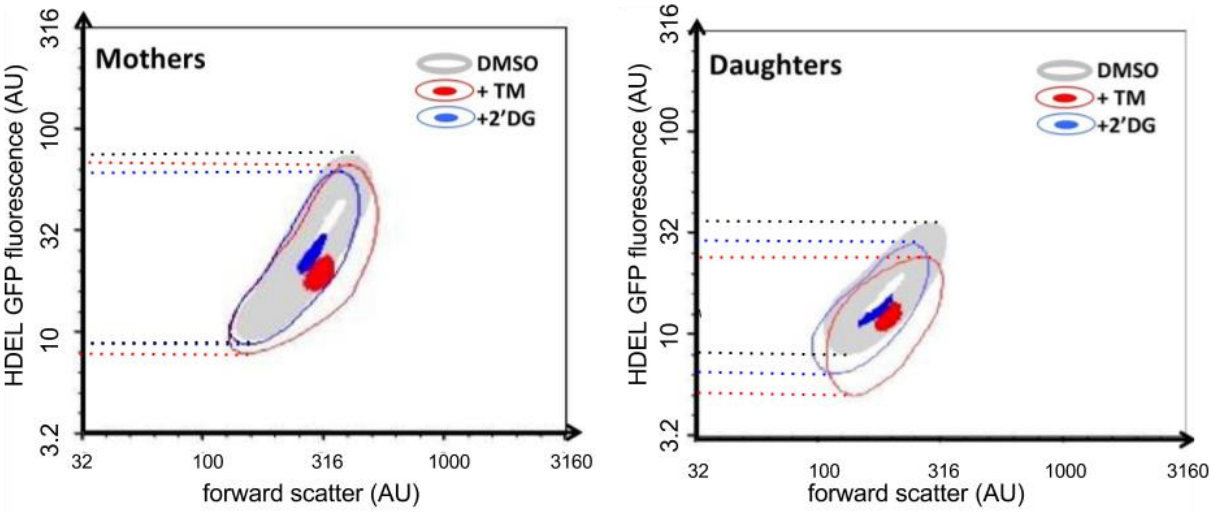

Figure 5.8: Impact of ER stress on the HDEL-GFP fluorescence and forward scatter of mother and daughter cells after cytokinesis.

Forward scatter and HDEL-GFP fluorescence of synchronised and ConA-stained wild-type cells with constitutive HDEL-GFP expression (FJ4741.17) after two cell divisions in YPD medium with DMSO (grey), 1 mM 2'-deoxy-glucose (+2'DG, blue) or 100 ng/ml tunicamycin (+TM, red) were measured with flow cytometry and analysed with FlowJo. TRITC fluorescence was used to separate mother (left) from daughter (right) cells during the analysis. (The hollow and filled contour represent the outline that comprises 90% and 10% of the population, respectively, during each treatment. The plots show one representative sample per condition, n=3, both axis in log scale on a 3.16 basis).

Tunicamycin and 2'DG reduced overall HDEL-GFP fluorescence and forward scatter more strongly in daughter than in mother cells (downward shift of treatment curves, figure 5.8). Fluorescence decreased more strongly in mother cells with a high forward scatter than in mother

cells with small forward scatter. In contrast, the fluorescence decrease in daughter cells was independent of the cell size. The changes in HDEL-GFP fluorescence indicated a reduced HDEL-GFP content that depended on cell size in mother but not in daughter cells. The size-independent decrease in HDEL-GFP in daughter cells suggested a lower inheritance, which decreased the amount of HDEL-GFP and ER content in all daughter cells. The size-dependent decrease in HDEL-GFP in mother cells suggested an unaffected initial amount and a slower accumulation during cell growth, which would mainly decrease the HDEL-GFP and ER content of bigger mother cells. Together the lower initial HDEL-GFP content in daughter cells and the constant initial HDEL-GFP content in mother cells suggested a more asymmetric ER content distribution during cytokinesis at low ER stress, which might contribute to the previously observed asymmetric UPR activation (see figure 5.5).

5.7 At low ER stress, the HAC1 activity of WHI5-deficient mother and daughter cells were more similar in than in wild-type cells

The deletion of the cell cycle regulator WHI5 increases the duration of the budded phase and reduces the size and content differences between mother and daughter cells after cytokinesis [354,355]. WHI5 knock-out can thus be used to force a more symmetric inheritance in *S. cerevisiae* [356].

To determine the relative importance of asymmetric ER inheritance for heterogeneous UPR activation, the UPR activity of WHI5-deficient mother and daughter cells at different tunicamycin concentrations was measured with the HAC1-activity reporter.

To distinguish between mother and daughter cells, exponentially growing WHI5-deficient cells with the HAC1-activity reporter (FJ4741WHI5Δ.1) were stained with TRITC-ConA and resuspended in YPD medium with DMSO or different tunicamycin concentrations (100, 200 ng/ml). After 200 minutes, the cellular fluorescence in each sample was determined with flow cytometry and the TRITC fluorescence was used to distinguish between younger and older cells during the analysis (see figure 5.9).

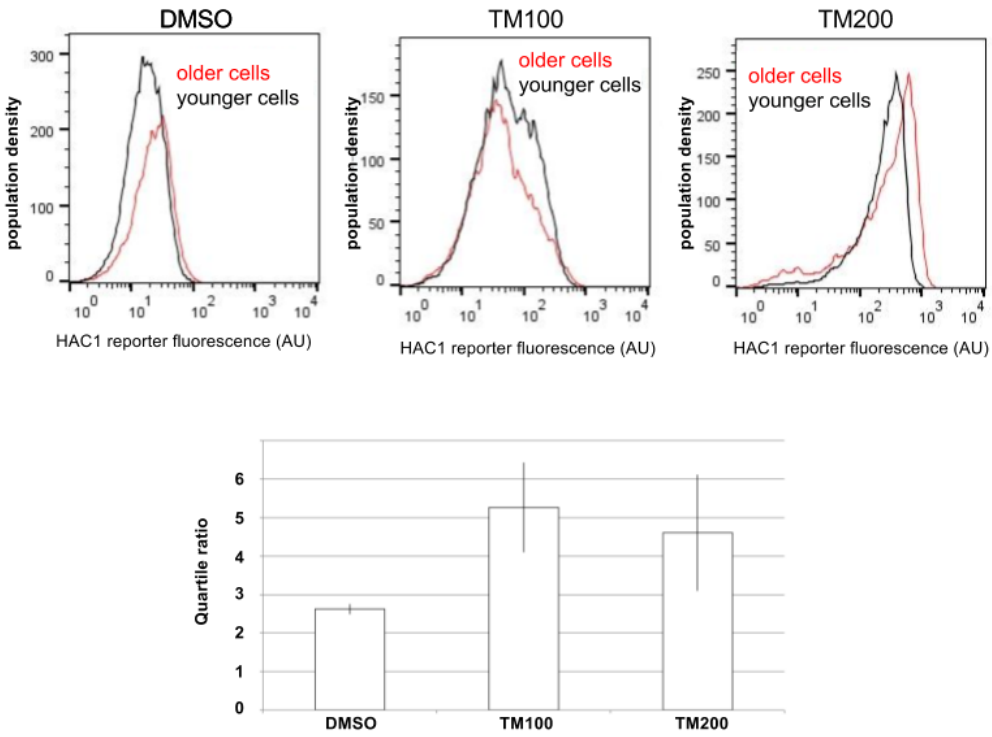

Figure 5.9: Distribution of HAC1-activity reporter fluorescence in WHI5-deficient cells born before and during the exposure to different tunicamycin concentrations.

Upper panels: Histograms of HAC1 reporter fluorescence in WHI5-deficient cells 200 minutes after TRITC-ConA staining and growth in YPD medium with DMSO or different tunicamycin concentrations (100 ng/ml: TM100 or 200 ng/ml: TM200) as determined with flow cytometry and analysed with FlowJo (red line: older, stained cells that were born before the staining and treatment, black line: younger, unstained cells that were born after the staining and during the treatment; n=2 and the plots represent one exemplary sample). Lower panels: the quartile ratio of the HAC1 reporter fluorescence in the entire population in DMSO or at different tunicamycin concentrations (TM100: 100 ng/ml and TM200: 200 ng/ml)

As in wild-type cells, the distribution of the HAC1-activity reporter fluorescence was almost identical in younger and older cells in YPD medium (see figure 5.9, left). At low tunicamycin concentrations, the distribution shifted to higher reporter fluorescence values in both subpopulations (see figure 5.9, middle), and the overlap between both distributions was larger than in the wild-type cells (compare figure 5.5 with figure 5.9).

The more similar reporter profile indicated a more similar HAC1-activity in younger and older cells. This suggested that a more symmetric distribution of cellular resources and possibly ER content reduced the differences in UPR activation and ER perturbation between mother and daughter cells at low ER stress. This further suggested that asymmetric cell division is an important factor for the heterogeneous UPR activation in wild-type cells.

Interestingly, the quartile ratio of the total population, which initially indicated heterogeneous UPR activation, also increased in WHI5-deficient strains at low tunicamycin concentrations (see figure 5.9). This, in turn, suggested that asymmetric ER inheritance is not required for heterogeneous UPR activation at low ER stress, while the remaining difference between the reporter fluorescence of younger and older cells suggested that WHI5 knock-out and symmetric cell division are not sufficient to alleviate all differences between the ER homeostasis of mother and daughter cells.

5.8 Secreted proteins were enriched in the daughter-specific transcription program

These remaining differences possibly resulted from a stronger expression of secreted proteins in daughter cells. The daughter-specific expression program, which is induced by two transcription factors, ACE2 and ASH1, leads to G1 delay, repression of the mating type switch and cell separation [141,357]. In particular, cell separation requires several secreted enzymes, and this suggested that protein secretion might increase ER load contribute to daughter-specific UPR activity. To better estimate the overall ER load from the daughter-specific expression program, the subcellular destination and function of all ACS2 and ASH1 targets was evaluated via their gene ontology (GO).

The lists of 70 ASH1 and 77 ACE2 targets were obtained from published data sets (see appendix B for full lists) [358–360]. The GO term enrichment in the individual lists was then tested against the yeast genome with YeastMine, Holm-Bonferroni correction and a p-value cut-off of 0.05 (see table 5.1) [361] .

Table 5.1: GO term enrichment of ACE2 and ASH1 targets.

The GO term enrichment in the known ACE2 and ASH1 targets was analysed with YeastMine [358–361]. (The first row indicates the transcription factor and the total number of target genes: '*ACE2'* and '*ASH1'* include all ACE2 and ASH1 targets, and *'ASH1 (heat-independent)'* omits ASH1 targets that were found after heat shock [360]. In the subsequent rows, the first, third and fifth column indicate the GO term and p-value for the enrichment in brackets. The superscript indicates the GO term category: 1: biological process and 2: cellular component. The second, fourth and sixth column indicate the number of target genes that are regulated by the TF and belong to a specific GO term.)

ACE2	**77**	***ASH1***	**70**	***ASH1 (heat-independent)***	**29**
cell separation after cytokinesis[1] (0.0079)	6			Cell wall organisation[1] (0.005625)	8
extracell. region[2] (4.1e-6)	12	extracell. region[2] (0.029)	8	fungal type cell wall[2] (0.001287)	7
cell periphery[2] (8.9e-4)	24				

This analysis revealed that genes that localise to the extracellular region and the cell periphery are significantly enriched among the ACE2 targets (see table 5.1, left column), but the 70 ASH1 targets contained a much lower number and less significant enrichment for proteins in the extracellular space (see table 5.1, middle column). However, excluding the heat-dependent ASH1 targets leaves 29 heat-independent ASH1 targets, of which 7 participate in cell wall organisation [360] (see table 5.1, right column).

ACE2 and ASH1 share 7 heat-independent target genes and the GO term enrichment in the unified list of 99 genes, which are regulated by ACE2 and ASH1 without heat shock, was also evaluated (see table 5.2).

Table 5.2: GO term enrichment in the unified list of ACE2 and ASH1 targets.

The GO term enrichment of the combined list of 99 targets was evaluated as before with YeastMine (the superscript indicates the GO term category: 1: biological process, 2: cellular component, and 3: molecular function)

GO-Term	P-value	GO-specific Targets
Cell wall organization or biogenesis[1]	4.02e-4	17
Cell periphery[2]	8.00e-6	32
Vacuole[2]	0.037	22
Hydrolase activity, acting on glycosyl bonds[3]	8.27e-4	10

Like the targets of the individual transcription factors, the common targets were significantly enriched for genes that regulate cell wall organisation (17) or localised in the cell periphery (32). Interestingly, the unified list also showed a significant enrichment for proteins that localise to the vacuole and also need to pass through the endoplasmic reticulum.

This strong enrichment of secreted proteins among the target genes of the daughter-specific transcription factors indicated that daughter cells express many secreted proteins.

Depending on the expression strength of individual genes, the daughter-specific transcription profile could increase the secretion load and perturb ER homeostasis already without external ER stress. However, the similar HAC1 activity of mother and daughter cells in YPD medium with DMSO (see figure 5.5) and the low impact of ACE2 or ASH1 knock-out on basal UPR activity indicated no inherent ER stress and UPR activation from the daughter-specific expression program [196].

However, a closer examination of both knock-out strains at low tunicamycin concentrations would be necessary to experimentally validate the role of daughter-specific gene expression at low ER stress.

5.9 Sphingosine hydroxylation was not required for heterogeneous UPR activation but increased ER stress at low tunicamycin concentrations

Clay *et al.* [165] reported that a ceramide- and SUR2-dependent diffusion barrier in the bud neck separates mother from daughter ER and regulates ER content inheritance. In order to test the role of this diffusion barrier for the cell-to-cell differences at low ER stress, the median strength

and distribution of UPR activity in SUR2-deficient cells was assessed with the HAC1-activity reporter.

To induce different ER stress levels, exponentially growing, SUR2-deficient cells with the HAC1-activity reporter (FJ4741SUR2Δ.1) were diluted into YPD medium with DMSO and four different tunicamycin concentrations; 100, 200, 400, and 800 ng/ml. After a 2.5-hour incubation, the cellular reporter fluorescence was measured with flow cytometry and analysed with FlowJo. For each condition, the relative reporter fluorescence after tunicamycin treatment was calculated as the ratio between the median reporter fluorescence in tunicamycin-containing medium and the median reporter fluorescence of the solvent control medium (DMSO). Additionally, the quartile ratio was determined as described previously (see subchapter 5.2 and figure 5.10 for results).

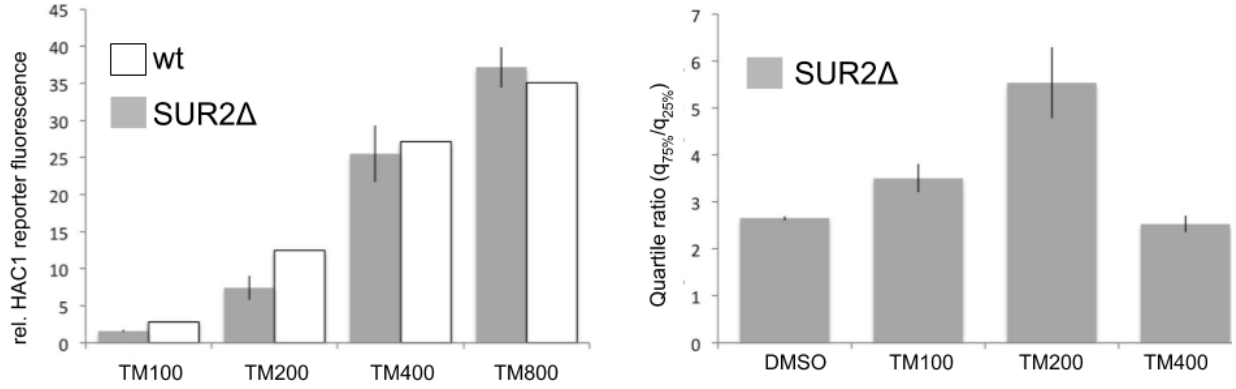

Figure 5.10: Median and quartile ratio of the HAC1-activity reporter fluorescence of SUR2-deficient cells at different tunicamycin concentrations.

Reporter fluorescence of SUR2-deficient (FJ4741SUR2Δ.1, SUR2Δ) or wild-type (FJ4741.1, wt) strains with the HAC1-activity reporter after 2.5 hour in YPD medium with DMSO or different tunicamycin concentrations (TM100, TM200, TM400, TM800: 100, 200, 400, 800 ng/ml) was determined with flow cytometry and analysed with FlowJo. Left: Relative HAC1-activity reporter fluorescence of different strains (SUR2Δ: grey, wt: white) was calculated as the ratio between the median reporter fluorescence at a tunicamycin concentration and the median reporter fluorescence in the solvent control (n=3 for SUR2Δ, error bars indicate the standard deviation between the biological replicates, n=1 for wt). Right: The quartile ratio of the HAC1-activity reporter fluorescence in DMSO and at different tunicamycin concentrations was calculated as described previously (see subchapter 5.2) (n=3, and the error bars represent the standard deviation between the different biological replicates).

At low tunicamycin concentrations (i.e. 100 ng/ml, 200 ng/ml), the relative HAC1-activity reporter fluorescence of SUR2-deficient cells was lower than in wild-type cells, and only the relative HAC1-activity reporter fluorescence at tunicamycin concentrations above 400 ng/ml was comparable between both strains (see figure 5.10). The quartile ratio at 100 ng/ml tunicamycin was lower than in the wild-type cells (3 vs. 5, see figure 5.3) and only slightly higher than in the solvent control

(DMSO: 2.5). However, the quartile ratio at 200 ng/ml was similar to wild-type cells and higher than in the solvent control (5 vs. 2.5). The quartile ratio at 400 ng/ml was lower than in the solvent control and similar to the wild-type cells.

Firstly, the lower relative HAC1 reporter fluorescence at 100 ng/ml tunicamycin after SUR2 knock-out suggested that higher tunicamycin concentrations, e.g. 200 ng/ml, are necessary to induce low ER stress without sphingosine hydroxylation. The increased quartile ratio at 200 ng/ml indicated heterogeneous HAC1 activity and suggested that sphingosine hydroxylation by SUR2 is not required for heterogeneous UPR activation. However, heterogeneous UPR activation does not necessitate daughter-specific UPR activation (see subchapter 5.7), and only additional experiments that distinguish between mother and daughter cells would be able to test if SUR2 is required for daughter-specific UPR activation or lower ER content inheritance (see subchapter 7.3).

5.10 Phytoceramide supplementation lowered HAC1 activity at low tunicamycin concentrations

The previous experiments indicated that stress-dependent asymmetric ER content inheritance and maybe the daughter-specific transcription profile induced a daughter-specific UPR activation at low ER stress. The decreased HAC1 activity in SUR2-deficient cells further suggested that UPR activation and ER stress at different tunicamycin concentrations depend on sphingolipid (SL) metabolism.

Similarly, external sphingolipid precursors such as phytoceramide could influence SL metabolism of wild-type cells and modify their reaction, i.e. UPR activation and ER inheritance, to low tunicamycin concentrations. Wild-type cells with the HAC1-activity reporter were then used to determine the impact of phytoceramide supplementation on the UPR activation at low tunicamycin concentrations.

Exponentially growing HAC1-activity reporter cells (FJ4741.1) were diluted into YPD medium with or without phytoceramide supplementation (20 µM) and different tunicamycin concentrations (DMSO, 100 ng/ml or 200 ng/ml). After 2 hours, the cellular reporter fluorescence in each sample was measured with flow cytometry and analysed with FlowJo (see figure 5.11).

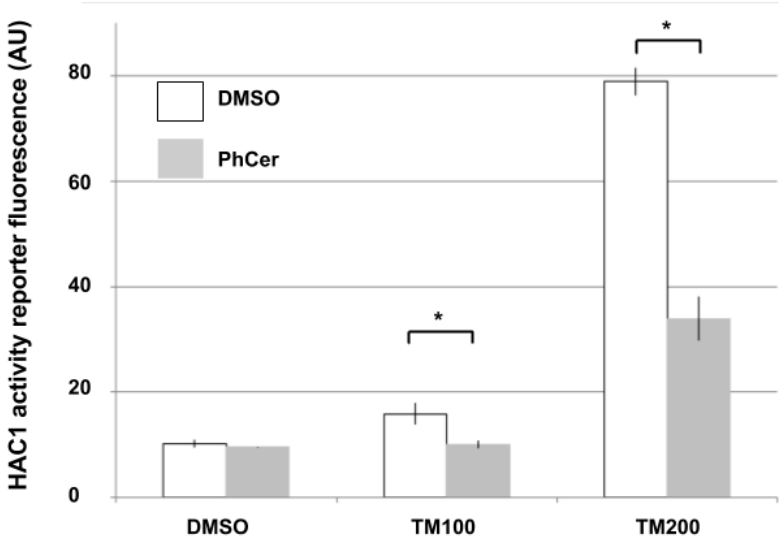

Figure 5.11: The effect of phytoceramide supplementation on the fluorescence of the HAC1-activity reporter at different tunicamycin concentrations.

The fluorescence of wild-type strains with the HAC1-activity reporter after 2 hours in YPD medium with (PhCer) and without (DMSO) phytoceramide supplementation (20µM) and at different tunicamycin concentrations (DMSO: solvent control, TM100: 100 ng/ml and TM200: 200 ng/ml) was determined with flow cytometry and analysed with FlowJo. (n=3, error bars indicate the standard deviation between the individual samples, asterisks indicate significant differences ($p<0.05$) with student's t-test)

Phytoceramide alone did not change the reporter fluorescence in YPD medium, but phytoceramide supplementation lowered the reporter fluorescence in YPD medium with each tunicamycin concentration.

The decreased HAC1-activity reporter fluorescence in phytoceramide-supplemented cultures at both tunicamycin concentrations indicated a lower UPR activation and suggested that external phytoceramide either inhibits UPR activation or alleviates ER stress at low tunicamycin concentrations.

5.11 Phytoceramide supplementation increased growth rate of wild-type, UPR-deficient and ERSU-deficient cells at low tunicamycin concentrations

When comparing the two possible effects of phytoceramide supplementation, lower ER stress should be reflected by an increased growth rate of wild-type cells and a higher survival of UPR-deficient strains, while an inhibited UPR activation might hinder adaptation and lower the growth rate of wild-type cells at low tunicamycin concentrations.

Therefore, the relative growth rate at low tunicamycin concentrations with and without phytoceramide supplementation was determined for wild-type cells. In addition the relative effect of phytoceramide on cells with a perturbed ER stress adaptation, i.e. UPR-deficient after HAC1 and IRE knock-out or ER-surveillance-(ERSU)-deficient after SLT2 knock-out (see chapter 1) [146], was also determined.

Exponentially growing cells from each genotype, i.e. wild-type, SLT2-deficient (ERSU), HAC1-deficient and IRE1-deficient (BY4741, BY4741.SLT2Δ, BY4741.HAC1Δ and BY4741.IRE1Δ), were diluted into microwells with fresh YPD medium with or without phytoceramide supplementation (20 µM) and different tunicamycin concentrations, i.e. 0 (DMSO), 100, 200, and 400 ng/ml. Every 5 minutes during a 24-hour incubation, OD600 was determined for each well, and the growth curves were used to calculate the exponential growth rate of each genotype in each condition. The relative growth rate for each genotype at each condition was then calculated as the ratio between the absolute growth rate in a specific environment and the growth rate of the same genotype in unsupplemented YPD medium without tunicamycin (see figure 5.12).

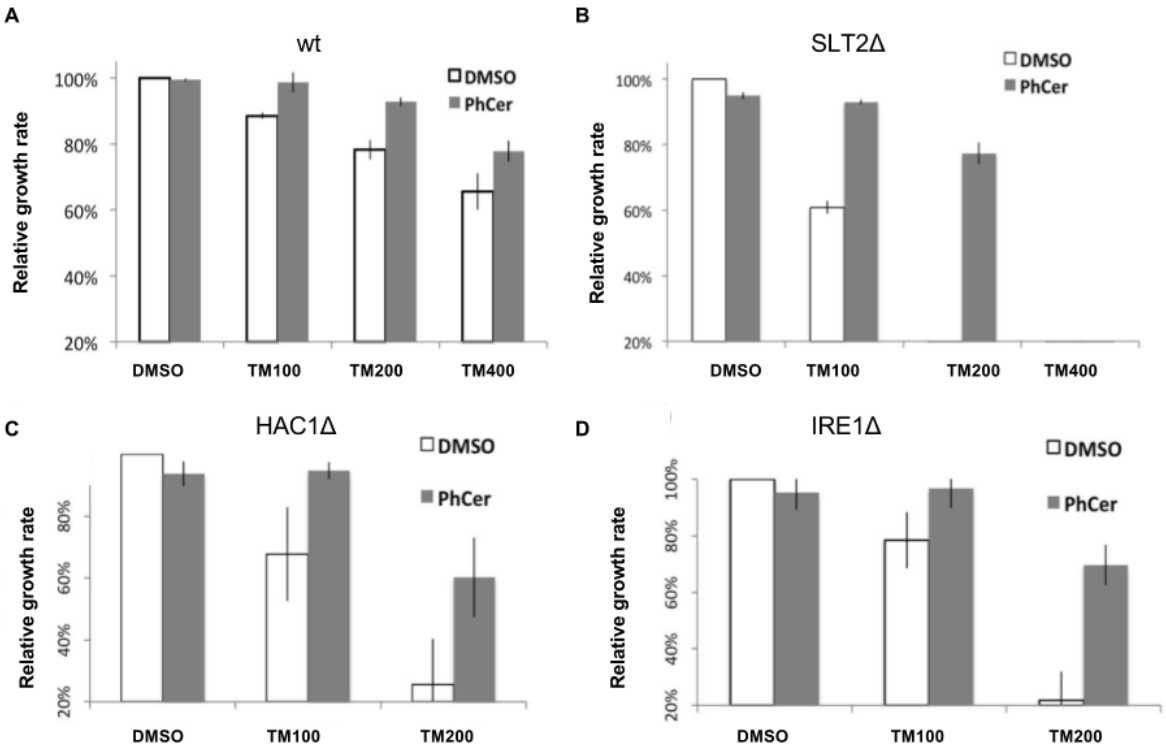

Figure 5.12: The effect of phytoceramide supplementation on the growth rate of wild-type, ERSU-deficient and UPR-deficient strains at low tunicamycin concentrations

The exponential growth rate of wild-type (A), SLT2-deficient (B), HAC1-deficient (C) and IRE1-deficient (D) cells at different tunicamycin concentrations (DMSO: solvent control, TM100, 200, 400 : 100, 200 and 400 ng/ml tunicamycin) and with (PhCer, grey bars) or without phytoceramide supplementation (DMSO, white bars) was determined in 96-well microtiter plates. The relative growth rate of each strain in each condition was calculated as the ratio between the growth rate in this condition and the growth rate in normal YPD medium without tunicamycin (n=3, and the error bars indicate the standard deviation between the biological replicates).

For all tunicamycin concentrations, the relative growth rate of the wild-type cells in phytoceramide-supplemented YPD medium was higher than in the normal YPD medium (figure 5.12 A). The relative growth rate of the SLT2-, HAC1- and IRE1-deficient strains in normal YPD medium with low tunicamycin concentrations, was much lower than the relative growth rate of the wild-type strain in the same environment, but phytoceramide supplementation increased their growth rate at 100 ng/ml and 200 ng/ml tunicamycin much stronger than in the wild-type cells.

The increased growth rate of the wild-type strains indicated a reduced environmental stress at low tunicamycin concentrations with phytoceramide supplementation. The stronger effect of phytoceramide supplementation in ERSU- and UPR-deficient cells indicated a decreased importance of UPR and ERSU activation in this environment. This further implied that

phytoceramide supplementation reduced ER stress at low tunicamycin concentrations and thereby reduced UPR activation.

5.12 Phytoceramide supplementation increased the inheritance of ER content to the daughter cells at low but not intermediate tunicamycin concentrations

Phytoceramide supplementation and low ER stress might also prevent the reduction of ER content inheritance at low tunicamycin concentrations. As previously, HDEL-GFP and daughter selection were used to investigate the effect of phytoceramide supplementation on ER content inheritance at low tunicamycin concentrations.

For daughter selection, wild-type cells with HDEL-GFP (FJ4741.17) were synchronised with Nocodazole, stained with TRITC-ConA (see subchapter 5.6) and released into YPD medium with or without phytoceramide or ceramide supplementation (20 µM) and different tunicamycin concentrations (DMSO: solvent control, or 100 and 300 ng/ml). After two cell divisions, the fluorescence of all cells was measured with flow cytometry, and the TRITC fluorescence was used to separate between mother and daughter cells during the analysis with FlowJo.

To exclude clone-specific effects, the relative HDEL-GFP fluorescence of daughter cells for each sample was subsequently defined as the ratio between the median HDEL-GFP fluorescence of the TRITC-negative cells in a sample and the median HDEL-GFP fluorescence of the TRITC-negative cells from the same clone in non-supplemented tunicamycin-free YPD medium (see figure 5.13).

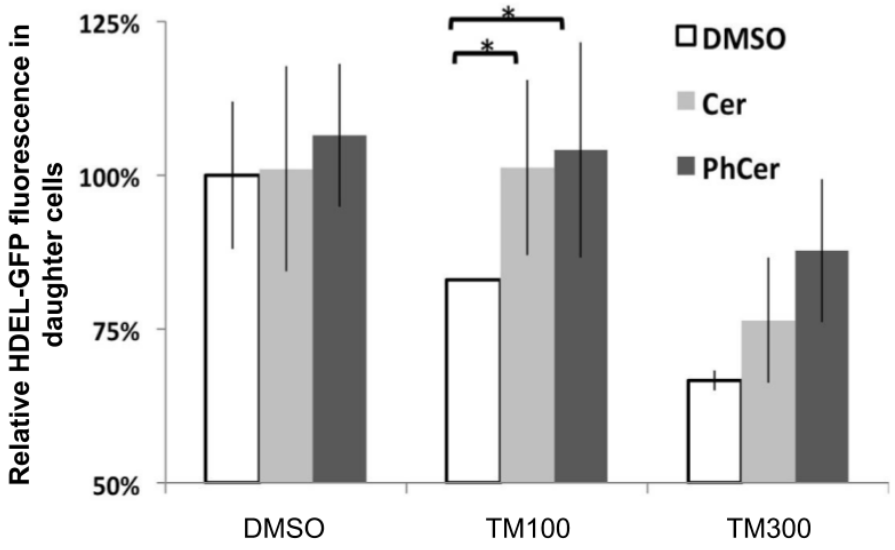

Figure 5.13: The effect of phytoceramide supplementation on HDEL-GFP inheritance at low tunicamycin concentrations.

HDEL-GFP fluorescence and TRITC fluorescence of synchronised, wild-type cells with constitutive HDEL-GFP expression two doublings after TRITC-ConA staining and growth in YPD medium with solvent control (DMSO) or with phytoceramide or ceramide supplementation (PhCer: 20 µM Phytoceramide, dark grey; Cer: 20 µM Ceramide, light grey) and at different tunicamycin concentrations (DMSO: solvent control, TM100, TM300: 100, 300 ng/ml tunicamycin) was determined with flow cytometry. The relative HDEL-GFP fluorescence of daughter cells for each conditions was subsequently calculated as the ratio between the median HDEL-GFP fluorescence of TRITC-negative cells (i.e. cells born at the second cell division) in a certain condition and the median HDEL-GFP fluorescence of TRITC-negative cells of the same clone in normal YPD medium without tunicamycin (n=3, error bars indicate the standard deviation between the biological replicates and asterisks indicate significant differences, $p<0.05$, with student's t-test).

The relative HDEL-GFP fluorescence of daughter cells in YPD medium with ceramide or phytoceramide supplementation was not significantly higher than the relative fluorescence in normal YPD medium. At 100 ng/ml tunicamycin, the relative fluorescence of the daughter cells in the phytoceramide- or ceramide-supplemented YPD medium was significantly higher than the relative fluorescence of daughter cells in non-supplemented YPD medium. At 300 ng/ml tunicamycin, the relative fluorescence of daughter cells was much lower than at 100 ng/ml.

The higher relative fluorescence at 100 ng/ml tunicamycin with phytoceramide supplementation indicated a larger inheritance of HDEL-GFP and probably other lumenal ER-resident proteins to the daughter cells and suggested that phytoceramide supplementation also prevented the reduction of ER inheritance at low tunicamycin concentrations. Ceramide only differs from endogenous phytoceramide in the hydroxylation pattern, and the larger inheritance with ceramide supplementation thus suggested that non-endogenous ceramides also alleviated ER stress from

tunicamycin. At 300 ng/ml, the reduced relative fluorescence of all daughter cells further indicated reduced ER content inheritance. As this tunicamycin concentration was higher than the HAC1-activating tunicamycin concentration (see figure 5.11), this result also suggested that phytoceramide was not able to directly promote ER inheritance at low ER stress, but primarily reduced ER stress from low tunicamycin concentrations and indirectly increased ER inheritance at low tunicamycin concentrations.

5.13 High tunicamycin concentrations or phytoceramide supplementation but not low tunicamycin concentrations induced ER stress in minimal SC medium

Like ceramide supplementation and SUR2 deficiency, different nutrient compositions could change metabolism and modulate ER stress at low tunicamycin concentrations. To investigate the effect of the nutrient composition on ER stress, the growth rates of wild-type and HAC1-deficient cells were determined in minimal synthetic complete medium with or without phytoceramide supplementation and at different tunicamycin concentrations.

Exponentially growing wild-type (BY4741) or HAC1-deficient cells (BY4741HAC1Δ*)* from minimal SC medium were diluted into 96-well microtiter plates with phytoceramide-supplemented (20 µM) or unsupplemented minimal SC medium and different tunicamycin concentrations (200, 400, 800, and 1600 ng/ml). In each well, the OD600 was measured every 10 minutes during a 30-hour incubation and used to determine the exponential growth rate. The relative growth rate was subsequently calculated as the ratio between the exponential growth rate of a genotype in a specific condition and that of this genotype in minimal SC medium (see Figure 5.14).

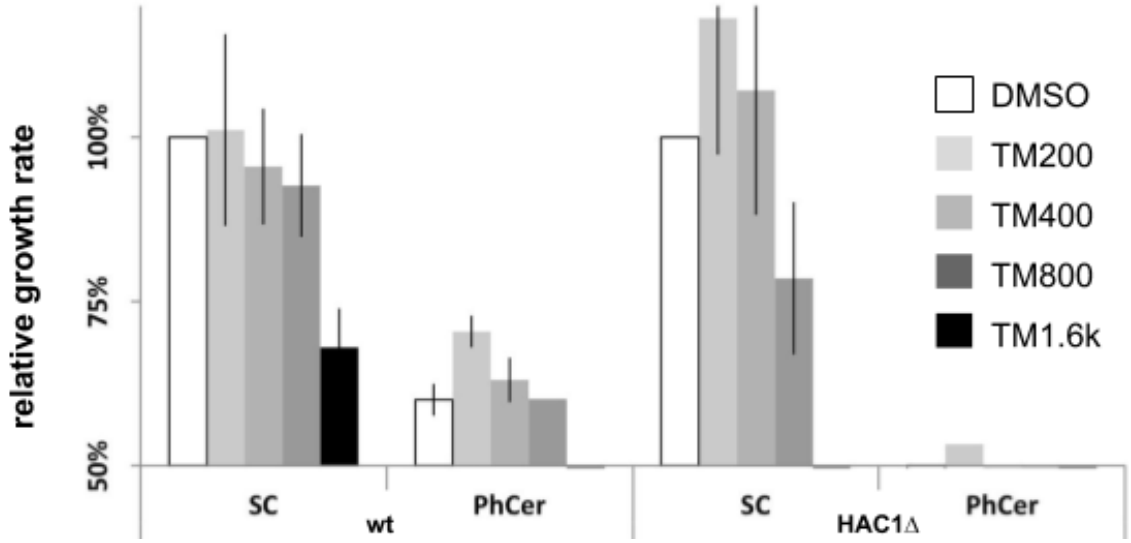

Figure 5.14: Minimal SC medium reverses the impact of low tunicamycin concentrations and phytoceramide on cell growth of wild-type and UPR-deficient strains.

The exponential growth rate of wild-type and HAC1-deficient cells (BY4741, wt and BY4741HAC1Δ, HAC1Δ) in minimal synthetic complete medium with or without phytoceramide (20 µM) supplementation (PhCer or SC) and at different tunicamycin concentrations (DMSO: solvent control; TM200, 400, 800, 1.6k: 200, 400, 800 and 1600 ng/ml tunicamycin) was determined from the growth curve in a 96-well microtiter plate. The relative growth rate was calculated as the ratio between the growth rate of a clone in a specific condition and the growth rate of the same clone in unsupplemented SC medium and without tunicamycin (n=3, error bars indicate the standard deviation between the biological replicates).

In minimal SC medium, only 1.6 µg/ml tunicamycin reduced the relative growth rate of wild-type and prevented the growth of HAC1-deficient cells. 800 ng/ml only reduced the growth of HAC1-deficient cells. On the other hand, phytoceramide supplementation reduced the relative growth rate of wild-type cells and prevented the growth of HAC1-deficient cells, independent of the tunicamycin concentration.

The small effect of 200 ng/ml and 400 ng/ml on the growth rate of wild-type and HAC1-deficient strains indicated ER homeostasis and suggested that higher tunicamycin concentrations are necessary to induce ER stress in minimal SC medium. The growth defect of wild-type cells in phytoceramide-supplemented SC medium and the growth inhibition of UPR-deficient cells indicated an ER homeostasis-dependent phytoceramide toxicity in minimal SC medium.

5.14 Low ER stress delayed the progression of daughter cells from G1- to S-Phase

Overall, the prior experiments indicated asymmetric ER inheritance, daughter-specific UPR activation and decreased population growth at low ER stress but were not able to attribute the decreased growth to a slower cell division in one of the two subpopulations. Therefore, the cell cycle progression of mother and daughter cells at 100 ng/ml tunicamycin was investigated. In *S. cerevisiae,* the progression from G1 to S phase is characterised by the appearance of a bud, which remains with the cell until the end of the cell cycle, when the bud becomes the new daughter cell. In an exponentially growing population unbudded cells are therefore in G1, while budded cells are in one of the three subsequent cell cycle phases, i.e. S, G2 and M (see figure 5.16).

Because cells in non-synchronised cultures are equally distributed along the cell cycle, the fraction of budded cells corresponds to the cumulative relative length of the S, G2 and M phase, and the budding index (fraction of budding cells in a population) can serve as a morphological measure for cell cycle progression: a high budding index indicates a short G1 in comparison to the remaining phases and a relatively fast G1-S progression, while a lower budding index indicates a relatively long G1 and relatively slow G1-S progression [362].

This phenotypic characterisation was combined with ConA staining to evaluate cell cycle progression in younger and older cells after tunicamycin treatment. Exponentially growing wild-type cells with the HAC1-activity reporter (FJ4741.1) from YPD medium were stained with TRITC-ConA and diluted into fresh YPD medium with DMSO or 100 ng/ml tunicamycin. After three hours (i.e. around two cell cycles) and under each condition, the morphology, i.e. budded vs. unbudded, of at least 100 random cells from the TRITC-positive and negative subpopulation was quantified with epifluorescence microscopy. The subpopulation-specific budding index was then calculated as the fraction of budded cells in TRITC-positive and negative cells (see figure 5.15)

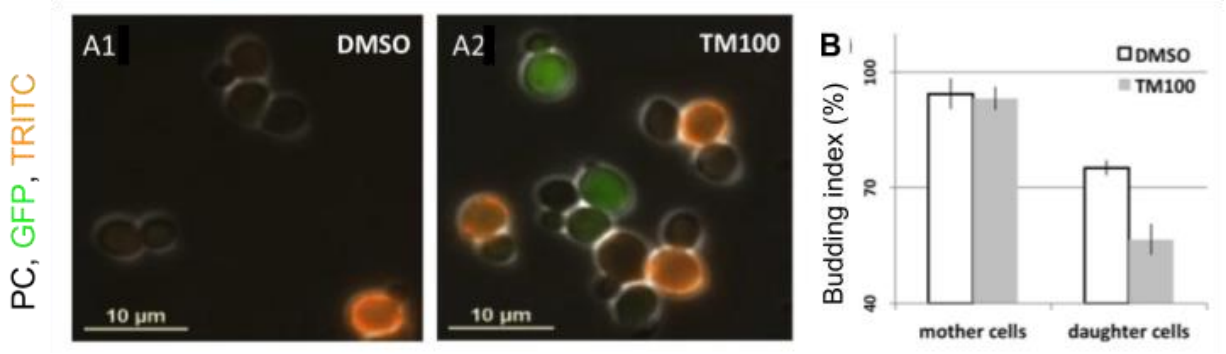

Figure 5.15: Cell cycle progression and UPR activation of mother and daughter cells after weak ER disruption. **A1,2:** The budding of TRITC-ConA-stained HAC1-activity reporter cells (FJ4741.1) after three hours of growth in YPD with DMSO or 100 ng/ml tunicamycin (TM100) was manually quantified with epifluorescence microscopy (phase contrast (PC), reporter fluorescence: green channel (GFP), TRITC fluorescence: red channel). **B:** The TRITC-fluorescence was subsequently used to distinguish cells born before and after the treatment and the budding index calculated for both subpopulations (n=3; at least 100 counted cells per subpopulation and biological replicate, error bars indicate the standard deviation between the biological replicates).

The budding index of TRITC-positive cells was 95% in the DMSO-containing YPD medium and 94% in the tunicamycin-treated samples. For the TRITC-negative subpopulation, the budding index was 75% in YPD medium with DMSO and only 57% in YPD medium with 100 ng/ml tunicamycin.

In both media, the higher budding index of TRITC-positive cells indicated that older cells spent relatively less time than younger cells in G1 compared to the other cell cycle phases. After two divisions, all stained cells are mother cells that have already completed more than one cell cycle, while most of the unstained cells are daughter cells (see figure 5.4). The higher indices therefore suggested a relatively short G1 phase in mother cells, while the largely unchanged budding index in mother cells at 100 ng/ml tunicamycin further indicated that the relative length of their G1 phase is not affected by low ER stress. In younger cells, the decreased budding index at 100 ng/ml tunicamycin suggested that low ER stress increased the relative G1 duration of daughter cells and delayed their G1-to-S progression.

5.15 Tunicamycin increased absolute G1 and G2 duration of both cell types

The previous experiment indicated an increased relative G1 duration for daughter cells at low tunicamycin concentrations, but did not give any insights into the absolute duration of the cell cycle phases in mother or daughter cells under each condition. The different budding indices in younger and older cells further showed an asymmetric dividing population with two different G1

durations (see figure 5.16). While it is straightforward to calculate the absolute cell cycle duration, T_{CC}, from the exponential growth rate, g, of symmetric dividing cells ($T_{CC}= ln(2)/g$), several assumptions were made to calculate the cell cycle duration of mother and daughter cell in YPD medium with and without 100 ng/ml tunicamycin:

(A0) The cell cycle of every cell consists of a budded phase and an unbudded phase (see figure 5.16).
(A1) The absolute duration of the budded phase in mother and daughter cells is similar [363,364].
(A2) During the cell cycle, the resource pool of cells from both subpopulations grows exponentially with the same rate that matches the population growth rate [355].
(A3) Mother and daughter cells divide with the same amount of cellular resources.
(A4) During cell division, the bud becomes the daughter cell and inherits resources that were previously in the bud.

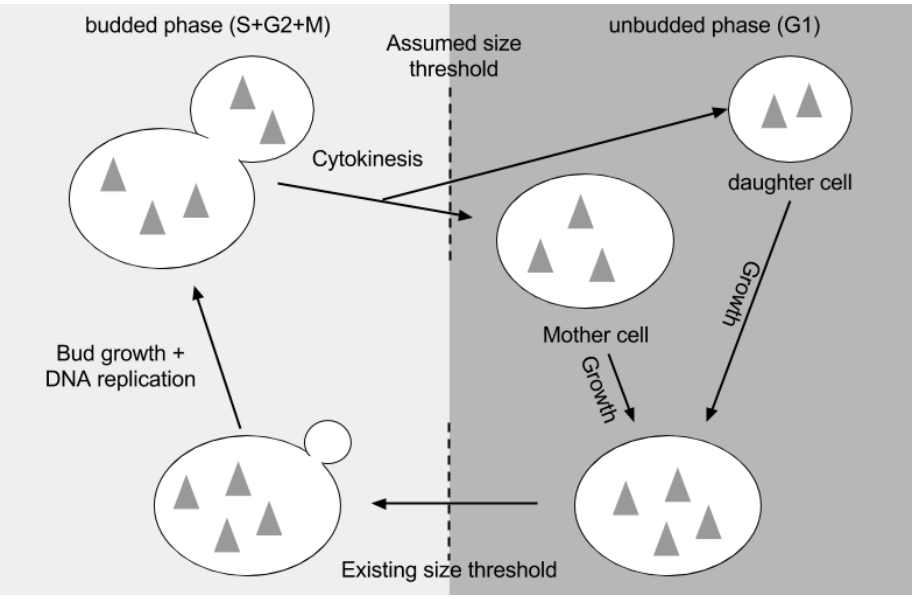

Figure 5.16: The life cycle of *Saccharomyces cerevisiae.*
During cytokinesis cellular resources (grey triangles) are split between mother and daughter cells. After birth, both cells accumulate cellular resources until they reach a certain amount to cross the size threshold, start DNA replication (S Phase) and initiate budding. Due to their lower starting amount of cellular resources this growth phase takes longer in daughter cells. DNA replication, the additional growth phase (G2 phase) and mitosis (M phase) are assumed to take the same time in mother and daughter cells, end with cytokinesis and give rise to a daughter cell and a mother cell. (Dotted lines indicate the experimentally proven size threshold [365], and the size threshold which is assumed in subchapter 5.17).

The necessary parameters values to calculate the absolute duration of each cell cycle stage, i.e. subpopulation-specific budding indices and growth rates, were derived from the experimental data (see table 5.3) and the numerical calculations performed with WolframAlpha®.

Table 5.3: Parameters and variables to calculate the absolute phase durations in both cell types

The values for growth rate and budding index in the different media were taken from subchapter 3.6, 5.1 and 5.14. The exact values of the missing variables are either not necessary ($R_{D0,}$ $R_{M0,}$ R_2) or calculated during the analysis. '*YPD*' corresponds to the growth of yeast in fresh YPD medium, and '*YPD+TM*' corresponds to the growth of yeast cells in YPD medium with 100 ng/ml of tunicamycin. The right column indicates if the quantity was fixed, variable or calculated during the analysis.

Symbol	**Explanation**	**Value**
R_{D0}	Resource pool of a daughter cell after cytokinesis	*variable*
R_{M0}	Resource pool of a mother cell after cytokinesis	*variable*
R_2	Resource pool before cytokinesis	*variable*
x	Relative size of the resource pool in the bud compared to the whole cell before cytokinesis	*calculated*
g	Exponential growth rate (see subsection 5.1)	0.0081 min^{-1} in YPD and 0.0064 min^{-1} in YPD+TM
T_D	Cell cycle duration of daughter cells	*calculated*
T_M	Cell cycle duration of mother cells	*calculated*
T_2	Duration of the budded phase	*calculated*
T_{D1} ; T_{M1}	G1 duration of daughter; G1 duration of mother cells	*calculated*
bi_D ; bi_M	Budding index of daughter; budding index of mother cells (see subsection 5.13)	0.75; 0.95 in YPD and 0.54; 0.94 in YPD+TM

From assumption A4: $R_2 = R_{D0} + R_{M0}$;

$R_{D0} = x\, R_2$ **(5.1);** $R_{M0} = (1 - x)\, R_2$ **(5.2)**

From assumptions A2 and A3: $R_2 = R_{D0}\, exp(g\, T_D)$ **(5.3)**; $R_2 = R_{M0}\, exp(g\, T_M)$ **(5.4)**

equation (eq.) 5.1 in 5.3, 5.2 in 5.4: $R_2 = x\, R_2\, exp(g\, T_D)$; $R_2 = (1 - x)\, R_2 exp(g\, T_M)$

=> $0 = ln\,(x)\; + g\,T_D;$ $0 = ln\,(1-x)\; + g\,T_M$

=> $-ln\,(x)\; = g\,T_D$ **(5.5)** $-ln\,(1-x)\; = g\,T_M$ **(5.6)**

(eq. 5.6/5.5): $\frac{ln(1-x)}{ln(x)} = \frac{T_M}{T_D}$ **(5.7)**

and from assumption A1: $T_2 = T_M bi_M = T_D bi_D$

=> $\frac{T_M}{T_D} = \frac{bi_D}{bi_M}$ **(5.8)**

(eq. 5.7 = 5.8): $\frac{ln\,(1-x)}{ln\,(x)} = \frac{bi_D}{bi_M}$

bi_D and bi_M were then substituted with the experimentally determined budding indices in for YPD and YPD+TM (see table 5.3) and the respective x-values calculated with WolframAlpha:

$x(YPD) = \; 0.459$ and $x(YPD + TM) = 0.405$

x(YPD) and x(YPD+TM) and g in eq. 5.5:

$$T_D = \frac{-ln\,(x)}{g} \Rightarrow T_D(YPD) = 96.1\;min\,; T_D(YPD + TM) = 141.2\;min$$

x(YPD) and x(YPD+TM) and g in eq. 5.6:

$$T_M = \frac{-ln\,(1-x)}{g} => T_M(YPD) = 75.8\;min\,; T_M(YPD + TM) = 81.1\;min$$

From assumption A0 and A1:

$T_2 = bi_D T_D$, $T_{D1} = T_D - T_2$ and $T_{M1} = T_M - T_2$

$T_2(YPD) = 72.0\;min, T_{D1}(YPD) = 24.2\;min, T_{M1}(YPD) \; = 3.8\;min$

$T_2(YPD + TM) = 76.2\;min, T_{D1}(YPD + TM) = 65.0\;min, T_{M1}(YPD + TM) \; = 4.9\;min$

The calculated G1 duration of mother / daughter cells was 3.8 / 24.2 minutes in YPD medium, and 4.9 / 65.0 minutes in YPD medium with 100 ng/ml tunicamycin. The absolute G2 duration of both cell types was 72.0 or 76.2 minutes in YPD medium with DMSO or with 100 ng/ml tunicamycin. The calculated relative size of the resource pool in the bud, x which is inherited to the daughter cell after cytokinesis, was ten percent lower for 100 ng/ml tunicamycin than in YPD medium with DMSO.

This calculation suggested that compared to unperturbed growth, low ER stress also increased the G2 duration of both subpopulations (+6%) as well as the G1 duration of mother cells (+29%), but not to the same extent as the G1 duration of daughter cells (+165%). The decrease in the relative resource pool of the bud (x) from 45.9% to 40.5% at 100 ng/ml tunicamycin suggested a reduced inheritance of cellular resources to daughter cells at low environmental stress.

Based on the overall cell cycle durations, i.e. 141.2 (or 96.1) minutes in daughter cells with (or. without) tunicamycin and 81.1 (or 75.8) minutes in mother cells with (or without) tunicamycin. These results also indicated that the division rate (cell-cycle-duration^{-1}) decreased much stronger

in daughter than mother cells (-31.1% vs. -6.5%), and the relative division rate of daughter cells, i.e. division rate of daughter cells versus division rate of mother cells, thus decreased from 78.9% to 57% at low tunicamycin concentrations.

Interestingly, the relative division rate, which is defined by the cell cycle durations of both subpopulations (T_M/T_D), can be calculated from the relative size of the resource pool in daughter cells after cell division, which decreases at 100 ng/ml tunicamycin (see eq. 5.7).

$$\frac{T_M}{T_D} = \frac{ln(1-x)}{ln(x)}.$$

5.16 The fraction of daughter increases with a decreasing relative division rate of daughter cells

Both the division of a daughter or a mother cell results in one mother and one daughter cell, and both subpopulations thus interact with each other (see figure 5.16):

mother cell ➞ mother cell + daughter cell

daughter cell ➞ mother cell + daughter cell

The net-effect of a daughter cell division is an additional mother cell, while the net-effect of a mother cell division is an additional daughter cell. The division of daughter cells thus increases the number of mother cells and *vice versa*.

Due to this relation, the growth of one subpopulation depends on the division rate of the other subpopulation, and conditions that mainly affect the division rate of one subpopulation, e.g. low ER stress, might have an unexpected impact on the growth of both subpopulations. A model, which accounts for this interaction, can be used to calculate the impact of such conditions on the population growth in both subpopulations and the overall population from the division rate of both subpopulations and to predict the population-wide changes during the adaptation to low ER stress.

First, two new assumptions were made to connect the division rates of both cell types, i.e. mother and daughter cell, with the growth of both subpopulations and the overall population:

(A5) Cells in both subpopulations are completely asynchronous.

(A6) Cell division follows the law of mass action and first order kinetics.

Then, the growth of both subpopulations, M: mother cells and D: daughter cells, at time t, $M'(t)$ and $D'(t)$, and the total population, $P'(t)$, was described with the following formulas, where k_D or k_M denote the division rate of the daughter or mother cell (see table 5.4 for complete list of variables):

$$M'(t) = D(t)\,k_D \textbf{ (5.9)}; \; D'(t) = M(t)\,k_M \textbf{ (5.10)}; \; P'(t) = M'(t) + D'(t) \textbf{ (5.11)}$$

Table 5.4: Names, definitions and comments for the variables of the model, which was used to analyse the growth of both subpopulations and the total population.

Variable	Definition	Comment
$M(t)$	Number of mother cells at time t	$M(t)>0$
$D(t)$	Number of daughter cells at time t	$D(t)>0$
$P(t)$	Total number of cells at time t	$P(t)=M(t)+D(t)>0$
$M'(t)$, $D'(t)$, $P'(t)$	Growth of the mother or daughter subpopulation and the total population	$M'(t)=d\,M(t)/d\,t$, aso
k_M	Division rate of the mother cells	$k_M>0$
k_D	Division rate of the daughter cells	$k_D>0$
$r(t)$	Subpopulation ratio, i.e. daughters per mother cell, at time t	$r(t)=D(t)/M(t)$
r_O	Stable subpopulation ratio	$r_O>0$
$r^*(t)$	Inverse subpopulation ratio, i.e. mothers per daughter cell, at time t	$r^*(t)=M(t)/D(t)=1/r(t)$

The auxiliary variable, $r(t)$, was subsequently defined as the ratio of daughter to mother cells at time t:

$$r(t) = \frac{D(t)}{M(t)} \textbf{ (5.12)},$$

and used to write the relative division rate of each subpopulation, i.e. $D'(t)/D(t)$ and $M'(t)/M(t)$, and the total population, $P'(t)/P(t)$, as:

(eq. 5.12 in 5.9, 5.10 and 5.11):

$$\frac{M\prime(t)}{M(t)} = r(t)\ k_D \textbf{ (5.13)}, \frac{D\prime(t)}{D(t)} = \frac{1}{r(t)} k_M \textbf{ (5.14)}, \frac{P\prime(t)}{P(t)} = \frac{k_M + r(t)k_D}{1+r(t)} \textbf{ (5.15)}$$

These equations showed that relative growth rates only depend on the subpopulation ratio and their division rates but not on absolute sizes. However, divisions of mother and daughter cells alter this ratio continuously. The temporal development of the ratio, *r'(t),* was thus determined with the quotient rule and from the growth of the mother and daughter subpopulation, i.e. *M'(t)* (eq. 5.9) and *D'(t)* (eq. 5.10)*:*

$$r'(t) = \frac{D\prime(t)M(t) - M\prime(t)D(t)}{M(t)^2} = k_M - (\frac{D(t)}{M(t)})^2 k_D$$

$$r'(t) = -r(t)^2 k_D + k_M \textbf{ (5.16)}$$

This highlighted that also *r'(t)* is independent of the absolute cell number and only depends on the subpopulation ratio at time *t* and the division rates of both subpopulations. Because division rates and subpopulation ratios cannot be negative, the phase-plane *r'(t)* vs *r(t)*, is only considered for positive *r(t)* values. In this phase-plane, equation 5.16 corresponds to a downwards-facing parabola with a vertex at $r'(t)=k_M$, $r=0$ and a single positive root (fixed point), r_O (see figure 5.17). As ratios smaller than the fixed ratio grow ($r'(r(t)<r_O)>0$) and bigger ratios shrink ($r'(r(t)>r_O)<0$), a simple stability analysis based on this phase-plane showed that this fixed point, r_O, is asymptotically stable.

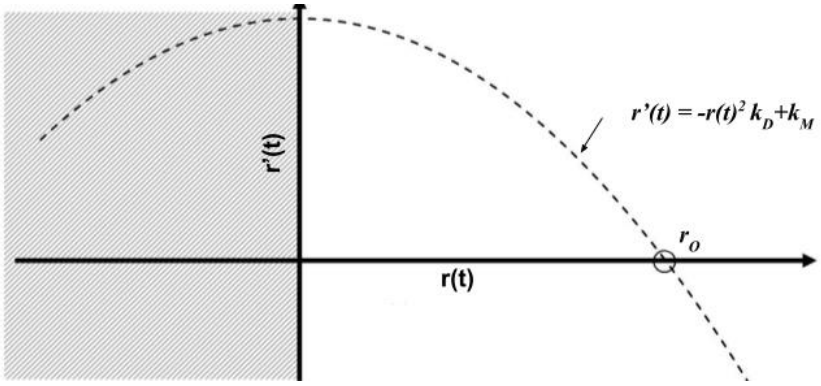

Figure 5.17: The rate of change of the subpopulation ratio r'(t) depends on the subpopulation r(t) in asymmetric dividing cell populations.

The time derivative of the population ratio is plotted against the population ratio. The grey shading indicates the biologically irrelevant parameter space with negative population ratios and the dashed line indicates an exemplary parabola that described the calculated relation between the time derivative and value of the subpopulation ratios in asymmetrically dividing cell-populations (see equation 5.16). r_O indicates the the fixed population ratio. A simple stability analysis shows that this fixed point is asymptotically stable.

The analytical expression of the fixed point r_O was obtained as follows:

eq. 5.16=0: $r'(r_{O1,O2}) = 0$

=> $-{r_{O1,O2}}^2 k_D + k_M = 0$

=> $r_{O1,O2} = \pm\sqrt{k_M/k_D}$

=> $r_{O1} > 0 \; and \; r_{O2} < 0$

=> $r_O = \sqrt{k_M/k_D}$ **(5.17)**

This analytical solution for the fixed point showed that every division rate combination has one asymptotically stable population ratio, which is defined by the square root of the fraction of the subpopulation division rates, i.e. the inverse of the relative daughter cell division rate (see equation 5.17 and figure 5.18).

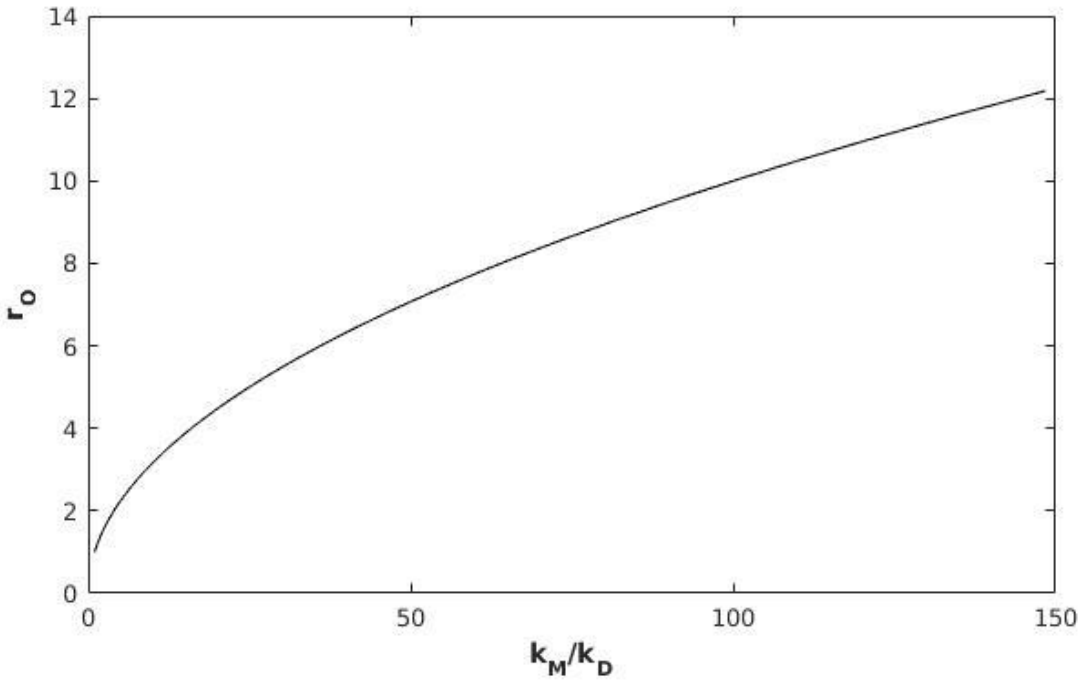

Figure 5.18: Stable population of asymmetric dividing cells only depended on the relative subpopulation division rates.

Stable ratio (r_O), i.e. r'(r_O) =0 is plotted against the relative division rate of the mother cells (k_M/ k_D). The solid line is a square root function that determines the stable ratio for every biologically relevant division rate (i.e. $0 < k_M/ k_D < \infty$). The stable ratio (r_O) is calculated with equation 5.17 and for different ratios of subpopulation division rates (k_M and k_D) from 1 (i.e. the daughter cell divides as fast as the mother cell), to 150 (i.e. the mother cell divides 150 times faster than the daughter cell), and plotted against the relative division rate k_M/ k_D.

Additionally, equation (5.16) was solved analytically using WolframAlpha® to yield the general form of the solution. $r(t)$. This yielded:

$$r(t) = \sqrt{\frac{k_M}{k_D}}\ tanh\ (C + \sqrt{k_M k_D}\ t) = r_O\ tanh\ (C + \sqrt{k_M k_D}\ t)\ <\ r_O \quad \textbf{(5.18)}$$

with $C > 0\ \forall\ r(t = 0) > 0$

However, because the hyperbolic tangent $tanh(.)$ takes on only values smaller than one and approaches one asymptotically from below for large values of its argument $(tanh(x)<1\ \forall x \in R)$, only the time evolution of subpopulations with initial ratios $r(t=0)$ smaller than the stable ratio, $r(t=0) < r_O$, is described by equation 5.18.

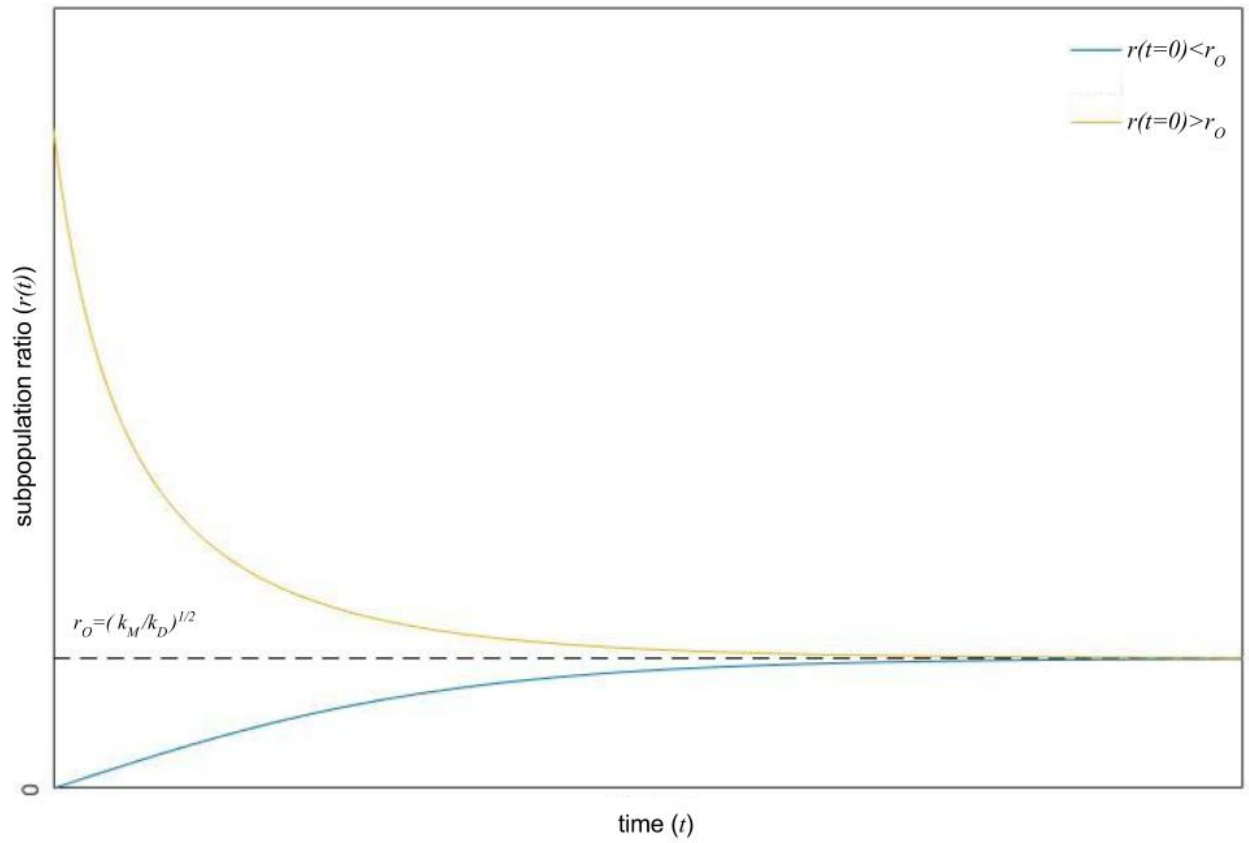

Figure 5.19: The ratio of mother and daughter cells converges towards a stable value.

Equations 5.18 and 5.22 were used to calculate the time evolution of two exemplary subpopulation ratios, one initially much bigger, i.e. $r(t=0)=10\ r_O$ (yellow line), and one initially smaller than the stable ratio, $r(t=0) = 0.01 * r_O$ (blue line).

In order to understand the evolution of subpopulation ratios initially larger than the stable ratio, i.e. $r(t=0)>r_O$, it was necessary to define an auxiliary variable $r^*(t)$, which corresponds ratio mother per daughter cell and is the inverse of ratio $r(t)$:

$$r^*(t) = \frac{M(t)}{D(t)} = \frac{1}{r(t)}$$ **(5.19)** (compare with eq. 5.12)

$$r^{*\prime}(t) = \frac{M\prime(t)D(t) - D\prime(t)M(t)}{D^2(t)} = \frac{k_D D^2(t) - k_M M^2(t)}{D^2(t)} = -r^{*2}(t)k_M + k_D$$ **(5.20)**

The inverse ratio of a stable population, r_O^*, is thus the inverse of the stable ratio:

eq. 5.20=0: $$0 = -r_O^{*2} k_M + k_D$$

$$r_O^* = \sqrt{\frac{k_D}{k_M}} = \frac{1}{r_O}$$ **(5.21)** (compare with eq. 5.17)

And the inverse ration is smaller than the inverse stable ratio, r_O^*, if *r(t)* is bigger than the stable ratio:

eq. 5.12 > r_O and eq. 5.21: $r(t) > r_O \Leftrightarrow \frac{1}{r(t)} < \frac{1}{r_O} \Leftrightarrow r^*(t) < r_O^*$

The differential equation of the inverse ratio (eq. 5.20) was then solved with WolframAlpha® to calculate the time evolution of populations whose population ratio is bigger than the stable ratio.

$$r^*(t) = \sqrt{\frac{k_D}{k_M}}\ tanh\ (C^* + \sqrt{k_M k_D}\ t)\ \forall\ r^*(t=0) < \frac{1}{r_O}$$

$$r(t) = \frac{1}{\sqrt{\frac{k_D}{k_M}} \tanh\left(C^* + \sqrt{k_M k_D}\ t\right)} = r_O \frac{1}{\tanh\left(C^* + \sqrt{k_M k_D}\ t\right)} > r_O\ \forall\ r(t=0) > r_O$$ **(5.22)**

Using this auxiliary variable, *r*(t)*, it was thus possible to show that the time evolution of larger population ratios is the product of the stable ratio and the inverse of a hyperbolic tangent. It thus also converges towards the stable ratio (see equation 5.22 and figure 5.19).

Together the analytic solutions proved that independent of the starting number of mother and daughter cells, the population always converges towards the stable ratio r_O. Typical time courses for both solutions of *r(t)*, i.e equation 5.18 and 5.22, are represented in figure 5.19.

Neglecting the transient required to reach the stable ratio r_O, and assuming that $r(t)=r_O$ gave:

eq. 5.17 in 5.15: $$k_p(r = r_O) = \frac{k_M + r_O k_D}{1 + r_O} = \frac{\sqrt{k_D}\,(k_M + \sqrt{k_M\, k_D})}{\sqrt{k_D}(1 + r_O)} = \sqrt{k_M\ k_D}\ \sim\ g$$ **(5.23)**

where k_P, i.e. the average division rate of a population that has already reached the stable ratio r_O, is equal to the geometric mean of the subpopulation-specific division rates (see equation 5.23). This result suggested that a mechanism, which decreases the division rate of one subpopulation but increases the division rate of the other subpopulation, does not necessarily change the population growth rate.

Interestingly, the geometric mean of division rates of both subpopulations, $\sqrt{k_M\ k_D}$, is also the time scaling factor in the argument of the hyperbolic tangent that described the time evolution of the population ratio (see equations 5.18 and 5.22). As the hyperbolic tangent rapidly approaches one, *tanh(3)>0.99,* this stipulated that few doublings would be sufficient to closely approach the stable

population ratio from any starting population. It thus seems appropriate to neglect transients and assume populations have already reached their stable ratio, r_O, in long-term experiments.
Overall, this theoretical investigation suggested that environmental conditions such as low ER stress, which decrease the division rate of daughter cells stronger than mother cells, also increase the fraction of daughter cells and lead to a population growth rate, which is defined by the geometric mean of the individual division rates, over the long run.

5.17 Asymmetric inheritance of growth-limiting resources lowers the average resource amount of the total population

The two previous analyses revealed two growth rate-independent features of asymmetric cell division: (A) The division rate ratio of descending cells, i.e. mother and daughter, is determined by the inheritance of the limiting resources. (B) Independent of the initial conditions and after a few cell divisions, the subpopulation ratio remains constant and is defined by the relative division rates of both subpopulations.
Furthermore, changes in the inheritance also influence the average resources in both subpopulations. The average amount of limiting resources per cell sets the resource demand of a growing population, which is another insightful characteristic of the population. The impact of lower inheritance to the daughter cell, i.e. a smaller x, on the average resource amount of both subpopulations and the total population was thus investigated theoretically. Two additional assumption were made to calculate resource pool size in an average cell of both subpopulations and the total population:

(A7) Independent of the growth rate or the environment, cell division is always initiated at the same critical amount of the limiting resource, i.e. R_2.
(A8) The environment is stable and the population has already reached the stable subpopulation ratio, r_O.

The exponential model for cell growth (see eq. 5.3 and 5.4) was subsequently used to calculate the evolution of limiting resources over the mother or daughter cell cycle for any critical resource amount, R_2, using the experimentally determined values for the relative inheritance, x, and the growth rate, g, in pure YPD medium (see figure 5.20).

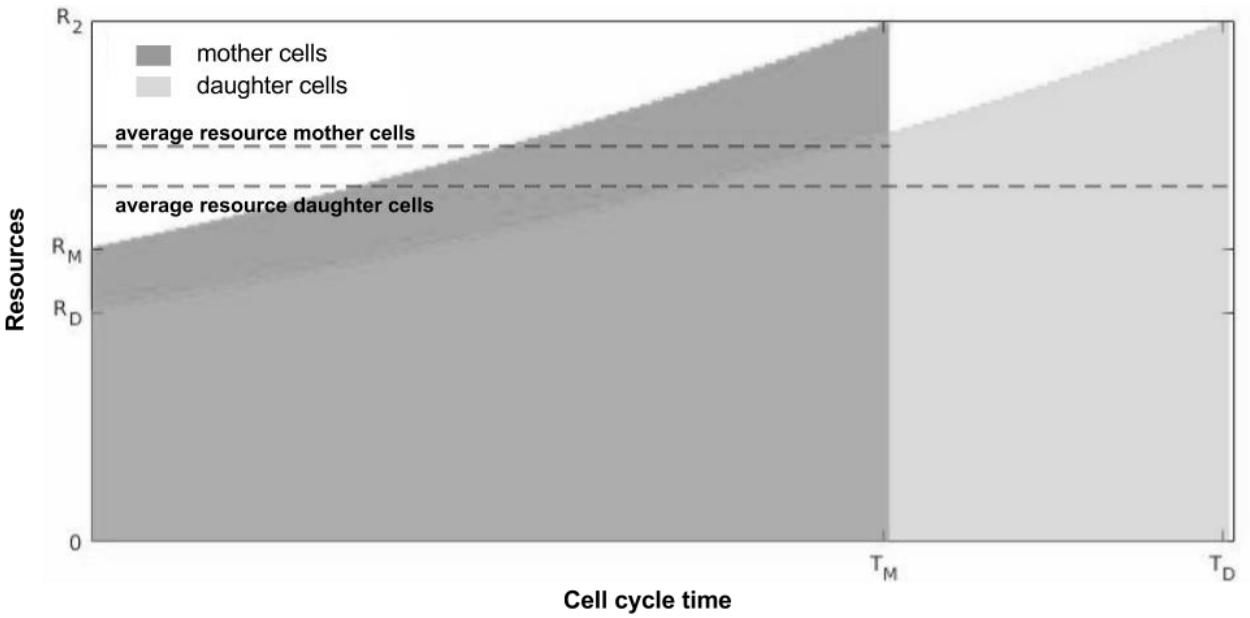

Figure 5.20: The evolution of cellular resources in mother and daughter cells over the cell cycle.
The resource amount at each point of the cell cycle of daughter (light grey, back) and mother (dark grey, front) cells were calculated with equations 5.3 and 5.4 and the experimentally determined inheritance fraction and growth rate in YPD medium (x = 0.44, g=0.081 min^{-1}). The average resource amount of mother and daughter cells was calculated with formulas 5.24 and 5.25.

Because cells of each subpopulation are asynchronous and uniformly distributed over the cell cycle (see A5), the average cellular resource in each subpopulations, R_D or R_M, is equal to the time average of an individual cell over the entire cell cycle, i.e. ergodicity. The average resources in both subpopulations can thus be expressed with the general variables of table 5.5 as follows:
For daughter cells:

Assumption A5: $$R_D = \frac{\int_0^{T_D} R_D(t)\, dt}{T_D}$$

Assumptions A2, A4: $$R_D = \frac{\int_0^{T_D} x R_2\, e^{gt}\, dt}{T_D} = \frac{x\, R_2\, (e^{gT_D} - 1)}{g\, T_D}$$

see eq. 5.5 ($-ln(x) = gT_D$) : $$R_D = \frac{R_2 - x\, R_2}{-ln(x)} = \frac{R_2\, (1-x)}{-ln(x)}$$ **(5.24)**

Analogues for mother cells: $$R_M = \frac{R_2\, x}{-ln(1-x)}$$ **(5.25)**

Table 5.5: Parameters and variables to calculate the average resource pool size in each subpopulation and the overall population in dependence of the inherited fraction.

The symbol and description of each quantity that was used in the model. The right column indicates if the quantity was fixed, variable or calculated during the analysis.

Symbol	Definition	Value
$R_D(t)$	Amount of the limiting resource in a daughter cell at time t	*variable*
$R_M(t)$	Amount of the limiting resource in a mother cell at time t	*variable*
R_2	Amount of R that is required to initiate cell division	*Fixed (A7)*
g	Exponential growth rate	*variable*
x	Relative amount of the resource at birth in the daughter cell ($1>x>0.5$ just switches the mother-daughter relation)	$0<x<0.5$
R_D	Average resource content of a daughter cell	*calculated*
R_M	Average resource content of mother cell	*calculated*
R_P	Average resource content of any cell in the population	*calculated*
T_D and T_M	Cell cycle duration of daughter and mother cell	*variable*

This calculation showed that the average resource content in both subpopulations is determined by the relative inheritance and the final resource amount but is independent of the growth rate in a given environment.

To investigate the change of the average resource content in both subpopulations with x, the first derivatives of the average resource amount in mother and daughter cells (see equations 5.24 and 5.25) ($d/dx\ R_D(x)$ and $d/dx\ R_M(x)$) were calculated.

$$\frac{d}{d\,x}R_D(x) = -R_2\left(\frac{-ln(x)+(1-x)x^{-1}}{ln^2(x)}\right) = R_2\,\frac{x\,ln(x)+1-x}{x\,ln^2(x)} > 0, \forall\, x > 0 \quad \textbf{(5.26)}$$

$$\frac{d}{d\,x}R_M(x) = -R_2\,\frac{ln\,(1-x)+x\,(1-x)^{-1}}{ln^2(1-x)} = R_2\,\frac{(1-x)\,ln(1-x)+x}{(x-1)\,ln^2(1-x)} < 0, \forall\, 1 > x > 0 \quad \textbf{(5.27)}$$

This showed that the first derivative of R_D is always larger than zero for all x-values larger than zero (see equation 5.26), and the first derivative of R_M is smaller than zero for all x-values between

zero and one (see equation 5.27). These boundaries indicated that a bigger relative inheritance to the daughter cell reduced the average resource content of mother cells and increased the average resource content of the daughter cells (see figure 5.21 for x from 0 to 0.5).

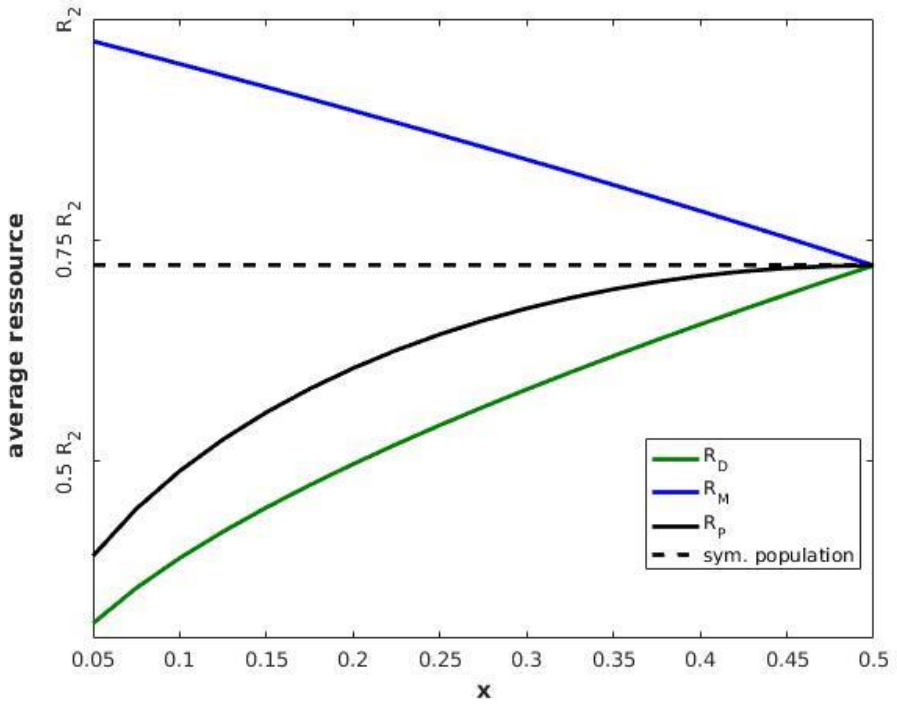

Figure 5.21: Average cellular resources in an asymmetric dividing population decreases with decreasing inheritance.

The average resources in mother (R_M, blue line) or daughter cells (R_D, green line) for the different relative inheritance values, i.e. x, were calculated with equations 5.26 and 5.27. Equation 5.28 was used to subsequently calculate the resource content of an average cell for the different x-values (R_P, black line) (dashed line indicates the average resources in symmetrically dividing cells).

The relative inheritance to the daughter cell also determines the relative growth rate ratio of the daughter cells (see eq. 5.7) and thus the stable population ratio, r_O (see eq. 5.17):

eq. 5.7: $$\frac{ln(1-x)}{ln(x)} = \frac{T_M}{T_D} = \frac{k_D}{k_M}$$ **(5.28)**

eq 5.28 in 5.17: $$r_O = \sqrt{\frac{ln\,(x)}{ln\,(1-x)}}$$ **(5.29)**

The average resource content in the population, R_P, which is defined by the number of mother and daughter cells in the population and the average resources in each subpopulation, can be calculated from the subpopulation ratio and the average resource content in each subpopulation:

$$R_P = \frac{M(t)\,R_M + D(t)\,R_D}{D(t)+M(t)} = \frac{M(t)\,(R_M + r(t)\,R_D)}{M(t)\,(1+r(t))}$$

With assumption A8: $$R_P = \frac{R_M + r_O R_D}{1+r_O}$$ **(5.30)**

Equations 5.26, 5.20 and 5.29 were used to define R_P in dependence of x:

$$R_P = -R_2 \frac{\frac{x}{ln(1-x)} + \sqrt{\frac{ln(x)}{ln(1-x)}}\frac{(1-x)}{ln(x)}}{1+\sqrt{\frac{ln(x)}{ln(1-x)}}} = -R_2 \frac{\frac{x\sqrt{ln(x)} + (1-x)\sqrt{ln(1-x)}}{ln(1-x)\sqrt{ln(x)}}}{\frac{\sqrt{ln(1-x)}+\sqrt{ln(x)}}{\sqrt{ln(1-x)}}} = -R_2 \frac{x\sqrt{ln(x)} + (1-x)\sqrt{ln(1-x)}}{\sqrt{ln(x)}\sqrt{ln(1-x)}(\sqrt{ln(x)}+\sqrt{ln(1-x)})}$$

$$R_P = -R_2 \frac{1}{(\sqrt{ln(x)}+\sqrt{ln(1-x)})}\left(\frac{x}{\sqrt{ln(1-x)}} + \frac{1-x}{\sqrt{ln(x)}}\right)$$ **(5.31)**

This calculation confirmed that relative inheritance to the daughter cell determines the average cellular resource content in asymmetric dividing populations. A numeric calculation of average resource contents for all x-values from 0 to 0.5 further showed that it is smaller than the average resource content in symmetric dividing populations and increases with inheritance until $x=0.5$, i.e. when mother and daughter inherit the same amount of cellular resources (see figure 5.21).
Overall, this theoretical exploration of asymmetric cell division suggested that it enables an organism to lower the average cellular resource pool and the resource demand of growing populations without affecting the exponential growth rate.

5.18 Discussion

To understand how cells adequately respond to quantitatively different ER stress levels, chemical agents and reporter proteins were used to study the phenotypic consequences of different ER stress levels in wild-type cells and cells with a perturbed adaptation.
Firstly, the growth rate of wild-type or UPR-deficient cells and the HAC1-activity reporter stipulated that different tunicamycin concentrations provoked different levels of ER stress, which are characterised by different growth rates and UPR activities of wild-type cells. Moreover, the impact of the medium composition and SUR2 knock-out highlighted the importance of the metabolic state for the effect of tunicamycin and phytoceramide.
Reduced tunicamycin effect in minimal medium most probably resulted from slower growth (see chapter 4), while SUR2 knock-out or phytoceramide supplementation in rich medium could directly affect ER homeostasis [54] but also just hinder the import of tunicamycin into the cell [366]. No previous studies connected phytoceramide toxicity to ER homeostasis [367,368], the

strong effect on HAC1-deficient cells hence probably resulted from secondary effects of HAC1 knock-out and not ER disruption.

The experiments with an ER-localised fluorescent protein and a symmetric-dividing *S. cerevisiae* mutant as well as a bioinformatic evaluation of published data further implied that asymmetric ER content inheritance and maybe daughter-specific transcription contributed to daughter-specific UPR activation at low ER stress. The budding behaviour of wild-type cells with and without tunicamycin addition highlighted that low ER stress primarily slows G1 progression of daughter cells. However, a calculation, which accounted for asymmetric cell division and the lower growth rate in tunicamycin, showed that low tunicamycin concentrations actually increased the absolute duration of the G1 and G2 phase in mother and daughter cells, but the relative impact on the daughter cells was bigger.

A summarising model for exponential cell growth and asymmetric cell division suggested that the stress-dependent inheritance regulation, which caused the daughter-specific effect, also increases the fraction of daughter cells during long-term growth and reduces the average cellular resource demand of the total population.

Decreased ER content inheritance under low ER stress resembled two established mechanisms of ER inheritance control, CWI-dependent ER surveillance (ERSU) and the ceramide-dependent bud neck barrier [146,165,166,369], but the initial experiments were not able to connect it to or separate it from one of them. A low ER stress regime with intermediate growth inhibition could not be established for tunicamycin-sensitive ERSU-deficient cells, i.e. CWI-deficient SLT2 knock-out cells (see subchapter 5.11). Moreover, SUR2 knock-out, which perturbed SL biosynthesis and lowered the bud neck barrier in minimal SC medium [165], did not prevent heterogeneous UPR activation at low ER stress and might not perturb ceramide synthesis in peptide-rich YPD medium (see subchapter 4.7). However, as inherited ER is primarily synthesized during G2 [44], increased G2 duration might not compensate slower cortical ER synthesis at low ER stress, which then results in lower inheritance even without active regulation.

Interestingly, the investigated mechanism benefitted the division of mother cells and seemed to oppose most other mechanisms for organelle inheritance that rejuvenate the daughter cell [165,186,188,370,371]. However, these previous investigations focussed on the nature of the preferentially inherited molecules, e.g. ageing factors, protein aggregates or mitochondria, and did not determine the impact of asymmetric cell division on the doubling time of mother and daughter cells in normal or stress conditions. Because mother cells, which retain growth-promoting factors like the translation machinery or chaperones, probably divide faster than their daughter cells [186,370], both effects (i.e. daughter rejuvenation and mother preference) could

actually be two sides of the same coin: rejuvenated but slowly dividing daughter cells and rapidly dividing but ageing mother cells.

As outlined in the introduction, the observed heterogeneous UPR activation at low ER stress was not observed in previous investigations of ER homeostasis that used long-lived fluorescent proteins [154,168,339]. Even though other cellular parameters, i.e. protein translation and protein degradation, could possibly cause the observed differences between mother and daughter cells, the previously used reporters, which took much longer to respond to high chemical concentrations (2 vs. 4 hours), were most probably not able to detect the transient cell-to-cell differences in low-stress conditions, i.e. lower chemical concentrations or protein overexpression.

Accordingly, a fluorescent reporter for ER redox potential, i.e. eroGFP, already indicated differences in ER homeostasis of individual cells during inositol starvation or protein overexpression, but the simultaneously measured long-lived HAC1 reporter did not to detect corresponding differences in UPR activity [168]. As most previous investigations were performed in minimal SC medium, it would further be interesting to re-evaluate the UPR activity in those conditions with the fast-degrading reporter and test if cell-to-cell differences in UPR activity are a common feature of low ER stress or only pronounced in nutrient-rich environments (e.g. YPD medium).

Apart from the UPR, cell-to-cell differences have been shown previously for other cellular processes, e.g. growth, sugar metabolism or the adaptation to hyperosmotic stress [206,342,372–376]. Because these differences similarly correlated with other cellular parameters such as cell size, replicative age or sugar concentration, they were probably generated by a non-stochastic mechanism. In contrast to this project, those studies did not consider or investigate the effect of asymmetric cell division, which could explain the observed correlations.

For the decreased budding index, an ER-homeostasis-dependent G1-S transition has been proposed previously [377]. However, in contrast to the UPR-dependent repression of cyclins in mammalian cells [378], the UPR in yeast was only shown to be important for cytokinesis and no other cell cycle phases [194,195]. Strong chaperone, i.e. KAR2, expression at the end of G1 and ER-localised cell cycle regulators could still support and sense ER homeostasis before DNA replication and connect G1-to-S-transition to ER homeostasis independently of the UPR [293,379,380].

With respect to the two types of heterogeneity and since daughter cells turn into mother cells with their first cell division, the observed asymmetric UPR activation could represent temporal, i.e. cells deactivate their UPR after the first cell cycle, or cellular heterogeneity, i.e. cells born after

tunicamycin exposure activate the UPR. It is thus necessary to determine UPR activity of post-treatment cells after their first cell division to distinguish between both cases:
If they shut off the UPR after cell division, it can be regarded as temporal heterogeneity, but if they maintain the UPR activity, it needs to be regarded as cellular heterogeneity. In the latter case, the median fluorescence of the total population should increase with the dilution of original cells, but an ER homeostasis dependent G1-S-progression would still be sufficient for an adequate average response to different stress levels, i.e. more stress would extend G1 phase and UPR activation for all cells.
The theoretical model suggested that asymmetric inheritance increases the number of daughter cells and provides a growth-rate-independent way to minimise the relative resource demand of a yeast population. This benefit has already been simulated and experimentally validated during zinc starvation but could also underlie the smaller daughter cell size in poorer carbon sources [356,363,381,382].
In contrast to previous models, the constructed model offered an analytical solution, and its predictions were thus independent of most parameters and less sensitive to experimental errors. Even though most assumptions were justified experimentally, the assumptions of a fixed resource pool at the end of cytokinesis, i.e. A3 and A7, were not supported by experimental data and only made to simplify the calculations.
The actual prerequisites for cytokinesis at the end of G2 are currently not known [383–385], and the assumptions rather disagreed with some experimental evidence that indicated a continuous growth of mother cells during subsequent cell divisions and a smaller size at cytokinesis under different environmental conditions [363,386,387]. The resource content of *S. cerevisiae* is actually monitored at the G1-to-S-transition, i.e. budding. An accordingly adjusted model would most likely reiterate the results but relies on the relation between budded phase duration and growth rate in different environments, which first need to be quantified with live cell microscopy or through the budding index at different tunicamycin concentrations.
The predicted resource savings, which are independent of the growth rate, could also be achieved in an optimal environment, but the model did not indicate any particular benefit of the increased asymmetry in stressed conditions. In this respect, a lower asymmetry under good conditions could store resources for later use in worse environments, and it would be interesting to investigate this potential benefit of heterogeneous populations experimentally (see chapter 7).

6 Discussion

6.1 Summary of results

The purpose of this work was to better understand transcriptional adaptation after perturbations that do not require the full activation of a single signaling pathway but instead require a combined activation of different signaling pathways. However, due to a lack of tools to investigate yeast metabolism and transcription in single cells and at the desired temporal resolution, it was first necessary to develop the appropriate tools before studying the transcriptional response to two representative complex perturbations, i.e. inositol starvation representing a diversified lipid perturbation with a multi-faceted transcriptional response and weak ER stress representing graded stress.

After explaining the general motivation as well as presenting background knowledge in the first chapter and introducing the applied experimental methods in the second chapter, the feasibility of two different tools, i.e. destabilised transcriptional reporter proteins and fluorescently labeled lipid metabolites, to study the transcriptional and metabolic changes of single yeast cells was explored in the third chapter.

For the first tool and based on a quantitative model, transcription factor-specific promoter sequences were combined with a fast-folding, actively-degraded fluorescent protein to develop reporter systems for the three transcription factors that induce most transcriptional changes after inositol starvation, RLM1, HAC1 and INO2/4. After transcription factor stimulation, the reporter fluorescence increased on a timescale (~15 minutes) that resembled gene induction and was shorter than the doubling time of *S. cerevisiae*. Moreover, reporter fluorescence was relatively unaffected by environmental changes that did not affect promoter activity, and the basal reporter expression did not interfere with cell growth.

As reporter for changes in sphingolipid metabolism, *in vivo* staining with the lipid analogue NBD-C6-ceramide resulted in an NBD fluorescence that changed its subcellular localisation and increased after chemical IPC synthesis inhibition. However, since NBD fluorescence is very sensitive to the environment [268], those observations possibly resulted from unknown side effects, e.g. a perturbed ergosterol metabolism, and not directly from changes in sphingolipid metabolism.

In the fourth chapter, the developed reporters were first used to compare the similarities and differences between inositol depletion, which rapidly changes overall lipid metabolism, and SUR2 knock-out, which only affects SL biosynthesis. Increased RLM1 activity during inositol starvation or after SUR2 knock-out at elevated temperatures and GAP1 trafficking suggested that

sphingolipid metabolism is mainly required for trafficking along the secretory pathway and to maintain cell wall integrity under normal and stress conditions. From the different UPR activities after both treatments and ceramide synthase inhibition during inositol starvation emerged that ER stress during inositol starvation was not triggered by SL metabolism but by an unrelated change in phospholipid metabolism, while SUR2 knock-out or slow growth supported ER homeostasis after tunicamycin treatment. In line with the higher SUR2 expression in rich media and the elongated G2 phase during inositol starvation, a bioinformatic analysis of published data further showed that SL biosynthesis is probably induced during the budded phase of dividing cells.

For the multi-faceted transcriptional response, the reporter dynamics after inositol starvation and the phenotype of different genetic mutants argued against an immediate adaptation and proposed a temporal sequence of metabolic and transcriptional changes that is characterised by three possibly interdependent steps: (I) PA accumulation and INO2/4 activation; (II) an ER disruption, which possibly depends on INO2/4 activation and PC accumulation, UPR activation and decreased AUR1 activity; (III) a UPR-dependent cell wall perturbation and RLM1 activation, which probably resulted from lower IPC synthesis.

In the fifth chapter, the dynamic HAC1 reporter and established fluorescent reporters for replicative age or ER content were used to investigate the maintenance of ER homeostasis in single cells at different ER stress levels. The distinction between mother and daughter cells during low ER stress, which doesn't require full UPR activation, revealed that such a graded perturbation reduced the inheritance of ER content to the daughter cell and then triggered the daughter-specific UPR activation. This asymmetric response also delayed G1 progression of daughter cells. However, a calculation, which accounted for the measured growth rate reduction in tunicamycin, further suggested a minor elongation for the G1 phase of mother cells and for the budded phase of both cell types.

These results motivated the development of an abstract model for asymmetric cell division, whose analysis implied that decreased inheritance of important resources eventually increases the fraction of daughter cells and lowers the demand for the limiting resource. Even though the experimental verification of this prediction for ER inheritance at low ER stress exceeded is project, both properties of asymmetric cell division were already verified for the inheritance of the vesicle in low zinc environments [356].

6.2 Evaluation of the approach

In addition to generating new insights into sphingolipid metabolism, ER homeostasis and fungal adaptation, the fourth and fifth chapter also demonstrated the potential of the modular reporter system and NBD-C6-ceramide.

In comparison to unbiased, genome-wide approaches such as microarrays, RNA sequencing or protein mass spectroscopy, targeted techniques, e.g. fluorescent reporter proteins, require prior knowledge and cannot be used to investigate completely new biological processes or organisms [388,389]. However, in a well-studied model organism such as *Saccharomyces cerevisiae* and for relatively well-understood processes such as ER homeostasis or sphingolipid metabolism, this restriction is less problematic.

For low ER stress and inositol starvation, the two alternative methods to investigate specific transcriptional responses, i.e. long-lived reporter proteins and endogenously tagged signaling components, might not enable the same insights as actively-degraded reporter proteins.

Long-lived reporter proteins might fail to detect the transient differences between mother and daughter cells at low ER stress or differences in the transcription factor dynamics after inositol depletion. This disadvantage might explain why Merksamer *et al.* [168] detected cell-to-cell differences with a reporter for ER redox potential but not with a long-lived reporter for UPR activation. Moreover, the rapid response of reporters might be particularly important to detect transcriptional changes before cell death from toxic treatments (e.g. Aureobasidin A or Fumonisin B1 [33,83]) or auxotrophic strains. The main advantage of stable reporter proteins is a higher sensitivity during long-term experiments, which seems unnecessary for this project as the fast-degrading fluorescent proteins enabled a clear signal detection with all tested promoters. If reporter fluorescence is an issue in future studies, tandem GFP molecules could amplify the fluorescence from less-active promoters [390].

For GFP-tagged signaling components, the abundance of signaling components does not necessarily change after a specific stimulus, and subcellular relocalisation is commonly used to determine pathway activity [391–393]. While transcriptional changes are a common feature of most signaling pathways [7], this subcellular relocalisation already differs between the three investigated pathways: IRE1 clusters and HAC1 re-localises to the nucleus during UPR activation [25]. RLM1 resides in the nucleus independent of cell wall disruption and also no other component of the kinase cascade is known to relocalise [238]. The inhibitor OPI1 re-localizes from the nucleus to the ER membrane, but the INO2/4 complex remains permanently inside the nucleus in response to phosphatidic acid accumulation [393].

These differences prevent the development of a general scheme for all signaling pathways and complicate data analysis. N- or C-terminal GFP tags might further perturb the native function of a signaling component and, in the worst case, change the adaptative response [394].

In contrast to the clear benefits of destabilised reporter proteins, the data suggested that the potential application of NBD-C6-ceramide is limited. NBD fluorescence increase might not be specific to the rate of IPC synthesis, and NBD-C6-ceramide did not provide any insights that cannot be gained with large-scale techniques.

The lack of specificity is a strong argument against any method. Even though the inositol dependency of IPC synthesis might have enabled the detection of changes in lipid metabolism with NBD-C6-ceramide in this project, NBD-C6-ceramide might fail to detect changes in SL metabolism that decrease IPC synthesis but have a different effect on ergosterol synthesis or might falsely react to changes in ergosterol metabolism in future studies. Moreover, the main motivation to substitute population-wide measurements with fluorescent probes was to detect cell-to-cell differences in lipid metabolism under different conditions, but the cellular NBD fluorescence mostly followed a uniform distribution, which indicated no cell-to-cell differences, and suggested that population-wide measurements would also detect the differences in lipid metabolism between the different conditions [395].

However, sample preparation for conventional lipidomic techniques is more demanding than simple staining, and NBD-C6-ceramide might be a valuable tool to screen ergosterol and sphingolipid metabolism in many different environmental conditions or after genetic perturbations, before a limited in-depth investigation with large-scale techniques is carried out [396].

In addition to these reporters, mathematic models were, for example, applied to connect the phenotypes of individual cells to the overall growth rate and understand the evolutionary advantage of asymmetric inheritance.

On the one hand, the calculated duration of the individual cell cycle phases, which only relied on two robust measures (i.e. budding index and growth rate), facilitated to assign the impact of certain conditions on the different cell cycle phases (i.e. budded or unbudded) and life stages (i.e. mother or daughter cell) of *S. cerevisiae.* However, the sensitivity of this approach should be verified under conditions for which the individual cell cycle durations were already determined with single-cell microscopy, e.g. gene knock-outs [355], before a future application.

On the other hand, the insights from the more elaborated model, e.g. reduced resource demand from asymmetric cell division, partially relied on simplifying assumptions that were not exclusively based on experimental results, e.g. constant resource content at cell division. However, ER stress and UPR induction actually increased ER content and size [156,397], and this model might be

less applicable to such actively regulated resources and more useful to understand resources that are not actively managed by the cell, e.g. the vacuole during metal starvation [356].

6.3 Concluding remarks

In this study and with a set of novel reporter proteins, transcriptional changes were measured on single-cell level and with higher temporal resolution than in previous studies. This resolution helped to better understand the adaptation of eukaryotic organisms to environmental stimuli that do not require the full activation of one signaling pathway but rather a graded activation or the activation of multiple signaling pathways.

For multiple signaling pathways, the sequential transcription factor activation during inositol starvation suggested that adaptation is not always an instantaneous process, where the final response is immediately triggered by a specific perturbation, but can be a dynamic process, in which different interacting signaling pathways are affected at different times and by different changes (e.g. phospholipid metabolism, ER homeostasis and cell wall integrity) after the initial stimuli. This modularisation delays the final response and differs from the concept of master regulators or hubs, i.e. certain transcription factors in mammalian development that alone can trigger big phenotypic changes [398] (see figure 6.1).

Slow modularisation might represent a disadvantage in fast-fluctuating environments but seems more adjustable to variations of the initial stimulus that do not have the same effect on all modules [7]: An elevated growth temperature during inositol starvation, for example, probably increases the perturbation of cell wall integrity but might have a much smaller impact on ER homeostasis or lipid metabolism. A modular mechanism could subsequently respond with a higher PKC activity but similar UPR and INO2/4 activities [23]. Due to this trade-off between speed and flexibility, the transcriptional adaptation to frequent and highly reproducible environmental changes that require rapid adaptation such as amino acid starvation might rather be controlled by a master regulator [399], while the adaptation to less frequent and more variable changes, e.g. inositol depletion or gene knock-out [400], is probably governed by the interaction of modules that do not all detect the initial stimulus.

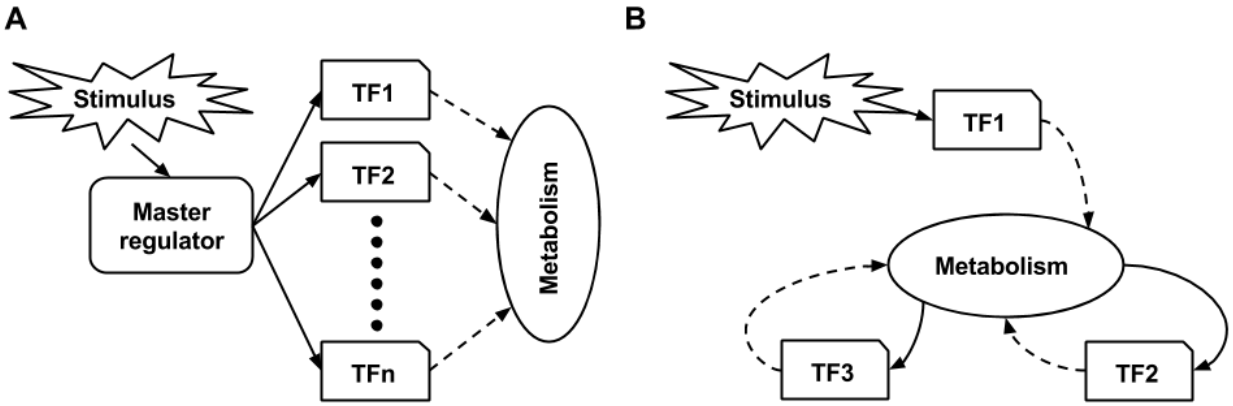

Figure 6.1: Two alternative ways to activate multiple transcription pathways and adapt to complex perturbation. **A**, Master regulator or hubs detect the initial stimulus and subsequently activate the necessary transcription factors (TF). **B,** A stimulus activates one transcription factor, which induces the expression of genes that change metabolism and this change subsequently activates other transcription factors.

For quantitatively different stresses, the coordination of asymmetric ER inheritance and UPR activation at low ER stress suggested that cells use an additional level of complexity, i.e. cell-to-cell differences and temporal separation, to achieve an adequate response and minimize the cost of transcriptional adaptation. Therefore, the life cycle of *S. cerevisiae* is probably divided into two consecutive phases: a growth phase, i.e. unbudded period of daughter cells, and a replication phase, i.e. budded period of mother and daughter cell (see figure 6.2).

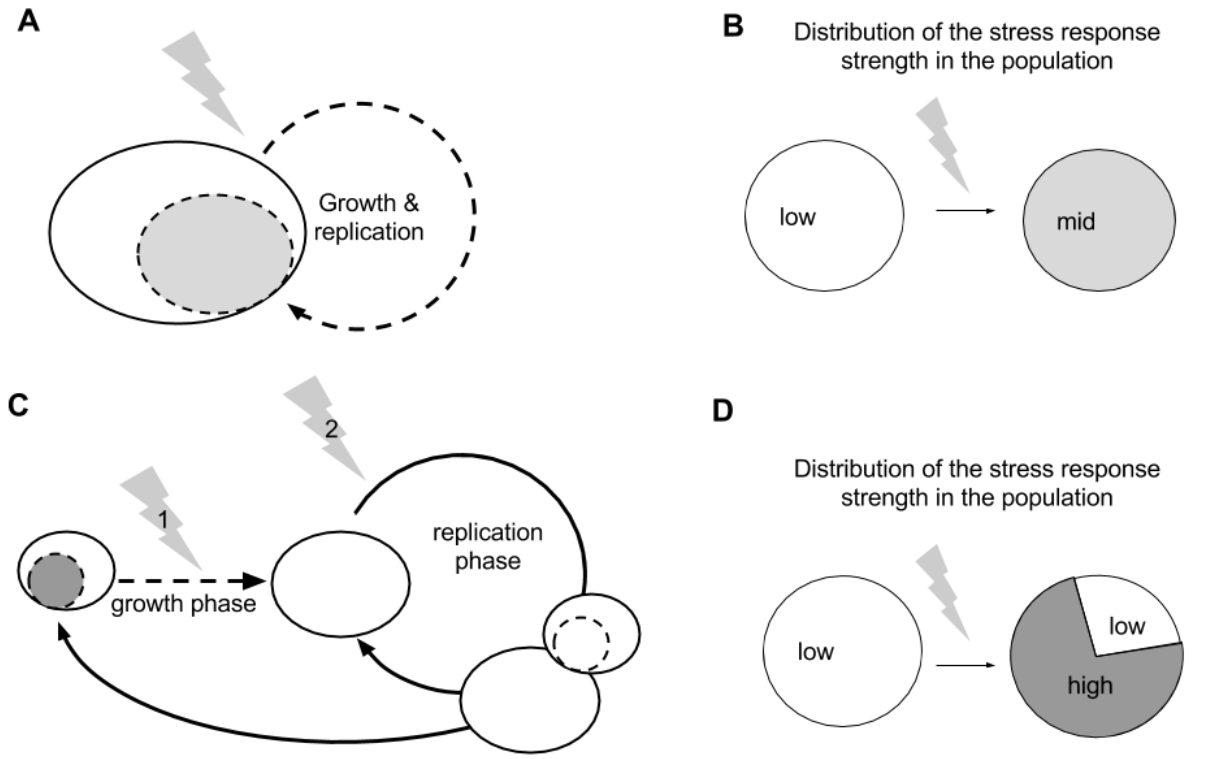

Figure 6.2: A divided life cycle and population heterogeneity.

A, In a homogenous life cycle, environmental stress results in a longer cell cycle (dashed lines) and affects all cells equally (dashed, grey cell).The population thus, consists of equally affected cells that all need to respond to the stress (**B**). **C,** In a divided life cycle, environmental stress results in a longer growth phase of new-born cells (1, dashed line) and handicapped new-born cells (2, dashed dark grey cells). But does not affect the duration of the replication phase or the phenotype of the existing cells**.** Therefore, the population consists of a small fraction of non-affected cells and a much larger fraction of handicapped cells with a strong stress response (**D**).

Because cells actively respond to environmental changes during the first phase, perturbations lead to big metabolic rearrangements, e.g. UPR activation, and unbudded phase extension. During the replication phase, cells are less responsive towards environmental changes, and environmental perturbations thus have a small impact on the duration of the budded phase but mainly cause defects in new-born daughter cells, e.g. lower ER inheritance.

Similar to low ER stress, conditions that reduce protein translation primarily changed the duration of the unbudded phase of daughter cells [364], and this then led to the proposal of a size-dependent G1-to-S transition, which separates between the environmental-sensitive growth phase and the robust replication phase [365].

Independent of the molecular mechanism, which enables this cellular '*division of labor'* among responding and nonresponding cell during low ER stress, the model proposed that the observed

asymmetric ER stress distribution leads to a condition where the stress level is not reflected by the strength of the adaptive response in individual cells but by the fraction of daughter cells and the duration of their G1 phase, i.e. more daughter cells with longer G1 for higher stress levels [29,363].

The transient activation of signaling pathways during the G1 phase also limits the maximal duration of possible oscillations and the cost of over-compensations due to burst-like transcription. Interestingly, other organisms that do not have a size-dependent checkpoint for DNA replication and are believed to divide symmetrically, e.g. *S. pombe* and *E. coli*, also use asymmetric inheritance to concentrate toxic substances in a specific subpopulation [401–405]. This way to establish a cellular *division of labour* might thus represent a general evolutionary advantage. Moreover, stochastic fluctuations from cellular noise, which are an alternative way to establish heterogeneous populations and respond to less-frequent complex environmental stimuli, were so far only described for simple prokaryotes and might be too wasteful for more complex eukaryotes [406–408].

7 Future Directions

7.1 Reporter development

The developed transcriptional reporter proteins were sufficient to detect cell-to-cell differences and distinguish between different dynamics in this project, but some modifications might yet increase their potential:

Firstly, as outlined before, the reporter should be tested with fast-maturing fluorescent proteins, which have different fluorescent spectra and enable the parallel measurement of multiple signaling pathways in single cells. Yeast-codon-optimised fast-folding versions of blue fluorescent proteins or GFP-derivatives, i.e. yellow fluorescent protein (YFP) and cyan fluorescent protein (CFP) [264], would be suitable but were not available at the start of this study. Moreover, their selective marker, histidine prototrophy, unnecessarily limits the reporter proteins to histidine-auxotroph yeast strains, i.e. BY4741 and derivatives, and should be replaced by an antibiotic resistance, i.e. Hygromycin, G418 and Nourseothricin, to extend the set of possible host strains [409–411].

Recent studies indicated that the terminator of a gene influences the stability and translation efficiency of its mRNA [412]. As mRNA half-life probably has a small impact on reporter dynamics, a new terminator might increase reporter output without extending the response time.

Without these modifications, the current reporter proteins can already be used to measure the dynamics of other transcriptional changes in single yeast cells, which have previously been studied with long-lived reporter proteins or on a population-wide level. This higher resolution could enable researchers to better understand the effect of different perturbations on the sequential gene activation during the cell cycle, which is the most prominent example for a time-dependent expression profile [293,413], and also enrich the study of other adaptational responses such as the general stress response, osmotic homeostasis or phosphate starvation, which are believed to be more complex than a single ON/OFF-switch [207,391,392].

In contrast to the transcriptional reporter proteins, there is no obvious way to improve NBD-C6-ceramide. To investigate IPC synthesis, the two main disadvantages of NBD-C6-ceramide are that (a) non-metabolised NBD-C6-ceramide can remain inside the cell (see chapter 3), and that (b) NBD fluorescence depends on its concentration but also on its chemical environment.

It seems impossible to overcome the first disadvantage as most intermediates of sphingolipid metabolism are lipophilic substances and preferentially localise to cellular membranes. However, it might be possible to reduce the starting concentration, perform several washing steps or apply a counterstaining of subcellular compartments to differentiate between metabolised NBD-IPC in

the Golgi and non-metabolised NBD-C6-ceramide in the ER [414–416]. The environment-sensitive NBD fluorophore could further be replaced by the more robust BODIPY [417], but it remains to be validated experimentally if BODIPY-ceramide would be suited to determine AUR1 activity.

Reporter proteins represent another way to measure metabolic changes and have already been developed for some lipid species [393,418]. Sphingosine-binding domains of endogenous proteins could analogously be used to construct fluorescent reporters for sphingolipid metabolism but might be less specific or compete with endogenous proteins [327]. As an alternative, a set of endogenous proteins, which reacts to known perturbations of SL metabolism, e.g. AUR1 inhibition, could be determined, and endogenously GFP-tagged versions used to study unknown conditions [419,420].

Even though the results from chapters 4 and 5 indicated that dynamic reporter proteins are a valuable tool to study transcriptional changes in *S. cerevisiae,* they might not be suited to detect dynamic transcription patterns in other model organisms (e.g. *E. coli*, *C. elegans* and *D. melanogaster*) or mammalian cell culture.

In *E.coli*, active degradation by an endogenous protease was used to develop dynamic reporter proteins with half-lives around 40 minutes [215]. However, this half-life is longer than the doubling time of *E.coli* in optimal conditions, and protein dilution via cell division probably remains the main determinant for reporter dynamics. This reporter could still be used to study dynamic transcription in slow growing bacteria but might interfere with the proteolytic regulation of important processes [210,421].

In more complex eukaryotic organisms, specific protein domains induce active degradation and reduce protein half-lives to one or two hours [422,423]. Because the average mRNA half-life in these organisms is several hours, protein stability might not be the bottleneck for the dynamics of reporter proteins [424,425]. However, the investigation of processes that involve active mRNA degradation, e.g. circadian clock or development, might still benefit from destabilised fluorescent proteins in these organisms [422,426].

7.2 Inositol starvation and sphingolipid metabolism

During inositol starvation, the dynamic reporter proteins indicated a temporal sequence of events, but future studies need to validate the proposed causal connections that determined it.

For the delayed HAC1 activation after inositol depletion, the lipid profile and UPR activity of INO2/4-deficient cells are necessary to resolve if the first transcriptional change, INO2/4 activation, perturbed ER homeostasis via an increased PC synthesis. To better understand the

importance of lipid homeostasis for cell physiology [46], it might also be useful to further investigate the inositol-auxotrophy of UPR-deficient cells, which is characterised by an unbalanced lipid metabolism and rescued by the overexpression of PC degrading enzymes [181,185].

Regarding the observed SL-dependent PKC activation, several published results, e.g. RLM1 activation after partial AUR1 inhibition and inositol auxotrophy at high temperatures after SL metabolism perturbation [23, 276], further support the hypothesis that it results from reduced IPC production [55]. The hypothesis could directly be tested through external sphingolipid supplementation, e.g. glucosylceramide [427], which should prevent RLM1 activation and rescue the inositol auxotrophy of yeast cells with a disrupted CWI response.

It remains unknown why PKC activation depended on UPR activation, but the RLM1 promoter and knock-out mutants could be used to investigate the effect of individual UPR target genes, i.e. ORM1/2, on the PKC activation during inositol starvation.

Causal connections between the individual processes, i.e. phospholipid biosynthesis, ER homeostasis, sphingolipid (SL) biosynthesis and cell wall integrity, probably exist independently of inositol starvation. They might thus help to understand the transcriptional adaptation of *S. cerevisiae* to other conditions such as elevated temperatures, genetic modifications or ethanol exposure, which at least involve one of the investigated signaling pathways [428].

Additional fluorescence labels or live cell imaging could further reveal the relation between observed transcriptional dynamics and cellular phenotype, e.g. cell size, cell cycle stage, replicative age or cell death [176,375], and help to understand the trade-off between transcriptional adaptation and other processes such as cell growth and cell division [429].

For sphingolipid metabolism, the cell-cycle-dependent SUR2 and LAC1 expression stipulated by Cyclebase.org and the high transcriptional activity of the SUR2 promoter in YPD medium already suggested an increased ceramide production during the budded phase. However and depending on the actual flux through sphingolipid biosynthesis, the induction of SUR2 and LAC1 might only have a minor impact on ceramide synthesis and direct measurements of lipid metabolites are necessary to proof a connection between sphingolipid metabolism and cell cycle progression, which was already shown for other metabolites or in other organisms [430,431].

The results from SUR2-deficient cells further suggested that less-conserved steps of sphingolipid metabolism downstream of ceramide are important for cellular trafficking in *S. cerevisiae*.

Interestingly, sphingolipid metabolism seems to expand with the complexity of the secretory pathway in different organisms: while *S. cerevisiae* only has a single mature sphingolipid class (IPC and derivatives) and unstructured Golgi vesicles, *Pichia pastoris* has two different classes

and a stacked Golgi apparatus [432,433], and mammalian cells have at least two different SL classes and a stacked Golgi apparatus with several subcompartments. As SL biosynthesis only happens in specific subcellular compartments [256,434–436], and the disruption of Golgi structure perturbs SL metabolism [437], it would be interesting to further investigate the relation between these two eukaryotic-specific process and understand if compartmentalisation enables a more complex SL biosynthesis or *vice versa.*

7.3 Population asymmetry

So far, the molecular basis of heterogeneous UPR activation under low-stress conditions was only investigated with the HAC1 reporter and SUR2-deficient cells, but this method was rather indirect and poses two major problems that should be solved to properly address the participation of the ceramide-dependent bud neck barrier. On one hand, even a different HAC1 activity in mother and daughter cells, which could be assessed via an additional ConA-based staining, is no proof for regulated ER inheritance, and only an ER marker such as HDEL-GFP or SEC63-GFP could directly determine ER inheritance [165,438]. On the other hand, as SUR2 knock-out might not be sufficient to disturb ceramide biosynthesis in YPD medium, chemical inhibitors of ceramide biosynthesis (Myriocin, Fumonisin B1) should be applied to perturb the ceramide-dependent barrier in YPD medium [81,82]. The relation of the discovered mechanism to known ER inheritance regulation, i.e. ERSU and the bud neck barrier, is crucial to determine if daughter rejuvenation and mother preference are consequences of the same mechanism during ER inheritance like they seem to be during vacuole inheritance [356,439].

Moreover, the correlation between HAC1 activity and different cellular parameters, e.g. cell cycle phase, growth rate or cell size, could be measured with live imaging and help to determine if additional mechanisms such as stochastic noise, cell cycle progression or growth rate also generate cell-to-cell differences that affect ER homeostasis and influence the adaptation to ER stress [406,440–444]. Live imaging and cell synchronisation could further be used to validate the proposed ER homeostasis-dependent G1 progression. However, as the high autofluorescence of YPD medium interferes with reporter fluorescence, it is first necessary to establish a low ER stress regime with heterogeneous UPR activity in synthetic complete medium [168,445], which probably requires much higher tunicamycin concentrations (see chapter 4).

The experimental validation of the model and a test of its last prediction, i.e. asymmetric cell division improves population fitness in changing environments, exceeded the scope of this project. Interestingly, the very small daughter cells and reduced overall cell size in conditions where cell size and cell growth limit cell division, i.e. poor carbon sources, already agree with the

model prediction [39]. Different carbon source might thus be a better experimental condition than low ER stress to investigate the effect of asymmetric inheritance on the population fitness in changing environments. Growth competition of asymmetric-dividing wild-type cells against symmetric-dividing WHI5-deficient cells, for example, could then reveal a new benefit of asymmetric cell division in addition to daughter rejuvenation [371,446,447].

8 References

1. Van Schaftingen E, Hers HG. Inhibition of fructose-1,6-bisphosphatase by fructose 2,6-biphosphate. Proc Natl Acad Sci U S A. 1981;78: 2861–2863.
2. Ramaiah A, Hathaway JA, Atkinson DE. ADENYLATE AS A METABOLIC REGULATOR. EFFECT ON YEAST PHOSPHOFRUCTOKINASE KINETICS. J Biol Chem. 1964;239: 3619–3622.
3. Walsh DA, Perkins JP, Krebs EG. An adenosine 3',5'-monophosphate-dependant protein kinase from rabbit skeletal muscle. J Biol Chem. 1968;243: 3763–3765.
4. López-Maury L, Marguerat S, Bähler J. Tuning gene expression to changing environments: from rapid responses to evolutionary adaptation. Nat Rev Genet. 2008;9: 583–593.
5. Jacobs FA, Bird RC, Sells BH. Differentiation of rat myoblasts. Regulation of turnover of ribosomal proteins and their mRNAs. Eur J Biochem. 1985;150: 255–263.
6. Geyer PK, Meyuhas O, Perry RP, Johnson LF. Regulation of ribosomal protein mRNA content and translation in growth-stimulated mouse fibroblasts. Mol Cell Biol. 1982;2: 685–693.
7. Gasch AP, Spellman PT, Kao CM, Carmel-Harel O, Eisen MB, Storz G, et al. Genomic expression programs in the response of yeast cells to environmental changes. Mol Biol Cell. 2000;11: 4241–4257.
8. Ghaemmaghami S, Huh W-K, Bower K, Howson RW, Belle A, Dephoure N, et al. Global analysis of protein expression in yeast. Nature. 2003;425: 737–741.
9. Dermitzakis ET, Clark AG. Evolution of transcription factor binding sites in Mammalian gene regulatory regions: conservation and turnover. Mol Biol Evol. 2002;19: 1114–1121.
10. Tirosh I, Reikhav S, Levy AA, Barkai N. A yeast hybrid provides insight into the evolution of gene expression regulation. Science. 2009;324: 659–662.
11. Wang X, Sato R, Brown MS, Hua X, Goldstein JL. SREBP-1, a membrane-bound transcription factor released by sterol-regulated proteolysis. Cell. 1994;77: 53–62.
12. Hua X, Yokoyama C, Wu J, Briggs MR, Brown MS, Goldstein JL, et al. SREBP-2, a second basic-helix-loop-helix-leucine zipper protein that stimulates transcription by binding to a sterol regulatory element. Proc Natl Acad Sci U S A. 1993;90: 11603–11607.
13. Levin DE. Regulation of cell wall biogenesis in Saccharomyces cerevisiae: the cell wall integrity signaling pathway. Genetics. 2011;189: 1145–1175.
14. Suter DM, Molina N, Gatfield D, Schneider K, Schibler U, Naef F. Mammalian genes are transcribed with widely different bursting kinetics. Science. 2011;332: 472–474.
15. Nazarenko VG. [Effect of delay on auto-oscillations in cell populations]. Biofizika. 1976;21: 352–356.
16. Friesen WO, Block GD. What is a biological oscillator? Am J Physiol. 1984;246: R847–53.
17. Porter SL, Wadhams GH, Armitage JP. Signal processing in complex chemotaxis pathways. Nat Rev Microbiol. 2011;9: 153–165.
18. Paget MS. Bacterial Sigma Factors and Anti-Sigma Factors: Structure, Function and

Distribution. Biomolecules. 2015;5: 1245–1265.

19. Hughes TR, de Boer CG. Mapping yeast transcriptional networks. Genetics. 2013;195: 9–36.
20. Alberts B. Molecular Biology of the Cell with CD. Garland; 2008;
21. Kholodenko BN, Hancock JF, Kolch W. Signalling ballet in space and time. Nat Rev Mol Cell Biol. 2010;11: 414–426.
22. Senft D, Ronai ZA. UPR, autophagy, and mitochondria crosstalk underlies the ER stress response. Trends Biochem Sci. 2015;40: 141–148.
23. Villa-García MJ, Choi MS, Hinz FI, Gaspar ML, Jesch SA, Henry SA. Genome-wide screen for inositol auxotrophy in Saccharomyces cerevisiae implicates lipid metabolism in stress response signaling. Mol Genet Genomics. 2011;285: 125–149.
24. Scrimale T, Didone L, de Mesy Bentley KL, Krysan DJ. The unfolded protein response is induced by the cell wall integrity mitogen-activated protein kinase signaling cascade and is required for cell wall integrity in Saccharomyces cerevisiae. Mol Biol Cell. 2009;20: 164–175.
25. Walter P, Ron D. The unfolded protein response: from stress pathway to homeostatic regulation. Science. 2011;334: 1081–1086.
26. Henry SA, Kohlwein SD, Carman GM. Metabolism and regulation of glycerolipids in the yeast Saccharomyces cerevisiae. Genetics. 2012;190: 317–349.
27. Jazwinski SM. The retrograde response: a conserved compensatory reaction to damage from within and from without. Prog Mol Biol Transl Sci. 2014;127: 133–154.
28. Vendrell A, Martínez-Pastor M, González-Novo A, Pascual-Ahuir A, Sinclair DA, Proft M, et al. Sir2 histone deacetylase prevents programmed cell death caused by sustained activation of the Hog1 stress-activated protein kinase. EMBO Rep. 2011;12: 1062–1068.
29. Brauer MJ, Huttenhower C, Airoldi EM, Rosenstein R, Matese JC, Gresham D, et al. Coordination of growth rate, cell cycle, stress response, and metabolic activity in yeast. Mol Biol Cell. 2008;19: 352–367.
30. Hao N, Budnik BA, Gunawardena J, O'Shea EK. Tunable signal processing through modular control of transcription factor translocation. Science. 2013;339: 460–464.
31. Lin Y, Sohn CH, Dalal CK, Cai L, Elowitz MB. Combinatorial gene regulation by modulation of relative pulse timing. Nature. 2015;527: 54–58.
32. McCammon MT, Parks LW. Lipid synthesis in inositol-starved Saccharomyces cerevisiae. Biochim Biophys Acta. 1982;713: 86–93.
33. Ulaszewski S, Woodward JR, Cirillo VP. Membrane damage associated with inositol-less death in Saccharomyces cerevisiae. J Bacteriol. 1978;136: 49–54.
34. Kozutsumi Y, Segal M, Normington K, Gething MJ, Sambrook J. The presence of malfolded proteins in the endoplasmic reticulum signals the induction of glucose-regulated proteins. Nature. 1988;332: 462–464.
35. Martínez-Pastor MT, Marchler G, Schüller C, Marchler-Bauer A, Ruis H, Estruch F. The Saccharomyces cerevisiae zinc finger proteins Msn2p and Msn4p are required for transcriptional induction through the stress response element (STRE). EMBO J. 1996;15: 2227–2235.
36. Cox JS, Walter P. A novel mechanism for regulating activity of a transcription factor that controls the unfolded protein response. Cell. 1996;87: 391–404.

37. Bar-Even A, Paulsson J, Maheshri N, Carmi M, O'Shea E, Pilpel Y, et al. Noise in protein expression scales with natural protein abundance. Nat Genet. 2006;38: 636–643.

38. Newman JRS, Ghaemmaghami S, Ihmels J, Breslow DK, Noble M, DeRisi JL, et al. Single-cell proteomic analysis of S. cerevisiae reveals the architecture of biological noise. Nature. 2006;441: 840–846.

39. Tyson CB, Lord PG, Wheals AE. Dependency of size of Saccharomyces cerevisiae cells on growth rate. J Bacteriol. 1979;138: 92–98.

40. Geisberg JV, Moqtaderi Z, Fan X, Ozsolak F, Struhl K. Global analysis of mRNA isoform half-lives reveals stabilizing and destabilizing elements in yeast. Cell. 2014;156: 812–824.

41. Chaudhuri B, Delany NS, Stephan C. The unfolded-protein-response element discriminates misfolding induced by different mutant pro-sequences of yeast carboxypeptidase Y. Biochem Biophys Res Commun. 1995;209: 31–39.

42. Frand AR, Kaiser CA. The ERO1 gene of yeast is required for oxidation of protein dithiols in the endoplasmic reticulum. Mol Cell. 1998;1: 161–170.

43. J. Cox D, Strudwick N, Ali AA, Paton AW, Paton JC, Schröder M. Chapter fifteen - Measuring Signaling by the Unfolded Protein Response. In: P. Michael Conn, editor. Methods in Enzymology. Academic Press; 2011. pp. 261–292.

44. Du Y, Ferro-Novick S, Novick P. Dynamics and inheritance of the endoplasmic reticulum. J Cell Sci. 2004;117: 2871–2878.

45. Mori K, Sant A, Kohno K, Normington K, Gething MJ, Sambrook JF. A 22 bp cis-acting element is necessary and sufficient for the induction of the yeast KAR2 (BiP) gene by unfolded proteins. EMBO J. 1992;11: 2583–2593.

46. Thibault G, Shui G, Kim W, McAlister GC, Ismail N, Gygi SP, et al. The membrane stress response buffers lethal effects of lipid disequilibrium by reprogramming the protein homeostasis network. Mol Cell. 2012;48: 16–27.

47. Orlean P, Menon AK. Thematic review series: lipid posttranslational modifications. GPI anchoring of protein in yeast and mammalian cells, or: how we learned to stop worrying and love glycophospholipids. J Lipid Res. 2007;48: 993–1011.

48. Hanson BA, Lester RL. Effects of inositol starvation on phospholipid and glycan syntheses in Saccharomyces cerevisiae. J Bacteriol. 1980;142: 79–89.

49. Gardocki ME, Jani N, Lopes JM. Phosphatidylinositol biosynthesis: biochemistry and regulation. Biochim Biophys Acta. 2005;1735: 89–100.

50. Cox JS, Shamu CE, Walter P. Transcriptional induction of genes encoding endoplasmic reticulum resident proteins requires a transmembrane protein kinase. Cell. 1993;73: 1197–1206.

51. Nunez LR, Jesch SA, Gaspar ML, Almaguer C, Villa-Garcia M, Ruiz-Noriega M, et al. Cell wall integrity MAPK pathway is essential for lipid homeostasis. J Biol Chem. 2008;283: 34204–34217.

52. Megyeri M, Riezman H, Schuldiner M, Futerman AH. Making Sense of the Yeast Sphingolipid Pathway. J Mol Biol. 2016; doi:10.1016/j.jmb.2016.09.010

53. Montefusco DJ, Matmati N, Hannun YA. The yeast sphingolipid signaling landscape. Chem Phys Lipids. 2014;177: 26–40.

54. Breslow DK. Sphingolipid homeostasis in the endoplasmic reticulum and beyond. Cold

Spring Harb Perspect Biol. 2013;5: a013326.

55. Jesch SA, Gaspar ML, Stefan CJ, Aregullin MA, Henry SA. Interruption of inositol sphingolipid synthesis triggers Stt4p-dependent protein kinase C signaling. J Biol Chem. 2010;285: 41947–41960.

56. Bailis AM, Lopes JM, Kohlwein SD, Henry SA. Cis and trans regulatory elements required for regulation of the CHO1 gene of Saccharomyces cerevisiae. Nucleic Acids Res. 1992;20: 1411–1418.

57. Kamada Y, Jung US, Piotrowski J, Levin DE. The protein kinase C-activated MAP kinase pathway of Saccharomyces cerevisiae mediates a novel aspect of the heat shock response. Genes Dev. 1995;9: 1559–1571.

58. Carmona-Gutierrez D, Reisenbichler A, Heimbucher P, Bauer MA, Braun RJ, Ruckenstuhl C, et al. Ceramide triggers metacaspase-independent mitochondrial cell death in yeast. Cell Cycle. 2011;10: 3973–3978.

59. Knoblach B, Sun X, Coquelle N, Fagarasanu A, Poirier RL, Rachubinski RA. An ER-peroxisome tether exerts peroxisome population control in yeast. EMBO J. European Molecular Biology Organization; 2013;advance on. doi:10.1038/emboj.2013.170

60. Kornmann B, Walter P. ERMES-mediated ER-mitochondria contacts: molecular hubs for the regulation of mitochondrial biology. J Cell Sci. The Company of Biologists Ltd; 2010;123: 1389–1393.

61. Elbaz Y, Schuldiner M. Staying in touch: the molecular era of organelle contact sites. Trends Biochem Sci. 2011;36: 616–623.

62. Gurel PS, Hatch AL, Higgs HN. Connecting the cytoskeleton to the endoplasmic reticulum and Golgi. Curr Biol. 2014;24: R660–72.

63. Natter K, Leitner P, Faschinger A, Wolinski H, McCraith S, Fields S, et al. The spatial organization of lipid synthesis in the yeast Saccharomyces cerevisiae derived from large scale green fluorescent protein tagging and high resolution microscopy. Mol Cell Proteomics. 2005;4: 662–672.

64. Wiedmann M, Kurzchalia TV, Hartmann E, Rapoport TA. A signal sequence receptor in the endoplasmic reticulum membrane. Nature. 1987;328: 830–833.

65. Hasselbach W. ATP-DRIVEN ACTIVE TRANSPORT OF CALCIUM IN THE MEMBRANES OF THE SARCOPLASMIC RETICULUM. Proc R Soc Lond B Biol Sci. 1964;160: 501–504.

66. Morin-Ganet MN, Rambourg A, Deitz SB, Franzusoff A, Képès F. Morphogenesis and dynamics of the yeast Golgi apparatus. Traffic. 2000;1: 56–68.

67. Hoepfner D, Schildknegt D, Braakman I, Philippsen P, Tabak HF. Contribution of the Endoplasmic Reticulum to Peroxisome Formation. Cell. Elsevier; 2005;122: 85–95.

68. Thiam AR, Farese RV Jr, Walther TC. The biophysics and cell biology of lipid droplets. Nat Rev Mol Cell Biol. 2013;14: 775–786.

69. van Meer G, Voelker DR, Feigenson GW. Membrane lipids: where they are and how they behave. Nat Rev Mol Cell Biol. 2008;9: 112–124.

70. Simons K, Sampaio JL. Membrane organization and lipid rafts. Cold Spring Harb Perspect Biol. 2011;3: a004697.

71. Koch B, Schmidt C, Daum G. Storage lipids of yeasts: a survey of nonpolar lipid metabolism in Saccharomyces cerevisiae, Pichia pastoris, and Yarrowia lipolytica.

FEMS Microbiol Rev. 2014;38: 892–915.

72. Ejsing CS, Sampaio JL, Surendranath V, Duchoslav E, Ekroos K, Klemm RW, et al. Global analysis of the yeast lipidome by quantitative shotgun mass spectrometry. Proc Natl Acad Sci U S A. 2009;106: 2136–2141.

73. Tamura Y, Onguka O, Itoh K, Endo T, Iijima M, Claypool SM, et al. Phosphatidylethanolamine biosynthesis in mitochondria: phosphatidylserine (PS) trafficking is independent of a PS decarboxylase and intermembrane space proteins UPS1P and UPS2P. J Biol Chem. 2012;287: 43961–43971.

74. Kodaki T, Yamashita S. Characterization of the methyltransferases in the yeast phosphatidylethanolamine methylation pathway by selective gene disruption. Eur J Biochem. 1989;185: 243–251.

75. Donahue TF, Henry SA. myo-Inositol-1-phosphate synthase. Characteristics of the enzyme and identification of its structural gene in yeast. J Biol Chem. 1981;256: 7077–7085.

76. Melcher K, Entian KD. Genetic analysis of serine biosynthesis and glucose repression in yeast. Curr Genet. 1992;21: 295–300.

77. Funato K, Riezman H. Vesicular and nonvesicular transport of ceramide from ER to the Golgi apparatus in yeast. J Cell Biol. 2001;155: 949–959.

78. Haak D, Gable K, Beeler T, Dunn T. Hydroxylation of Saccharomyces cerevisiae Ceramides Requires Sur2p and Scs7p. J Biol Chem. 1997;272: 29704–29710.

79. Huh W-K, Falvo JV, Gerke LC, Carroll AS, Howson RW, Weissman JS, et al. Global analysis of protein localization in budding yeast. Nature. 2003;425: 686–691.

80. Nagiec MM, Nagiec EE, Baltisberger JA, Wells GB, Lester RL, Dickson RC. Sphingolipid synthesis as a target for antifungal drugs. Complementation of the inositol phosphorylceramide synthase defect in a mutant strain of Saccharomyces cerevisiae by the AUR1 gene. J Biol Chem. 1997;272: 9809–9817.

81. Miyake Y, Kozutsumi Y, Nakamura S, Fujita T, Kawasaki T. Serine palmitoyltransferase is the primary target of a sphingosine-like immunosuppressant, ISP-1/myriocin. Biochem Biophys Res Commun. 1995;211: 396–403.

82. Wu WI, McDonough VM, Nickels JT Jr, Ko J, Fischl AS, Vales TR, et al. Regulation of lipid biosynthesis in Saccharomyces cerevisiae by fumonisin B1. J Biol Chem. 1995;270: 13171–13178.

83. Endo M, Takesako K, Kato I, Yamaguchi H. Fungicidal action of aureobasidin A, a cyclic depsipeptide antifungal antibiotic, against Saccharomyces cerevisiae. Antimicrob Agents Chemother. 1997;41: 672–676.

84. Gururaj C, Federman RS, Federman R, Chang A. Orm proteins integrate multiple signals to maintain sphingolipid homeostasis. J Biol Chem. 2013;288: 20453–20463.

85. Swain E, Baudry K, Stukey J, McDonough V, Germann M, Nickels JT Jr. Sterol-dependent regulation of sphingolipid metabolism in Saccharomyces cerevisiae. J Biol Chem. 2002;277: 26177–26184.

86. Fügi MA, Kaiser M, Tanner M, Schneiter R, Mäser P, Guan XL. Match-making for posaconazole through systems thinking. Trends Parasitol. 2015;31: 46–51.

87. Parks LW. Metabolism of sterols in yeast. CRC Crit Rev Microbiol. 1978;6: 301–341.

88. Fieser Louis F FM. STEROIDS. by Fieser Louis F, Fieser Mary: New York Reinhold

Publishing 1959. F - Lawrence's Books [Internet]. New York Reinhold Publishing 1959.; 1959 [cited 24 Oct 2016]. Available: http://www.abebooks.com/STEROIDS-Fieser-Louis-F-Mary-New/200375418/bd

89. Klug L, Daum G. Yeast lipid metabolism at a glance. FEMS Yeast Res. 2014;14: 369–388.

90. Hampton RY, Rine J. Regulated degradation of HMG-CoA reductase, an integral membrane protein of the endoplasmic reticulum, in yeast. J Cell Biol. 1994;125: 299–312.

91. Vik A, Rine J. Upc2p and Ecm22p, dual regulators of sterol biosynthesis in Saccharomyces cerevisiae. Mol Cell Biol. 2001;21: 6395–6405.

92. Hartl FU, Bracher A, Hayer-Hartl M. Molecular chaperones in protein folding and proteostasis. Nature. 2011;475: 324–332.

93. Tu BP, Weissman JS. Oxidative protein folding in eukaryotes: mechanisms and consequences. J Cell Biol. 2004;164: 341–346.

94. Nyathi Y, Wilkinson BM, Pool MR. Co-translational targeting and translocation of proteins to the endoplasmic reticulum. Biochim Biophys Acta. 2013;1833: 2392–2402.

95. Panzner S, Dreier L, Hartmann E, Kostka S, Rapoport TA. Posttranslational protein transport in yeast reconstituted with a purified complex of Sec proteins and Kar2p. Cell. 1995;81: 561–570.

96. Ye Y, Meyer HH, Rapoport TA. The AAA ATPase Cdc48/p97 and its partners transport proteins from the ER into the cytosol. Nature. 2001;414: 652–656.

97. Corsi AK, Schekman R. The lumenal domain of Sec63p stimulates the ATPase activity of BiP and mediates BiP recruitment to the translocon in Saccharomyces cerevisiae. J Cell Biol. 1997;137: 1483–1493.

98. Normington K, Kohno K, Kozutsumi Y, Gething MJ, Sambrook J. S. cerevisiae encodes an essential protein homologous in sequence and function to mammalian BiP. Cell. 1989;57: 1223–1236.

99. Rose MD, Misra LM, Vogel JP. KAR2, a karyogamy gene, is the yeast homolog of the mammalian BiP/GRP78 gene. Cell. 1989;57: 1211–1221.

100. Behnke J, Feige MJ, Hendershot LM. BiP and its nucleotide exchange factors Grp170 and Sil1: mechanisms of action and biological functions. J Mol Biol. 2015;427: 1589–1608.

101. Kampinga HH, Craig EA. The HSP70 chaperone machinery: J proteins as drivers of functional specificity. Nat Rev Mol Cell Biol. 2010;11: 579–592.

102. Woycechowsky KJ, Raines RT. Native disulfide bond formation in proteins. Curr Opin Chem Biol. 2000;4: 533–539.

103. Farquhar R, Honey N, Murant SJ, Bossier P, Schultz L, Montgomery D, et al. Protein disulfide isomerase is essential for viability in Saccharomyces cerevisiae. Gene. 1991;108: 81–89.

104. Frand AR, Cuozzo JW, Kaiser CA. Pathways for protein disulphide bond formation. Trends Cell Biol. 2000;10: 203–210.

105. Holst B, Tachibana C, Winther JR. Active site mutations in yeast protein disulfide isomerase cause dithiothreitol sensitivity and a reduced rate of protein folding in the endoplasmic reticulum. J Cell Biol. 1997;138: 1229–1238.

106. Frand AR, Kaiser CA. Ero1p oxidizes protein disulfide isomerase in a pathway for disulfide bond formation in the endoplasmic reticulum. Mol Cell. 1999;4: 469–477.

107. Cuozzo JW, Kaiser CA. Competition between glutathione and protein thiols for disulphide-bond formation. Nat Cell Biol. 1999;1: 130–135.

108. Stolz A, Wolf DH. Endoplasmic reticulum associated protein degradation: a chaperone assisted journey to hell. Biochim Biophys Acta. 2010;1803: 694–705.

109. D'Alessio C, Caramelo JJ, Parodi AJ. UDP-GlC:glycoprotein glucosyltransferase-glucosidase II, the ying-yang of the ER quality control. Semin Cell Dev Biol. 2010;21: 491–499.

110. Xu X, Azakami H, Kato A. P-domain and lectin site are involved in the chaperone function of Saccharomyces cerevisiae calnexin homologue. FEBS Lett. 2004;570: 155–160.

111. Szathmary R, Bielmann R, Nita-Lazar M, Burda P, Jakob CA. Yos9 protein is essential for degradation of misfolded glycoproteins and may function as lectin in ERAD. Mol Cell. 2005;19: 765–775.

112. Gardner RG, Swarbrick GM, Bays NW, Cronin SR, Wilhovsky S, Seelig L, et al. Endoplasmic reticulum degradation requires lumen to cytosol signaling. Transmembrane control of Hrd1p by Hrd3p. J Cell Biol. 2000;151: 69–82.

113. Heifetz A, Keenan RW, Elbein AD. Mechanism of action of tunicamycin on the UDP-GlcNAc:dolichyl-phosphate GlcNAc-1-phosphate transferase. Biochemistry. American Chemical Society; 1979;18: 2186–2192.

114. Datema R, Schwarz RT. Interference with glycosylation of glycoproteins. Inhibition of formation of lipid-linked oligosaccharides in vivo. Biochem J. 1979;184: 113–123.

115. Resh MD. Covalent lipid modifications of proteins. Curr Biol. 2013;23: R431–5.

116. Doering TL, Schekman R. GPI anchor attachment is required for Gas1p transport from the endoplasmic reticulum in COP II vesicles. EMBO J. 1996;15: 182–191.

117. Malkus P, Jiang F, Schekman R. Concentrative sorting of secretory cargo proteins into COPII-coated vesicles. J Cell Biol. 2002;159: 915–921.

118. Spang A. Retrograde traffic from the Golgi to the endoplasmic reticulum. Cold Spring Harb Perspect Biol. 2013;5. doi:10.1101/cshperspect.a013391

119. Emr S, Glick BS, Linstedt AD, Lippincott-Schwartz J, Luini A, Malhotra V, et al. Journeys through the Golgi--taking stock in a new era. J Cell Biol. 2009;187: 449–453.

120. Fujiwara T, Oda K, Yokota S, Takatsuki A, Ikehara Y. Brefeldin A causes disassembly of the Golgi complex and accumulation of secretory proteins in the endoplasmic reticulum. J Biol Chem. 1988;263: 18545–18552.

121. Schwank S, Ebbert R, Rautenstrauss K, Schweizer E, Schüller HJ. Yeast transcriptional activator INO2 interacts as an Ino2p/Ino4p basic helix-loop-helix heteromeric complex with the inositol/choline-responsive element necessary for expression of phospholipid biosynthetic genes in Saccharomyces cerevisiae. Nucleic Acids Res. 1995;23: 230–237.

122. Lopes JM, Hirsch JP, Chorgo PA, Schulze KL, Henry SA. Analysis of sequences in the INO1 promoter that are involved in its regulation by phospholipid precursors. Nucleic Acids Res. 1991;19: 1687–1693.

123. Bailis AM, Lopes JM, Kohlwein SD, Henry SA. Cis and trans regulatory elements required for regulation of the CHO1 gene of Saccharomyces cerevisiae. Nucleic Acids

Res. 1992;20: 1411–1418.

124. Hoppen J, Repenning A, Albrecht A, Geburtig S, Schüller H-J. Comparative analysis of promoter regions containing binding sites of the heterodimeric transcription factor Ino2/Ino4 involved in yeast phospholipid biosynthesis. Yeast. 2005;22: 601–613.

125. Graves JA, Henry SA. Regulation of the yeast INO1 gene. The products of the INO2, INO4 and OPI1 regulatory genes are not required for repression in response to inositol. Genetics. 2000;154: 1485–1495.

126. Carman GM, Han G-S. Regulation of phospholipid synthesis in yeast. J Lipid Res. 2009;50 Suppl: S69–73.

127. Karanasios E, Han G-S, Xu Z, Carman GM, Siniossoglou S. A phosphorylation-regulated amphipathic helix controls the membrane translocation and function of the yeast phosphatidate phosphatase. Proc Natl Acad Sci U S A. National Academy of Sciences; 2010;107: 17539–17544.

128. Loewen CJR, Gaspar ML, Jesch SA, Delon C, Ktistakis NT, Henry SA, et al. Phospholipid metabolism regulated by a transcription factor sensing phosphatidic acid. Science. 2004;304: 1644–1647.

129. Young BP, Shin JJH, Orij R, Chao JT, Li SC, Guan XL, et al. Phosphatidic acid is a pH biosensor that links membrane biogenesis to metabolism. Science. 2010;329: 1085–1088.

130. Gardner R, Cronin S, Leader B, Rine J, Hampton R, Leder B. Sequence determinants for regulated degradation of yeast 3-hydroxy-3-methylglutaryl-CoA reductase, an integral endoplasmic reticulum membrane protein. Mol Biol Cell. 1998;9: 2611–2626.

131. Smith SJ, Crowley JH, Parks LW. Transcriptional regulation by ergosterol in the yeast Saccharomyces cerevisiae. Mol Cell Biol. 1996;16: 5427–5432.

132. Marie C, Leyde S, White TC. Cytoplasmic localization of sterol transcription factors Upc2p and Ecm22p in S. cerevisiae. Fungal Genet Biol. 2008;45: 1430–1438.

133. Davies BSJ, Wang HS, Rine J. Dual activators of the sterol biosynthetic pathway of Saccharomyces cerevisiae: similar activation/regulatory domains but different response mechanisms. Mol Cell Biol. 2005;25: 7375–7385.

134. Han S, Lone MA, Schneiter R, Chang A. Orm1 and Orm2 are conserved endoplasmic reticulum membrane proteins regulating lipid homeostasis and protein quality control. Proc Natl Acad Sci U S A. 2010;107: 5851–5856.

135. Liu M, Huang C, Polu SR, Schneiter R, Chang A. Regulation of sphingolipid synthesis through Orm1 and Orm2 in yeast. J Cell Sci. 2012;125: 2428–2435.

136. Shimobayashi M, Oppliger W, Moes S, Jenö P, Hall MN. TORC1-regulated protein kinase Npr1 phosphorylates Orm to stimulate complex sphingolipid synthesis. Mol Biol Cell. 2013;24: 870–881.

137. Niles BJ, Joslin AC, Fresques T, Powers T. TOR complex 2-Ypk1 signaling maintains sphingolipid homeostasis by sensing and regulating ROS accumulation. Cell Rep. 2014;6: 541–552.

138. Kondo K, Inouye M. TIP 1, a cold shock-inducible gene of Saccharomyces cerevisiae. J Biol Chem. 1991;266: 17537–17544.

139. Klebl F, Tanner W. Molecular cloning of a cell wall exo-beta-1,3-glucanase from Saccharomyces cerevisiae. J Bacteriol. 1989;171: 6259–6264.

140. Cappellaro C, Mrsa V, Tanner W. New potential cell wall glucanases of Saccharomyces cerevisiae and their involvement in mating. J Bacteriol. 1998;180: 5030–5037.

141. O'Conallain C, Doolin MT, Taggart C, Thornton F, Butler G. Regulated nuclear localisation of the yeast transcription factor Ace2p controls expression of chitinase (CTS1) in Saccharomyces cerevisiae. Mol Gen Genet. 1999;262: 275–282.

142. Ozaki K, Tanaka K, Imamura H, Hihara T, Kameyama T, Nonaka H, et al. Rom1p and Rom2p are GDP/GTP exchange proteins (GEPs) for the Rho1p small GTP binding protein in Saccharomyces cerevisiae. EMBO J. 1996;15: 2196–2207.

143. Drgonová J, Drgon T, Tanaka K, Kollár R, Chen GC, Ford RA, et al. Rho1p, a yeast protein at the interface between cell polarization and morphogenesis. Science. 1996;272: 277–279.

144. Jung US, Levin DE. Genome-wide analysis of gene expression regulated by the yeast cell wall integrity signalling pathway. Mol Microbiol. 1999;34: 1049–1057.

145. Brodsky JL. Cleaning up: ER-associated degradation to the rescue. Cell. Elsevier; 2012;151: 1163–1167.

146. Babour A, Bicknell AA, Tourtellotte J, Niwa M. A surveillance pathway monitors the fitness of the endoplasmic reticulum to control its inheritance. Cell. 2010;142: 256–269.

147. Schuck S, Gallagher CM, Walter P. ER-phagy mediates selective degradation of endoplasmic reticulum independently of the core autophagy machinery. J Cell Sci. 2014; jcs.154716–.

148. Kimata Y, Oikawa D, Shimizu Y, Ishiwata-Kimata Y, Kohno K. A role for BiP as an adjustor for the endoplasmic reticulum stress-sensing protein Ire1. J Cell Biol. 2004;167: 445–456.

149. Gardner BM, Walter P. Unfolded Proteins Are Ire1-Activating Ligands that Directly Induce the Unfolded Protein Response. Science. 2011;333: 1891–1894.

150. Korennykh AV, Egea PF, Korostelev AA, Finer-Moore J, Zhang C, Shokat KM, et al. The unfolded protein response signals through high-order assembly of Ire1. Nature. 2009;457: 687–693.

151. Chapman RE, Walter P. Translational attenuation mediated by an mRNA intron. Curr Biol. 1997;7: 850–859.

152. Morl K, Ma W, Gething M-J, Sambrook J. A transmembrane protein with a cdc2+CDC28-related kinase activity is required for signaling from the ER to the nucleus. Cell. 1993;74: 743–756.

153. Cox JS, Chapman RE, Walter P. The unfolded protein response coordinates the production of endoplasmic reticulum protein and endoplasmic reticulum membrane. Mol Biol Cell. 1997;8: 1805–1814.

154. Rubio C, Pincus D, Korennykh A, Schuck S, El-Samad H, Walter P. Homeostatic adaptation to endoplasmic reticulum stress depends on Ire1 kinase activity. J Cell Biol. 2011;193: 171–184.

155. Maurel M, Chevet E, Tavernier J, Gerlo S. Getting RIDD of RNA: IRE1 in cell fate regulation. Trends Biochem Sci. 2014;39: 245–254.

156. Travers KJ, Patil CK, Wodicka L, Lockhart DJ, Weissman JS, Walter P. Functional and genomic analyses reveal an essential coordination between the unfolded protein response and ER-associated degradation. Cell. 2000;101: 249–258.

157. Gauss R, Jarosch E, Sommer T, Hirsch C. A complex of Yos9p and the HRD ligase integrates endoplasmic reticulum quality control into the degradation machinery. Nat Cell Biol. 2006;8: 849–854.

158. Gauss R, Sommer T, Jarosch E. The Hrd1p ligase complex forms a linchpin between ER-lumenal substrate selection and Cdc48p recruitment. EMBO J. 2006;25: 1827–1835.

159. Xie W, Kanehara K, Sayeed A, Ng DTW. Intrinsic conformational determinants signal protein misfolding to the Hrd1/Htm1 endoplasmic reticulum-associated degradation system. Mol Biol Cell. 2009;20: 3317–3329.

160. Hamasaki M, Noda T, Baba M, Ohsumi Y. Starvation triggers the delivery of the endoplasmic reticulum to the vacuole via autophagy in yeast. Traffic. 2005;6: 56–65.

161. Lipatova Z, Segev N. A Role for Macro-ER-Phagy in ER Quality Control. PLoS Genet. 2015;11: e1005390.

162. Bernales S, McDonald KL, Walter P. Autophagy counterbalances endoplasmic reticulum expansion during the unfolded protein response. PLoS Biol. 2006;4: e423.

163. Estrada P, Kim J, Coleman J, Walker L, Dunn B, Takizawa P, et al. Myo4p and She3p are required for cortical ER inheritance in Saccharomyces cerevisiae. J Cell Biol. 2003;163: 1255–1266.

164. Luedeke C, Frei SB, Sbalzarini I, Schwarz H, Spang A, Barral Y. Septin-dependent compartmentalization of the endoplasmic reticulum during yeast polarized growth. J Cell Biol. 2005;169: 897–908.

165. Clay L, Caudron F, Denoth-Lippuner A, Boettcher B, Buvelot Frei S, Snapp EL, et al. A sphingolipid-dependent diffusion barrier confines ER stress to the yeast mother cell. Elife. 2014;3: e01883.

166. Piña FJ, Niwa M. The ER Stress Surveillance (ERSU) pathway regulates daughter cell ER protein aggregate inheritance [Internet]. 2015. doi:10.7554/eLife.06970

167. Lee MV, Topper SE, Hubler SL, Hose J, Wenger CD, Coon JJ, et al. A dynamic model of proteome changes reveals new roles for transcript alteration in yeast. Mol Syst Biol. 2011;7: 514.

168. Merksamer PI, Trusina A, Papa FR. Real-time redox measurements during endoplasmic reticulum stress reveal interlinked protein folding functions. Cell. 2008;135: 933–947.

169. Daniel Gietz R, Woods RA. Transformation of yeast by lithium acetate/single-stranded carrier DNA/polyethylene glycol method. In: Christine Guthrie and Gerald R. Fink, editor. Methods in Enzymology. Academic Press; 2002. pp. 87–96.

170. Winzeler EA, Shoemaker DD, Astromoff A, Liang H, Anderson K, Andre B, et al. Functional characterization of the S. cerevisiae genome by gene deletion and parallel analysis. Science. 1999;285: 901–906.

171. Daniel Gietz R, Woods RA. Transformation of yeast by lithium acetate/single-stranded carrier DNA/polyethylene glycol method. In: Christine Guthrie and Gerald R. Fink, editor. Methods in Enzymology. Academic Press; 2002. pp. 87–96.

172. Khmelinskii A, Meurer M, Duishoev N, Delhomme N, Knop M. Seamless gene tagging by endonuclease-driven homologous recombination. Hardwick KG, editor. PLoS One. Public Library of Science; 2011;6: e23794.

173. Xiao W, editor. Yeast Protocols: Springer New York; 2014.

174. Toussaint M, Conconi A. High-throughput and sensitive assay to measure yeast cell

growth: a bench protocol for testing genotoxic agents. Nat Protoc. Nature Publishing Group; 2006;1: 1922–1928.

175. Livak KJ, Schmittgen TD. Analysis of relative gene expression data using real-time quantitative PCR and the 2(-Delta Delta C(T)) Method. Methods. 2001;25: 402–408.

176. Rines DR, Thomann D, Dorn JF, Goodwin P, Sorger PK. Live cell imaging of yeast. Cold Spring Harb Protoc. 2011;2011. doi:10.1101/pdb.top065482

177. Sikorski RS, Hieter P. A system of shuttle vectors and yeast host strains designed for efficient manipulation of DNA in Saccharomyces cerevisiae. Genetics. 1989;122: 19–27.

178. Levin DE. Cell wall integrity signaling in Saccharomyces cerevisiae. Microbiol Mol Biol Rev. 2005;69: 262–291.

179. Promlek T, Ishiwata-Kimata Y, Shido M, Sakuramoto M, Kohno K, Kimata Y. Membrane aberrancy and unfolded proteins activate the endoplasmic reticulum stress sensor Ire1 in different ways. Mol Biol Cell. 2011;22: 3520–3532.

180. Shamu CE, Cox JS, Walter P. The unfolded-protein-response pathway in yeast. Trends Cell Biol. 1994;4: 56–60.

181. Chang HJ, Jones EW, Henry SA. Role of the Unfolded Protein Response Pathway in Regulation of INO1 and in the sec14 Bypass Mechanism in Saccharomyces cerevisiae. Genetics. 2002;162: 29–43.

182. Henry SA, Donahue TF, Culbertson MR. Selection of spontaneous mutants by inositol starvation in yeast. Mol Gen Genet. 1975;143: 5–11.

183. Tan S-X, Teo M, Lam YT, Dawes IW, Perrone GG. Cu, Zn superoxide dismutase and NADP(H) homeostasis are required for tolerance of endoplasmic reticulum stress in Saccharomyces cerevisiae. Mol Biol Cell. 2009;20: 1493–1508.

184. Chen Y, Feldman DE, Deng C, Brown JA, De Giacomo AF, Gaw AF, et al. Identification of mitogen-activated protein kinase signaling pathways that confer resistance to endoplasmic reticulum stress in Saccharomyces cerevisiae. Mol Cancer Res. 2005;3: 669–677.

185. Fernández-Murray JP, Gaspard GJ, Jesch SA, McMaster CR. NTE1-encoded phosphatidylcholine phospholipase b regulates transcription of phospholipid biosynthetic genes. J Biol Chem. 2009;284: 36034–36046.

186. Yang J, McCormick MA, Zheng J, Xie Z, Tsuchiya M, Tsuchiyama S, et al. Systematic analysis of asymmetric partitioning of yeast proteome between mother and daughter cells reveals “aging factors” and mechanism of lifespan asymmetry. Proc Natl Acad Sci U S A. 2015; doi:10.1073/pnas.1506054112

187. Colman-Lerner A, Chin TE, Brent R. Yeast Cbk1 and Mob2 activate daughter-specific genetic programs to induce asymmetric cell fates. Cell. 2001;107: 739–750.

188. Vevea JD, Swayne TC, Boldogh IR, Pon LA. Inheritance of the fittest mitochondria in yeast. Trends Cell Biol. 2014;24: 53–60.

189. Avraham N, Soifer I, Carmi M, Barkai N. Increasing population growth by asymmetric segregation of a limiting resource during cell division. Mol Syst Biol. 2013;9: 656.

190. New AM, Cerulus B, Govers SK, Perez-Samper G, Zhu B, Boogmans S, et al. Different levels of catabolite repression optimize growth in stable and variable environments. PLoS Biol. 2014;12: e1001764.

191. Wang J, Atolia E, Hua B, Savir Y, Escalante-Chong R, Springer M. Natural variation in

preparation for nutrient depletion reveals a cost-benefit tradeoff. PLoS Biol. 2015;13: e1002041.

192. DeGennaro CM, Savir Y, Springer M. Identifying Metabolic Subpopulations from Population Level Mass Spectrometry. PLoS One. 2016;11: e0151659.

193. Di Talia S, Wang H, Skotheim JM, Rosebrock AP, Futcher B, Cross FR. Daughter-specific transcription factors regulate cell size control in budding yeast. PLoS Biol. 2009;7: e1000221.

194. Henry KA, Blank HM, Hoose SA, Polymenis M. The unfolded protein response is not necessary for the G1/S transition, but it is required for chromosome maintenance in Saccharomyces cerevisiae. PLoS One. 2010;5: e12732.

195. Bicknell AA, Babour A, Federovitch CM, Niwa M. A novel role in cytokinesis reveals a housekeeping function for the unfolded protein response. J Cell Biol. 2007;177: 1017–1027.

196. Jonikas MC, Collins SR, Denic V, Oh E, Quan EM, Schmid V, et al. Comprehensive characterization of genes required for protein folding in the endoplasmic reticulum. Science. 2009;323: 1693–1697.

197. Gaspar ML, Hofbauer HF, Kohlwein SD, Henry SA. Coordination of storage lipid synthesis and membrane biogenesis: evidence for cross-talk between triacylglycerol metabolism and phosphatidylinositol synthesis. J Biol Chem. 2011;286: 1696–1708.

198. Maity S, Basak T, Bhat A, Bhasin N, Ghosh A, Chakraborty K, et al. Cross-compartment proteostasis regulation during redox imbalance induced ER stress. Proteomics. 2014;14: 1724–1736.

199. Aragón T, van Anken E, Pincus D, Serafimova IM, Korennykh AV, Rubio CA, et al. Messenger RNA targeting to endoplasmic reticulum stress signalling sites. Nature. Macmillan Publishers Limited. All rights reserved; 2009;457: 736–740.

200. Cowart LA, Shotwell M, Worley ML, Richards AJ, Montefusco DJ, Hannun YA, et al. Revealing a signaling role of phytosphingosine-1-phosphate in yeast. Mol Syst Biol. 2010;6: 349.

201. Travers KJ, Patil CK, Wodicka L, Lockhart DJ, Weissman JS, Walter P. Functional and genomic analyses reveal an essential coordination between the unfolded protein response and ER-associated degradation. Cell. 2000;101: 249–258.

202. Jesch SA, Zhao X, Wells MT, Henry SA. Genome-wide analysis reveals inositol, not choline, as the major effector of Ino2p-Ino4p and unfolded protein response target gene expression in yeast. J Biol Chem. 2005;280: 9106–9118.

203. Trcek T, Chao JA, Larson DR, Park HY, Zenklusen D, Shenoy SM, et al. Single-mRNA counting using fluorescent in situ hybridization in budding yeast. Nat Protoc. 2012;7: 408–419.

204. Nagalakshmi U, Wang Z, Waern K, Shou C, Raha D, Gerstein M, et al. The transcriptional landscape of the yeast genome defined by RNA sequencing. Science. 2008;320: 1344–1349.

205. Lashkari DA, DeRisi JL, McCusker JH, Namath AF, Gentile C, Hwang SY, et al. Yeast microarrays for genome wide parallel genetic and gene expression analysis. Proc Natl Acad Sci U S A. 1997;94: 13057–13062.

206. Pelet S, Rudolf F, Nadal-Ribelles M, de Nadal E, Posas F, Peter M. Transient activation of the HOG MAPK pathway regulates bimodal gene expression. Science. 2011;332:

732–735.

207. Vardi N, Levy S, Gurvich Y, Polacheck T, Carmi M, Jaitin D, et al. Sequential feedback induction stabilizes the phosphate starvation response in budding yeast. Cell Rep. 2014;9: 1122–1134.

208. Houser JR, Ford E, Chatterjea SM, Maleri S, Elston TC, Errede B. An improved short-lived fluorescent protein transcriptional reporter for Saccharomyces cerevisiae. Yeast. 2012;29: 519–530.

209. Dantuma NP, Lindsten K, Glas R, Jellne M, Masucci MG. Short-lived green fluorescent proteins for quantifying ubiquitin/proteasome-dependent proteolysis in living cells. Nat Biotechnol. 2000;18: 538–543.

210. Cookson NA, Mather WH, Danino T, Mondragón-Palomino O, Williams RJ, Tsimring LS, et al. Queueing up for enzymatic processing: correlated signaling through coupled degradation. Mol Syst Biol. 2011;7: 561.

211. Belle A, Tanay A, Bitincka L, Shamir R, O'Shea EK. Quantification of protein half-lives in the budding yeast proteome. Proc Natl Acad Sci U S A. 2006;103: 13004–13009.

212. Milo R, Jorgensen P, Moran U, Weber G, Springer M. BioNumbers—the database of key numbers in molecular and cell biology. Nucleic Acids Res. 2010;38: D750–D753.

213. Megerle JA, Fritz G, Gerland U, Jung K, Rädler JO. Timing and dynamics of single cell gene expression in the arabinose utilization system. Biophys J. 2008;95: 2103–2115.

214. Yaglom J, Linskens MH, Sadis S, Rubin DM, Futcher B, Finley D. p34Cdc28-mediated control of Cln3 cyclin degradation. Mol Cell Biol. 1995;15: 731–741.

215. Andersen JB, Sternberg C, Poulsen LK, Bjorn SP, Givskov M, Molin S. New unstable variants of green fluorescent protein for studies of transient gene expression in bacteria. Appl Environ Microbiol. 1998;64: 2240–2246.

216. Salama SR, Hendricks KB, Thorner J. G1 cyclin degradation: the PEST motif of yeast Cln2 is necessary, but not sufficient, for rapid protein turnover. Mol Cell Biol. 1994;14: 7953–7966.

217. Bachmair A, Finley D, Varshavsky A. In vivo half-life of a protein is a function of its amino-terminal residue. Science. 1986;234: 179–186.

218. Bachmair A, Finley D, Varshavsky A. Methods of generating desired amino-terminal residues in proteins. World Patent. 1989; Available: http://www.google.com/patents/WO1989009829A2?cl=en

219. Tasaki T, Sriram SM, Park KS, Kwon YT. The N-end rule pathway. Annu Rev Biochem. 2012;81: 261–289.

220. Mogk A, Schmidt R, Bukau B. The N-end rule pathway for regulated proteolysis: prokaryotic and eukaryotic strategies. Trends Cell Biol. 2007;17: 165–172.

221. Akashi H. Translational selection and yeast proteome evolution. Genetics. 2003;164: 1291–1303.

222. Kane JF. Effects of rare codon clusters on high-level expression of heterologous proteins in Escherichia coli. Curr Opin Biotechnol. 1995;6: 494–500.

223. Gilchrist MA, Wagner A. A model of protein translation including codon bias, nonsense errors, and ribosome recycling. J Theor Biol. 2006;239: 417–434.

224. Zhang SP, Zubay G, Goldman E. Low-usage codons in Escherichia coli, yeast, fruit fly and primates. Gene. 1991;105: 61–72.

225. Prasher DC, Eckenrode VK, Ward WW, Prendergast FG, Cormier MJ. Primary structure of the Aequorea victoria green-fluorescent protein. Gene. 1992;111: 229–233.

226. Tian J, Gong H, Sheng N, Zhou X, Gulari E, Gao X, et al. Accurate multiplex gene synthesis from programmable DNA microchips. Nature. 2004;432: 1050–1054.

227. Kunkel TA. Rapid and efficient site-specific mutagenesis without phenotypic selection. Proc Natl Acad Sci U S A. 1985;82: 488–492.

228. Adhikari AN, Freed KF, Sosnick TR. De novo prediction of protein folding pathways and structure using the principle of sequential stabilization. Proc Natl Acad Sci U S A. 2012;109: 17442–17447.

229. Lindorff-Larsen K, Piana S, Dror RO, Shaw DE. How fast-folding proteins fold. Science. 2011;334: 517–520.

230. Fisher AC, DeLisa MP. Laboratory evolution of fast-folding green fluorescent protein using secretory pathway quality control. PLoS One. 2008;3: e2351.

231. Rosenman DJ, Huang Y-M, Xia K, Fraser K, Jones VE, Lamberson CM, et al. Green-lighting green fluorescent protein: faster and more efficient folding by eliminating a cis-trans peptide isomerization event. Protein Sci. 2014;23: 400–410.

232. Aliye N, Fabbretti A, Lupidi G, Tsekoa T, Spurio R. Engineering color variants of green fluorescent protein (GFP) for thermostability, pH-sensitivity, and improved folding kinetics. Appl Microbiol Biotechnol. 2015;99: 1205–1216.

233. Ai H-W, Baird MA, Shen Y, Davidson MW, Campbell RE. Engineering and characterizing monomeric fluorescent proteins for live-cell imaging applications. Nat Protoc. 2014;9: 910–928.

234. Shaner NC, Campbell RE, Steinbach PA, Giepmans BNG, Palmer AE, Tsien RY. Improved monomeric red, orange and yellow fluorescent proteins derived from Discosoma sp. red fluorescent protein. Nat Biotechnol. 2004;22: 1567–1572.

235. Verkhusha VV, Akovbian NA, Efremenko EN, Varfolomeyev SD, Vrzheshch PV. Kinetic analysis of maturation and denaturation of DsRed, a coral-derived red fluorescent protein. Biochemistry . 2001;66: 1342–1351.

236. Reid BG, Flynn GC. Chromophore formation in green fluorescent protein. Biochemistry. 1997;36: 6786–6791.

237. Pédelacq J-D, Cabantous S, Tran T, Terwilliger TC, Waldo GS. Engineering and characterization of a superfolder green fluorescent protein. Nat Biotechnol. Nature Publishing Group; 2006;24: 79–88.

238. Jung US, Sobering AK, Romeo MJ, Levin DE. Regulation of the yeast Rlm1 transcription factor by the Mpk1 cell wall integrity MAP kinase. Mol Microbiol. 2002;46: 781–789.

239. Mager WH, Planta RJ. Multifunctional DNA-binding proteins mediate concerted transcription activation of yeast ribosomal protein genes. Biochim Biophys Acta. 1990;1050: 351–355.

240. Brachmann CB, Davies A, Cost GJ, Caputo E, Li J, Hieter P, et al. Designer deletion strains derived from Saccharomyces cerevisiae S288C: a useful set of strains and plasmids for PCR-mediated gene disruption and other applications. Yeast. 1998;14: 115–132.

241. Chang DT-H, Huang C-Y, Wu C-Y, Wu W-S. YPA: an integrated repository of promoter features in Saccharomyces cerevisiae. Nucleic Acids Res. 2011;39: D647–52.

242. Ridgway GJ, Douglas HC. Unbalanced growth of yeast due to inositol deficiency. J Bacteriol. 1958;76: 163–166.

243. Causton HC, Ren B, Koh SS, Harbison CT, Kanin E, Jennings EG, et al. Remodeling of yeast genome expression in response to environmental changes. Mol Biol Cell. 2001;12: 323–337.

244. Truman AW, Millson SH, Nuttall JM, Mollapour M, Prodromou C, Piper PW. In the yeast heat shock response, Hsf1-directed induction of Hsp90 facilitates the activation of the Slt2 (Mpk1) mitogen-activated protein kinase required for cell integrity. Eukaryot Cell. 2007;6: 744–752.

245. Kuravi VK, Kurischko C, Puri M, Luca FC. Cbk1 kinase and Bck2 control MAP kinase activation and inactivation during heat shock. Mol Biol Cell. 2011;22: 4892–4907.

246. Graves JA, Henry SA. Regulation of the yeast INO1 gene. The products of the INO2, INO4 and OPI1 regulatory genes are not required for repression in response to inositol. Genetics. 2000;154: 1485–1495.

247. Kafri M, Metzl-Raz E, Jona G, Barkai N. The Cost of Protein Production. Cell Rep. 2016;14: 22–31.

248. Zenobi R. Single-cell metabolomics: analytical and biological perspectives. Science. 2013;342: 1243259.

249. Wu H, Volponi JV, Oliver AE, Parikh AN, Simmons BA, Singh S. In vivo lipidomics using single-cell Raman spectroscopy. Proc Natl Acad Sci U S A. 2011;108: 3809–3814.

250. Tantama M, Martínez-François JR, Mongeon R, Yellen G. Imaging energy status in live cells with a fluorescent biosensor of the intracellular ATP-to-ADP ratio. Nat Commun. 2013;4: 2550.

251. Zou C, Wang Y, Shen Z. 2-NBDG as a fluorescent indicator for direct glucose uptake measurement. J Biochem Biophys Methods. 2005;64: 207–215.

252. Lipsky NG, Pagano RE. Sphingolipid metabolism in cultured fibroblasts: microscopic and biochemical studies employing a fluorescent ceramide analogue. Proc Natl Acad Sci U S A. 1983;80: 2608–2612.

253. Kirkeby S, Thomsen CE. Quantitative immunohistochemistry of fluorescence labelled probes using low-cost software. J Immunol Methods. 2005;301: 102–113.

254. Fery-Forgues S, Fayet J-P, Lopez A. Drastic changes in the fluorescence properties of NBD probes with the polarity of the medium: involvement of a TICT state? J Photochem Photobiol A Chem. 1993;70: 229–243.

255. Haldar S, Chattopadhyay A. Application of NBD-Labeled Lipids in Membrane and Cell Biology. In: Mély Y, Duportail G, editors. Fluorescent Methods to Study Biological Membranes. Springer Berlin Heidelberg; 2012. pp. 37–50.

256. Levine TP, Wiggins CA, Munro S. Inositol phosphorylceramide synthase is located in the Golgi apparatus of Saccharomyces cerevisiae. Mol Biol Cell. 2000;11: 2267–2281.

257. Zhong W, Murphy DJ, Georgopapadakou NH. Inhibition of yeast inositol phosphorylceramide synthase by aureobasidin A measured by a fluorometric assay. FEBS Lett. 1999;463: 241–244.

258. Takesako K, Kuroda H, Inoue T, Haruna F, Yoshikawa Y, Kato I, et al. Biological properties of aureobasidin A, a cyclic depsipeptide antifungal antibiotic. J Antibiot . 1993;46: 1414–1420.

259. Li X, Zhao X, Fang Y, Jiang X, Duong T, Fan C, et al. Generation of destabilized green fluorescent protein as a transcription reporter. J Biol Chem. 1998;273: 34970–34975.

260. Lanza AM, Curran KA, Rey LG, Alper HS. A condition-specific codon optimization approach for improved heterologous gene expression in Saccharomyces cerevisiae. BMC Syst Biol. 2014;8: 33.

261. Lopes JM, Henry SA. Interaction of trans and cis regulatory elements in the INO1 promoter of Saccharomyces cerevisiae. Nucleic Acids Res. 1991;19: 3987–3994.

262. Li B, Nierras CR, Warner JR. Transcriptional elements involved in the repression of ribosomal protein synthesis. Mol Cell Biol. 1999;19: 5393–5404.

263. Blount BA, Weenink T, Vasylechko S, Ellis T. Rational diversification of a promoter providing fine-tuned expression and orthogonal regulation for synthetic biology. PLoS One. 2012;7: e33279.

264. Shaner NC, Steinbach PA, Tsien RY. A guide to choosing fluorescent proteins. Nat Methods. 2005;2: 905–909.

265. Hackett EA, Esch RK, Maleri S, Errede B. A family of destabilized cyan fluorescent proteins as transcriptional reporters in S. cerevisiae. Yeast. 2006;23: 333–349.

266. Khmelinskii A, Keller PJ, Bartosik A, Meurer M, Barry JD, Mardin BR, et al. Tandem fluorescent protein timers for in vivo analysis of protein dynamics. Nat Biotechnol. 2012;30: 708–714.

267. Breslow DK, Collins SR, Bodenmiller B, Aebersold R, Simons K, Shevchenko A, et al. Orm family proteins mediate sphingolipid homeostasis. Nature. 2010;463: 1048–1053.

268. Martin OC, Comly ME, Blanchette-Mackie EJ, Pentchev PG, Pagano RE. Cholesterol deprivation affects the fluorescence properties of a ceramide analog at the Golgi apparatus of living cells. Proc Natl Acad Sci U S A. 1993;90: 2661–2665.

269. Mao C, Xu R, Bielawska A, Szulc ZM, Obeid LM. Cloning and characterization of a Saccharomyces cerevisiae alkaline ceramidase with specificity for dihydroceramide. J Biol Chem. 2000;275: 31369–31378.

270. Fröhlich F, Petit C, Kory N, Christiano R, Hannibal-Bach H-K, Graham M, et al. The GARP complex is required for cellular sphingolipid homeostasis. Elife. 2015;4. doi:10.7554/eLife.08712

271. Nikawa J, Yamashita S. Molecular cloning of the gene encoding CDPdiacylglycerol-inositol 3-phosphatidyl transferase in Saccharomyces cerevisiae. Eur J Biochem. 1984;143: 251–256.

272. Henry SA, Atkinson KD, Kolat AI, Culbertson MR. Growth and metabolism of inositol-starved Saccharomyces cerevisiae. J Bacteriol. 1977;130: 472–484.

273. Jadhav S, Greenberg ML. Harnessing the power of yeast to elucidate the role of sphingolipids in metabolic and signaling processes pertinent to psychiatric disorders. Clin Lipidol. 2014;9: 533–551.

274. Epstein S, Riezman H. Sphingolipid signaling in yeast: potential implications for understanding disease. Front Biosci . 2013;5: 97–108.

275. Swinnen E, Wilms T, Idkowiak-Baldys J, Smets B, De Snijder P, Accardo S, et al. The protein kinase Sch9 is a key regulator of sphingolipid metabolism in Saccharomyces cerevisiae. Mol Biol Cell. 2014;25: 196–211.

276. Voynova NS, Roubaty C, Vazquez HM, Mallela SK, Ejsing CS, Conzelmann A.

Saccharomyces cerevisiae Is Dependent on Vesicular Traffic between the Golgi Apparatus and the Vacuole When Inositolphosphorylceramide Synthase Aur1 Is Inactivated. Eukaryot Cell. 2015;14: 1203–1216.

277. Morimoto Y, Tani M. Synthesis of mannosylinositol phosphorylceramides is involved in maintenance of cell integrity of yeast Saccharomyces cerevisiae. Mol Microbiol. 2015;95: 706–722.

278. Nakase M, Tani M, Morita T, Kitamoto HK, Kashiwazaki J, Nakamura T, et al. Mannosylinositol phosphorylceramide is a major sphingolipid component and is required for proper localization of plasma-membrane proteins in Schizosaccharomyces pombe. J Cell Sci. 2010;123: 1578–1587.

279. Sütterlin C, Doering TL, Schimmöller F, Schröder S, Riezman H. Specific requirements for the ER to Golgi transport of GPI-anchored proteins in yeast. J Cell Sci. 1997;110 (Pt 21): 2703–2714.

280. Martínez-Montañés F, Schneiter R. Following the flux of long-chain bases through the sphingolipid pathway in vivo using mass spectrometry. J Lipid Res. 2016;57: 906–915.

281. Giaever G, Chu AM, Ni L, Connelly C, Riles L, Véronneau S, et al. Functional profiling of the Saccharomyces cerevisiae genome. Nature. 2002;418: 387–391.

282. Hofman-Bang J. Nitrogen catabolite repression in Saccharomyces cerevisiae. Mol Biotechnol. 1999;12: 35–73.

283. Pachkov M, Balwierz PJ, Arnold P, Ozonov E, van Nimwegen E. SwissRegulon, a database of genome-wide annotations of regulatory sites: recent updates. Nucleic Acids Res. 2013;41: D214–20.

284. Franceschini A, Szklarczyk D, Frankild S, Kuhn M, Simonovic M, Roth A, et al. STRING v9.1: protein-protein interaction networks, with increased coverage and integration. Nucleic Acids Res. 2013;41: D808–15.

285. Kispal G, Sipos K, Lange H, Fekete Z, Bedekovics T, Janáky T, et al. Biogenesis of cytosolic ribosomes requires the essential iron-sulphur protein Rli1p and mitochondria. EMBO J. 2005;24: 589–598.

286. Johnston LH, Thomas AP. The isolation of new DNA synthesis mutants in the yeast Saccharomyces cerevisiae. Mol Gen Genet. 1982;186: 439–444.

287. Craig KL, Tyers M. The F-box: a new motif for ubiquitin dependent proteolysis in cell cycle regulation and signal transduction. Prog Biophys Mol Biol. 1999;72: 299–328.

288. Cherry JM, Hong EL, Amundsen C, Balakrishnan R, Binkley G, Chan ET, et al. Saccharomyces Genome Database: the genomics resource of budding yeast. Nucleic Acids Res. 2012;40: D700–5.

289. Merz S, Westermann B. Genome-wide deletion mutant analysis reveals genes required for respiratory growth, mitochondrial genome maintenance and mitochondrial protein synthesis in Saccharomyces cerevisiae. Genome Biol. 2009;10: R95.

290. Spiegel S, Milstien S. Sphingosine-1-phosphate: an enigmatic signalling lipid. Nat Rev Mol Cell Biol. 2003;4: 397–407.

291. Hibbs MA, Hess DC, Myers CL, Huttenhower C, Li K, Troyanskaya OG. Exploring the functional landscape of gene expression: directed search of large microarray compendia. Bioinformatics. 2007;23: 2692–2699.

292. Gauthier NP, Larsen ME, Wernersson R, de Lichtenberg U, Jensen LJ, Brunak S, et al.

Cyclebase.org--a comprehensive multi-organism online database of cell-cycle experiments. Nucleic Acids Res. 2008;36: D854–9.

293. Spellman PT, Sherlock G, Zhang MQ, Iyer VR, Anders K, Eisen MB, et al. Comprehensive identification of cell cycle-regulated genes of the yeast Saccharomyces cerevisiae by microarray hybridization. Mol Biol Cell. 1998;9: 3273–3297.

294. Cho RJ, Campbell MJ, Winzeler EA, Steinmetz L, Conway A, Wodicka L, et al. A genome-wide transcriptional analysis of the mitotic cell cycle. Mol Cell. 1998;2: 65–73.

295. Granovskaia MV, Jensen LJ, Ritchie ME, Toedling J, Ning Y, Bork P, et al. High-resolution transcription atlas of the mitotic cell cycle in budding yeast. Genome Biol. 2010;11: R24.

296. Pramila T, Wu W, Miles S, Noble WS, Breeden LL. The Forkhead transcription factor Hcm1 regulates chromosome segregation genes and fills the S-phase gap in the transcriptional circuitry of the cell cycle. Genes Dev. 2006;20: 2266–2278.

297. Teixeira MC, Monteiro PT, Guerreiro JF, Gonçalves JP, Mira NP, dos Santos SC, et al. The YEASTRACT database: an upgraded information system for the analysis of gene and genomic transcription regulation in Saccharomyces cerevisiae. Nucleic Acids Res. 2014;42: D161–6.

298. Koch C, Moll T, Neuberg M, Ahorn H, Nasmyth K. A role for the transcription factors Mbp1 and Swi4 in progression from G1 to S phase. Science. 1993;261: 1551–1557.

299. Sidorova J, Breeden L. Analysis of the SWI4/SWI6 protein complex, which directs G1/S-specific transcription in Saccharomyces cerevisiae. Mol Cell Biol. 1993;13: 1069–1077.

300. Saito T, Mitsui K, Hamada Y, Tsurugi K. Regulation of the Gts1p level by the ubiquitination system to maintain metabolic oscillations in the continuous culture of yeast. J Biol Chem. 2002;277: 33624–33631.

301. Harbison CT, Gordon DB, Lee TI, Rinaldi NJ, Macisaac KD, Danford TW, et al. Transcriptional regulatory code of a eukaryotic genome. Nature. 2004;431: 99–104.

302. Iyer VR, Horak CE, Scafe CS, Botstein D, Snyder M, Brown PO. Genomic binding sites of the yeast cell-cycle transcription factors SBF and MBF. Nature. 2001;409: 533–538.

303. Chua G, Morris QD, Sopko R, Robinson MD, Ryan O, Chan ET, et al. Identifying transcription factor functions and targets by phenotypic activation. Proc Natl Acad Sci U S A. 2006;103: 12045–12050.

304. Travers KJ, Patil CK, Wodicka L, Lockhart DJ, Weissman JS, Walter P. Functional and genomic analyses reveal an essential coordination between the unfolded protein response and ER-associated degradation. Cell. 2000;101: 249–258.

305. VanderSluis B, Hess DC, Pesyna C, Krumholz EW, Syed T, Szappanos B, et al. Broad metabolic sensitivity profiling of a prototrophic yeast deletion collection. Genome Biol. 2014;15: R64.

306. Proszynski TJ, Klemm RW, Gravert M, Hsu PP, Gloor Y, Wagner J, et al. A genome-wide visual screen reveals a role for sphingolipids and ergosterol in cell surface delivery in yeast. Proc Natl Acad Sci U S A. 2005;102: 17981–17986.

307. Cain NE, Kaiser CA. Transport activity-dependent intracellular sorting of the yeast general amino acid permease. Mol Biol Cell. 2011;22: 1919–1929.

308. Roberg KJ, Bickel S, Rowley N, Kaiser CA. Control of amino acid permease sorting in the late secretory pathway of Saccharomyces cerevisiae by SEC13, LST4, LST7 and

LST8. Genetics. 1997;147: 1569–1584.

309. Cowart LA, Hannun YA. Selective substrate supply in the regulation of yeast de novo sphingolipid synthesis. J Biol Chem. 2007;282: 12330–12340.

310. Nanduri J, Tartakoff AM. The arrest of secretion response in yeast: signaling from the secretory path to the nucleus via Wsc proteins and Pkc1p. Mol Cell. 2001;8: 281–289.

311. Heinisch JJ, Lorberg A, Schmitz HP, Jacoby JJ. The protein kinase C-mediated MAP kinase pathway involved in the maintenance of cellular integrity in Saccharomyces cerevisiae. Mol Microbiol. 1999;32: 671–680.

312. Daquinag A, Fadri M, Jung SY, Qin J, Kunz J. The yeast PH domain proteins Slm1 and Slm2 are targets of sphingolipid signaling during the response to heat stress. Mol Cell Biol. 2007;27: 633–650.

313. Patton JL, Srinivasan B, Dickson RC, Lester RL. Phenotypes of sphingolipid-dependent strains of Saccharomyces cerevisiae. J Bacteriol. 1992;174: 7180–7184.

314. Barnes G, Hansen WJ, Holcomb CL, Rine J. Asparagine-linked glycosylation in Saccharomyces cerevisiae: genetic analysis of an early step. Mol Cell Biol. 1984;4: 2381–2388.

315. Kapitzky L, Beltrao P, Berens TJ, Gassner N, Zhou C, Wüster A, et al. Cross-species chemogenomic profiling reveals evolutionarily conserved drug mode of action. Mol Syst Biol. 2010;6: 451.

316. Epstein S, Castillon GA, Qin Y, Riezman H. An essential function of sphingolipids in yeast cell division. Mol Microbiol. 2012;84: 1018–1032.

317. Surma MA, Klose C, Peng D, Shales M, Mrejen C, Stefanko A, et al. A lipid E-MAP identifies Ubx2 as a critical regulator of lipid saturation and lipid bilayer stress. Mol Cell. 2013;51: 519–530.

318. Ambroziak J, Henry SA. INO2 and INO4 gene products, positive regulators of phospholipid biosynthesis in Saccharomyces cerevisiae, form a complex that binds to the INO1 promoter. J Biol Chem. 1994;269: 15344–15349.

319. Cox JS, Chapman RE, Walter P. The unfolded protein response coordinates the production of endoplasmic reticulum protein and endoplasmic reticulum membrane. Mol Biol Cell. 1997;8: 1805–1814.

320. Haak D, Gable K, Beeler T, Dunn T. Hydroxylation of Saccharomyces cerevisiae ceramides requires Sur2p and Scs7p. J Biol Chem. 1997;272: 29704–29710.

321. Yoshikawa K, Tanaka T, Furusawa C, Nagahisa K, Hirasawa T, Shimizu H. Comprehensive phenotypic analysis for identification of genes affecting growth under ethanol stress in Saccharomyces cerevisiae. FEMS Yeast Res. 2009;9: 32–44.

322. Dudley AM, Janse DM, Tanay A, Shamir R, Church GM. A global view of pleiotropy and phenotypically derived gene function in yeast. Mol Syst Biol. 2005;1: 2005.0001.

323. Guan XL, Souza CM, Pichler H, Dewhurst G, Schaad O, Kajiwara K, et al. Functional interactions between sphingolipids and sterols in biological membranes regulating cell physiology. Mol Biol Cell. 2009;20: 2083–2095.

324. Abe F, Hiraki T. Mechanistic role of ergosterol in membrane rigidity and cycloheximide resistance in Saccharomyces cerevisiae. Biochim Biophys Acta. 2009;1788: 743–752.

325. Wickner W. Membrane fusion: five lipids, four SNAREs, three chaperones, two nucleotides, and a Rab, all dancing in a ring on yeast vacuoles. Annu Rev Cell Dev Biol.

2010;26: 115–136.

326. Lai Y, Zhao L, Bu B, Lou X, Li D, Ji B, et al. Lipid molecules influence early stages of yeast SNARE-mediated membrane fusion. Phys Biol. 2015;12: 025003.

327. Gallego O, Betts MJ, Gvozdenovic-Jeremic J, Maeda K, Matetzki C, Aguilar-Gurrieri C, et al. A systematic screen for protein-lipid interactions in Saccharomyces cerevisiae. Mol Syst Biol. 2010;6: 430.

328. LeBlanc MA, McMaster CR. Lipid binding requirements for oxysterol-binding protein Kes1 inhibition of autophagy and endosome-trans-Golgi trafficking pathways. J Biol Chem. 2010;285: 33875–33884.

329. Mousley CJ, Yuan P, Gaur NA, Trettin KD, Nile AH, Deminoff SJ, et al. A sterol-binding protein integrates endosomal lipid metabolism with TOR signaling and nitrogen sensing. Cell. 2012;148: 702–715.

330. Holthuis JCM, Menon AK. Lipid landscapes and pipelines in membrane homeostasis. Nature. 2014;510: 48–57.

331. Hanscho M, Ruckerbauer DE, Chauhan N, Hofbauer HF, Krahulec S, Nidetzky B, et al. Nutritional requirements of the BY series of Saccharomyces cerevisiae strains for optimum growth. FEMS Yeast Res. 2012;12: 796–808.

332. Volmer R, Ron D. Lipid-dependent regulation of the unfolded protein response. Curr Opin Cell Biol. 2015;33: 67–73.

333. Volmer R, van der Ploeg K, Ron D. Membrane lipid saturation activates endoplasmic reticulum unfolded protein response transducers through their transmembrane domains. Proc Natl Acad Sci U S A. 2013;110: 4628–4633.

334. Chumnanpuen P, Nookaew I, Nielsen J. Integrated analysis, transcriptome-lipidome, reveals the effects of INO-level (INO2 and INO4) on lipid metabolism in yeast. BMC Syst Biol. 2013;7 Suppl 3: S7.

335. Atkinson KD, Kolat AI, Henry SA. Osmotic imbalance in inositol-starved spheroplasts of Saccharomyces cerevisiae. J Bacteriol. 1977;132: 806–817.

336. Gasch AP. Comparative genomics of the environmental stress response in ascomycete fungi. Yeast. 2007;24: 961–976.

337. Kimata Y, Ishiwata-Kimata Y, Ito T, Hirata A, Suzuki T, Oikawa D, et al. Two regulatory steps of ER-stress sensor Ire1 involving its cluster formation and interaction with unfolded proteins. J Cell Biol. 2007;179: 75–86.

338. Leber JH, Bernales S, Walter P. IRE1-independent gain control of the unfolded protein response. PLoS Biol. Public Library of Science; 2004;2: E235.

339. Pincus D, Chevalier MW, Aragón T, van Anken E, Vidal SE, El-Samad H, et al. BiP binding to the ER-stress sensor Ire1 tunes the homeostatic behavior of the unfolded protein response. Kelly JW, editor. PLoS Biol. Public Library of Science; 2010;8: e1000415.

340. Pincus D, Aranda-Díaz A, Zuleta IA, Walter P, El-Samad H. Delayed Ras/PKA signaling augments the unfolded protein response. Proc Natl Acad Sci U S A. 2014;111: 14800–14805.

341. Behar M, Hao N, Dohlman HG, Elston TC. Dose-to-duration encoding and signaling beyond saturation in intracellular signaling networks. PLoS Comput Biol. 2008;4: e1000197.

342. Siegal ML. Shifting sugars and shifting paradigms. PLoS Biol. 2015;13: e1002068.

343. Diamond S, Jun D, Rubin BE, Golden SS. The circadian oscillator in Synechococcus elongatus controls metabolite partitioning during diurnal growth. Proc Natl Acad Sci U S A. 2015;112: E1916–25.

344. Shapiro HM. Practical Flow Cytometry. Wiley; 2005.

345. Koch AL. The logarithm in biology 1. Mechanisms generating the log-normal distribution exactly. J Theor Biol. 1966;12: 276–290.

346. Mager WH, Planta RJ. Coordinate expression of ribosomal protein genes in yeast as a function of cellular growth rate. Mol Cell Biochem. 1991;104: 181–187.

347. Laabs TL, Markwardt DD, Slattery MG, Newcomb LL, Stillman DJ, Heideman W. ACE2 is required for daughter cell-specific G1 delay in Saccharomyces cerevisiae. Proc Natl Acad Sci U S A. 2003;100: 10275–10280.

348. Smith EE, Smith ZH, Goldstein IJ. Protein-carbohydrate interaction. A turbidimetric study of the interaction of concanavalin A with amylopectin and glycogen and some of their enzymic and chemical degradation products. Biochem J. 1968;107: 715–724.

349. Pagny S, Lerouge P, Faye L, Gomord V. Signals and mechanisms for protein retention in the endoplasmic reticulum. J Exp Bot. 1999;50: 157–164.

350. Davey HM, Kell DB. Flow cytometry and cell sorting of heterogeneous microbial populations: the importance of single-cell analyses. Microbiol Rev. 1996;60: 641–696.

351. Foltman M, Molist I, Sanchez-Diaz A. Synchronization of the Budding Yeast Saccharomyces cerevisiae. Methods Mol Biol. 2016;1369: 279–291.

352. Wang Y, Burke DJ. Checkpoint genes required to delay cell division in response to nocodazole respond to impaired kinetochore function in the yeast Saccharomyces cerevisiae. Mol Cell Biol. 1995;15: 6838–6844.

353. Schröder M, Chang JS, Kaufman RJ. The unfolded protein response represses nitrogen-starvation induced developmental differentiation in yeast. Genes Dev. 2000;14: 2962–2975.

354. White MA, Riles L, Cohen BA. A systematic screen for transcriptional regulators of the yeast cell cycle. Genetics. 2009;181: 435–446.

355. Soifer I, Barkai N. Systematic identification of cell size regulators in budding yeast. Mol Syst Biol. 2014;10: 761.

356. Avraham N, Soifer I, Carmi M, Barkai N. Increasing population growth by asymmetric segregation of a limiting resource during cell division. Mol Syst Biol. EMBO Press; 2013;9: 656.

357. Sil A, Herskowitz I. Identification of asymmetrically localized determinant, Ash1p, required for lineage-specific transcription of the yeast HO gene. Cell. 1996;84: 711–722.

358. MacIsaac KD, Wang T, Gordon DB, Gifford DK, Stormo GD, Fraenkel E. An improved map of conserved regulatory sites for Saccharomyces cerevisiae. BMC Bioinformatics. 2006;7: 113.

359. Hu Z, Killion PJ, Iyer VR. Genetic reconstruction of a functional transcriptional regulatory network. Nat Genet. 2007;39: 683–687.

360. Venters BJ, Wachi S, Mavrich TN, Andersen BE, Jena P, Sinnamon AJ, et al. A comprehensive genomic binding map of gene and chromatin regulatory proteins in Saccharomyces. Mol Cell. 2011;41: 480–492.

361. Balakrishnan R, Park J, Karra K, Hitz BC, Binkley G, Hong EL, et al. YeastMine--an integrated data warehouse for Saccharomyces cerevisiae data as a multipurpose tool-kit. Database . 2012;2012: bar062.

362. Zettel MF, Garza LR, Cass AM, Myhre RA, Haizlip LA, Osadebe SN, et al. The budding index of Saccharomyces cerevisiae deletion strains identifies genes important for cell cycle progression. FEMS Microbiol Lett. 2003;223: 253–258.

363. Lord PG, Wheals AE. Asymmetrical division of Saccharomyces cerevisiae. J Bacteriol. 1980;142: 808–818.

364. Hartwell LH, Unger MW. Unequal division in Saccharomyces cerevisiae and its implications for the control of cell division. J Cell Biol. 1977;75: 422–435.

365. Turner JJ, Ewald JC, Skotheim JM. Cell size control in yeast. Curr Biol. 2012;22: R350–9.

366. Bassik MC, Kampmann M. Knocking out the door to tunicamycin entry. Proc Natl Acad Sci U S A. 2011;108: 11731–11732.

367. Fishbein JD, Dobrowsky RT, Bielawska A, Garrett S, Hannun YA. Ceramide-mediated growth inhibition and CAPP are conserved in Saccharomyces cerevisiae. J Biol Chem. 1993;268: 9255–9261.

368. Pacheco A, Azevedo F, Rego A, Santos J, Chaves SR, Côrte-Real M, et al. C2-phytoceramide perturbs lipid rafts and cell integrity in Saccharomyces cerevisiae in a sterol-dependent manner. PLoS One. 2013;8: e74240.

369. Piña FJ, Fleming T, Pogliano K, Niwa M. Reticulons Regulate the ER Inheritance Block during ER Stress. Dev Cell. 2016;37: 279–288.

370. Song J, Yang Q, Yang J, Larsson L, Hao X, Zhu X, et al. Essential genetic interactors of SIR2 required for spatial sequestration and asymmetrical inheritance of protein aggregates. PLoS Genet. 2014;10: e1004539.

371. Knoblach B, Rachubinski RA. Sharing the cell's bounty - organelle inheritance in yeast. J Cell Sci. 2015;128: 621–630.

372. Roberts RG. Stressed Yeast Paint a Picture of Dorian Gray. PLoS Biol. Public Library of Science; 2014;12: e1001885.

373. Levy SF, Ziv N, Siegal ML. Bet hedging in yeast by heterogeneous, age-correlated expression of a stress protectant. Hurst LD, editor. PLoS Biol. Public Library of Science; 2012;10: e1001325.

374. Carlquist M, Fernandes RL, Helmark S, Heins A-L, Lundin L, Sørensen SJ, et al. Physiological heterogeneities in microbial populations and implications for physical stress tolerance. Microb Cell Fact. 2012;11: 94.

375. Llamosi A, Gonzalez-Vargas AM, Versari C, Cinquemani E, Ferrari-Trecate G, Hersen P, et al. What Population Reveals about Individual Cell Identity: Single-Cell Parameter Estimation of Models of Gene Expression in Yeast. PLoS Comput Biol. 2016;12: e1004706.

376. Venturelli OS, Zuleta I, Murray RM, El-Samad H. Population diversification in a yeast metabolic program promotes anticipation of environmental shifts. PLoS Biol. 2015;13: e1002042.

377. Vai M, Popolo L, Alberghina L. Effect of tunicamycin on cell cycle progression in budding yeast. Exp Cell Res. 1987;171: 448–459.

378. Brewer JW, Hendershot LM, Sherr CJ, Diehl JA. Mammalian unfolded protein response inhibits cyclin D1 translation and cell-cycle progression. Proc Natl Acad Sci U S A. 1999;96: 8505–8510.

379. Pramila T, Wu W, Miles S, Noble WS, Breeden LL. The Forkhead transcription factor Hcm1 regulates chromosome segregation genes and fills the S-phase gap in the transcriptional circuitry of the cell cycle. Genes Dev. 2006;20: 2266–2278.

380. Vergés E, Colomina N, Garí E, Gallego C, Aldea M. Cyclin Cln3 is retained at the ER and released by the J chaperone Ydj1 in late G1 to trigger cell cycle entry. Mol Cell. 2007;26: 649–662.

381. Vanoni M, Rossi RL, Querin L, Zinzalla V, Alberghina L. Glucose modulation of cell size in yeast. Biochem Soc Trans. 2005;33: 294–296.

382. Schmidt-Glenewinkel H, Barkai N. Loss of growth homeostasis by genetic decoupling of cell division from biomass growth: implication for size control mechanisms. Mol Syst Biol. 2014;10: 769.

383. Saracino F, Bassler J, Muzzini D, Hurt E, Agostoni Carbone ML. The yeast kinase Swe1 is required for proper entry into cell cycle after arrest due to ribosome biogenesis and protein synthesis defects. Cell Cycle. 2004;3: 648–654.

384. Booher RN, Deshaies RJ, Kirschner MW. Properties of Saccharomyces cerevisiae wee1 and its differential regulation of p34CDC28 in response to G1 and G2 cyclins. EMBO J. 1993;12: 3417–3426.

385. McNulty JJ, Lew DJ. Swe1p responds to cytoskeletal perturbation, not bud size, in S. cerevisiae. Curr Biol. 2005;15: 2190–2198.

386. Soifer I, Robert L, Amir A. Single-Cell Analysis of Growth in Budding Yeast and Bacteria Reveals a Common Size Regulation Strategy. Curr Biol. 2016;26: 356–361.

387. Lord PG, Wheals AE. Variability in individual cell cycles of Saccharomyces cerevisiae. J Cell Sci. 1981;50: 361–376.

388. Mäder U, Nicolas P, Richard H, Bessières P, Aymerich S. Comprehensive identification and quantification of microbial transcriptomes by genome-wide unbiased methods. Curr Opin Biotechnol. 2011;22: 32–41.

389. Aebersold R, Mann M. Mass-spectrometric exploration of proteome structure and function. Nature. 2016;537: 347–355.

390. Hocine S, Raymond P, Zenklusen D, Chao JA, Singer RH. Single-molecule analysis of gene expression using two-color RNA labeling in live yeast. Nat Methods. 2013;10: 119–121.

391. Zi Z, Liebermeister W, Klipp E. A quantitative study of the Hog1 MAPK response to fluctuating osmotic stress in Saccharomyces cerevisiae. PLoS One. 2010;5: e9522.

392. AkhavanAghdam Z, Sinha J, Tabbaa OP, Hao N. Dynamic control of gene regulatory logic by seemingly redundant transcription factors. Elife. 2016;5. doi:10.7554/eLife.18458

393. Loewen CJR, Roy A, Levine TP. A conserved ER targeting motif in three families of lipid binding proteins and in Opi1p binds VAP. EMBO J. 2003;22: 2025–2035.

394. Yofe I, Weill U, Meurer M, Chuartzman S, Zalckvar E, Goldman O, et al. One library to make them all: streamlining the creation of yeast libraries via a SWAp-Tag strategy. Nat Methods. 2016;13: 371–378.

395. Ejsing CS, Sampaio JL, Surendranath V, Duchoslav E, Ekroos K, Klemm RW, et al. Global analysis of the yeast lipidome by quantitative shotgun mass spectrometry. Proceedings of the National Academy of Sciences. 2009;106: 2136–2141.

396. Singh A, Del Poeta M. Sphingolipidomics: An Important Mechanistic Tool for Studying Fungal Pathogens. Front Microbiol. 2016;7: 501.

397. Schuck S, Prinz WA, Thorn KS, Voss C, Walter P. Membrane expansion alleviates endoplasmic reticulum stress independently of the unfolded protein response. J Cell Biol. 2009;187: 525–536.

398. Ohno S. Major Sex-Determining Genes. Springer Berlin Heidelberg; 2013.

399. Natarajan K, Meyer MR, Jackson BM, Slade D, Roberts C, Hinnebusch AG, et al. Transcriptional profiling shows that Gcn4p is a master regulator of gene expression during amino acid starvation in yeast. Mol Cell Biol. 2001;21: 4347–4368.

400. Szamecz B, Boross G, Kalapis D, Kovács K, Fekete G, Farkas Z, et al. The genomic landscape of compensatory evolution. PLoS Biol. 2014;12: e1001935.

401. Coelho M, Lade SJ, Alberti S, Gross T, Tolić IM. Fusion of protein aggregates facilitates asymmetric damage segregation. Walter P, editor. PLoS Biol. Public Library of Science; 2014;12: e1001886.

402. Minois N, Frajnt M, Dölling M, Lagona F, Schmid M, Küchenhoff H, et al. Symmetrically dividing cells of the fission yeast schizosaccharomyces pombe do age. Biogerontology. 2006;7: 261–267.

403. Zhang J, Hulme L, Liu J-L. Asymmetric inheritance of cytoophidia in Schizosaccharomyces pombe. Biol Open. 2014;3: 1092–1097.

404. Mitchison JM. The growth of single cells. I. Schizosaccharomyces pombe. Exp Cell Res. 1957;13: 244–262.

405. Lindner AB, Madden R, Demarez A, Stewart EJ, Taddei F. Asymmetric segregation of protein aggregates is associated with cellular aging and rejuvenation. Proc Natl Acad Sci U S A. 2008;105: 3076–3081.

406. Swain PS, Elowitz MB, Siggia ED. Intrinsic and extrinsic contributions to stochasticity in gene expression. Proc Natl Acad Sci U S A. 2002;99: 12795–12800.

407. Uphoff S, Lord ND, Okumus B, Potvin-Trottier L, Sherratt DJ, Paulsson J. Stochastic activation of a DNA damage response causes cell-to-cell mutation rate variation. Science. 2016;351: 1094–1097.

408. Süel GM, Kulkarni RP, Dworkin J, Garcia-Ojalvo J, Elowitz MB. Tunability and noise dependence in differentiation dynamics. Science. 2007;315: 1716–1719.

409. Webster TD, Dickson RC. Direct selection of Saccharomyces cerevisiae resistant to the antibiotic G418 following transformation with a DNA vector carrying the kanamycin-resistance gene of Tn903. Gene. 1983;26: 243–252.

410. Gritz L, Davies J. Plasmid-encoded hygromycin B resistance: the sequence of hygromycin B phosphotransferase gene and its expression in Escherichia coli and Saccharomyces cerevisiae. Gene. 1983;25: 179–188.

411. Krügel H, Fiedler G, Haupt I, Sarfert E, Simon H. Analysis of the nourseothricin-resistance gene (nat) of Streptomyces noursei. Gene. 1988;62: 209–217.

412. Curran KA, Karim AS, Gupta A, Alper HS. Use of expression-enhancing terminators in Saccharomyces cerevisiae to increase mRNA half-life and improve gene expression

control for metabolic engineering applications. Metab Eng. 2013;19: 88–97.

413. Skotheim JM, Di Talia S, Siggia ED, Cross FR. Positive feedback of G1 cyclins ensures coherent cell cycle entry. Nature. 2008;454: 291–296.

414. Wood EJ. Molecular probes: Handbook of fluorescent probes and research chemicals: By R P Haugland. pp 390. Interchim (Molecular Probes Inc, PO Box 22010 Eugene, OR 97402-0414, USA, or 15 rue des Champs, 92600 Asnieres, Paris). 1992–1994. $15. Biochem Educ. Headington Hill Hall; 1994;22: 83–83.

415. Cole L, Davies D, Hyde GJ, Ashford AE. ER-Tracker dye and BODIPY-brefeldin A differentiate the endoplasmic reticulum and golgi bodies from the tubular-vacuole system in living hyphae of Pisolithus tinctorius. J Microsc. 2000;197: 239–249.

416. Deng Y, Bennink JR, Kang HC, Haugland RP, Yewdell JW. Fluorescent conjugates of brefeldin A selectively stain the endoplasmic reticulum and Golgi complex of living cells. J Histochem Cytochem. 1995;43: 907–915.

417. Arroyo IJ, Hu R, Merino G, Tang BZ, Peña-Cabrera E. The smallest and one of the brightest. Efficient preparation and optical description of the parent borondipyrromethene system. J Org Chem. 2009;74: 5719–5722.

418. Roy A, Levine TP. Multiple pools of phosphatidylinositol 4-phosphate detected using the pleckstrin homology domain of Osh2p. J Biol Chem. 2004;279: 44683–44689.

419. Kang J, Hsu C-H, Wu Q, Liu S, Coster AD, Posner BA, et al. Improving drug discovery with high-content phenotypic screens by systematic selection of reporter cell lines. Nat Biotechnol. 2016;34: 70–77.

420. Tkach JM, Yimit A, Lee AY, Riffle M, Costanzo M, Jaschob D, et al. Dissecting DNA damage response pathways by analysing protein localization and abundance changes during DNA replication stress. Nat Cell Biol. 2012;14: 966–976.

421. Camberg JL, Hoskins JR, Wickner S. The Interplay of ClpXP with the Cell Division Machinery in Escherichia coli. J Bacteriol. 2011;193: 1911–1918.

422. Li X, Zhao X, Fang Y, Jiang X, Duong T, Fan C, et al. Generation of destabilized green fluorescent protein as a transcription reporter. J Biol Chem. 1998;273: 34970–34975.

423. Gaudet J, Mango SE. Regulation of organogenesis by the Caenorhabditis elegans FoxA protein PHA-4. Science. 2002;295: 821–825.

424. Sharova LV, Sharov AA, Nedorezov T, Piao Y, Shaik N, Ko MSH. Database for mRNA half-life of 19 977 genes obtained by DNA microarray analysis of pluripotent and differentiating mouse embryonic stem cells. DNA Res. 2009;16: 45–58.

425. Yang E, van Nimwegen E, Zavolan M, Rajewsky N, Schroeder M, Magnasco M, et al. Decay rates of human mRNAs: correlation with functional characteristics and sequence attributes. Genome Res. 2003;13: 1863–1872.

426. Thomsen S, Anders S, Janga SC, Huber W, Alonso CR. Genome-wide analysis of mRNA decay patterns during early Drosophiladevelopment. Genome Biol. 2010;11: R93.

427. Sawada K, Sato T, Hamajima H, Jayakody LN, Hirata M, Yamashiro M, et al. Glucosylceramide Contained in Koji Mold-Cultured Cereal Confers Membrane and Flavor Modification and Stress Tolerance to Saccharomyces cerevisiae during Coculture Fermentation. Appl Environ Microbiol. 2015;81: 3688–3698.

428. Fuchs BB, Mylonakis E. Our paths might cross: the role of the fungal cell wall integrity pathway in stress response and cross talk with other stress response pathways.

Eukaryot Cell. 2009;8: 1616–1625.

429. Chu D, Barnes DJ. The lag-phase during diauxic growth is a trade-off between fast adaptation and high growth rate. Sci Rep. 2016;6: 25191.

430. Atilla-Gokcumen GE, Muro E, Relat-Goberna J, Sasse S, Bedigian A, Coughlin ML, et al. Dividing cells regulate their lipid composition and localization. Cell. 2014;156: 428–439.

431. Ewald JC, Kuehne A, Zamboni N, Skotheim JM. The Yeast Cyclin-Dependent Kinase Routes Carbon Fluxes to Fuel Cell Cycle Progression. Mol Cell. 2016;62: 532–545.

432. Ternes P, Wobbe T, Schwarz M, Albrecht S, Feussner K, Riezman I, et al. Two pathways of sphingolipid biosynthesis are separated in the yeast Pichia pastoris. J Biol Chem. 2011;286: 11401–11414.

433. Rossanese OW, Soderholm J, Bevis BJ, Sears IB, O'Connor J, Williamson EK, et al. Golgi structure correlates with transitional endoplasmic reticulum organization in Pichia pastoris and Saccharomyces cerevisiae. J Cell Biol. 1999;145: 69–81.

434. Futerman AH, Pagano RE. Determination of the intracellular sites and topology of glucosylceramide synthesis in rat liver. Biochem J. 1991;280 (Pt 2): 295–302.

435. Huitema K, van den Dikkenberg J, Brouwers JFHM, Holthuis JCM. Identification of a family of animal sphingomyelin synthases. EMBO J. 2004;23: 33–44.

436. Sato K, Noda Y, Yoda K. Kei1: a novel subunit of inositolphosphorylceramide synthase, essential for its enzyme activity and Golgi localization. Mol Biol Cell. 2009;20: 4444–4457.

437. Chandran S, Machamer CE. Acute perturbations in Golgi organization impact de novo sphingomyelin synthesis. Traffic. 2008;9: 1894–1904.

438. Fehrenbacher KL, Davis D, Wu M, Boldogh I, Pon LA. Endoplasmic reticulum dynamics, inheritance, and cytoskeletal interactions in budding yeast. Mol Biol Cell. 2002;13: 854–865.

439. Hill SM, Hao X, Grönvall J, Spikings-Nordby S, Widlund PO, Amen T, et al. Asymmetric Inheritance of Aggregated Proteins and Age Reset in Yeast Are Regulated by Vac17-Dependent Vacuolar Functions. Cell Rep. 2016;16: 826–838.

440. Colman-Lerner A, Gordon A, Serra E, Chin T, Resnekov O, Endy D, et al. Regulated cell-to-cell variation in a cell-fate decision system. Nature. 2005;437: 699–706.

441. Stewart-Ornstein J, Weissman JS, El-Samad H. Cellular Noise Regulons Underlie Fluctuations in Saccharomyces cerevisiae. Mol Cell. 2012;45: 483–493.

442. Volfson D, Marciniak J, Blake WJ, Ostroff N, Tsimring LS, Hasty J. Origins of extrinsic variability in eukaryotic gene expression. Nature. 2006;439: 861–864.

443. Ackermann M. A functional perspective on phenotypic heterogeneity in microorganisms. Nat Rev Microbiol. 2015;13: 497–508.

444. Rebnegger C, Graf AB, Valli M, Steiger MG, Gasser B, Maurer M, et al. In Pichia pastoris, growth rate regulates protein synthesis and secretion, mating and stress response. Biotechnol J. 2014;9: 511–525.

445. Zenklusen D, Wells AL, Condeelis JS, Singer RH. Imaging real-time gene expression in living yeast. CSH Protoc. 2007;2007: db.prot4870.

446. Higuchi-Sanabria R, Pernice WMA, Vevea JD, Alessi Wolken DM, Boldogh IR, Pon LA. Role of asymmetric cell division in lifespan control in Saccharomyces cerevisiae. FEMS

Yeast Res. 2014; doi:10.1111/1567-1364.12216

447. Fehrmann S, Paoletti C, Goulev Y, Ungureanu A, Aguilaniu H, Charvin G. Aging yeast cells undergo a sharp entry into senescence unrelated to the loss of mitochondrial membrane potential. Cell Rep. Elsevier; 2013;5: 1589–1599.

Appendix A: Coding DNA sequence of the reporter constructs

Table A.1: Sequences of the different features of the coding DNA sequence of the dynamic reporter constructs

Feature	Sequence (5'-> 3')
Start codon + UBI4 gene	ATGcagattttcgtcaagactttgaccggtaaaaccataacattggaagttgaatcttcc gataccatcgacaacgttaagtcgaaaattcaagacaaggaaggtatccctccagatc aacaaagattgatctttgccggtaagcagctagaagacggtagaacgctgtctgattac aacattcagaaggagtccaccttacatcttgtgctaaggctaagaggtggt
Linker with N-terminal aspartate (GAT)	GATGGGAAACTTGGTCGACAAGATCCACCTGTCGCCACCA TGGTT
Yeast codon optimised super folder GFP + stop codon	tccaagg gtgaagagct atttactggg gttgtaccca ttttggtaga actggacggagatgtaaacg gacataaatt ctctgttaga ggtgagggcg aaggcgatgc caccaatggt aaattgactc tgaagtttat atgcactacg ggtaaattac ctgttccttg gccaacccta gtaacaactt tgacatatgg tgttcaatgt ttctcaagat acccagacca tatgaaaagg catgatttct ttaaaagtgc tatgccagaa ggctacgtgc aagagagaac tatctccttt aaggatgacg gtacgtataa aacacgagca gaagtgaaat tcgaagggga tacactagtt aatcgcatcg aattaaaggg tatagacttt aaggaagatg gtaatattct cggccataaa cttgagtata atttcaactc gcataatgtg tacattacag ctgacaaaca aaagaacgga attaaagcga attttaaaat caggcacaac gtcgaagatg ggtctgttca acttgccgat cattatcagc aaaacacccc tattggtgat ggtccagtct tgttacccga taatcactac ttaagcacac agtctagatt gtcaaaagat ccgaatgaaa agcgtgatca catggtttta ttggaatttg tcaccgctgc aggaataact cacggaatgg acgagcttta taagggatcc TAA

Appendix B: Targets of ACE2 and ASH1

Table B.1: ORF and Name of all ACE2 targets

ORF	Name	ORF	Name	ORF	Name
YBR090C		YGL229C	SAP4	YNL078W	NIS1
YBR116C		YGR041W	BUD9	YNL079C	TPM1
YBR122C	MRPL36	YGR053C		YNL241C	ZWF1
YBR152W	SPP381	YGR057C	LST7	YNL242W	ATG2
YBR157C	ICS2	YGR283C		YNL327W	EGT2
YBR158W	AMN1	YHL028W	WSC4	YNL328C	MDJ2
YBR159W	IFA38	YHL029C	OCA5	YNR018W	RCF2
YDL127W	PCL2	YHR143W	DSE2	YNR067C	DSE4
YDR155C	CPR1	YIL104C	SHQ1	YOL084W	PHM7
YDR156W	RPA14	YJL159W	HSP150	YOL104C	NDJ1
YDR306C		YJL160C	PIR5	YOL158C	ENB1
YDR433W		YJR044C	VPS55	YOR034C	AKR2
YDR524C	AGE1	YJR145C	RPS4A	YOR138C	RUP1
YDR524C-B		YJR147W	HMS2	YOR140W	SFL1
YDR524W-C		YKL037W	AIM26	YOR263C	
YDR525W-A	SNA2	YKL096W	CWP1	YOR264W	DSE3
YDR527W	RBA50	YKL150W	MCR1	YOR382W	FIT2
YER124C	DSE1	YKL151C			
YER125W	RSP5	YKL178C	STE3		
YER177W	BMH1	YKR093W	PTR2		
YFR015C	GSY1	YLR042C			
YFR026C	ULI1	YLR214W	FRE1		
YGL006W	PMC1	YLR286C	CTS1		
YGL006W-A		YLR465C	BSC3		
YGL007C-A		YML099W-A			
YGL008C	PMA1	YML100W	TSL1		
YGL028C	SCW11	YML100W-A			
YGL089C	MF(ALPHA)2	YML101C	CUE4		
YGL133W	ITC1	YML108W			
YGL228W	SHE10	YNL066W	SUN4		

Table B.2: ORF and name of every ASH1 target

ORF	Name	ORF	Name	ORF	Name
YBL027W	RPL19B	YIL019W	FAF1	YNR059W	MNT4
YBR068C	BAP2	YIL046W	MET30	YOL007C	CSI2
YBR259W		YIL122W	POG1	YOL105C	WSC3
YDL055C	PSA1	YIL161W		YOL113W	SKM1
YDL135C	RDI1	YJL004C	SYS1	YOL114C	PTH4
YDL182W	LYS20	YJL194W	CDC6	YOR087W	YVC1
YDR054C	CDC34	YJL196C	ELO1	YOR168W	GLN4
YDR055W	PST1	YKL096W	CWP1	YOR270C	VPH1
YDR077W	SED1	YKL214C	YRA2	YOR310C	NOP58
YDR226W	ADK1	YKR041W		YPR063C	
YDR383C	NKP1	YKR042W	UTH1		
YDR447C	RPS17B	YLR141W	RRN5		
YDR451C	YHP1	YLR243W	GPN3		
YDR452W	PPN1	YLR272C	YCS4		
YDR461W	MFA1	YLR285W	NNT1		
YDR524C	AGE1	YLR300W	EXG1		
YDR524C-B		YLR344W	RPL26A		
YDR524W-C		YML020W			
YDR525W-A	SNA2	YML100W	TSL1		
YDR527W	RBA50	YMR108W	ILV2		
YER021W	RPN3	YMR121C	RPL15B		
YGR054W		YMR122W-A			
YGR189C	CRH1	YMR123W	PKR1		
YGR217W	CCH1	YMR238W	DFG5		
YGR220C	MRPL9	YMR305C	SCW10		
YGR229C	SMI1	YMR306W	FKS3		
YGR281W	YOR1	YMR315W-A			
YHR162W	MPC2	YNL289W	PCL1		
YHR166C	CDC23	YNR010W	CSE2		
YHR177W		YNR045W	PET494		

Table B.3: ORF and name of every heat-independent ASH1 target

ORF	Name
YDR054C	CDC34
YDR055W	PST1
YDR077W	SED1
YDR451C	YHP1
YDR452W	PPN1
YDR461W	MFA1
YDR524C	AGE1
YDR524C-B	
YDR524W-C	
YDR525W-A	SNA2
YDR527W	RBA50
YGR189C	CRH1
YIL122W	POG1
YJL194W	CDC6
YJL196C	ELO1
YKL096W	CWP1
YKR041W	
YKR042W	UTH1
YLR300W	EXG1
YML100W	TSL1
YMR121C	RPL15B
YMR122W-A	
YMR123W	PKR1
YMR305C	SCW10
YMR306W	FKS3
YNL289W	PCL1
YOL007C	CSI2
YOL113W	SKM1
YOL114C	PTH4